Università degli Studi di Torino

Scuola di Dottorato in

Scienze della Natura e Tecnologie Innovative

Dottorato in

Scienze Farmaceutiche e Biomolecolari

(XXXVI ciclo)

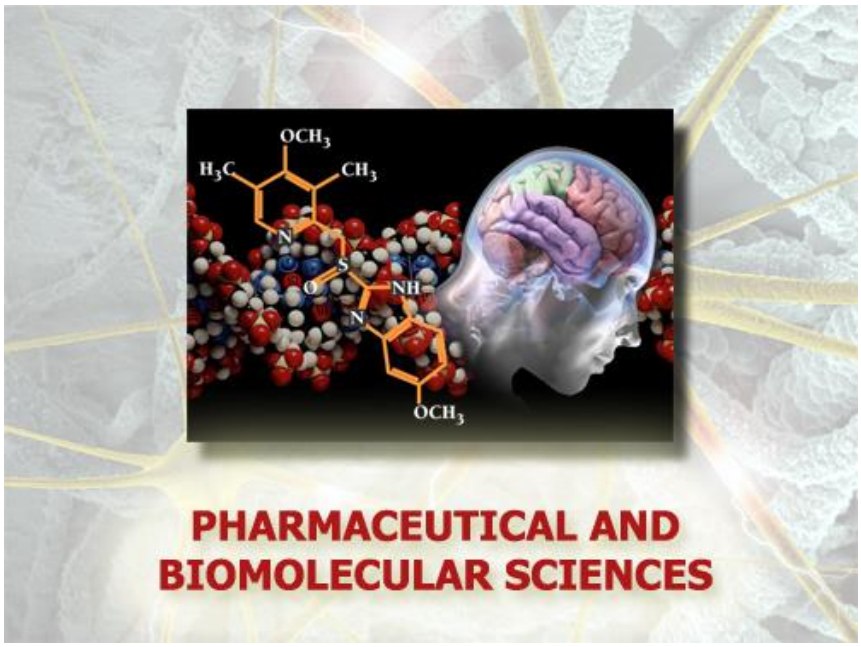

Development of electrochemical sensors for the determination of biomarkers, for application in the biomedical, food and environmental fields

Candidato: Dr. Paolo Inaudi **Tutor: Prof. Agnese Giacomino**

UNIVERSITÀ
DI TORINO

Ph.D. Program in Pharmaceutical and Biomolecular Sciences
Department of Drug Science and Technology

Cycle XXXVI

Thesis title: Development of electrochemical sensors for the determination of biomarkers, for application in the biomedical, food and environmental field

PhD candidate: Dr. Paolo Inaudi

Tutor: Prof. Agnese Giacomino

PhD. Coordinator: Prof. Roberta Cavalli

Academic years: 2020/2021 – 2021/2022 – 2022-2023

Scientific field of application: Analytical Chemistry (SSD - CHIM/01)

Table of Contents

ABSTRACT

This doctoral thesis focuses on the development of voltammetric sensors with applications spanning across diverse domains, including food analysis, healthcare, and environmental monitoring. The research explores three distinct topics, each contributing to the enhancement advancement of sensor technologies for voltammetric analyses, both in laboratory both for on-site application.

The first area of investigation involves the development of a portable procedure (pretreatment and analysis) for the speciation of mercury-methylmercury in fish samples, with a unique emphasis on enabling on-site analyses through the patenting of a novel resin for the efficient separation of the two mercury species. This innovation not only facilitates fast mercury speciation but also provides a practical solution for in-field assessments.

The second topic addresses the optimisation of a method for the determination of iron (III) in water. Originally, the interest for the determination of iron (total, iron III, iron II and iron complex) aimed at early diagnoses of neurodegenerative diseases, since this element is considered as a novel marker for these types of disease. Despite the initial goal, the research delves into the challenges and opportunities surrounding iron analysis in aquatic environments, contributing valuable insights for both environmental monitoring and potential medical applications.

The third focus area is the determination of chemical UV filters in water and sunscreens, given their significant correlation with environmental damage and their essential role in human health. The study explores the possibility of using voltammetry for on-site analysis of these filters; a good applicability of this technique has been demonstrated for monitoring contaminants in water and for checking the composition of sunscreens.

Overall, this thesis presents a comprehensive exploration of voltammetric sensor development, showcasing its applicability in addressing critical challenges across diverse fields, ranging from food safety and healthcare diagnostics to environmental monitoring. The innovative approaches and findings presented herein contribute to the advancement of analytical techniques with potential societal impact.

ABBREVIATIONS

AD - Alzheimer's disease

ASV - Anodic Stripping Voltammetry

BBB - Blood-Brain Barrier

BDNF - Brain-Derived Neurotrophic Factor

BMVEC - Brain MicroVascular Endothelial Cells

BP3 – Benzophenone-3

CE - Counter Electrode

CEC - Contaminants of Emerging Concern

CNS - Central Nervous System

CSV - Cathodic Stripping Voltammetry

CV - Cyclic Voltammetry

CV-AAS - Cold Vapor Atomic Absorption Spectrometry

CV-AFS - Cold Vapor Atomic Fluorescence Spectrometry

DcytB - Duodenal cytochrome B

DMA - Direct Mercury Analyzer

DMT1 - Divalent Metal Transporter-1

DPV - Differential Pulse Voltammetry

ECHA - European Chemicals Agency

EFSA - European Food Safety Authority

EHMC – Octinoxate

FDA – Food and Drug Administration

FGF - Fibroblast Growth Factor

Fpn – Ferroportin

GC - Gas Chromatography

GCE – Glassy Carbon Electrode

GSK-3B - Glycogen Synthase Kinase-3 Beta

Hb – Hemoglobin

HM – Heavy Metals

HPLC - High-Performance Liquid Chromatography

ICP AES/OES - Inductively Coupled Plasma Atomic Emission Spectrometry/Optical Emission Spectrometry

ICP MS - Inductively Coupled Plasma Mass Spectrometry

IFN-γ - Interferon-gamma

IGF-I - Insulin-like Growth Factor I

iNOS - inducible Nitric Oxide Synthase

LSV - Linear Sweep Voltammetry

NMDA - N-Methyl-D-Aspartate

NMR - Nuclear Magnetic Resonance

OC – Octocrylene

PABA - Para-AminoBenzoic Acid

PAN - 1-(2-Piridylazo)-2-Naphthol

RE - Reference Electrode

ROS - Reactive Oxygen Species

SbBiFE Antimony Bismuth Film Electrode

SCCS - Scientific Committee on Consumer Safety

SRM - Standard Reference Material

STCV - Staircase Voltammetry

SWV - Square Wave Voltammetry

SW-AdCSV - Square Wave Adsoptive Cathodic Stripping Voltammetry

Tf - Transferrin

TGF-β - Transform Growth Factor-beta

TLR - Toll-Like Receptor

TNF-α - Tumor Necrosis Factor-alpha

WE - Working Electrode

WWTPs - Wastewater Treatment Plants

XRF - X-ray Fluorescence Spectroscopy

Aims of the project

The aims of my PhD project focused on the development of sensors for the rapid determination of contaminants in different matrices, using a low-cost and easy-to-use voltammetric techniques that allows analysis directly in the field, with a focus on topics related to food, environment, and human health. Particular attention was paid to:

1. *Sensor development*: develop innovative sensors that can detect a wide range of contaminants in various matrices, including food, environmental samples, and human biological fluids. Optimize the sensor design for sensitivity, selectivity, and rapid response.

2. *Cost efficiency*: ensure that the sensor technology is cost-effective, making it accessible to a wide range of users, including resource-constrained areas and industries.

3. *Field-friendly technology*: development of a procedures that are user-friendly and suitable for on-site analysis, eliminating the need for extensive sample transportation to a laboratory and preparation. Design portable devices that can be easily operated by non-experts in the field.

4. *Contaminant scope*: target a broad spectrum of contaminants relevant to food safety, environmental monitoring, and human health, such as heavy metals and pharmaceutical/personal care products residues.

5. *Matrix compatibility*: ensure that the sensors are adaptable to various sample matrices, including water, soil, feathers, food products, and biological sample.

6. *Sensitivity and selectivity*: enhance the sensitivity and selectivity of the voltammetric technique to detect contaminants at low concentrations and distinguish different species or compounds, without matrix effects.

7. *Rapid detection*: aim for real-time detection capabilities to provide timely information for decision-making.

8. *Validation and certification*: ensure that the developed sensors meet regulatory standards and are suitable for certification and validation processes.

9. *Education and outreach*: conduct training programs and awareness campaigns to educate users, including field workers, food inspectors, and healthcare professionals, on the proper use of the technology.

10. *Environmental impact*: assess and minimize the environmental footprint of the sensor production process and disposal of sensor components.

11. *Collaboration*: foster collaboration with relevant stakeholders, including government agencies, research institutions, and industry partners, to promote the adoption of the technology and its integration into existing monitoring systems.

12. *Continuous improvement*: establish a mechanism for ongoing research and development to continually improve sensor performance, expand the range of detectable contaminants, and address emerging challenges.

By addressing these aims, the project can contribute significantly to the advancement of sensor technology for the rapid determination of contaminants in food, environmental samples, and human health applications, ultimately enhancing safety and well-being in these critical areas.

1. INTRODUCTION

1.1 Mercury – Methylmercury in fish samples

1.1.1 Mercury

Mercury is acknowledged as a hazardous contaminant with the characteristics of being both persistent and mobile. It resists environmental degradation and gains mobility due to the volatile nature of the element and certain compounds. Additionally, mercury possesses the capability to travel vast distances within air masses. [1]

Mercury falls within the definition of heavy metal, i.e. elements with a density greater than 5.0 g/cm^3 are classified as such.

Overall, HMs are elements found in the Earth's crust in traces (< 0.1%). They typically behave as cations, have low solubility of their hydrates, a strong tendency to form complexes, and exhibit various oxidation states depending on pH conditions. Elements such as iron (a cofactor in hemoglobin and cytochromes), cobalt (a cofactor in vitamin B12), chromium, manganese, zinc, copper, molybdenum, and selenium are present in our bodies, performing essential functions for the proper functioning of vital processes. Some of these elements cannot be completely replaced, which is why they are referred to as "essential" mineral components, while others are termed "non-essential" metals, and are commonly toxic and harmful to organisms above a threshold concentration value. Mercury belongs to the category of "non-essential" metals and exerts toxic effects in all its forms, leading to bioaccumulation and biomagnification phenomena.

Heavy metal pollution is the most significant component of overall environmental pollution, mainly because HM are widely used in many industrial activities, and therefore, their emission and concentration in the environment need to be carefully monitored. [2]

1.1.2 Chemical-physical properties

Mercury is a chemical element with the symbol Hg and atomic number 80; it has a silvery colour and is the only metal that is liquid at ordinary temperature and pressure. It is positioned in the periodic table among the transition metals of the "d-block".

Mercury exhibits unique chemical and physical characteristics. It is liquid at room temperature, solidifies at -38.5 °C, and boils at 357.25 °C, forming monoatomic vapours. It has an exceptionally high density for a liquid, at 13.6 g/cm^3. As a metal, mercury is a good conductor of electricity but is considered a poor conductor of heat. There are seven stable isotopes of mercury, with Hg-202 being the most common (29.72 % of the total). The radioisotopes with the longest half-lives are Hg-194 with a half-life of 444 years and Hg-203 with a half-life of 46,612 days. The rest of the radioisotopes have half-lives not exceeding one, and these elements are generally studied using nuclear magnetic resonance (NMR) techniques.

Special attention is given to the spectroscopic properties of mercury. It exhibits numerous emission lines in the ultraviolet spectral range, with the most intense ones at 184.950 nm, 253.652 nm, and 194.164 nm. In the visible spectrum, it shows a strong green emission line at 546.1 nm [3].

The chemical behaviour of the metal resembles that of noble metals; at room temperature, it does not oxidize in the air, and only near its boiling point does it combine with oxygen to form mercuric oxide, HgO. The oxides corresponding to the two oxidation states are weak bases. It directly

combines with sulphur and halogens; it is unaffected by water and saline solutions, while it is oxidized by nitric acid to produce mercurous nitrate ($Hg_2(NO_3)_2$) and mercuric nitrate ($Hg(NO_3)_2$) and dissolves in concentrated sulfuric acid.

Among the mercury salts still in use, noteworthy are mercuric chloride $HgCl_2$, a potent poison; mercury fulminate $Hg(ONC)_2$, which has detonating properties and is used in explosives; mercuric sulphate HgS, used as a vermilion pigment in painting; and mercurous chloride Hg_2Cl_2, also known as calomel.

It readily forms alloys with almost all common metals, especially with gold and silver; these alloys are known as amalgams, all of which possess more or less pronounced toxic properties.

1.1.3 Natural availability and use

Mercury is present in very low concentrations in the Earth's crust and is, in fact, considered a rare element. It exhibits a relative chemical inertness when combining with other elements, so its minerals are very rich, with percentages reaching up to 2.5% (a considerable amount when compared to other metals). This makes mercury one of the least expensive metals to purify. It is rarely found as native metal and more often in cinnabar, cordierite, livingstonite, and other minerals. The main cinnabar mines are located in China, Mexico, the United States, Tajikistan, Peru; Italy was also one of the leading countries in extraction and processing with mines in Mount Amiata in Tuscany for many years. The Mediterranean Sea is characterized by the presence of large cinnabar deposits (HgS), accounting for about 65% of the world's mercury reserves, even if it covers only about 1% of the world's oceans [4]. Over time, the mineral deposits have been depleted (the last mine discovered in Algeria in the 1970s) or extraction has become uneconomical, leading to a progressive decline in the global annual production, which currently stands at around 1,600 tons per year.

The peculiarities of mercury make it suitable for multiple applications.

Historically it was used for dental fillings, for the processing of hats, as antifungal in agriculture and for the extraction of gold from gold minerals in mines using the amalgams it forms with this element (all these uses are now obsolete). It displays a constant thermal expansion rate over a wide temperature range and for this reason has been used for the construction of mercury thermometers (banned in 2009), as a coolant in some types of nuclear power plants and to make liquid mirror telescopes. Mercury is an important component in electronics, it is still present in fluorescence lamps and is used in "chlor-soda" processes to conduct the electrolysis of sodium chloride in water, yielding gaseous chlorine and sodium hydroxide.

However, the use of metallic mercury is very low compared to the use of its compounds:

- sodium ethylmercurithiosalicylate (Thimerosal) is used as a preservative in vaccines, disinfectant solutions for ophthalmological and nasal use and tattoo inks;
- calomel (Hg_2Cl_2) is used in electrochemical measurements as a component of reference electrodes, in the past it was also used as a diuretic, local disinfectant and laxative in medicine;
- mercuric chloride ($HgCl_2$) is used as an insecticide, in rat poison, and as a disinfectant; in the past it was also used to treat syphilis;
- mercuric oxide (HgO) can be present in skin ointments as a whitening agent, but its use is banned from Europe;

- "mercury fulminate" ($Hg(CNO)_2$), is used as a detonator;
- merbromine and other mercury-based organomethyls are used as antiseptics.

1.1.4 Chemical forms and toxicity

Table 1.1 shows the main forms of mercury. Its elemental state (Hg^0) is very rare, and the only source is the vapours produced in post-mining extraction processes. Among the inorganic forms, in various environmental compartments, mercuric ion (Hg^{2+}) predominates. This ion binds to sulfur, giving rise to mercuric sulfide and to the -SH groups of proteins; this affinity is particularly important in anoxic water chemistry and sediments, where the high concentration of HS^- and S^{2-} leads to the formation of mercury sulfide, a solid with low solubility ($K_{sp} = 2x10^{-49}$) that tends to accumulate, regulating the availability of mercury in the environmental compartment.

In natural waters, Hg^{2+} ion is not found as a free ion but easily forms complexes with Cl^-, OH^-, and HS^- ions, to which it is affinitive. Organic species originate from the transformation of inorganic ones through processes promoted by biotic species. The formation of methylmercury occurs through the action of reducing bacteria present in sediments; these microorganisms transform inorganic mercury present in the water into the methylated species. The formed species are poorly soluble in water and tend to volatilize, but they are very stable and soluble in biological matrices. Solubility in such matrices is due to the presence of alkyl groups (-CH_3, -CH_2CH_3, -C_6H_5-, etc...) that confer high solubility in lipids, high permeability in membranes, and greater binding and accumulation capacity in tissues. The lipophilic properties of methylmercury result in bioaccumulation processes along the food chain, increasing the toxic effect of these chemical species on ecosystems, especially on higher organisms. Methylation reactions primarily occur in sediments (under reducing conditions) and biotic species, while they are less effective in natural waters due to the presence of oxidizing species and partial decomposition by sunlight.

Table 1.1 Elemental mercury and major mercury ions/species in environmental and biological samples (adapted from Kuban et al. (2007)).

			CAS number
Elemental mercury		Hg^0	92786-62-4
Inorganic mercury ions	Mercurous ion	Hg_2^{2+}	n/a
	Mercuric ion	Hg^{2+}	7439-97-6
Organic mercury ions/species	Methylmercury	CH_3Hg^+	22967-92-6
	Dimethylmercury	$(CH_3)_2Hg$	593-74-8
	Ethylmercury	$CH_3CH_2Hg^+$	627-44-1
	Phenylmercury	$C_6H_5Hg^+$	23172-37-4

n/a: not available.

The toxicity of mercury is high even at low concentrations and is also higher than that of arsenic and lead. In accordance with Regulation (EC) 1272/2008 on the classification and labelling of dangerous substances, mercury and its compounds are classified as toxic and dangerous to the environment [5]. Moreover the Water Framework Directive WFD D. Lgs 172/2015 regulates the Hg levels allowed for example in sediments and seas.

The tolerable threshold values for mercury have been progressively lowered as scientific research progresses; currently the maximum tolerable dose is set by the European Food Safety

Authority (EFSA) as 4 μg kg^{-1} body weight, of which not more than 1.6 μg kg^{-1} body weight of methylmercury [6]. The toxicological properties of mercury depend on its chemical and physical form.

Elemental mercury is highly volatile and is absorbed through the respiratory tract by inhalation, while it is hardly absorbed through the skin. It can cause pulmonary edema, pneumonia, and permanent damage to the bronchi. It has affinity for lipid substances, it can cross the blood-brain barrier, and cause damage to the brain and central nervous system. Mercurial erethism is a symptom of mercury inhalation syndrome, characterized by excessive shyness and social phobia.

Both acute and chronic intoxication (mercurialism) lead to permanent damage and the death of the target organism. Inorganic mercury salts, Hg^{+} and Hg^{2+}, are absorbed by the body through the skin and oral cavity, primarily causing damage to the digestive system and kidneys. However, they exhibit lower toxicity if they are absorbed in fractions not exceeding 10%. The most widespread form in the environment and in many respects more dangerous is methylmercury, whose affinity to lipid matrices and to thiol groups allows it to bind to enzymes, proteins, causing inactivation and blocking of enzymatic and hormonal functions and interference in ion channels [7]. In addition to the liver and kidneys the most affected apparatus is the Central Nervous System (CNS): the symptoms expressed are generally tremor, memory problems, severe depression, hallucinations and delirium, sialorrhea and gingivitis up to serious neurodegenerative diseases such as Parkinson's and Alzheimer's disease [8].

The most tragic event caused by environmental pollution by mercury occurred in Minamata Bay in Japan in the 1950s. An industry producing plastics and chemical fertilizers, the "Chisso Corporation", poured its methylmercury-contaminated wastewater into Minamata Bay, permanently polluting the seabed and ecosystems of the bay sea (called Shiranui) rich in fish species and shellfish farms, a source of livelihood for most of the inhabitants of this area. These species were the main targets of methylmercury originally dispersed in coastal waters and then absorbed in plankton; due to the phenomenon of biomagnification the toxic substance reached the human population of the region causing all the symptoms listed above. The first effects were observed in domestic animals; the felines in the specific were seized by convulsions and literally "went mad": for this the syndrome initially took the name of "dancing cat disease". The disease in humans had equally devastating effects causing permanent criticalities and death in hundreds of individuals over the years, particularly in children. The tragic effects had their peak in the 60s and in many respects they still last, also because of the teratogenicity of the pollutant.

1.1.5 Pollution sources and biogeochemical cycle of mercury

The release of mercury into the biosphere occurs through both natural and anthropogenic sources [9]. In nature, mercury primarily derives from the erosion of rocks and minerals by atmospheric agents, volcanic eruptions, and the volatilization of Hg^{0} from marine and terrestrial surfaces. Anthropogenic emissions are attributed to losses related to the use of mercury in paint and pesticide industries, battery production, paper processing, the use of fossil fuels as an energy source, and waste combustion.

Overall, mercury is a stable metal; Hg^{0} vapors have a residence time of about one year in the atmosphere and are considered persistent, thus showing a uniform distribution in this environmental compartment. Hg in the gaseous phase has high mobility and can therefore be

transported over long distances, while the particulate-bound fraction is less mobile but equally dangerous to health. In the atmosphere, the processes of oxidation from Hg^0 to Hg^{2+} are slow, and the return of mercury to the ground occurs through precipitation. In surface waters, the reduction of Hg^{2+} to Hg^0 is significant through microbial or photo-reduction (direct or catalyzed) processes [10].

In anaerobic environments, mercuric ions form stable bonds with thiol groups and sulfide ions, producing low-solubility salts that tend to sediment. The methylation reaction of Hg^{2+} occurs in sediments, involving the transfer of a methyl group from an organic compound to the metal. This reaction takes place in the presence of catalysis through microbial activity or solar radiation [9].

Methylmercury is stable in natural waters because the hydrolysis of the C-Hg bond is slow. This stability is the basis for the high toxicity of methylmercury and its tendency to bioaccumulate. Mercuric organometals, especially CH_3Hg^+ and $(CH_3)_2Hg$ (the most mobile species), undergo biomagnification along the food chain, starting from bacteria and plankton up to macroorganisms like herbivorous and piscivorous fish (see Figure 1.1.). The half-life of methylmercury in fish is high (approximately 72 days), so its concentration increases significantly at each step of the food chain. This is why it can reach very high levels (even a million times higher) in predatory fish such as tuna, mackerel, and swordfish [11].

The widespread consumption of fish products makes fish and other aquatic species the most significant sources of methylmercury for humans. Therefore, it is necessary to monitor the concentration of mercury and methylmercury in environmental compartments and biota using sensitive analytical techniques applicable to various matrices.

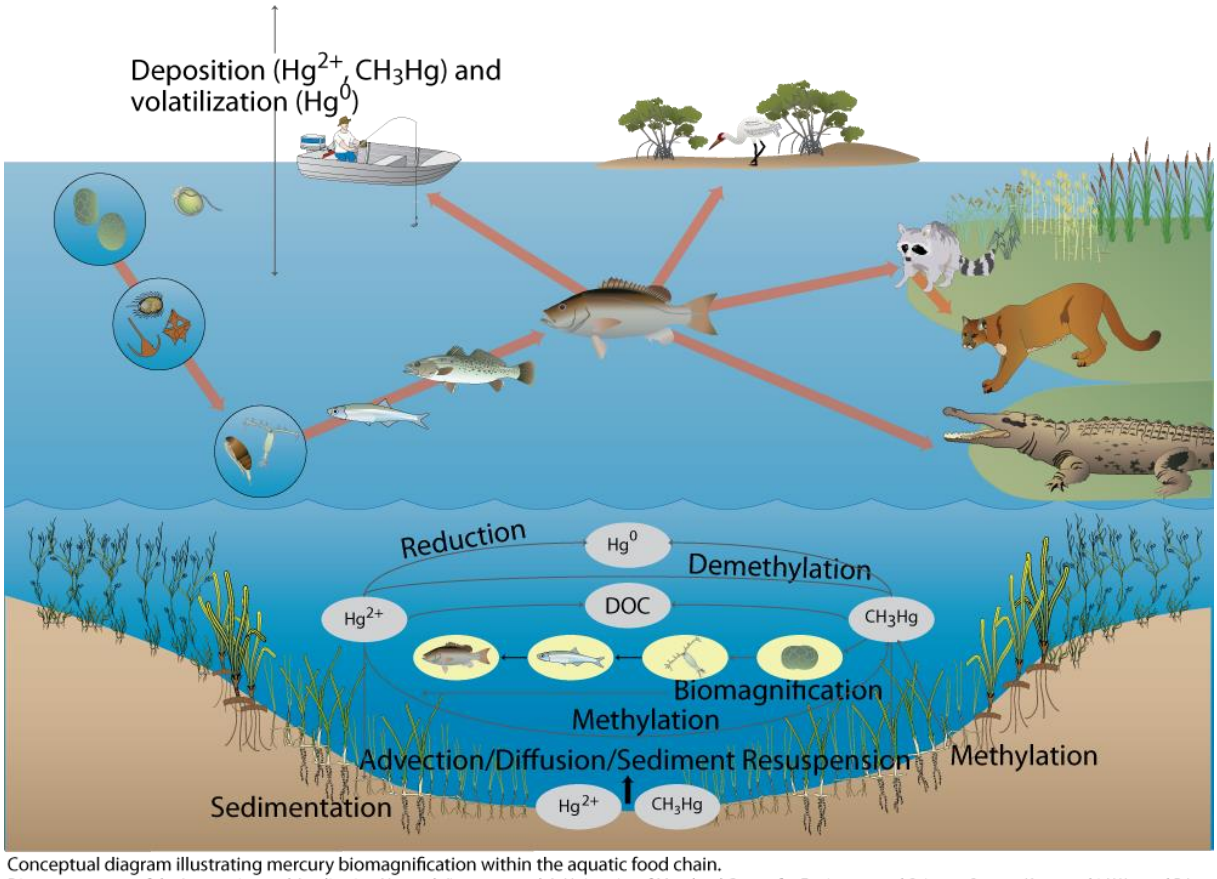

Conceptual diagram illustrating mercury biomagnification within the aquatic food chain.
Diagram courtesy of the Integration and Application Network (ian.umces.edu), University of Maryland Center for Environmental Science. Source: Kruczynski, W.L., and P.J. Fletcher (eds.). 2012. Tropical Connections: South Florida's marine environment. IAN Press, University of Maryland Center for Environmental Science, Cambridge, Maryland. 492 pp.

Figure 1.1 – Mercury biomagnification

The pollution of natural waters with mercury is reflected in the living organisms that inhabit this environmental compartment. As pointed out above, fish is therefore contaminated by the metal, especially by its organic compounds, such as CH_3Hg^+ and $(CH_3)_2Hg$, which are stable in water; mercury contamination begins in the plankton, and through the biomagnification phenomenon, it amplifies along the food chain, reaching higher organisms. The highest concentration of mercury is observed in predatory fish such as mackerel, tuna, swordfish, and even in some freshwater species like pike or carp.

The transfer of methylmercury to humans occurs through the diet, and the human population's consumption of fish products is enormous, with tuna being the most consumed fish by far. Tunas (*Tuna's species*) are migratory predators that occupy high positions in the food chain in marine ecosystems and are important fishing resources for many nations. Because they are large and long-lived predators, tunas accumulate more mercury in their tissues than smaller fish. Furthermore, due to their migratory movements during their life cycle, the presence of Hg contamination can be considered a global indicator of sea pollution [10].

The content of Hg is influenced by the fishing location and the age of the caught animal. White tuna (*Thunnus alalunga*), which reaches adulthood in five years, contains about four times more mercury than skipjack tuna (*Katsuwonus pelamis*), which is caught at a younger age. The same applies to bluefin tuna (*Thunnus thynnus*), one of the largest predators in the Mediterranean. For food safety reasons, the contamination of local and imported tuna products is a concern for many nations, and

their widespread consumption requires careful monitoring of the food placed on the market. Legal limits for higher fish are applied to the "muscle," the part of the animal where the pollutant is mostly accumulated. The European Community has established through Regulation (EC) No. 420/2011 the concentration limits for mercury, which are 0.5 mg kg^{-1} for fish products and fish muscle and 1 mg kg^{-1} for predatory fish [12].

1.1.6 Analytical methods for the determination of mercury

Given all these premises, analytical techniques suitable for the measurement of traces and ultra-traces of mercury in environmental matrices are necessary.

In natural waters, mercury is present in traces, and the legal limit for drinking water is set at 1 $\mu g\ L^{-1}$ (D.M. 29/12/2003 (Ministerial Decree), 2003). Sampling and storage are conducted using Teflon material (not glass, as the latter can cause adsorption/release of metals) and under acidic conditions. Any potential interferents that may degrade CH_3Hg^+ need to be eliminated.

Sediment collection is carried out using a bucket sampling system, box corer, or coring devices. Samples should be analysed immediately or lyophilized and frozen.

Biological samples are challenging to preserve due to their susceptibility to deterioration and bacterial contamination, and because the behaviour of different mercury species over time is not fully understood. Generally, lyophilization, freezing, and sterilization processes are applied [3]. However, repeated temperature fluctuations are always avoided.

Mercury in the atmosphere exists either in a free state or bound to particulate matter. Sampling is carried out using traps and quartz tubes coated with adsorbents for gases or specialized equipment for particulate sampling (pumps, impactors, filters, etc.). Subsequent steps involve pyrolysis or dissolution of filters or thermal desorption from the adsorbed phase.

Most analytical techniques involve dissolving the matrix to allow for the analysis of the target analyte in liquid or gaseous phase. Additionally, the complexity of biological matrices often makes analysis challenging, necessitating pretreatments before instrumental analysis.

For the determination of total mercury in complex biological matrices such as fish, acid digestion is employed to dissolve the organic matter and release the mercury content in the sample, achieving a quantitative recovery of the analyte [13]. Dissolution is carried out using a microwave oven with reagents such as aqua regia, HNO_3, H_3BO_3, H_2SO_4, H_2O_2, HF, combined in various mixtures depending on the pre-treatment requirements [14]. The rather harsh dissolution conditions in terms of acidity and oxidizing strength do not allow for the speciation of organic mercury.

Techniques for sample treatment compatible with the speciation of organic mercury alternatively involve:

- Acid digestion of the sample and solvent extraction [15]
- Alkaline digestion of the sample and solvent extraction [16]
- Acid volatilization and preconcentration [17]

Most analytical techniques for mercury are based on spectroscopy and exploit the absorption or emission of electromagnetic radiations by the analyte under certain conditions.

- *Cold Vapor Atomic Absorption Spectrometry* (CV-AAS): this is the reference spectroscopic technique for mercury determination. Mercury in solution is reduced to Hg^0 by a reducing agent,

such as stannous chloride ($SnCl_2$) or sodium borohydride ($NaBH_4$). The vapor of Hg^0 is quantified by the absorption of radiation emitted by a mercury discharge lamp (λ = 253.7 nm). The radiation is absorbed proportionally to the concentration of the analyte in the sample. The technique is highly sensitive, with a detection limit < 10 ng L^{-1}, providing rapid analyses while mitigating interferences, since mercury is separated from the matrix through volatilization.

- *Cold Vapor Atomic Fluorescence Spectrometry* (CV-AFS): this technique differs from CV-AAS in the principle of analyte determination. Vapours are irradiated with UV radiation at 253.7 nm, and mercury atoms absorb the radiation, reaching an excited state configuration. The power of the atomic fluorescence radiation, emitted as atoms relax back to the ground state, is measured. CV-AFS is a very sensitive and selective technique (detection limit of 0.05 ng L^{-1}) but is less commonly used compared to CV-AAS.

- *Direct Mercury Analyzer* (DMA): is a selective analyser that allows mercury determination without preliminary steps. The sample (solid or liquid) undergoes disintegration through combustion with oxygen in a furnace in the presence of a catalyst. Mercury vapours are trapped and concentrated on a gold trap, followed by thermal desorption and analysis by absorption of radiation produced by a mercury discharge lamp (λ = 253.7). Oxygen serves as the carrier gas and acts as a combustion agent in the matrix combustion reaction. The direct analysis of the sample without the need for a separate pretreatment step (since sample mineralization takes place in the analytical device), the possibility of fast and sequential analyses, and low quantification limits make this technique one of the most widely used for mercury determination in various matrices. The LOD for the DMA is 0.1 μg L^{-1}.

- *Inductively Coupled Plasma Optical Emission Spectrometry* (ICP-OES): this is the most commonly used instrumental technique for the simultaneous determination of multiple metals. The sample is vaporized and atomized by heating with inductively coupled argon plasma reaching average temperatures of 9000-10000 K. The measured signal consists of the radiative emission of excited atoms in the ICP torch: the power of the emitted electromagnetic radiation is proportional to the concentration of the element under examination. ICP-OES has higher detection limits for mercury compared to the previously mentioned techniques (18 μg L^{-1}).

- *Inductively Coupled Plasma Mass Spectrometry* (ICP-MS): in this instrumental technique, sample components are atomized and partially ionized through an ICP torch. The actual ionization occurs through an ionizing gas and is discriminated in the mass spectrometer based on the m/z ratio. The quadrupole is the most used mass analyzer, but there can be various variants. ICP-MS allows for lower detection limits (0.5 μg L^{-1})compared to ICP-OES but entails higher operational costs.

These techniques are considered "traditional" in the field of metal determination and are found in many laboratories.

Less common techniques for metal determination include gas chromatography (GC) and high-performance liquid chromatography (HPLC) coupled to ICP-OES or ICP-MS, X-ray Fluorescence Spectroscopy (XRF), and Neutron Activation Analysis (NAA) [18]. Chromatographic techniques are particularly used in studies of speciation of organometallic compounds, with GC often involving

sample derivatization for thermal stability and non-polarity. XRF relies on the measurement of X-Rays emitted by mercury atoms (irradiated with a beam of primary X-Rays) and is widely used for the analysis and mapping of solid samples. NAA is a non-destructive method requiring minimal sample manipulation, suitable for speciation studies, but its instrumentation comes with high costs due to the need for a neutron source.

Electrochemical techniques for metal analysis, particularly mercury, have seen a significant increase since the 1990s. The ability to perform rapid, low-cost analyses with very high sensitivity has led to the consideration of Anodic Stripping Voltammetry (ASV) as a potential future reference technique for the analysis of this element.

The analytical principle is based on the ability to preconcentrate Hg (II) by electrochemical reduction on the electrode surface, followed by subsequent reoxidation upon the application of a potential scan towards more positive values. The result of the analysis is a voltammogram from which the current intensity is obtained, and it is proportional to the concentration of the analyte.

Voltammetric techniques, to be explored in detail in chapter 2, enable the conduct of analyses with very low detection limits, at affordable costs, and with the possibility of field use.

1.2. Iron speciation for the early diagnosis of neurodegenerative diseases

1.2.1 Iron

Iron is the most abundant metal on Earth, constituting 34.6% of the mass and 5% of the crust. It is believed that the Earth's core is primarily characterized by an alloy of iron and nickel, the same composition found in about 5% of meteorites. Although rare, meteorites are the main source of naturally occurring metallic iron. In its pure state, iron is seldom used except in certain chemical analyses and in the production of magnetic cores. Instead, iron alloys are of great importance, particularly those with carbon (iron-carbon alloys), which produce cast iron and steel that are fundamental in the steel industry and in the preparation of plenty of manufacts.

1.2.2 The role in human biology

The adult human body contains between 3.5 to 5 grams of iron. The daily requirement varies depending on individual characteristics and is 5 mg for adults and 15 mg for children. During pregnancy, the need for iron increases, becoming two to five times higher, as it must meet not only the increased demands of the mother, but also those of the fetus.

Iron obtained from the diet can be divided into heme iron, present in the heme group, and non-heme iron. The former is provided by meat and is absorbed more rapidly than the latter, which primarily comes from vegetables and cereals. Non-heme iron is ingested as ferric ions, which are insoluble at physiological pH and must be reduced to ferrous ions, which are water-soluble and can be absorbed in the duodenum.

This reduction is carried out by duodenal cytochrome B (DcytB) located on the apical surface of enterocytes, epithelial cells present in the inner surface of the small and large intestines, whose major role is the uptake of nutrients. The reduced iron is then transported by Divalent Metal Transporter-1 (DMT1), a protein which brings Fe(II) into intestinal cells, while ferroportin (Fpn) mediates its exit through the epithelial barrier. On the serosal side, ceruloplasmin ferroxidases oxidize Fe(II) to Fe(III), promoting its binding to transferrin (Tf) [19]. In tissues, it is stored in the oxidized form in ferritin and hemosiderin.

In the plasma, after binding to transferrin as Fe(III), approximately 80 % of iron is released into the bone marrow, where it is used for hemoglobin synthesis. The remaining 20 % is utilized for the synthesis of myoglobin, heme enzymes such as cytochromes, catalases, peroxidases, and non-heme enzymes such as NADH dehydrogenase, xanthine oxidase, succinic dehydrogenase. All conjugated proteins containing iron in the prosthetic group are known as iron proteins, and they play crucial roles in biological functions, including oxygen transport and catalysis of numerous biological redox reactions.

Entering into the composition of hemoglobin (Hb), it consists of a protein portion (globin) and a prosthetic group (heme), which, in turn, is formed by a molecule of protoporphyrin that coordinates Fe(II). This coordination allows oxygen to bind reversibly, facilitating its transport and delivery to tissues.

Finally, it is important to note that forms of excess metal excretion are not known. This explains why continuous administrations or repeated transfusions can lead to accumulations in tissues, giving rise to adverse effects, such as nausea, vomiting, diarrhea and, at high concentrations, even serious damages to liver, pancreas and brain.

1.2.3 The cerebral homeostasis

The brain is among the metabolically most active organs, consuming 20% of the body's energy; therefore, an adequate supply of iron is necessary to support its energy needs. Our understanding of the role of iron in normal brain function has greatly improved in the last decade, with significant attention focused on deciphering the cellular and molecular signals that guide iron transport and metabolism. These studies have outlined the essential role of iron as a cofactor in various physiological processes, including oxidative metabolism, myelination, and neurotransmitter biosynthesis.

Iron levels are tightly regulated to ensure the normal function of the central nervous system. It is crucial to note that iron absorption is strictly controlled to respond to the body's needs, being enhanced in deficiency but reduced in overload conditions; such control mechanisms are important also because of the lack of metal excretion processes, as outlined above. Once in circulation, the entry from the blood is controlled by the Blood-Brain Barrier (BBB), which is formed by Brain Microvascular Endothelial Cells (BMVEC), pericytes, and astrocytes. Iron bound to transferrin circulating outside the CNS cannot directly cross the BBB and must enter the brain through BMVEC in a multi-step process. Transferrin binding to TfR receptors facilitates iron absorption through receptor-mediated endocytosis. The subsequent fate of the Tf-TfR complex within brain endothelial cells is not entirely clear, and the mechanism of iron release into the brain is highly controversial.

The iron in the cytoplasm of BMVEC, following receptor-mediated endocytosis of Tf, appears as Fe(III). After detaching from Tf, in the acidic endosomal environment, it is reduced to Fe(II) and exits the endosome through DMT1. At this point, the metal may be utilized for metabolic purposes by endothelial cells, stored in their ferritin (Ftn), or released into the brain via ferroportin.

Another source of iron is ferritin, which plays a crucial role in iron homeostasis. In fact, the genetic loss of ferritin function leads to the failure of iron homeostasis. The brain can acquire exogenous ferritin through transcellular transport across the blood-brain barrier (BBB), or this protein can be produced by endothelial cells and be released on demand. Other endogenous sources of brain ferritin are possible, including its synthesis by microglia [19].

1.2.4 The functions performed in the CNS

Iron plays an indispensable role in ATP production, acting as a cofactor for cytochromes and iron-sulphur complexes in the oxidative phosphorylation chain. The primary substrate for brain energy production is glucose, which undergoes complete oxidation, as well as ketone bodies that can meet energy needs under certain conditions. The brain consumes nearly 20 % of the body's energy, although it represents only about 2 % of its weight. Approximately 80 % of the energy supports neuronal activity, while the residual part is used to maintain the "clean-up" functions of astrocytes, oligodendrocytes, and microglia; furthermore, the energy demand for neuronal activity is mainly required at the figure post-synaptic level.

Therefore, iron support becomes essential in oxidative phosphorylation, which provides energy in the form of ATP at the mitochondrial level. Figure 1.2 illustrates the mitochondrial electron transport chain, which features multiple iron-sulphur clusters and heme-containing proteins essential for ATP synthesis. NADH dehydrogenase (Complex I) contains eight Fe–S clusters, succinate dehydrogenase (Complex II) has three Fe–S clusters and a heme portion, while Complex III (cytochrome bc1) contains an Fe–S cluster and several heme groups vital for its function. Complex IV (cytochrome c oxidase) also includes two heme fractions. Aconitase, a key enzyme catalyzing the stereospecific isomerization of citrate to isocitrate via cis-aconitate in the tricarboxylic acid (TCA) cycle, contains a single Fe–S cluster.

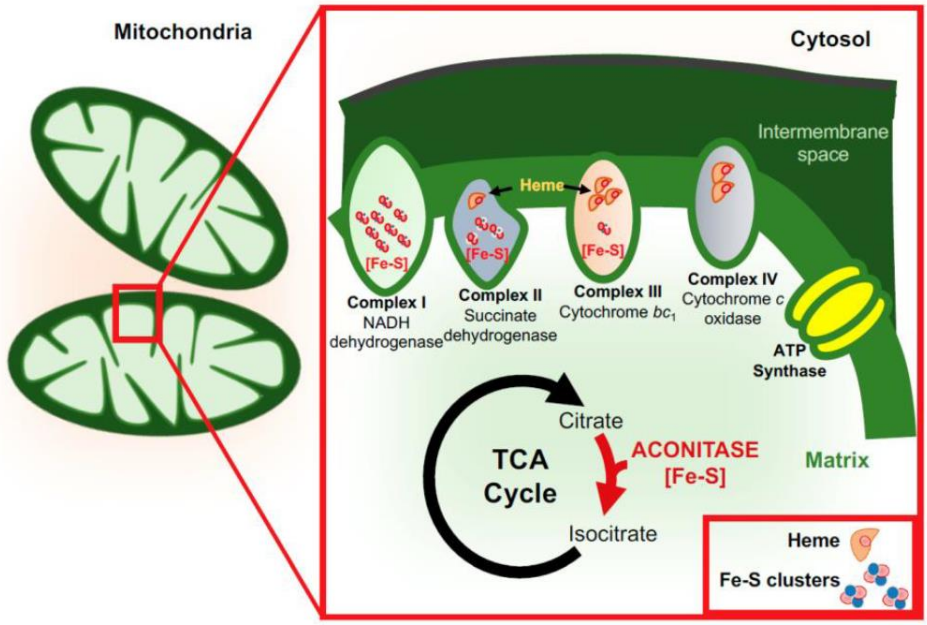

Figure 1.2 - Iron and mitochondrial function. (Nnah et al, 2018)

Oligodendrocytes, responsible for myelin production, also require high amounts of ATP. Not only do many of the enzymes involved in ATP production require an iron supply, but also the processes of cholesterol and fatty acid synthesis, necessary for myelination, are dependent on this element. Some of the enzymes involved in this pathway include NADH dehydrogenase, HMG-CoA reductase, succinate dehydrogenase, dioxygenases, and glucose-6-phosphate dehydrogenase.

Finally, neurotransmitters serve as a means of communication between neurons, and this process includes biosynthesis, transport, storage in vesicles for preservation, controlled release, and binding

to receptors on post-synaptic neurons with the induction of cellular responses. The role of iron in each of these processes has been extensively described in the scientific literature, especially in the case of monoaminergic neurotransmitters such as dopamine and serotonin, which are involved in the regulation of cognitive processes.

1.2.5 The interaction with microglia

Microglia are resident cells of the brain that regulate brain development, maintenance of neuronal networks, and injury repair. Microglia serve as brain macrophages: they are responsible for the elimination of microbes, dead cells, redundant synapses, protein aggregates, and other particulate and soluble antigens that may endanger the CNS. Furthermore, as the primary source of proinflammatory cytokines, microglia are pivotal mediators of neuroinflammation and can induce or modulate a broad spectrum of cellular responses. Alterations in microglia functionality are implicated in brain development and aging, as well as in neurodegeneration.

Microglial activation in response to pro- and anti-inflammatory stimuli is often characterized as classical M1 or alternative M2 activation. M1 activation is pro-inflammatory and neurotoxic, primarily induced through toll-like receptor (TLR) signalling and interferon-gamma (IFN-γ) activation. M1 microglia synthesize and release pro-inflammatory cytokines and chemokines such as tumor necrosis factor-alpha (TNF-α), interleukins including IL-6, IL-1β, IL-12, and CC Motif Chemokine Ligand 2 (CCL2). In this reactive state, microglia also express inducible nitric oxide synthase (iNOS), converting arginine to nitric oxide. The accumulation of nitric oxide enhances the toxic effects of glutamate, thereby potentiating N-methyl-D-aspartate (NMDA) receptor-mediated neurotoxicity.

In the M2 state, microglia release anti-inflammatory cytokines such as interleukin-10 (IL-10) and transform growth factor-beta (TGF-β). M2 microglia also induce arginase 1 to promote the conversion of arginine into polyamines. These cells can also release insulin-like growth factor I (IGF-I), fibroblast growth factor (FGF), and neurotrophic factors including nerve growth factor (NGF) and brain-derived neurotrophic factor (BDNF) to resolve inflammation and promote synaptic plasticity. Microglia can, therefore, express both neurotoxic and neuroprotective factors in disease conditions. An important characteristic of neuroinflammation is the activation leading to increased extracellular iron acquisition and subsequent negative regulation of proteins interacting with this metal, causing intracellular sequestration. This phenomenon may play a similar role in the brain to reduce metal availability; however, intracellular accumulation is associated with neuronal degeneration underlying most neurological disorders. In turn, these pro-inflammatory mediators have been shown to strongly influence iron transport and metabolism in microglia.

Microglial cells interact with both transferrin-bound and non-transferrin-bound iron. For the absorption of non-transferrin-bound iron by DMT1, an endogenous cell surface ferrireductase catalyzes the reduction of Fe(III) to Fe(II) in a pH-dependent manner. Transferrin-bound iron is taken up through endocytosis of the Tf-TfR complex; after release in the acidic endosomal environment, iron is translocated into the cytosol by DMT1 or other transporters. More recently, researchers have demonstrated that microglial iron transport pathways are differentially active in response to pro- and anti-inflammatory stimuli at both transcriptional and protein levels. Pro-inflammatory mediators increase the absorption of non-transferrin-bound iron and enhance the ferritin storage pool. The uptake of non-transferrin-bound iron by microglia limits free extracellular

iron and reduces reactive oxygen species (ROS), potentially harmful in the neural environment. In this pro-inflammatory M1 state, microglia also exhibit increased glycolysis, with extracellular acidification supporting changes in the microenvironment, favouring the absorption of non-transferrin-bound iron by the pH-dependent transporter DMT1. Inflammatory mediators reduce oxidative respiration, induce heme oxygenase-1, and decrease intracellular heme levels. These changes are associated with an increase in intracellular "labile iron," suggesting that microglia can sequester both intracellular iron released from heme catabolism and extracellular iron absorbed by DMT1. In contrast, IL-4 increases TfR expression to promote the absorption of transferrin-bound iron. It is possible that this shift in iron transport is associated with the release of ferritin deposits by M2 microglia to support neuron regeneration and oligodendrocyte activity. Based on these data, a study proposed a model in which microglial cells actively modify transport pathways and metabolism in response to the iron status of their environment.

Figure 1.3, on the left side, highlights how pro-inflammatory stimuli increase the expression of DMT1 and the absorption of non-transferrin-bound iron. These effects are associated with an increase in labile iron and an increased ferritin pool. On the right side of the figure, anti-inflammatory stimuli responsible for an increase in transferrin receptor (TfR) levels are shown to enhance the absorption of transferrin-bound iron through receptor-mediated endocytosis. In endosome recycling, low pH promotes the release of Fe^{3+} for iron reduction. Fe^{2+} can be released into the cytosol through DMT1 or another channel, then utilized in mitochondria to promote heme production. Finally, the hypothesis is presented that, in anti-inflammatory conditions, microglia may release ferritin-bound iron through lysosomal exocytosis to support oligodendrocyte function and neuronal repair [19].

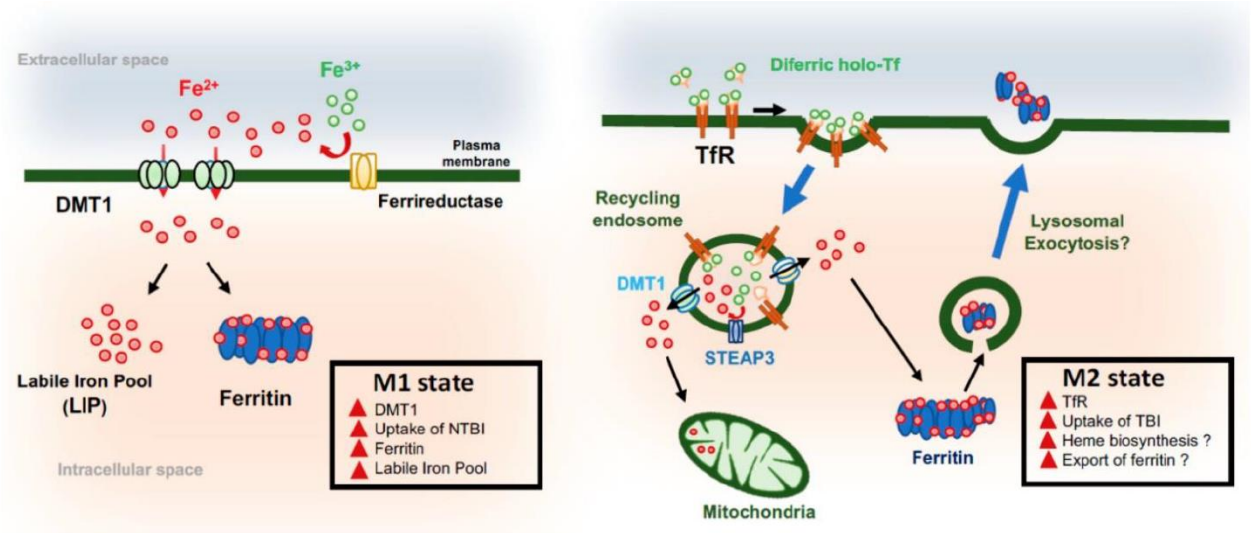

Figure 1.3 - Iron and microglia

1.2.6 The mechanisms of neurotoxicity

An important role in iron transport is played by DMT1, which is essential not only for its absorption but also for that of many divalent metals, including Mn. Since DMT1 expression levels are regulated by various factors such as body iron status, genetic polymorphism, and inflammation, they may also alter the transport and neurotoxicity of such metals. Iron deficiency, in turn, regulates DMT1 intestinal levels, increasing manganese absorption and neurotoxicity. This metal has a crucial

function in the central nervous system where it is essential for life but toxic when tolerable levels are exceeded. At the cellular level, iron is necessary for growth; however, excess iron causes oxidative stress and cell death. Iron levels are, therefore, tightly regulated by a process called iron homeostasis. The primary protective strategy to prevent overload in the brain is represented by the blood-brain barrier (BBB), which limits the quantity through highly regulated selective transport systems. Within the brain, multiple feedback circuits form an elaborate control system for cellular iron levels, ensuring a precisely balanced amount for the normal functioning of the central nervous system.

In the brain, absorption occurs through the BBB: iron is absorbed by the endothelial cell through TfR, in the form of transferrin-Fe^{3+}. Subsequently, it is transported into the brain compartment by the basolateral membrane of the endothelial cells and made available to neurons and glia.

Bound iron is considered non-toxic or minimally toxic, but free iron is more likely to exchange electrons with nearby molecules and produce free radicals. Normal metabolic processes in mitochondria form hydrogen peroxide as a result of molecular oxygen reduction. Hydrogen peroxide alone is not particularly toxic, but in the presence of free iron, it forms the $^{\cdot}OH$ radical when an electron is donated to H_2O_2 through the Fenton reaction.

$$Fe^{2+} + H_2O_2 \rightarrow Fe^{3+} + OH^{\cdot} + OH^{-}$$

$$Fe^{3+} + H_2O_2 \rightarrow Fe^{2+} + OOH^{\cdot} + H^{+}$$

This free radical can interact with oxygen and other molecules in the brain to form additional free radicals that initiate a deleterious positive feedback loop. Hydroxyl radicals can attack proteins, DNA, and lipid membranes to the extent of disrupting cellular integrity and function, ultimately leading to apoptosis.

A deficiency of iron can increase the absorption of other metals, such as lead, cadmium, aluminium, and manganese. Previous studies have indeed shown that iron deficiency increases blood levels of Mn in adults since the concentration of both Fe and Mn, as well as other essential metals, is regulated by transferrin and TfR, as well as DMT1. Iron deficiency increases transferrin and DMT1, and consequently Mn absorption, leading to an increase in Mn accumulation in the brain. Fe and Mn, in fact, compete for the same transport system for both TfR and DMT1, which are involved in the regulation of their cerebral influx. Similarly, other essential metals that share transporters can be altered: rats during lactation, for example, if exposed to low-iron or iron-integrated milk with Mn, increase Cu levels in the brain while lowering iron levels. The results of this study confirmed that there is a homeostatic relationship between different essential metals in the brain, not just between Fe and Mn. Indeed, Fe deficiency is a known risk factor for metal toxicity, resulting in increased absorption and accumulation of other divalent metals. In particular, deficient states of Fe are associated with increased Mn accumulation in a specific brain region; elevated Mn levels observed with Fe deficiency are more pronounced in the caudate putamen and globus pallidus. Another clinical study evaluated Mn levels in the brains of anaemic patients, and the results showed that deficiency is related to increased Mn deposition in the basal ganglia. Furthermore, dietary iron deficiency upregulated DMT1 expression in the intestine, leading to an increase in basal Mn levels in various tissues, including the brain, heart, kidney, testicle, femoral muscle, and tibia.

Despite the crucial roles of Fe in the brain, there is evidence supporting a strong link between high brain concentrations and induced neurotoxicity. In Alzheimer's disease, widespread accumulation occurs in various brain regions, such as the cortex and hippocampus, with higher amounts at senile plaque sites. Toxic effects from brain overload can also be caused by oxidative stress induced by iron itself, particularly dangerous because it can cause further release of Fe from

proteins containing it, such as ferritin, heme proteins, and sulphur-Fe clusters, thus aggravating the toxic effects of cerebral overload [20].

1.2.7 The role of Fe in the pathogenesis of Alzheimer's disease

In recent years, numerous studies have revealed that excess iron in the brain is a cause of certain neurodegenerative diseases. Iron ions in the brains of Alzheimer's disease (AD) patients can interact with H_2O_2 to produce highly reactive hydroxyl radicals. These hydroxyl radicals act on proteins, nucleic acids, and the cell membrane, which contains a large amount of unsaturated fatty acids, causing oxidative stress damage. Excessive iron, in particular, damages the mitochondrial respiratory chain, leading to the formation of free radicals and subsequent cell death. Accumulated iron can also alter the mitochondrial membrane potential, activate the caspase-3-dependent apoptotic pathway, leading to the onset of AD [41].

Various studies have provided evidence of iron accumulation in senile plaques in patients with Alzheimer's disease. Furthermore, brain imaging of subjects with early-stage AD has shown increased iron concentrations in β-amyloid plaques, responsible for both the development and progression of the disease. An increase in iron levels is believed to result in higher β-amyloid production through negative regulation of furin, a proprotein convertase involved in amyloid precursor protein (APP) processing, dependent on α-secretase, which, in turn, activates β-secretase implicated in β-amyloid generation. SH5SY cells exposed to ferric ammonium citrate confirm an increase in β-secretase levels, coupled with increased Aβ42 production; moreover, iron treatment promotes APP accumulation. Specifically, some studies show that ferrous iron induces a change in the structural conformation of β-amyloid towards a β-sheet structure that tends to form oligomers and fibrils, while other research groups demonstrate that ferric iron can promote the aggregation of Aβ40 and Aβ42 and cytotoxicity in vitro. Therefore, prolonged iron overload can lead to high levels of β-amyloid, a central constituent of extracellular plaques in individuals with AD.

Tauopathies, including Alzheimer's disease, as well as corticobasal degeneration and frontotemporal dementia, are characterized by neurofibrillary tangles, the core of which consists of helical filaments coupled to hyperphosphorylated tau protein. The functions of tau protein, which, under normal conditions, facilitates microtubule stabilization, regulation of axonal transport, neurotransmission, and iron metabolism, can be disrupted following self-phosphorylation of the protein itself. Iron appears to mediate this modification depending on its redox state: while Fe(II) gives rise to a reversible interaction through threonine residues, Fe(III) induces an irreversible conformational change; both phenomena promote tau protein aggregation. Tau hyperphosphorylation, a key step towards aggregation, can be induced by iron through the (CDK25)/P25 complex and GSK-3B. Fe(III) can also mediate nitration of this protein, thereby preventing microtubule stabilization. The accumulation of tau protein in tangles leads to the induction of heme oxygenase 1, an antioxidant that promotes the release of redox-active Fe(II) and, consequently, the release of free radicals to generate oxidative stress. This, in turn, causes hyperphosphorylation and aggregation of the protein in question.

Iron plays a crucial role in the brain: on the one hand, it maintains respiratory activity in the brain supporting myelination and the production of various neurotransmitters; on the other hand, it can be responsible for the loss of balance between oxidative damage and antioxidant defence in brain tissue. Oxidative stress is, in fact, a common pathological feature in the development and

pathogenesis of various neurodegenerative diseases, including Alzheimer's disease, to the extent of contributing to β-amyloid production and, consequently, to neurotoxicity.

In recent years, many studies have confirmed that all intracellular macromolecules, such as lipids, proteins, and nucleic acids, are more present in oxidized form in the brain tissue of AD patients. Regarding lipid peroxidation, it has been revealed that it involves three distinct mechanisms: free radical-mediated oxidation, non-enzymatic free radical-independent oxidation, and enzymatic oxidation. Lipid peroxidation has also been shown to induce disturbances in membrane organization and functional disorder of proteins and DNA. However, lipid peroxidation products also act as redox mediators. In the presence of metal ions such as iron and copper, hydrogen peroxide undergoes the Fenton reaction (see chapter 1.2.6), resulting in the formation of hydroxyl radicals and oxidative damage. On the other hand, oxidative stress and lipid peroxidation have been shown to induce Aβ accumulation during the progression of Alzheimer's disease. Iron homeostasis, moreover, is tightly regulated under normal physiological conditions, as excessive amounts of iron cause cellular susceptibility and, consequently, DNA and RNA damage through the ROS mechanism. Accumulation of DNA and RNA affected by oxidative damage has been observed in cortical and hippocampal neurons in the brains of subjects with AD in the early stages of pathology. Damage to nucleic acids that is not repaired is particularly deleterious to neurons, as it can trigger alterations in transcriptional regulation and chromosomal instability, as observed in AD.

Oxidative damage to DNA may be a fundamental aspect of neuronal degeneration in AD patients due to the crucial role of DNA in cellular function. Without effective repair capacity in the brains of Alzheimer's patients, mutations can lead to neuron death due to defects in oxidative phosphorylation. Furthermore, higher concentrations of oxidized pyrimidines and purines have been detected in lymphocytes and leukocytes of AD patients compared to healthy controls; recent findings indicate increased oxidative damage in leukocytes and brain tissue of subjects with mild cognitive impairment (MCI), highlighting how DNA oxidation may represent an early diagnostic element in the progression of AD, before cytopathological changes, contributing to the pathogenesis of the disease itself.

Mitochondria are essential for regulating iron balance throughout the cell; consequently, mitochondrial dysfunction has long been associated with various neurodegenerative diseases, including AD. Abnormal accumulation of iron in the brain tissue of AD patients is likely one of the main causes of neuronal death. In the early stages of AD, morphologically and functionally compromised mitochondria are identified, leading to a reduction in brain energy due to decreased ATP production. It has also been reported that mitochondria contain an active γ-secretase complex involved in processing APP to form Aβ, which, in turn, mediates toxicity associated with mitochondrial dysfunction and apoptosis. Mitochondria, therefore, function both as a source and a target of toxic ROS. However, it is debatable whether mitochondrial iron accumulation is to be considered the cause or a consequence of upstream events in AD.

Neuroinflammation plays a significant role in the pathogenesis of many neurodegenerative diseases to the extent that there is ample evidence suggesting that the pathogenesis of AD may be caused by inappropriate activation of the inflammatory response in the brain and a robust immune response, leading to cellular damage and death. In AD-related neuroinflammation, the deposition of β-amyloid alone may be sufficient to trigger an inflammatory reaction by binding to specific receptors, subsequently releasing inflammatory mediators that contribute to cognitive decline and disease progression. Assuming that β-amyloid deposition precedes cognitive deficits, it can be

hypothesized that exogenous or endogenous factors, including systemic inflammation, obesity, iron accumulation, and head trauma, may modify the innate immune response. Activation of microglia and astrocytes, stimulated by Aβ deposition, induces reactive gliosis and a pro-inflammatory signalling cascade. Alterations in the morphology and quantity of microglia and astrocytic cells have been observed in the brains of AD patients, and both are involved in iron homeostasis. In particular, microglial cells interact with both transferrin-bound and non-transferrin-bound iron. It is interesting to note that intracellular iron accumulation is associated with neuronal degeneration, underlying most neurological disorders, and microglial secretion of inflammatory cytokines such as TNF-α and IL-1β, enhances neuronal iron uptake. In turn, these pro-inflammatory mediators have been shown to strongly influence iron transport and metabolism in microglia. However, despite establishing the connection between inflammation and iron metabolism, the relationship between these two processes in neurodegenerative diseases is not fully understood.

Synaptic loss and neuronal death are among the main pathological hallmarks of Alzheimer's disease: synapses are formed at the junction between two neurons, allowing neuronal cells to transmit signals to another cell. Evidence suggests that dysfunction and loss of synaptic connections may be an early event underlying the progression of AD, more than other pathological changes. Damage to synapses from Aβ oligomers includes alterations in synaptic numbers, transmission, and synaptic plasticity. The molecular mechanisms leading to synaptic degeneration are not well-defined but are implicated in various pathways such as altered metal homeostasis, oxidative stress, mitochondrial dysfunction, and neuroinflammation. Some findings suggest that iron influences mitochondrial dynamics, with the potential to trigger synaptic and apoptotic loss. Therefore, the profound synapse degeneration in AD is characterized by worsening cognitive function, loss of synaptic transmission, and neuronal cell death. There is also great evidence on how oxidative damage to proteins and lipids caused by iron can give rise to synaptic dysfunction and neuronal cell death, both fundamental features of AD.

In recent years, neuroimaging studies have revealed micro and macrostructural anomalies in white matter in the risk and progression of AD. Analysis of post-mortem brain tissue from AD patients has highlighted a chemical alteration in white matter compared to non-demented individuals. Anomalies present in the white matter of AD patients primarily manifest in changes to myelin and oligodendrocytes, the cells responsible for the production and maintenance of myelin, which lose the ability to repair myelin damage. In the brain, iron is a key substance involved in the process of synthesizing myelin proteins and fatty acids in oligodendrocytes. The deposition of iron in the brains of AD patients, leading to increased oxidative stress, can cause a rise in cellular damage. It has also been reported that myelinating oligodendrocytes contain lower levels of antioxidants compared to other glial cells. Therefore, the high iron content and low quantity of antioxidants make oligodendrocytes among the most susceptible cells to oxidative stress in the central nervous system.

Ceruloplasmin is a metalloprotein with a molecular weight of 151,000 Daltons, containing eight copper atoms in its molecule [42]. It serves as the primary copper transport protein in the blood and plays a role in iron metabolism. It is, in fact, an enzyme with ferroxidase activity, capable of catalysing the reaction $4\ Fe(II) + 4\ H^+ + O_2 \rightleftarrows 4\ Fe(III) + 2\ H_2O$. The significance of this protein becomes apparent when macrophages, at the end of red blood cell phagocytosis and digestion, release iron, largely in the ferrous state. For this iron to be recovered by ferritin and transferrin, it needs to be oxidized to the ferric state. Regarding ceruloplasmin, some researchers have noted elevated levels in the blood of individuals with AD. Consequently, as an increase in the content of this protein might

be associated with neurodegenerative diseases such as Alzheimer's dementia, it is useful to perform specific tests aimed at measuring ceruloplasmin.

Iron has been extensively studied in various brain regions in patients with AD, and the results vary. Some researchers used ICP-MS to detect iron levels in the hippocampus in 12 AD patients (10 females, 2 males) and 12 control subjects (4 females, 8 males). From the obtained data, it was observed that iron levels in this region in AD patients are significantly increased compared to the control group. This result was also confirmed by another study that used the same method to detect cortical iron levels in 12 AD patients and 11 control subjects. Another study used ICP-OES to detect iron in 5 AD patients (2 females, 3 males) and 5 control subjects (2 females, 3 males): the levels in AD patients were significantly increased compared to the control group. Other researchers used ICP-MS to detect the iron content in the cerebellum and parietal cortex of 4 AD patients and 4 healthy individuals and found no significant differences between the two groups. Others, using AAS, discovered that the iron content in the hippocampus in AD patients is slightly increased compared to that in healthy controls, although the increase was not statistically significant. Regarding the use of instrumental neutron activation analysis (INAA) to detect the iron content in the whole brain of 5 AD patients and 5 control individuals, no significant difference was detected. On the contrary, in another analysis using the same method, it was highlighted that the iron content in multiple brain regions of AD patients is significantly increased. Autopsy results have shown that iron is unevenly involved in the pathological process of Alzheimer's disease [21].All the methods for iron speciation are reported in paragraph 1.2.8.

The authors of a review, comparing the results of multiple studies on iron content in the brain, concluded that, despite different results, this metal deposits in various brain regions of AD patients; the fact that it is found in areas dedicated to memory could justify the loss of this brain function. Therefore, according to the authors of the review, the increase in iron content in the brain could be one method for diagnosing AD. Finally, to study the pathological development of AD and search for biomarkers for early-stage identification, it has been learned that neuroimaging data do not directly measure AD-related pathology but suggest neurodegeneration; in particular, the non-invasive detectability of Aβ plaques in magnetic resonance imaging has so far been widely attributed to focal iron deposition accompanying plaques in the preclinical stages of Alzheimer's dementia development.

1.2.8 Analytical methods for iron speciation

Numerous analytical techniques have been developed to quantify concentrations of Fe species, including spectrophotometry [22], [23], atomic absorption spectrometry (AAS) [24], [25], inductively coupled plasma-mass spectrometry (ICP-MS) [26], chemiluminescence [27], and fluorescence [28], among others. However, the majority of these methods necessitate complex and expensive analytical equipment, thereby restricting their potential applications. Electrochemical methods have emerged as highly sensitive for Fe determination, offering advantages such as minimal equipment requirements, cost-effectiveness, low detection limits, rapid analysis speed, and straightforward automation [29]. Various complexing agents, such as 1-(2-pyridylazo)-2-naphthol (PAN) [30], 1-nitroso-2-naphthol (NN), and 2,3-dihydroxynaphthalene (DHN) [31], have been employed to accumulate Fe complexes onto electrode surfaces.

1.3. Monitoring environmental pollutants (UV Filters)

1.3.1 Contaminants of Emerging Concern

Due to demographic and economic growth, the rapid intensification of chemical production and use, the reduction of river flow due to climate change and the improved sensitivity of analytical techniques, the number of chemicals detected in the environment, and in particular in aquatic ecosystems, is increasing rapidly. [32]

These include the so-called emerging contaminants or contaminants of emerging concern (CECs). There are several definitions of emerging contaminants. The Norman Network (Network of references laboratories, research centres and related organisations for monitoring of emerging environmental substances), is a European network that deals with aspects of research and control of emerging contaminants in the environment and has identified what is believed to be the most complete definition: "Contaminants which are not currently included in routine monitoring programmes at European and/or national level and which may be eligible for future regulation on the basis of their ecotoxicity, potential health effects, public perception and based on monitoring data concerning their frequency in the various environmental compartments".

Emerging contaminants belong to several classes of substances including: i) pharmaceuticals and products for personal care, ii) industrial chemical products, iii) agricultural chemicals, iv) substances for the treatment of water, v) nanoparticles, vi) persistent toxic substances and vii) metabolites of drugs and hormones.

The quality of water resources has deteriorated over the years due to contamination as a result of urbanisation, rapid population growth, agricultural activities and industrial development. [33]

Traditionally, water quality surveys focus on nutrients, bacteria, heavy metals, and compounds with known health effects, such as pesticides and industrial chemicals. However, recent research has found the presence of hundreds of organic contaminants in wastewater having an impact on urban surface water. These new contaminants belong to several classes of compounds, as outlined above, and are detected in concentrations ranging between ng L^{-1} to μg L^{-1}, although concentrations reach, in some cases, 100 μg L^{-1}. [34]

CECs enter water from different sources. These substances can result from household discharges, hospital discharges, industrial activities and agricultural practices. In addition, these substances can also result from leakage of sewage lines, landfills and wastes disposed of inappropriately. Once consumed or used by the population and aggregated to the sewerage system, CECs flow to sewage treatment plants that are only partially effective in removing them. The removal rate of CECs in sewage treatment plants, on average around 60 %, depends on the type of treatment, the incoming loads, the chemical-physical properties of the substance and the resistance to degradation. In particular, non-polar compounds are mainly distributed in sewage sludge, while water-soluble polar compounds remain in the aqueous phase and can be found in sewage effluents. [35]

The effects of emerging contaminants on the environment and human health can be significant and complex. These contaminants can affect various aspects of ecosystems and human life.

Aquatic ecosystems: CECs can alter the biodiversity of aquatic systems, can pollute water resources, impair drinking water quality, and affect aquatic life, altering the endocrine system of fish and other aquatic species [36].

Terrestrial ecosystems: some emerging contaminants can affect plant growth and insect survival, with cascading consequences on the food chain and terrestrial biodiversity. In addition, some chemicals can end up in the soil, affecting its chemical and biological composition.

Human health: CECs with endocrine activity can interfere with the human hormonal system causing reproductive problems and may also contribute to metabolic disorders such as obesity, diabetes and other related diseases.

Emerging contaminants include disinfection by-products (DBPs), which are formed by the addition of chlorinated disinfectants to natural waters.

These substances are found in purified water, and almost all humans are exposed to these compounds. Among the DBPs, trihalomethanes (THMs) are present. THMs in drinking water can cause colorectal and bladder tumors [37]. Furthermore, these substances can cause reproductive problems. In fact, as reported by Luben et al. in 2007, DBPs in tap water negatively impact sperm concentration and morphology [38]. Microplastics (MP) are tiny plastic particles measuring less than 5 millimeters, originating from plastic bottles, abrasives, and fabrics, and are considered emerging contaminants. Human exposure to MPs occurs through ingestion, inhalation, and skin contact [39]. MPs can be found in human blood and, through the bloodstream, can be transported to organs, causing intestinal toxicity, metabolic disruption, reproductive toxicity, neurotoxicity, and immunotoxicity [40]. Additionally, exposure to MPs can accelerate the onset and development of Inflammatory Bowel Disease (IBD) [41]. Some emerging contaminants are considered endocrine disruptors. These molecules interfere with hormones in the human body and affect how the body responds to hormones. Among these substances are flame retardants and bisphenol-A (BPA).

Manufactured nanomaterials, such as amorphous silica dioxide (SiO_2), carbon nanotubes (CNTs), and titanium dioxide (TiO_2), are considered emerging contaminants. These materials have dimensions ranging from 1-100 nm and are widely used in sunscreens, agriculture, transportation, healthcare, and information technologies [42]. Nanomaterials have adsorbent capabilities and can adsorb toxic gases, heavy metals, and biologically active substances on their surface. Furthermore, these materials are resistant to chemical and biological degradation and can undergo complex conversion processes and chemical reactions in the environment, leading to the formation of new pollutants.

Aquatic ecosystems are threatened due to their susceptibility to act as reservoirs or conduits, accumulating and transporting numerous chemical contaminants released from industrial, agricultural, and municipal sources [43]. Emerging contaminants can have significant impacts on the aquatic ecosystem as they can influence the health of aquatic organisms, water quality, and the overall balance of the aquatic ecosystem. Pharmaceuticals and personal care products (PPCPs) encompass numerous classes of chemicals. Pharmaceuticals include antibiotics, antidepressants, analgesics, and anti-inflammatory drugs, while personal care products include creams, perfumes, shampoos, toothpastes, and detergents. These substances are released into the environment through wastewater treatment plants and leaching from landfills, entering the aquatic ecosystem in the form of parent compounds, metabolites, and transformation products. These substances are considered emerging contaminants as they can affect aquatic life due to being persistent, potentially toxic, and prone to bioaccumulation [44].

Among pharmaceuticals, antibiotics have been identified as one of the most important class of emerging contaminants due to their widespread use in human and veterinary medicine and their persistence in the environment. The presence of antibiotics in aquatic environments causes

microorganisms exposed to these substances to develop antimicrobial-resistant genes (ARGs), and these genes are passed on to other microorganisms. This process leads to the formation of antibiotic-resistant bacteria or microorganisms capable of infecting other aquatic microorganisms. The continuous bioaccumulation of ARGs in aquatic environments results in their presence at various trophic levels, and the chronic exposure of fish, plants, and other aquatic organisms to ARGs poses a potential risk to the health of people and animals that consume them [45].

In addition to PPCPs, microplastics can also have negative impacts on aquatic ecosystems. Due to their size, shape, and composition, microplastics can be mistaken for food by aquatic animals and are naturally internalized by filter-feeding organisms. In the article by Impellittieri et al. (2023), the effects of microplastics on the Mediterranean mussel *M. galloprovincialis* and the small-spotted catshark *Scyliorhinus canicula* are described. Microplastics caused effects on digestive enzymes in mussels, leading to alterations that can affect the energy acquisition from food, depleting their energy reserves. In the catshark, MP ingestion showed an increase in the expression of immune genes, indicating that microplastic pollution in the Mediterranean Sea represents an emerging threat to catsharks and the Mediterranean food web [46]. In 2016, Meador et al. conducted a study to assess the presence of CECs in effluents from two wastewater treatment plants, estuaries, and two fish species: juvenile Chinook salmon and staghorn sculpin. Eighty-one analytes were detected in effluents, 25 in estuarine waters, and 42 in fish tissues. Among the substances found in fish tissues were pharmaceuticals (hormones, antibiotics, CNS agents, metabolic regulators), personal care products (triclosan, triclocarban), and industrial chemicals. Some of these compounds were found in both water and fish adipose tissue at concentrations that could cause adverse effects in fish. Furthermore, 29 CECs were detected in effluents and fish tissues but not in estuarine waters, indicating a high potential for bioaccumulation of these compounds [47].

1.3.2 UV filters

Sunscreen filters are substances capable of protecting the skin and eyes from the harmful effects of solar radiation, especially UV rays emitted by the sun. In addition to cosmetic products, UV filters are used in fabrics, paints, plastics and coatings to protect materials from photodegradation Sunscreen filters can be classified into two types: i) chemical or organic filters: substances capable of absorbing the energy of UVA and UVB radiations; ii) physical or inorganic filters: these filters have screening properties and block UVA and UVB radiations through the processes of reflection and dispersion.

UV filters, in order to protect individuals from damage associated with solar radiation, must possess certain characteristics:

- have a broad absorption spectrum (280-400 nm);
- be photostable and chemically stable;
- have a good toxicological profile, meaning they should have very low acute and long-term toxicity, should not be photosensitive, and should not exhibit percutaneous absorption;
- dissipate the absorbed energy through photophysical and photochemical pathways that exclude the formation of singlet oxygen, other reactive oxygen species, or other harmful reactive intermediates [48].

The most commonly used physical or inorganic UV filters are titanium dioxide (TiO_2) and zinc oxide (ZnO). These materials are called physical UV filters because they protect the skin from solar radiation through physical phenomena such as dispersion and reflection of UV radiation [49].

The characteristic of inorganic filters is to screen UV light across the entire UV-A/UV-B range (290-400 nm) through processes of absorption, diffusion, and reflection that depend on the particle size of TiO_2 and ZnO.

A mineral sunscreen that reflects light well tends to make the skin appear whitish and is consequently less accepted by consumers for cosmetic use in comparison to chemical UV filters. For this reason, the particle sizes of TiO_2 and ZnO have been reduced to 25-50 nm, and iron oxide (Fe_2O_3) is added to some sunscreens to give a brown colour to the cosmetic product. Inhaling TiO_2 nanoparticles can lead to lung toxicity, inflammation of the respiratory tract, and can even be carcinogenic. Moreover, TiO_2 nanoparticles can act as photocatalysts, reacting with UV rays and accelerating photochemical reactions, causing the oxidation of some biological molecules and generating free radicals that can lead to various diseases such as atherosclerosis, Parkinson's disease, and premature aging.

Chemical or organic UV filters are molecules that have single or multiple aromatic structures, sometimes conjugated with C-C double bonds and/or carbonyl portions, capable of attenuating solar radiation reaching the Earth. In particular, these molecules absorb photons, become excited, and quickly relax to the ground state by emitting thermal energy through a series of vibrational transitions. Therefore, if UV filters are not degraded, they can absorb photons and repeat the process, thus protecting the skin from UV radiation [50].

Organic filters are classified as UV-A filters: benzophenones, anthranilates, dibenzoylmethanes; or UV-B filters: PABA derivatives, salicylates, cinnamates, camphor derivatives.

Organic UV filters are almost always used in combination, as no single agent, used at currently permitted levels, can ensure high sun protection and broad-spectrum absorption. However, the FDA has limited the choice of combinations of organic UV filters UV-A/UV-B due to their photoinstability and possible unfavourable synergistic interactions that can occur between different agents.

Chemical UV filters are photounstable because, after the molecule has absorbed UV radiation, it must dissipate or convert the absorbed energy. The mechanisms that can occur are three: i) radiative decay: emission; ii) non-radiative decay: heat; iii) photochemical: the excited molecule undergoes photochemical changes that can lead to its breakdown and the formation of photoproducts that may no longer provide protection and can cause allergies or photoallergies.

The lack of photostability of organic UV filters is a problem as organic absorbers lose their photoprotective characteristics and may even become phototoxic agents [48].

UV filters have been identified in water bodies worldwide. It is interesting to note that these substances have also been found in the Arctic, suggesting that water currents are dispersing the filters even in remote environments, with potential significant impacts on the environment.

The widespread use of sun filters in various products has led to their presence in various water matrices, including seas, lakes, rivers, wastewater, and sludge [51]. Organic UV filters enter the environment through various mechanisms. They are absorbed through the skin and excreted in urine, which enters the water system. However, only 4% of the applied dose is excreted in urine, and the remaining portion on the skin is washed away by natural waters (sea, lakes, pools) during recreational activities or is washed away under the shower, and water containing UV filters enters the water discharge system. Furthermore, the production and disposal of waste from factories introduce organic filters into the water discharges. In particular, organic filters are present in wastes from sunscreen and cosmetics production facilities.

The concentrations of these substances in water matrices have seasonal variations, with higher concentrations in summer. This suggests an impact of human behaviour on the concentration of UV filters in water, which is due to both recreational activities and the likely increase in production to meet the growing demand [52].

In Schneider et al.'s (2019) article, attention is drawn to Waste Water Treatment Plants (WWTPs). The latter ones are crucial in the water recycling process; in fact, water used by humans passes through these plants for treatment before returning to rivers and streams [52]. In Switzerland, oxybenzone or benzophenone-3 (BP3), octinoxate (EHMC, ethylhexyl methoxycinnamate), and octocrylene (OC) were found in WWTPs [53], while in Brazil, BP3, OC, and EHMC were found in both raw and treated water [54].

WWTPs face difficulties in treating organic filters due to the chemical properties of these molecules. In fact, UV filters have low water solubility, high lipophilicity, and a high organic carbon-water coefficient, making it challenging for WWTPs to remove them [52]. Moreover, given their high lipophilicity and poor biodegradability, UV filters can accumulate in sewage sludge, which is then either disposed of in landfills or used in agriculture, potentially causing groundwater pollution [55].

In addition to being present in natural waters, UV filters have been identified in chlorinated water, such as in swimming pools. In these environments, organic filters can react with chlorine and bromine to form rather hazardous chlorinated or brominated transformation products. In the 2017 study by Manasfi et al., the presence and fate of 5 UV filters — dioxybenzone, oxybenzone, avobenzone, 2-ethylhexyl-4-methoxycinnamate, and octocrylene — were investigated in pools containing chlorinated seawater. The study showed that only octocrylene remained stable, while the other 4 filters were reactive and generated brominated transformation products and disinfection byproducts. Brominated transformation products originated from the reaction between UV filters and bromine. It was noted that the 4 reactive filters reacted with bromine to form bromoform, an extremely toxic and carcinogenic compound [56]. Furthermore, oxybenzone can react with chlorine through a chlorination reaction, leading to the formation of chlorinated oxybenzone, a cytotoxic compound. The 2011 study by Sherwood et al. highlighted that chlorinated oxybenzone caused significantly greater cell death compared to non-chlorinated oxybenzone.

To prevent the continuous accumulation of UV filters in aquatic environments, efforts are being made to optimize the removal of organic filters (particularly BP3) from water. In 2017, Chen et al. conducted a study with *Cyperus alternifolius L*, a plant found in wetlands capable of absorbing BP3 from its roots, accumulating it in its tissues, and converting it into chemical conjugates with lower toxicity [57].

When a substance is not metabolized or excreted at the rate at which it is ingested, it can undergo bioaccumulation and biomagnification. Bioaccumulation is the process through which toxic substances accumulate within an organism in concentrations higher than those found in the surrounding environment; this accumulation can occur through respiration, ingestion, or simple contact. Biomagnification is the process by which the accumulation of toxic substances in living organisms increases in concentration as one moves up the trophic levels, i.e., proceeding from the lower to the higher levels in the food chain. Therefore, when an animal ingests lower trophic-level organisms, it accumulates a higher concentration of a chemical contaminant, and this could have a negative implication for humans. Organic UV filters are lipophilic and hydrophobic molecules capable of accumulating in the lipophilic tissues of marine organisms such as fish and mollusks, as highlighted by Gago-Ferrero et al. (2012) [58]. OC, BP3, and EHMC, the UV filters that are most

scrutinized for potential risks to the environment and the aquatic ecosystem, have a logP > 1. This indicates that these molecules can accumulate in organic sediments and lipophilic tissues, initiating the processes of bioaccumulation and biomagnification. OC is among the sunscreens most frequently found in the environment. OC concentrates in the lipophilic tissues of aquatic organisms such as mussels, oysters, and dolphins [59]. Furthermore, OC disrupts the brain and liver development in zebrafish [52].

A study by Downs et al. (2016) demonstrated how BP3 can cause damage to mammals and fish. Studies on mice and rats have shown that general exposure to BP3 reduced body weight, increased liver, and kidney weight by 50 %, induced a 30 % increase in prostate weight, and caused a reduction in immune competence. In mammals, BP3 is known to have estrogenic and anti-androgenic activities, activating estrogen receptor proteins, and inhibiting androgen receptors. In fish, the actions of BP3 are similar to those in mammals. Indeed, BP3 causes endocrine disruption by modulating estrogen receptor signalling pathways, inducing reproductive pathologies, and reducing reproductive fitness. Chronic exposure to BP3 in fish has resulted in a reduction in egg production, induction of vitellogenin in males, and a decrease in egg hatching. These results raise the possibility of 'gender changes' in fish exposed to BP3 throughout their entire life history [60]. A paper by Schneider et al. (2019) shows that organic UV filters have been found in fish and aquatic organisms in various parts of Europe. In Switzerland, whitefish and perch in lakes had low but detectable amounts of UV filters. In Norway, cod liver contained OC and BP3. OC was found in 80% of the analysed samples, while BP3 was detected in 50% of the analysed samples. In Spain, UV filters were identified in rainbow trout, chub, perch, and mussels [52].

Coral reefs are highly diverse and sensitive marine ecosystems that develop through the growth of corals, colonial organisms known as polyps, which produce calcium carbonate, building hard and resilient skeletons. Coral reefs are primarily found in tropical and subtropical waters, where temperatures are warm enough to support coral growth. These ecosystems are among the most diverse in the world and host a wide range of marine species, including fish, mollusks, crustaceans, and other forms of marine life. Coral reefs play important ecological roles, serving as refuges for numerous marine species by providing habitats for reproduction, feeding, and protection. Additionally, they play a crucial role in maintaining the balance of marine ecosystems by contributing to nutrient cycling and protecting coastlines from erosion.

In recent decades, coral reefs have experienced episodes of bleaching worldwide. The main causes of decline have been: i) human activities, such as overfishing and wastewater discharge; ii) climate change, including high temperatures, sea level rise, and ocean acidification; iii) biological pollution, associated with the presence of viruses, bacteria, and pathogens; iv) chemical pollution, due to the presence of metals and organic substances in water.

Even UV filters can have a negative impact on coral reefs. In particular, oxybenzone has been identified as a threat to coral reefs worldwide. It is estimated that up to 14,000 tons of sunscreens, some containing up to 10 % BP3, are released annually in coral reef areas, putting approximately 10 % of global coral reefs and up to 40 % of coastal reefs at risk of coral bleaching [52].

In a study by Downs et al. (2016), the toxicological effects of exposure to variable concentrations of BP3 on the larval form (planula) of the Scleractinia coral *Stylophora pistillata*, the most abundant coral species in the northern Gulf of Aqaba, Red Sea, were examined. The study was conducted on planulae as they are more sensitive to the toxicological effects of pollution than adult corals. Planulae under control conditions have an elongated, cucumber-like morphology and are in

constant motion, being propelled by cilia covering the entire body. After 4 hours of exposure to BP3, the planulae's morphology significantly changed, taking on the shape of a deformed dewdrop. After 8 hours of exposure, the epidermal layer of the planulae had lost its typical transparency and assumed an opaque white hue, indicating increasingly evident coral bleaching [60].

BP3 can also have phototoxic properties. As demonstrated by Vuckovic et al. (2022), in the presence of UV radiation (290-370 nm), this filter caused increased mortality in both the sea anemone Aiptasia and the mushroom coral *Discosoma sp*. due to the metabolism of BP3, being converted in vivo into phototoxic glucoside conjugates. Indeed, upon contact with coral, oxybenzone is absorbed by coral tissue. In corals, BP3 acts as a UV filter and absorbs harmful UV radiation. Microbes present in coral tissue break down BP3 into metabolic byproducts, such as oxybenzone-glucoside, which have phototoxic properties. This can lead to the production of reactive oxygen and reactive halogens that can cause the degradation of essential molecules for corals [61].

The study conducted by Stien et al. (2019) demonstrated that the *P. damicornis* species, which is the reef-building species, was significantly affected after 7 days of exposure to 50 $\mu g\ L^{-1}$ of OC, while the highest non-toxic concentration was 5 $\mu g\ L^{-1}$. However, corals, as well as other marine species including mussels, oysters, and mollusks, are subject to long-term exposure to high concentrations of OC due to continuous release of OC into the environment [59].

Danovaro et al. (2008) conducted a study to assess the potential impacts of sunscreen ingredients on hard corals and their symbiotic algae. The study was conducted on various coral species such as *Acropora* (one of the most common hard corals), *Stylophora pistillata*, and *Millepora complanata* in different areas of the world such as the Celebes Sea (Pacific Ocean), the Caribbean Sea (Atlantic Ocean), the Andaman Sea, and the Red Sea (Indian Ocean). It was observed that in all samples and at all sampling sites, the addition of sunscreen, even in small quantities (10 $\mu g\ L^{-1}$), resulted in the release of large amounts of coral mucus (composed of zooxanthellae and coral tissue) within 14 - 48 hours and complete coral bleaching within 96 hours. The bleaching rate was faster both when higher amounts of UV filters were used and when the system was subjected to higher temperatures.

Furthermore, in the same study, sunscreen containing a higher amount of UV filters than that found in most natural environments was tested. The coral response to sunscreen was not dose-dependent, as the same effects were observed at both high and low concentrations [62].

In addition to cosmetic products, UV filters, especially BP3, are used in fabrics, paints, and plastics to protect materials from photodegradation, as already reported above. The use of UV filters in plastics can lead to the migration of these substances to environmental matrices. In fact, as reported by De Miranda et al. (2021), the analysis of water from the rural region of the Antarctic Peninsula identified several organic UV filters in all samples. Although some of this pollution may be attributed to a small amount of wastewater runoff from scientific stations, the data obtained suggest that UV filters from more populated areas are traveling long distances. The full extent of UV filter migration remains unknown, but one possibility is that the migration of UV filters is facilitated by microplastics (MP), as many plastic products contain these substances.

Moreover, micropellets in low-density polyethylene (LDPE) absorb BP3 from the environment and subsequently release it when consumed by an organism [63]. This is possible because organic filters, including BP3, are molecules with pronounced hydrophobic characteristics, leading to a high affinity for plastic surfaces [64]. O'Donovan et al. (2020) studied the effects of BP3 adsorbed on MPs on the marine clam *Scrobicularia plana*. It was found that MPs containing BP3

caused oxidative stress in the digestive system, an effect not observed when the clam was exposed to microplastics alone. This supports the hypothesis that the toxic effects of MPs and UV filters may be synergistic [65].

Sunscreens are defined by Regulation (EC) 1223/2009 on cosmetics as substances intended exclusively or predominantly to protect the skin from certain UV radiations through absorption, reflection, or scattering of this radiation [66]. Physical and chemical filters in Europe are marketed as cosmetic products, while in the United States, they are considered Over The Counter (OTC) drugs and are regulated by the FDA. In Europe, the permitted UV filters in cosmetic products are listed in Annex VI of Regulation No. 1223/2009, shown in Figure 1.4.

ANNEX VI

LIST OF UV FILTERS ALLOWED IN COSMETIC PRODUCTS

Reference number	Substance identification				Conditions			Wording of conditions of use and warnings
	Chemical name/INN/XAN	Name of Common Ingredients Glossary	CAS number	EC number	Product type, body parts	Maximum concentration in ready for use preparation	Other	
a	b	c	d	e	f	g	h	i
1	4-Aminobenzoic acid	PABA	150-13-0	205-753-0		5 %		
2	N,N,N-Trimethyl-4-(2-oxoborn-3-ylidenemethyl) anilinium methyl sulfate	Camphor Benzalkonium Methosulfate	52793-97-2	258-19 -8		6 %		
3	Benzoic acid, 2-hydroxy-, 3,3,5-trimethylcyclohexyl ester/Homosalate	Homosalate	118-56-9	204-260-8		10 %		
4	2-Hydroxy-4-methoxybenzophenone/Oxybenzone	Benzophenone-3	131-57-7	205-031-5		10 %		Contains Benzophenone-3 (1)
5	Moved or deleted							
6	2-Phenylbenzimidazole-5-sulfonic acid and its potassium, sodium and triethanolamine salts/Ensulizole	Phenylbenzimidazole Sulfonic Acid	27503-81-7	248-502-0		8 %(as acid)		
7	3,3'-(1,4-Phenylenedimethylene) bis(7, 7-dimethyl-2-oxobicyclo-[2.2.1]hept-1-yl-methanesu fonic acid) and its salts/Ecamsule	Terephthalylidene Dicamphor Sulfonic Acid	92761-26-7, 90457-82-2	410-960-6		10 %(as acid)		
8	1-(4-tert-Butylphenyl)-3-(4-methoxyphenyl)propane-1,3-dione/Avobenzone	Butyl Methoxydibenzoylmethane	70356-09-1	274-581-6		5 %		
9	alpha-(2-Oxoborn-3-ylidene)-toluene-4-sulphonic acid and its salts	Benzylidene Camphor Sulfonic Acid	56039-58-8			6 % (as acid)		
10	2-Cyano-3,3-diphenyl acrylic acid, 2-ethylhexyl ester/Octocrilene	Octocrylene	6197-30-4	228-250-8		10 % (as acid)		
11	Polymer of N-{(2 and 4)-[(2-oxoborn-3-ylidene)methyl-]benzyl} acrylamide	Polyacrylamidomethyl Benzylidene Camphor	113783-61-2			6 %		
12	2-Ethylhexyl 4-methoxycinnamate/Octinoxate	Ethylhexyl Methoxycinnamate	5466-77-3	226-775-7		10 %		
13	Ethoxylated ethyl-4-aminobenzoate	PEG-25 PABA	116242-27-4			10 %		
14	Isopentyl-4-methoxycinnamate/Amiloxate	Isoamyl p-Methoxycinnamate	71617-10-2	275-702-5		10 %		

Reference number	Substance identification				Conditions			Wording of conditions of use and warnings
	Chemical name/INN/XAN	Name of Common Ingredients Glossary	CAS number	EC number	Product type, body parts	Maximum concentration in ready for use preparation	Other	
a	b	c	d	e	f	g	h	i
15	2,4,6-Trianilino-(p-carbo-2'-ethylhexyl-1'-oxy)-1,3,5-triazine	Ethylhexyl Triazone	88122-99-0	402-070-1		5 %		
16	Phenol,2-(2H-benzotriazol-2-yl)-4-methyl-6-(2-methyl-3-(1,3,3,3-tetramethyl-1-(trimethylsilyl)oxy)-disiloxanyl)propyl)	Drometrizole Trisiloxane	155633-54-8			15 %		
17	Benzoic acid, 4,4-((6-((4-(((1,1-dimethylethyl)amino)carbonyl)phenyl)amino)-1,3,5-triazine-2,4-diyl)diimino)bis-, bis (2-ethylhexyl) ester/Iscotrizinol (USAN)	Diethylhexyl Butamido Triazone	154702-15-5			10 %		
18	3-(4-Methylbenzylidene)-d1 camphor/Enzacamene	4-Methylbenzylidene Camphor	38102-62-4/ 36861-47-9	- / 253-242-6		4 %		
19	3-Benzylidene camphor	3-Benzylidene Camphor	15087-24-8	239-139-9		2 %		
20	2-Ethylhexyl salicylate/Octisalate	Ethylhexyl Salicylate	118-60-5	204-263-4		5 %		
21	2-Ethylhexyl 4-(dimethylamino)benzoate/Padimate O (USAN:BAN)	Ethylhexyl Dimethyl PABA	21245-02-3	244-289-3		8 %		
22	2-Hydroxy-4-methoxybenzophenone-5-sulfonic acid and its sodium salt/Sulisobenzone	Benzophenone-4, Benzophenone-5	4065-45-6/ 6628-37-1	223-772-2 / -		5 % (as acid)		
23	2,2'-Methylene-bis(6-(2H-benzotriazol-2-yl)-4-(1,1,3,3-tetramethyl-butyl)phenol) / Bisoctrizole	Methylene Bis-Benzotriazolyl Tetramethylbutylphenol	103597-45-1	403-800-1		10 %		
24	Sodium salt of 2,2'-bis(1,4-phenylene)-1H-benzimidazole-4,6-disulfonic acid) / Bisdisulizole disodium (USAN)	Disodium Phenyl Dibenzimidazole Tetrasulfonate	180898-37-7	429-750-0		10 % (as acid)		
25	2,2'-(6-(4-Methoxyphenyl)-1,3,5-triazine-2,4-diyl)bis(5-((2-ethylhexyl)oxy)phenol) / Bemotrizinol	Bis-Ethylhexyloxyphenol Methoxyphenyl Triazine	187393-00-6			10 %		
26	Dimethicodiethylbenzalmalonate	Polysilicone-15	207574-74-1	426-000-4		10 %		
27	Titanium dioxide (2)	Titanium Dioxide	13463-67-7/ 1317-70-0/ 1317-80-2	236-675-5/ 205-280-1/ 215-282-2		25 %		
28	Benzoic acid, 2-[4-(diethylamino)-2-hydroxybenzoyl]-, hexylester	Diethylamino Hydroxybenzoyl Hexyl Benzoate	302776-68-7	443-860-6		10 % in sunscreen products		

(1) Not required if concentration is 0,5 % or less and when it is used only for product protection purposes.
(2) For use other than as a colorant, see Annex IV, No. 143.

Figure 1.4 - List of UV filters authorised in cosmetic products in the EU (Annex VI to Regulation 1223/2009)

With EU Regulation 621/2016 (Figure 1.5), an amendment to Annex VI of Regulation (EC) 1223/2009 is implemented, adding entries related to ZnO. Following clarification requests from the Commission, the Scientific Committee on Consumer Safety (SCCS) confirmed that the use of non-nano zinc oxide in cosmetic products was safe up to a maximum concentration of 25 %, and it was advisable to submit appropriate data for the risk assessment of nano-form ZnO. The Commission considers that non-nano zinc oxide should be authorized for use as a UV filter in cosmetic products; nano-form ZnO (according to SCCS - specifications) should be authorized for use as a UV filter in cosmetic products [67].

ANNEX

The following entries are added to Annex VI to Regulation (EC) No 1223/2009 as reference numbers 30 and 30a:

Reference number	Substance identification				Conditions			Wording of conditions of use and warnings
	Chemical name/INN	Name of Common Ingredients Glossary	CAS number	EC number	Product type, body parts	Maximum concentration in ready for use preparation	Other	
a	b	c	d	e	f	g	h	i
'30	Zinc oxide	Zinc Oxide	1314-13-2	215-222-5		25 % (*)	Not to be used in applications that may lead to exposure of the end-user's lungs by inhalation.	
30a	Zinc oxide	Zinc Oxide (nano)	1314-13-2	215-222-5		25 % (*)	Not to be used in applications that may lead to exposure of the end-user's lungs by inhalation. Only nanomaterials having the following characteristics are allowed: — purity ≥ 96 %, with wurtzite crystalline structure and physical appearance as clusters that are rod-like, star-like and/or isometric shapes, with impurities consisting only of carbon dioxide and water, whilst any other impurities are less than 1 % in total, — median diameter of the particle number size distribution D50 (50 % of the number below this diameter) > 30 nm and D1 (1 % below this size) > 20 nm, — water solubility < 50 mg/L — uncoated, or coated with triethoxycaprylylsilane, dimethicone, dimethoxydiphenylsilanetriethoxycaprylylsilane cross-polymer, or octyl triethoxy silane.	

(*) In case of combined use of zinc oxide and zinc oxide (nano), the sum shall not exceed the limit given in column g.'

Figure 1.5 - Extract from European Regulation 621/2016

The Annex VI of European Regulation 1223/2009 has been amended by EU Regulation 238/2017, shown in Figure 1.6. Entry 4 related to oxybenzone is modified. SCCS concluded, in its opinion of December 16, 2008, that the use of BP3 as a UV filter at a maximum concentration of 6 % w/w in cosmetic products for sun protection and 0.5 % w/w in other types of cosmetic products to protect the formulation poses no risks to human health, apart from potential contact allergenic and photoallergenic effects. Consequently, the current maximum concentration of 10 % w/w for BP3 used as a UV filter in cosmetic products should be reduced to 6 % w/w [68].

ANNEX

In Annex VI to Regulation (EC) No 1223/2009, entry 4 is replaced by the following:

Reference number	Substance identification				Conditions			Wordings of conditions of use and warnings
	Chemical name/INN/ XAN	Name of Common Ingredients Glossary	CAS number	EC number	Product type, body parts	Maximum concentration in ready for use preparation	Other	
a	b	c	d	e	f	g	h	i
'4	2-Hydroxy-4-methoxybenzophenone/ Oxybenzone	Benzophenone-3	131-57-7	205-031-5		6 %	Not more than 0,5 % to protect product formulation	Contains Benzophenone-3 (1)'

Figure 1.6 - Extract from the European Regulation 238/2017

Subsequently, with EU Regulation 1176/2022 (Figure 1.7), Annex VI (entries 4 and 10) of EU Regulation 1223/2009 was amended due to concerns regarding the potential endocrine-disrupting properties of OC and BP3 when used as UV filters in cosmetic products. An invitation to submit data

was published in 2019. The SCCS found that the use of BP3 as a UV filter up to a maximum concentration of 2.2 % in body creams and aerosol or pump sprays is safe for the consumer, provided there is no additional use of the same substance at 0.5 % in the same product to protect the cosmetic formulation. It also concluded that when BP3 is used at a concentration of 0.5 % in the same formulation, the levels of BP3 used as a UV filter in body creams and aerosol, or pump sprays should not exceed 1.7 %. Regarding OC, the SCCS concluded in its opinion of March 30 and 31, 2021, based on the safety assessment and considering concerns about potential endocrine-disrupting properties, that this substance is safe as a UV filter at concentrations up to 10 % in cosmetic products when used individually. The SCCS also noted that the use of OC at a maximum concentration of 10 % in sun creams or lotions, pump spray sunscreens, face creams, hand creams, and lipsticks is safe when used in combination, but its use at concentrations equal to or greater than 10 % in aerosol spray sunscreens is not safe when used in combination. The SCCS considered that the use of OC in such products is safe at a maximum concentration of 9 % when used in combination with face creams, hand creams, or lipsticks containing 10 % OC. In light of the opinions of the SCCS, it can be concluded that the use of BP3 and OC as UV filters in cosmetic products at the currently allowed concentrations poses a potential risk to human health. Therefore, the use of these substances should be limited to the maximum concentrations proposed by the SCCS.

ANNEX

In Annex VI to Regulation (EC) No 1223/2009, entries 4 and 10 are replaced by the following:

Reference number	Substance identification				Conditions			Wordings of conditions of use and warnings
	Chemical name/INN	Name of Common Ingredients Glossary	CAS number	EC number	Product type, body parts	Maximum concentration in ready use preparation	Other	
a	b	c	d	e	f	g	h	i
'4	2-Hydroxy-4-methoxy-benzophenone/ Oxybenzone (*)	Benzophenone-3	131-57-7	205-031-5	a) Face products, hand products, and lip products, excluding propellant and pump spray products	a) 6 %	For a) and b) Not more than 0,5 % to protect product formulation	For a) and b): Contains Benzophenone-3 (**)
					b) Body products, including propellant and pump spray products	b) 2,2 %	a) If used at 0,5 % to protect product formulation, the levels used as UV filter must not exceed 5,5 %.	
					c) Other products	c) 0,5 %	b) If used at 0,5 % to protect product formulation, the levels used as UV filter must not exceed 1,7 %.	
10	2-Cyano-3,3-diphenyl acrylic acid, 2- ethylhexyl ester/ Octocrylene (*) (***)	Octocrylene	6197-30-4	228-250-8	a) Propellant spray products	a) 9 %		
					b) Other products	b) 10 %		

(*) However, cosmetic products containing that substance and complying with the restrictions set out in Regulation (EC) No 1223/2009 as applicable on 27 July 2022 may be placed on the Union market until 28 January 2023 and be made available on the Union market until 28 July 2023.
(**) Not required if concentration is 0,5 % or less and when it is used only for product protection purposes.
(***) Benzophenone as an impurity and/or degradation product of Octocrylene shall be kept at trace level.'

Figure 1.7 Extract from the European Regulation 1176/2022

1.3.3 Analytical methods for the determination of UV filters

The most widely used analytical technique for the determination of UV filters is liquid chromatography (LC) coupled to an MS or UV-Vis detector.

In the literature there are several articles both concerning personal care products and for environmental or biological matrices, in which they are used: LC-UV/Vis [69], HPLC-UV/Vis [70], HPLC-MS/MS (ESI) [71], Ultra-High Performance Supercritical Fluid chromatography (UHPSFC-PDA) [72] or GC-MS/MS [73].

Some electrochemical methods have also been tested for a preliminary application in this field [74, 75].

References

[1] J. M. Pacyna, "Recent advances in mercury research," *Sci. Total Environ.*, vol. 738, p. 139955, Oct. 2020, doi: 10.1016/j.scitotenv.2020.139955.

[2] C. Roveta *et al.*, "Biomonitoring of Heavy Metals: The Unexplored Role of Marine Sessile Taxa," *Appl. Sci.*, vol. 11, no. 2, p. 580, Jan. 2021, doi: 10.3390/app11020580.

[3] H. Okyere, R. B. Voegborlo, and S. E. Agorku, "Human exposure to mercury, lead and cadmium through consumption of canned mackerel, tuna, pilchard and sardine," *Food Chem.*, vol. 179, pp. 331–335, Jul. 2015, doi: 10.1016/j.foodchem.2015.01.038.

[4] A. Annibaldi *et al.*, "Determination of Hg in Farmed and Wild Atlantic Bluefin Tuna (Thunnus thynnus L.) Muscle," *Molecules*, vol. 24, no. 7, p. 1273, Apr. 2019, doi: 10.3390/molecules24071273.

[5] "REGULATION (EC) No 1272/2008 OF THE EUROPEAN PARLIAMENT AND OF THE COUNCIL of 16 December 2008 on classification, labelling and packaging of substances and mixtures, amending and repealing Directives 67/548/EEC and 1999/45/EC, and amending Regulation (EC) No 1907/2006".

[6] EFSA Panel on Contaminants in the Food Chain (CONTAM), "Scientific Opinion on the risk for public health related to the presence of mercury and methylmercury in food," *EFSA J.*, vol. 10, no. 12, Dec. 2012, doi: 10.2903/j.efsa.2012.2985.

[7] P. Rivaro, C. Ianni, F. Soggia, and R. Frache, "Mercury speciation in environmental samples by cold vapour atomic absorption spectrometry with in situ preconcentration on a gold trap," *Microchim. Acta*, vol. 158, no. 3–4, pp. 345–352, May 2007, doi: 10.1007/s00604-006-0712-9.

[8] F. Zahir, S. J. Rizwi, S. K. Haq, and R. H. Khan, "Low dose mercury toxicity and human health," *Environ. Toxicol. Pharmacol.*, vol. 20, no. 2, pp. 351–360, Sep. 2005, doi: 10.1016/j.etap.2005.03.007.

[9] R. Agraz, M. T. Sevilla, and L. Hernandez, "Voltammetric quantification and speciation of mercury compounds," *J. Electroanal. Chem.*, vol. 390, no. 1–2, pp. 47–57, Jun. 1995, doi: 10.1016/0022-0728(95)03955-G.

[10] K. M. Rice, E. M. Walker, M. Wu, C. Gillette, and E. R. Blough, "Environmental Mercury and Its Toxic Effects," *J. Prev. Med. Pub. Health*, vol. 47, no. 2, pp. 74–83, Mar. 2014, doi: 10.3961/jpmph.2014.47.2.74.

[11] C.-Y. Chen, C.-C. Lai, K.-S. Chen, C.-C. Hsu, C.-C. Hung, and M.-H. Chen, "Total and organic mercury concentrations in the muscles of Pacific albacore (Thunnus alalunga) and bigeye tuna (Thunnus obesus)," *Mar. Pollut. Bull.*, vol. 85, no. 2, pp. 606–612, Aug. 2014, doi: 10.1016/j.marpolbul.2014.01.039.

[12] "Commission Regulation (EU) No 420/2011 of 29 April 2011 amending Regulation (EC) No 1881/2006 setting maximum levels for certain contaminants in foodstuffsText with EEA relevance".

[13] M. A. Augelli, R. A. A. Munoz, E. M. Richter, M. I. Cantagallo, and L. Angnes, "Analytical procedure for total mercury determination in fishes and shrimps by chronopotentiometric stripping analysis at gold film electrodes after microwave digestion," *Food Chem.*, vol. 101, no. 2, pp. 579–584, Jan. 2007, doi: 10.1016/j.foodchem.2006.02.017.

[14] M. Chen and C. Chou, "An Instrumental Correction for the Determination of Mercury in Biological and Sediment Samples Using Cold Vapor Atomic Absorption Spectrophotometry," *J. Chin. Chem. Soc.*, vol. 47, no. 5, pp. 1145–1153, Oct. 2000, doi: 10.1002/jccs.200000154.

[15] A. I. Cabañero Ortiz, Y. Madrid Albarrán, and C. Cámara Rica, "Evaluation of different sample pre-treatment and extraction procedures for mercury speciation in fish samples," *J Anal Spectrom*, vol. 17, no. 12, pp. 1595–1601, 2002, doi: 10.1039/B207334J.

[16] G. Tao and S. N. Willie, "Determination of total mercury in biological tissues by flow injection cold vapour generation atomic absorption spectrometry following tetramethylammonium hydroxide digestion," *The Analyst*, vol. 123, no. 6, pp. 1215–1218, 1998, doi: 10.1039/a802000k.

[17] Y. Li, J. Zhang, Y. Zhao, and C. Zheng, "Volatility and Speciation of Mercury during Pyrolysis and Gasification of Five Chinese Coals," *Energy Fuels*, vol. 25, no. 9, pp. 3988–3996, Sep. 2011, doi: 10.1021/ef2006904.

[18] I. Rodriguez Pereiro, A. Wasik, and R. Łobiński, "Determination of mercury species in fish reference materials by isothermal multicapillary gas chromatography with atomic emission detection after microwave-assisted solubilization and solvent extraction," *J Anal Spectrom*, vol. 13, no. 8, pp. 743–747, 1998, doi: 10.1039/A802154F.

[19] I. Nnah and M. Wessling-Resnick, "Brain Iron Homeostasis: A Focus on Microglial Iron," *Pharmaceuticals*, vol. 11, no. 4, p. 129, Nov. 2018, doi: 10.3390/ph11040129.

[20] L. Mezzaroba, D. F. Alfieri, A. N. Colado Simão, and E. M. Vissoci Reiche, "The role of zinc, copper, manganese and iron in neurodegenerative diseases," *NeuroToxicology*, vol. 74, pp. 230–241, Sep. 2019, doi: 10.1016/j.neuro.2019.07.007.

[21] Y.-Z. Chang, Ed., *Brain Iron Metabolism and CNS Diseases*, vol. 1173. in Advances in Experimental Medicine and Biology, vol. 1173. Singapore: Springer Singapore, 2019. doi: 10.1007/978-981-13-9589-5.

[22] W. Ruengsitagoon, "Reverse flow injection spectrophotometric determination of iron(III) using chlortetracycline reagent," *Talanta*, vol. 74, no. 5, pp. 1236–1241, Feb. 2008, doi: 10.1016/j.talanta.2007.08.031.

[23] L. L. Stookey, "Ferrozine---a new spectrophotometric reagent for iron," *Anal. Chem.*, vol. 42, no. 7, pp. 779–781, Jun. 1970, doi: 10.1021/ac60289a016.

[24] M. Grotti, M. L. Abelmoschi, F. Soggia, and R. Frache, "Determination of ultratrace elements in natural waters by solid-phase extraction and atomic spectrometry methods," *Anal. Bioanal. Chem.*, vol. 375, no. 2, pp. 242–247, Jan. 2003, doi: 10.1007/s00216-002-1676-1.

[25] D. J. Leao, M. M. S. Junior, G. C. Brandao, and S. L. C. Ferreira, "Simultaneous determination of cadmium, iron and tin in canned foods using high-resolution continuum source graphite furnace atomic absorption spectrometry," *Talanta*, vol. 153, pp. 45–50, Jun. 2016, doi: 10.1016/j.talanta.2016.02.023.

[26] J. Wu and E. A. Boyle, "Determination of iron in seawater by high-resolution isotope dilution inductively coupled plasma mass spectrometry after Mg(OH)2 coprecipitation," *Anal. Chim. Acta*, vol. 367, no. 1–3, pp. 183–191, Jul. 1998, doi: 10.1016/S0003-2670(98)00145-7.

[27] S. J. Ussher, I. Petrov, C. R. Quétel, and P. J. Worsfold, "Validation of a portable flow injection - chemiluminescence (FI-CL) method for the determination of dissolved iron in Atlantic open ocean and shelf waters by comparison with isotope dilution - inductively coupled plasma mass spectrometry (ID-ICPMS)," *Environ. Chem.*, vol. 7, no. 2, p. 139, 2010, doi: 10.1071/EN09092.

[28] Y. Du *et al.*, "Determination of iron(III) based on the fluorescence quenching of rhodamine B derivative," *Talanta*, vol. 106, pp. 261–265, Mar. 2013, doi: 10.1016/j.talanta.2012.10.078.

[29] M. Lin, D. Pan, X. Hu, F. Li, and H. Han, "A tin–bismuth alloy electrode for the cathodic stripping voltammetric determination of iron in coastal waters," *Anal. Methods*, vol. 7, no. 12, pp. 5169–5174, 2015, doi: 10.1039/C5AY00886G.

[30] R. Segura, M. I. Toral, and V. Arancibia, "Determination of iron in water samples by adsorptive stripping voltammetry with a bismuth film electrode in the presence of 1-(2-piridylazo)-2-naphthol," *Talanta*, vol. 75, no. 4, pp. 973–977, May 2008, doi: 10.1016/j.talanta.2007.12.038.

[31] C. M. G. Van Den Berg, "Chemical Speciation of Iron in Seawater by Cathodic Stripping Voltammetry with Dihydroxynaphthalene," *Anal. Chem.*, vol. 78, no. 1, pp. 156–163, Jan. 2006, doi: 10.1021/ac051441+.

[32] K. A. Baken, R. M. A. Sjerps, M. Schriks, and A. P. Van Wezel, "Toxicological risk assessment and prioritization of drinking water relevant contaminants of emerging concern," *Environ. Int.*, vol. 118, pp. 293–303, Sep. 2018, doi: 10.1016/j.envint.2018.05.006.

[33] N. Z. Arman *et al.*, "A Review on Emerging Pollutants in the Water Environment: Existences, Health Effects and Treatment Processes," *Water*, vol. 13, no. 22, p. 3258, Nov. 2021, doi: 10.3390/w13223258.

[34] A. Pal, Y. He, M. Jekel, M. Reinhard, and K. Y.-H. Gin, "Emerging contaminants of public health significance as water quality indicator compounds in the urban water cycle," *Environ. Int.*, vol. 71, pp. 46–62, Oct. 2014, doi: 10.1016/j.envint.2014.05.025.

[35] Q. Shi, Y. Xiong, P. Kaur, N. D. Sy, and J. Gan, "Contaminants of emerging concerns in recycled water: Fate and risks in agroecosystems," *Sci. Total Environ.*, vol. 814, p. 152527, Mar. 2022, doi: 10.1016/j.scitotenv.2021.152527.

[36] A. Pérez-Pereira, J. S. Carrola, M. E. Tiritan, and C. Ribeiro, "Enantioselectivity in ecotoxicity of pharmaceuticals, illicit drugs, and industrial persistent pollutants in aquatic and terrestrial environments: A review," *Sci. Total Environ.*, vol. 912, p. 169573, Feb. 2024, doi: 10.1016/j.scitotenv.2023.169573.

[37] C. M. Villanueva, S. Cordier, L. Font-Ribera, L. A. Salas, and P. Levallois, "Overview of Disinfection By-products and Associated Health Effects," *Curr. Environ. Health Rep.*, vol. 2, no. 1, pp. 107–115, Mar. 2015, doi: 10.1007/s40572-014-0032-x.

[38] T. J. Luben *et al.*, "The Healthy Men Study: An Evaluation of Exposure to Disinfection By-Products in Tap Water and Sperm Quality," *Environ. Health Perspect.*, vol. 115, no. 8, pp. 1169–1176, Aug. 2007, doi: 10.1289/ehp.10120.

[39] N. Hirt and M. Body-Malapel, "Immunotoxicity and intestinal effects of nano- and microplastics: a review of the literature," *Part. Fibre Toxicol.*, vol. 17, no. 1, p. 57, Dec. 2020, doi: 10.1186/s12989-020-00387-7.

[40] M. Liu *et al.*, "Research advances of microplastics and potential health risks of microplastics on terrestrial higher mammals: a bibliometric analysis and literature review," *Environ. Geochem. Health*, vol. 45, no. 6, pp. 2803–2838, Jun. 2023, doi: 10.1007/s10653-022-01458-8.

[41] X. Chen *et al.*, "Adverse health effects of emerging contaminants on inflammatory bowel disease," *Front. Public Health*, vol. 11, p. 1140786, Feb. 2023, doi: 10.3389/fpubh.2023.1140786.

[42] M. Lei *et al.*, "Overview of Emerging Contaminants and Associated Human Health Effects," *BioMed Res. Int.*, vol. 2015, pp. 1–12, 2015, doi: 10.1155/2015/404796.

[43] C. A. Grieshaber *et al.*, "Relation of contaminants to fish intersex in riverine sport fishes," *Sci. Total Environ.*, vol. 643, pp. 73–89, Dec. 2018, doi: 10.1016/j.scitotenv.2018.06.071.

[44] H. S. Srain, K. F. Beazley, and T. R. Walker, "Pharmaceuticals and personal care products and their sublethal and lethal effects in aquatic organisms," *Environ. Rev.*, vol. 29, no. 2, pp. 142–181, Jun. 2021, doi: 10.1139/er-2020-0054.

[45] E. S. Okeke *et al.*, "Antibiotic resistance in aquaculture and aquatic organisms: a review of current nanotechnology applications for sustainable management," *Environ. Sci. Pollut. Res.*, vol. 29, no. 46, pp. 69241–69274, Oct. 2022, doi: 10.1007/s11356-022-22319-y.

[46] F. Impellitteri, C. R. Multisanti, P. Rusanova, G. Piccione, F. Falco, and C. Faggio, "Exploring the Impact of Contaminants of Emerging Concern on Fish and Invertebrates Physiology in the Mediterranean Sea," *Biology*, vol. 12, no. 6, p. 767, May 2023, doi: 10.3390/biology12060767.

[47] J. P. Meador, A. Yeh, and E. P. Gallagher, "Adverse metabolic effects in fish exposed to contaminants of emerging concern in the field and laboratory," *Environ. Pollut.*, vol. 236, pp. 850–861, May 2018, doi: 10.1016/j.envpol.2018.02.007.

[48] N. Serpone, D. Dondi, and A. Albini, "Inorganic and organic UV filters: Their role and efficacy in sunscreens and suncare products," *Inorganica Chim. Acta*, vol. 360, no. 3, pp. 794–802, Feb. 2007, doi: 10.1016/j.ica.2005.12.057.

[49] E. B. Manaia, R. C. K. Kaminski, M. A. Corrêa, and L. A. Chiavacci, "Inorganic UV filters," *Braz. J. Pharm. Sci.*, vol. 49, no. 2, pp. 201–209, Jun. 2013, doi: 10.1590/S1984-82502013000200002.

[50] D. L. Giokas, A. Salvador, and A. Chisvert, "UV filters: From sunscreens to human body and the environment," *TrAC Trends Anal. Chem.*, vol. 26, no. 5, pp. 360–374, May 2007, doi: 10.1016/j.trac.2007.02.012.

[51] Y. Huang, J. C.-F. Law, T.-K. Lam, and K. S.-Y. Leung, "Risks of organic UV filters: a review of environmental and human health concern studies," *Sci. Total Environ.*, vol. 755, p. 142486, Feb. 2021, doi: 10.1016/j.scitotenv.2020.142486.

[52] S. L. Schneider and H. W. Lim, "Review of environmental effects of oxybenzone and other sunscreen active ingredients," *J. Am. Acad. Dermatol.*, vol. 80, no. 1, pp. 266–271, Jan. 2019, doi: 10.1016/j.jaad.2018.06.033.

[53] M. E. Balmer, H.-R. Buser, M. D. Müller, and T. Poiger, "Occurrence of Some Organic UV Filters in Wastewater, in Surface Waters, and in Fish from Swiss Lakes," *Environ. Sci. Technol.*, vol. 39, no. 4, pp. 953–962, Feb. 2005, doi: 10.1021/es040055r.

[54] C. P. Da Silva, E. S. Emídio, and M. R. R. De Marchi, "The occurrence of UV filters in natural and drinking water in São Paulo State (Brazil)," *Environ. Sci. Pollut. Res.*, vol. 22, no. 24, pp. 19706–19715, Dec. 2015, doi: 10.1007/s11356-015-5174-3.

[55] M. I. Cadena-Aizaga, S. Montesdeoca-Esponda, M. E. Torres-Padrón, Z. Sosa-Ferrera, and J. J. Santana-Rodríguez, "Organic UV filters in marine environments: An update of analytical methodologies, occurrence and distribution," *Trends Environ. Anal. Chem.*, vol. 25, p. e00079, Mar. 2020, doi: 10.1016/j.teac.2019.e00079.

[56] T. Manasfi, B. Coulomb, S. Ravier, and J.-L. Boudenne, "Degradation of Organic UV filters in Chlorinated Seawater Swimming Pools: Transformation Pathways and Bromoform Formation," *Environ. Sci. Technol.*, vol. 51, no. 23, pp. 13580–13591, Dec. 2017, doi: 10.1021/acs.est.7b02624.

[57] F. Chen, C. Huber, and P. Schröder, "Fate of the sunscreen compound oxybenzone in Cyperus alternifolius based hydroponic culture: Uptake, biotransformation and phytotoxicity," *Chemosphere*, vol. 182, pp. 638–646, Sep. 2017, doi: 10.1016/j.chemosphere.2017.05.072.

[58] P. Gago-Ferrero, M. S. Díaz-Cruz, and D. Barceló, "An overview of UV-absorbing compounds (organic UV filters) in aquatic biota," *Anal. Bioanal. Chem.*, vol. 404, no. 9, pp. 2597–2610, Nov. 2012, doi: 10.1007/s00216-012-6067-7.

[59] D. Stien *et al.*, "Metabolomics Reveal That Octocrylene Accumulates in *Pocillopora damicornis* Tissues as Fatty Acid Conjugates and Triggers Coral Cell Mitochondrial Dysfunction," *Anal. Chem.*, vol. 91, no. 1, pp. 990–995, Jan. 2019, doi: 10.1021/acs.analchem.8b04187.

[60] C. A. Downs *et al.*, "Toxicopathological Effects of the Sunscreen UV Filter, Oxybenzone (Benzophenone-3), on Coral Planulae and Cultured Primary Cells and Its Environmental Contamination in Hawaii and the U.S. Virgin Islands," *Arch. Environ. Contam. Toxicol.*, vol. 70, no. 2, pp. 265–288, Feb. 2016, doi: 10.1007/s00244-015-0227-7.

[61] D. Vuckovic, A. I. Tinoco, L. Ling, C. Renicke, J. R. Pringle, and W. A. Mitch, "Conversion of oxybenzone sunscreen to phototoxic glucoside conjugates by sea anemones and corals," *Science*, vol. 376, no. 6593, pp. 644–648, May 2022, doi: 10.1126/science.abn2600.

[62] R. Danovaro *et al.*, "Sunscreens Cause Coral Bleaching by Promoting Viral Infections," *Environ. Health Perspect.*, vol. 116, no. 4, pp. 441–447, Apr. 2008, doi: 10.1289/ehp.10966.

[63] L. L. R. De Miranda, K. E. Harvey, A. Ahmed, and S. C. Harvey, "UV-filter pollution: current concerns and future prospects," *Environ. Monit. Assess.*, vol. 193, no. 12, p. 840, Dec. 2021, doi: 10.1007/s10661-021-09626-6.

[64] S. Santana-Viera, S. Montesdeoca-Esponda, Z. Sosa-Ferrera, and J. J. Santana-Rodríguez, "UV filters and UV stabilisers adsorbed in microplastic debris from beach sand," *Mar. Pollut. Bull.*, vol. 168, p. 112434, Jul. 2021, doi: 10.1016/j.marpolbul.2021.112434.

[65] S. O'Donovan *et al.*, "Effects of the UV filter, oxybenzone, adsorbed to microplastics in the clam Scrobicularia plana," *Sci. Total Environ.*, vol. 733, p. 139102, Sep. 2020, doi: 10.1016/j.scitotenv.2020.139102.

[66] "Regulation (EC) No 1069/2009 of the European Parliament and of the Council of 21 October 2009 laying down health rules as regards animal by-products and derived products not intended for human consumption and repealing Regulation (EC) No 1774/2002 (Animal by-products Regulation)," p. 33.

[67] "COMMISSION REGULATION (EU) 2016/ 621 - of 21 April 2016 - amending Annex VI to Regulation (EC) No 1223 / 2009 of the European Parliament and of the Council on cosmetic products".

[68] "COMMISSION REGULATION (EU) 2017/ 238 - of 10 February 2017 - amending Annex VI to Regulation (EC) No 1223 / 2009 of the European Parliament and of the Council on cosmetic products".

[69] A. Chisvert, I. Tarazona, and A. Salvador, "A reliable and environmentally-friendly liquid-chromatographic method for multi-class determination of fat-soluble UV filters in cosmetic products," *Anal. Chim. Acta*, vol. 790, pp. 61–67, Aug. 2013, doi: 10.1016/j.aca.2013.06.032.

[70] D. Orsi *et al.*, "Simple Extraction and HPLC Determination of UV-A and UV-B Filters in Sunscreen Products," *Chromatographia*, vol. 64, no. 9–10, pp. 509–515, Nov. 2006, doi: 10.1365/s10337-006-0074-9.

[71] X. Meng, Q. Ma, H. Bai, Z. Wang, C. Han, and C. Wang, "Simultaneous separation and determination of 15 organic UV filters in sunscreen cosmetics by HPLC – ESI - MS / MS," *Int. J. Cosmet. Sci.*, vol. 39, no. 4, pp. 386–392, Aug. 2017, doi: 10.1111/ics.12387.

[72] M. A. Khalikova, E. Lesellier, E. Chapuzet, D. Šatínský, and C. West, "Development and validation of ultra-high performance supercritical fluid chromatography method for quantitative determination of nine sunscreens in cosmetic samples," *Anal. Chim. Acta*, vol. 1034, pp. 184–194, Nov. 2018, doi: 10.1016/j.aca.2018.06.013.

[73] M. Vila, J. P. Lamas, C. Garcia-Jares, T. Dagnac, and M. Llompart, "Optimization of an analytical methodology for the simultaneous determination of different classes of ultraviolet filters in cosmetics by pressurized liquid extraction–gas chromatography tandem mass spectrometry," *J. Chromatogr. A*, vol. 1405, pp. 12–22, Jul. 2015, doi: 10.1016/j.chroma.2015.05.061.

[74] V. S. Ferreira, J. B. G. Júnior, C. M. S. C. Oliveira, R. M. Takeuchi, A. L. Santos, and M. A. G. Trindade, "Voltammetric analysis of sun-block preparations containing octocrylene and its association with 2-Hydroxy-4-methoxybenzophenone and octyl methoxycinnamate," *Microchem. J.*, vol. 106, pp. 378–383, Jan. 2013, doi: 10.1016/j.microc.2012.10.002.

[75] J. B. G. Júnior, T. A. Araujo, M. A. G. Trindade, and V. S. Ferreira, "Electroanalytical determination of the sunscreen agent octocrylene in cosmetic products," *Int. J. Cosmet. Sci.*, vol. 34, no. 1, pp. 91–96, Feb. 2012, doi: 10.1111/j.1468-2494.2011.00686.x.

2. VOLTAMMETRY

This chapter will provide a general overview of the analytical technique used in this research study, in the various topics described above, i.e. mercury and iron determination and speciation and UV filter determination, for the quantification of analytes in synthetic solutions, in certified reference materials and in different real matrices.

2.1 Electrochemical methods - Voltammetry

Electrochemical methods can be divided into different categories, based on what is measured: potentiometry (a static technique in which the information about the sample composition is obtained measuring the difference in electrode potentials), voltammetry (the current due to the redox reaction of the analyte is measured) and coulometry (the charge flowing through the cell is measured over time).

Voltammetry is an analytical technique based on the measurement of the current passing through a working electrode (WE) immersed in a solution containing electroactive chemical species when it is subjected to a change in potential. This is a very versatile technique and allows to carry out studies on many aspects of electrochemical reactions in which electron exchanges between reagents and products take place.

One of the most important applications of voltammetry is the quantitative determination of chemical species in solution that can be oxidized or reduced. It is a technique that is applied to determine heavy metals and electroactive organic substances in different matrices such as water, soil, food, drugs.

Compared to other analytical methods, voltammetry has some advantages such as: i) inexpensive instrumentation, ii) low operating costs, iii) high sensitivity, iv) simple operating procedure and v) portable instrumentation, useful for in situ analysis.

The data obtained during a voltammetric experiment are represented in a voltammogram, which plots the current produced by the reduction of oxidation of the analyte versus the potential of the working electrode [1]. Table 2.1 collects the main electrochemical parameters involved in a voltammetric analysis.

Table 2.1 - Summary of the meanings of voltammetric parameters

Parameter	Meaning	Technique
$\mathbf{E_{begin}}$	Potential at which the scan begins	LSV, CV, DPV, SWV
$\mathbf{E_{end}}$	Potential at which the scan ends	LSV, CV, DPV, SWV
$\mathbf{E_{step}}$	Potential difference between one pulse and the next	LSV, CV, DPV, SWV
Scan rate	Determines the time between two steps and thus the sampling time	LSV, CV, DPV
$\mathbf{E_{pulse}}$	Height of the applied pulse	DPV
$\mathbf{t_{pulse}}$	Time length of the applied pulse	DPV
Amplitude	Amplitude of quare wave pulse (half peak-to-peak values)	SWV
Frequency	Frequency of the square wave	SWV
$\mathbf{E_{vertex}}$	Potential at which the scan is reversed	CV

*LS: Linear Sweep Voltammetry; CV: Cyclic Voltammetry, DPV: Differential Pulse Voltammetry; SWV: Square Wave Voltammetry

Assuming that the working electrode is immersed in a solution containing an electroactive (A_{ox}) species capable of being reduced according to the reaction: $\mathbf{A_{ox} + ne^- \rightarrow A_{red}}$ and that a more reducing (or more negative) potential is applied to the electrode than the reduction potential of the test species A_{ox}: under these conditions the A_{ox} discharge (i.e. reduction) occurs on the electrode surface. For the discharge to occur, A_{ox} must reach the electrode from the solution and receive electrons from the electrode. Thus, the discharge process is influenced by two kinetic factors: rate (v_1) with which A_{ox} reaches the electrode; electron exchange rate (v_2) between electrode and solution. Analytical-quantitative voltammetry requires v_2 to be greater than v_1. This means that the discharge of A_{ox} to the electrode surface can be considered instantaneous and the intensity of the discharge current depends exclusively on v_1 and therefore depends on the way A_{ox} reaches the electrode.

In solution, a chemical species can move through three processes, depicted in Figure 2.1: migration, convection, and diffusion. *Migration* is the movement caused by the attractive force of the electric field generated by the electrode against each opposite charge ion and the repulsion force by each ion with the same charge. *Convection* occurs when a solution is subject to agitation or when in solution there are inhomogeneities such as temperature or density gradients. In this case, the analyte and solvent molecules move according to a turbulent motion that becomes laminar near the electrode surface. *Diffusion* is the spontaneous movement that is generated in solution by those chemical species that are subjected to a gradient of concentration and thanks to this phenomenon the system tends to be homogeneous.

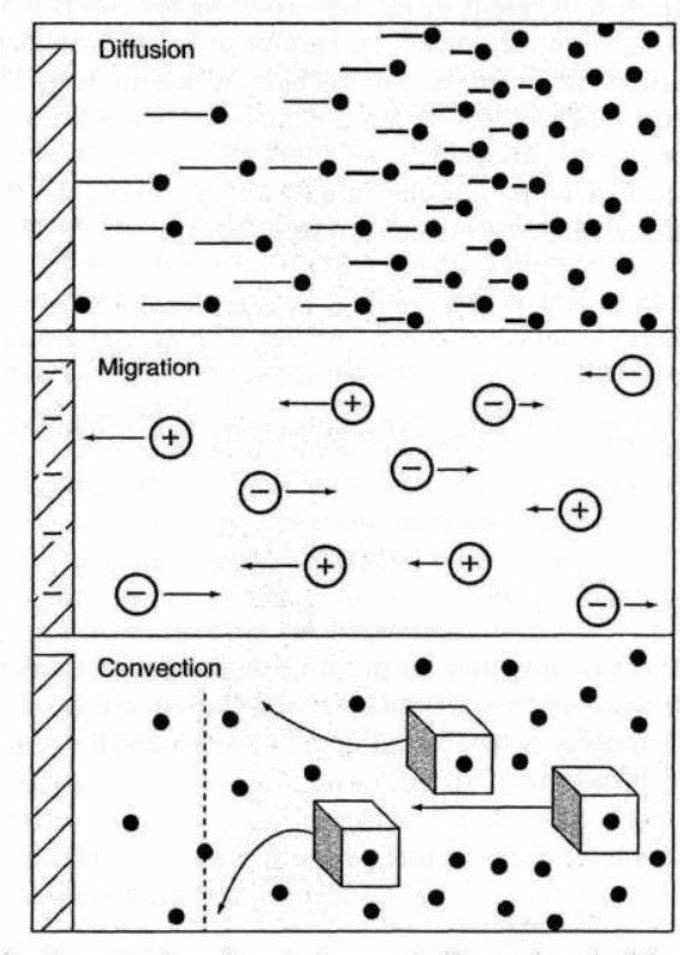

Figure 2-1 - The three modes of mass transport. Source: Maloy, 1983 [2].

The concentration gradient is proportional to the diffusion rate, expressible with Fick's first law:

$$J = -D\left(\frac{dC}{dx} + \frac{dC}{dy} + \frac{dC}{dz}\right)$$

where:

- J is the diffusion rate of the species (mol/m²s),

- D is the diffusion coefficient (m²/s),

- dC/dI is the concentration gradient along the coordinate I (x, y, and z),

The negative sign indicates that the flow is directed from the region of higher concentration to the region of lower concentration.

A *supporting electrolyte* is added in excess to the solution and consists of ions that do not discharge under the analytical conditions. Its function is to shield the electrode, that is, to surround it with ions that have the same charge as the electroactive species (depolarizing) that is discharged, reducing the electrostatic attraction towards the latter. This minimizes the migration of the analyte.

The supporting electrolyte for depolarizing must: i) be chemically inert; ii) do not hinder the spread and electronic exchange on the electrode surface; iii) have a different discharge potential (at least 100-200 mV) from that of the analyte; iv) have a high ionic conductivity so as to ensure low resistance to the passage of current.

The supporting electrolyte can be a salt, an acid, a base, a complexant or a buffer.

Potential scan

If a linear and fast potential scan is performed in a reversible redox system, characteristic segments are observed on the recorded voltammogram (potential vs. current) during the scan (Figure 2.2):

1. Initial residual current (Segment A): the potential is not sufficient to initiate the discharge of A_{ox}. The measured current, residual current, is due to various factors, including cell resistance, discharge of trace amounts of oxygen, and background noise in the circuit.
2. Rising part of the peak (Segment B): near the discharge potential, the curve sharply rises. Ions of the oxidized species A_{ox} discharge at an increasing rate on the electrode, and the diffusion layer (i.e. a layer at the electrode surface where the analyte only moves by diffusion) becomes increasingly depleted. This causes a spontaneous flow of A_{ox} ions from the bulk of the solution. The speed of A_{ox} ions towards the diffusion layer is proportional to their concentration in the solution.
3. Descending part of the peak (Segments C-D): in the solution layer in close contact with the working electrode, the concentration of A_{ox} is zero. Indeed, all oxidized species reaching the electrode are reduced, the diffusion layer becomes depleted, and the current tends to decrease.

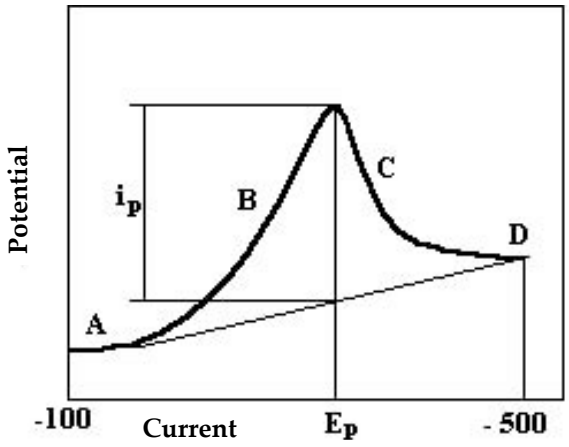

Figure 2.2 - Characteristic segments on recorded voltammogram (potential vs. current).

The maximum point of the peak identifies the peak current (i_P) and the peak potential (E_P). The peak potential is the point at which half of the A_{ox} ions reaching the electrode are discharged, and this potential deviates slightly from the standard potential of the redox couple. Therefore, E_P constitutes the voltammetric parameter that qualitatively characterizes a redox couple. The peak current corresponds to the peak height and is proportional to the concentration of the electroactive species present in the solution. Therefore, the peak current is the voltammetric parameter that quantitatively characterizes the species.

There are several voltammetric methods.

Linear Sweep Voltammetry.

Linear Sweep Voltammetry (LSV) is the simplest voltammetric technique. It involves applying a rapid potential scan to the working electrode, varying linearly, as shown in Figure 2.3; actually, the potential varies stepwise, being applied in a digital mode. The scan starts from a potential where no discharge occurs and ends beyond the discharge potential. It has detection limits on the order of mg L^{-1}.

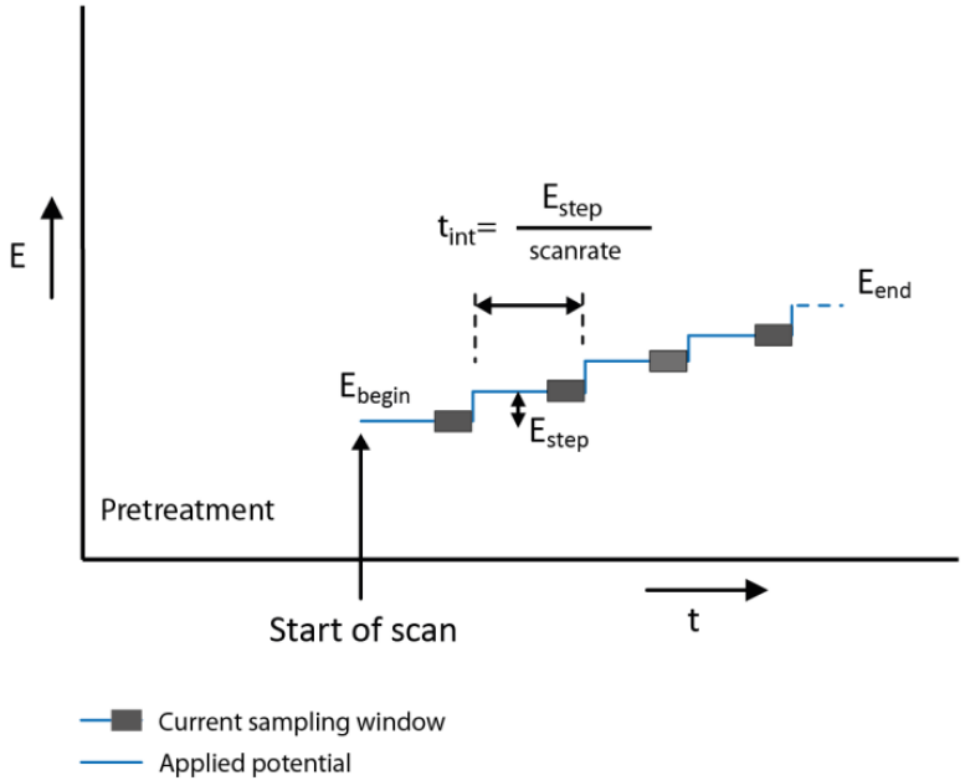

Figure 2.3 - Potential applied during Linear Sweep Voltammetry (LSV). Source: Metrohm PSTrace manual, 2019 [3].

Cyclic Voltammetry.

Cyclic Voltammetry (CV) is a particular type of LSV that applies a triangular scan to the working electrode, facilitating oxidation and then reduction (or vice versa) of the electroactive species. The scan mode is shown in Figure 2.4.

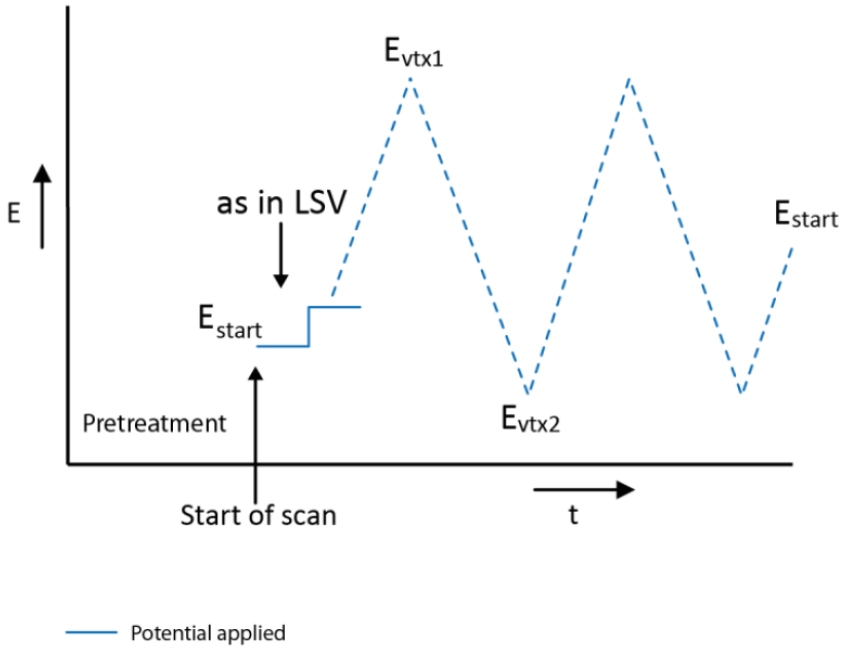

Figure 2.4 - Potential applied during CV. Source: Metrohm PSTrace manual, 2019 [3].

CV is useful to describe the redox process occurring during a voltammetric analysis, by means of the Nernst equation:

$$E = E^0 + \frac{RT}{nF}\ln\frac{(Ox)}{(Red)} = E^0 + 2.3026\frac{RT}{nF}log_{10}\frac{(Ox)}{(Red)}$$

where R is the universal gas constant (8.314 J·mol^{-1}), T is the temperature in Kelvin, *n* is the number of electrons and F is Faraday's constant (96485 C·mol^{-1}). (Ox) and (Red) are the activities of the oxidized and reduced forms of the analyte.

This equation relates the potential of an electrochemical cell (E) to the standard potential of a species (E°) and the relative activities of the oxidized (Ox) and reduced (Red) analyte in the system at equilibrium.

As an example, it is useful to consider the equilibrium between ferrocenium (Fc^+) and ferrocene (Fc), reported in Figure 2.5. Indeed, ferrocene is a highly stable organometallic compound, often used as an internal reference system in electrochemistry thanks to its reversible redox behaviour.

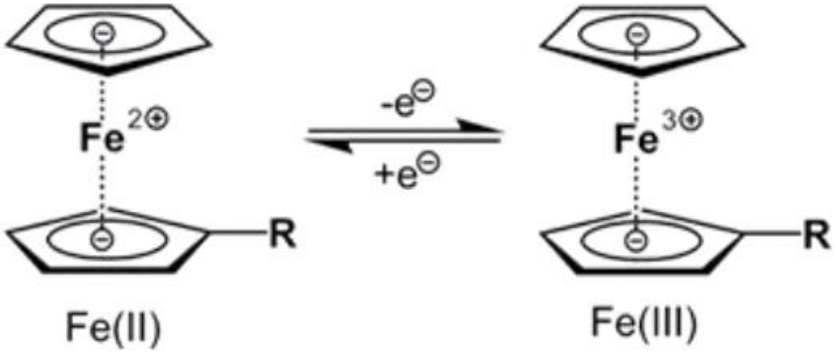

Figure 2.5 - Redox couple ferrocene (Fc)-ferrocenium (Fc^+). (R=H)

To better explain the study of redox behaviour, we can apply the Nernst equation to the one-electron reduction process of ferrocene. Since activities are not easily accessible experimentally, they are replaced with concentrations, the standard potential E^0 is replaced with the formal potential $E^{0'}$ (a term including activity coefficients), and *n* is equal to 1 as the process involves the exchange of one electron.

$$E = E^{0\prime} + \frac{RT}{F}\ln\frac{[Fc+]}{[Fc]} = E^{0\prime} + 2.3026\frac{RT}{F}log_{10}\frac{[Fc+]}{[Fc]}$$

The formal potential $E^{0'}$ depends on the experimental conditions employed and is often estimated through the experimentally determined $E_{1/2}$ value, i.e. the average potential between the cathodic and the anodic peaks (points C and F in Figure 2.6), where the concentrations of Fc^+ and Fc are the same and the logarithmic term becomes zero.

The Nernst equation allows predicting how a system will respond to changes in the electrode potential or concentration variations of species in solution. Resolving the equation, it is possible to predict that, under the application of a potential of $E = E^{0'} \approx E_{1/2}$, Fc^+ will be reduced to Fc until equilibrium is achieved ($[Fc^+] = [Fc]$). While the potential is scanned, the concentrations of the species in solution near the electrode change over time. The voltammogram reported in Figure 2.6 describes the process.

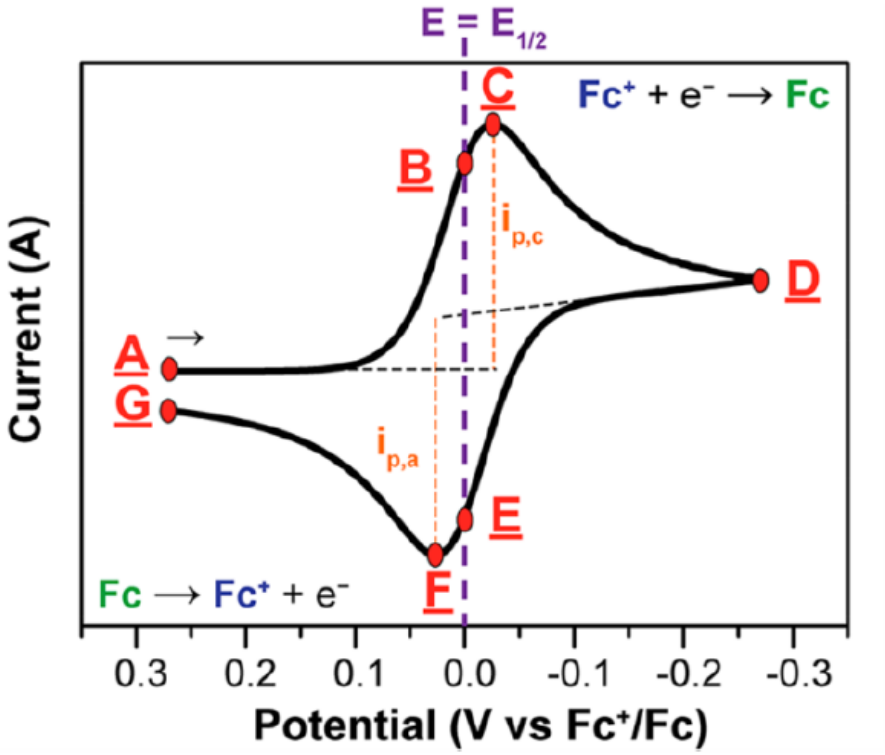

Figure 2.6 - Voltammogram of the reversible reduction of a Fc^+(ferrocenium) solution to Fc (ferrocene). Source: Elgrishi, N. et al., 2018 [4].

As the potential is scanned towards negative potentials (cathodically) from the starting point A (E_{start}) to the switch potential at point D, $[Fc^+]$ is steadily reduced to Fc, resulting in its depletion at the working electrode. The current increases from the residue value to a peak cathodic value ($i_{p,c}$), represented by point C.

The diffusion layer of Fc at the interface of the electrode continues to grow throughout the scan. This phenomenon slows down the rate of diffusion of Fc^+ from the bulk solution to the surface of the working electrode, causing a decrease in the current from point C to point D.

When the point D (switching potential) is reached, the scan direction is reversed, and the anodic trace is registered. As the applied potential becomes more positive, the Fc at the electrode surface is oxidised back to Fc^+. According to the Nernst equation, at points B and E equilibrium is reached, thus the concentrations of Fc^+ and Fc at the electrode surface are equal ($E = E_{1/2}$). As noted above, the $E_{1/2}$ value corresponds to the average potential between peaks C and F and allows us to estimate the formal potential $E^{0'}$.

As shown in Figure 2.6, if the redox process is reversible, the intensities of the anodic and cathodic peak currents are equal and the difference between their potentials (called peak-to-peak separation or ΔE_P) is 59 mV at 293 K. In this case, we observe a -so-called- "Nernstian" process,

because the fast electron transfers make the process electrochemically reversible and following the Nernst equation.

By contrast, when the process is electrochemically irreversible, the electron transfer requires more negative (or positive) potentials to observe redox reactions, giving rise to larger differences between the peaks' potentials (ΔEp) and more distorted, stretched, and flattened peaks. In fact, electrochemical reversibility is a result of fast electron transfer kinetics between the electrode and the analyte. Several species display intermediate behaviour between complete reversibility and irreversibility; for example, quasi-reversible redox reactions may occur.

Staircase Voltammetry.

Staircase Voltammetry (STCV) is a variant of LSV. It involves performing a stepwise scan, where the potential is increased at regular intervals, and the current is sampled in the last moments of the pulse, just before the next step.

Differential Pulse Voltammetry.

Differential Pulse Voltammetry (DPV) is derived from LSV O STCV, applying a periodic series of pulses with constant voltage, duration, and amplitude (Figure 2.7). By measuring the difference in current just before and at the end of the pulse, a differential measurement of the current is obtained, generating a peak-shaped voltammogram. DPV is a highly sensitive technique with detection limits around 10-100 μg L^{-1}.

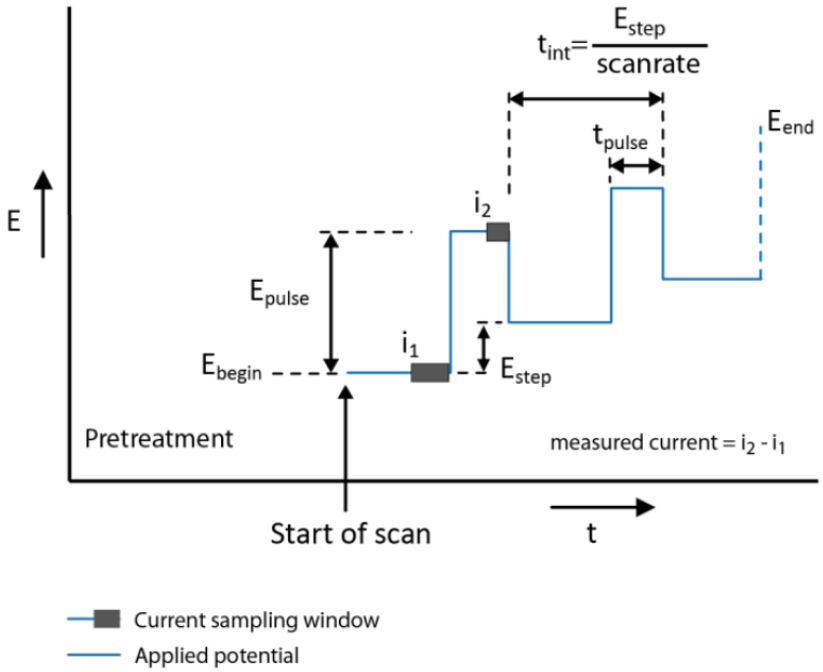

Figure 2.7 - Potential applied during Differential Pulse Voltammetry (DPV). Source: Metrohm PSTrace manual, 2019 [3].

Square Wave Voltammetry.

Square Wave Voltammetry (SWV) is an advancement of DPV. As Figure 2.8 shows, it applies a rapidly changing voltage in steps to the working electrode, overlaid with a square wave at a high

frequency (20-100 Hz). The current is sampled twice: at the end of the direct pulse and at the end of the return pulse. If the pulse is fast and the analysed redox couple is reversible, the electroactive species discharges in the first phase (e.g., reduces), while in the second phase, the reaction products undergo the reverse process (e.g., oxidize). The currents from the two processes add up, resulting in a more sensitive differential technique than DPV. Sensitivity can be increased by adjusting the square wave amplitude or frequency. Detection limits are on the order of 5-50 μg L^{-1}.

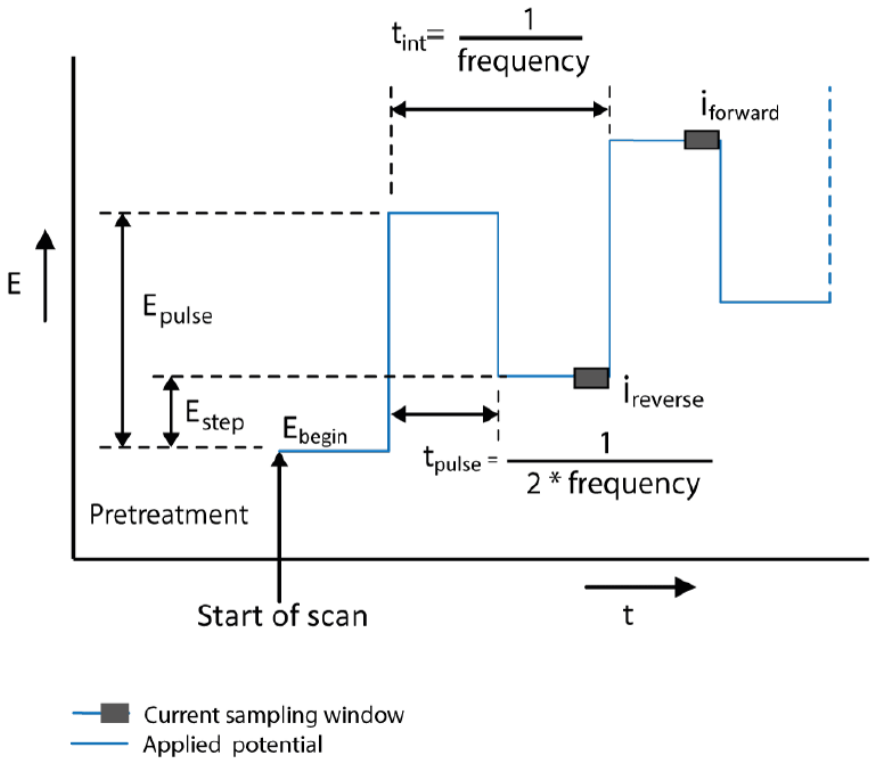

Figure 2.8 - Potential applied during Square Wave Voltammetry (SWV). Source: Metrohm PSTrace manual, 2019 [3].

Voltammetric stripping techniques

Each of the voltammetric methods previously described can be performed with stripping techniques [5].

These techniques are mostly used for trace analysis, since they allow to reach low limits of detection.

Voltammetric stripping analyses require two steps: firstly, the preconcentration of the analyte on the electrode surface; secondly, the stripping of the analyte.

The preconcentration step is carried out through the application of a proper potential, which allows the analyte to be accumulated on the electrode surface from the bulk solution. The duration of this step is inversely proportional to the concentration of the analytes. During this phase, the solution is stirred to ease the convective transport of the analyte. However, the stirring is stopped before moving on to the stripping step, to avoid any transport processes outside diffusion, and therefore have a better signal-to-noise ratio. The stripping step consists of a potential scan, giving rise to the oxidation of reduction of the species previously accumulated at the electrode.

Three different methods of performing voltammetric stripping analysis can be described:

- ✓ Anodic Stripping Voltammetry (ASV): based on the preconcentration of the analyte on the electrode surface by reduction, followed by an oxidative stripping step. ASV is generally used for the determination of metals.
- ✓ Cathodic Stripping Voltammetry (CSV): conversely to ASV, the preconcentration step is carried out in oxidative conditions. This leads to the generation of ions of the metal that constitutes the working electrode, which form slightly soluble salts with the analytes that accumulate at the electrode surface. The reduction of the metal during the stripping phase results in the release and indirect detection of the deposited species. CSV is usually adopted for the determination of inorganic and organic anionic compounds.
- ✓ Adsorptive Stripping Voltammetry (AdSV): it allows to perform trace and ultra-trace analysis of complex organic molecules and metal coordination complexes. The deposit of the analytes occurs by adsorption and the stripping is made by reducing the analytes through a cathodic scan or, less commonly, by oxidizing them during an anodic scan [6,7].

As noted above, these techniques allow the detection of low concentrations of analyte, since the preconcentration step leads to the accumulation of the analyte on the small surface of the electrode exposed to the solution, and therefore results in high stripping currents.

2.2 The electrochemical cell

Electrochemical cells are classified into:

- *Galvanic cells:* these cells involve a spontaneous reaction that generates a potential difference between the electrodes, leading to the production of electric current.

- *Electrolytic cells:* in these cells, an external source of electrical energy applies a potential, causing a non-spontaneous redox reaction.

For any voltammetric measure, an electrolytic cell is used. As these experiments require controlling the potential of an electrode immersed in the analytical solution while measuring the resulting current, at least two electrodes are needed. The working electrode (**WE**) assumes the required potential in a controlled way, and it is the one on which the reaction takes place. It facilitates the transfer of charge to and from the analyte. The second is the reference electrode (**RE**), which should act as the other half of the cell and must have a known potential. Moreover, the reference electrode should balance any charge added or removed by the working electrode. However, it is extremely difficult for this electrode to maintain a constant potential while passing current to balance redox events occurring at the working electrode. For this reason, the two tasks are split in the three-electrode cell, in which the reference electrode only acts as the half cell with a known potential, while the counter electrode (**CE**, also known as auxiliary electrode) passes the current needed to counteract the reactions at the WE.

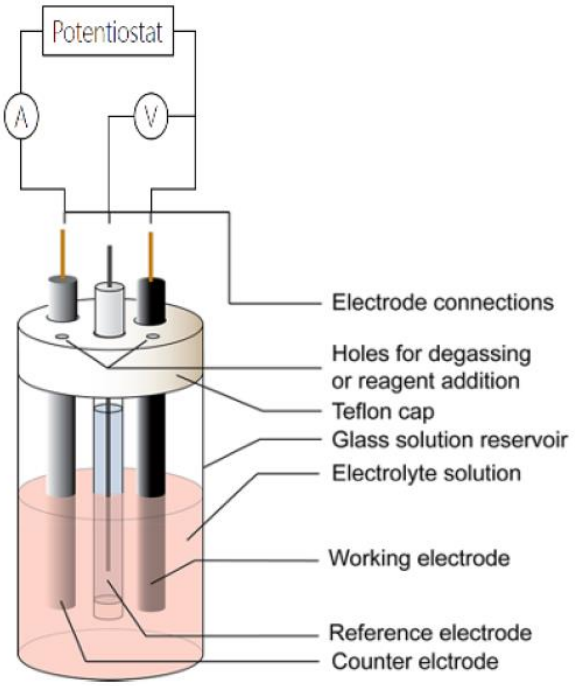

Figure 2.9 - Three-electrode voltammetric cell. Source: Elgrishi, 2018 [4].

As shown in Figure 2.9, the potential difference is set between the working and the reference electrodes, whilst the current flows between the working electrode and the counter electrode and is measured between them. Usually, the cell has a 5-50 mL capacity and it is filled with the sample solution; if the latter has a low ionic strength, a supporting electrolyte is added. The vessel can have different shapes and can be closed with a top designed to be fitted with the electrodes and a gas inlet/outlet for purging.

2.3 Electrodes

Counter Electrode (CE) or Auxiliary Electrode (AE)

The counter electrode is essential to balance any charge added or removed during the electrochemical reaction occurring at the working electrode. It is added to the two-electrode system so that only a negligible amount of current flows through the reference electrode. It can be made of any conductive material, even if it is usually a platinum wire or a graphite rod. Usually, the surface of the auxiliary electrode is larger than that of the working electrode to ensure that the kinetics of the half-reaction taking place at the auxiliary electrode is not a limit to the reaction occurring at the working electrode.

Reference Electrode (RE)

Reference electrodes has a constant potential, essential to know the potential applied to the WE and set it at the desired value. For this reason, voltammetry is classified as a controlled potential technique. The most widely used reference electrodes are saturated calomel (SCE) and Ag|AgCl electrodes.

The former is based on the redox equilibrium between elemental mercury and mercury(I) chloride:

$$Hg_2Cl_{2(s)} + 2e^- \rightleftharpoons 2Hg_{(l)} + 2Cl^-_{(aq)}$$

Hg_2Cl_2 (calomel) and Hg form two separate phases, so the potential of a calomel electrode is determined by the chloride concentration and is constant as long as [Cl^-] remains constant. The SCE is made of a glassware containing a saturated aqueous solution of KCl in contact with the mercury and the mercury(I) chloride (Figure 2.10). The electrical conductivity is assured by a platinum wire immersed in the liquid mercury and a porous frit maintains ionic contact between the KCl solution and the analytical one.

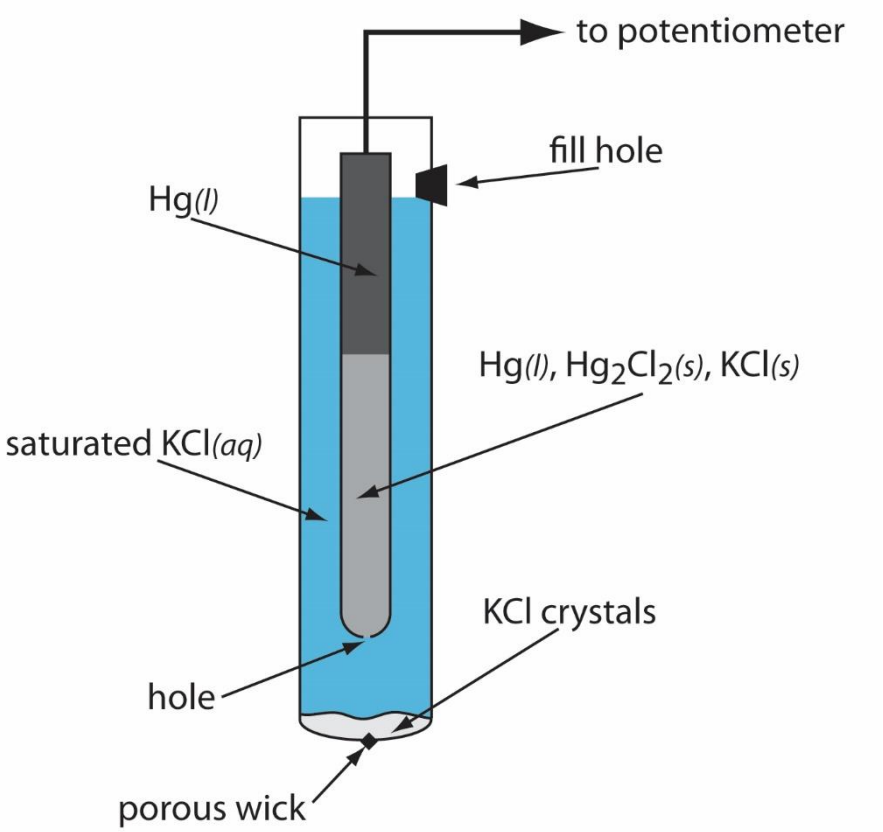

Figure 2.10 - Saturated Calomel Electrode (SCE).

The latter - Ag|AgCl electrode - has widely replaced the SCE, mostly for environmental reasons, even if the calomel electrode has a reputation of being more robust. The silver/silver chloride electrode functions on the basis of the redox equilibrium between the silver metal and its salt-silver(I) chloride:

$$AgCl_{(s)} + e^- \rightleftharpoons Ag_{(s)} + Cl^-_{(aq)}$$

The electrode is made by a silver wire coated with a thin layer of silver chloride, that can be deposited either by dipping the wire in molten silver chloride or by electroplating the wire in concentrated HCl or by oxidizing the silver in a chloride solution. As shown in Figure 2.11, the electrode body contains a saturated solution of KCl to stabilize the chloride concentration. As for the SCE, a porous frit allows contact between the analytic solution and the inner electrolyte, and the potential developed is determined by the chloride concentration in the RE body.

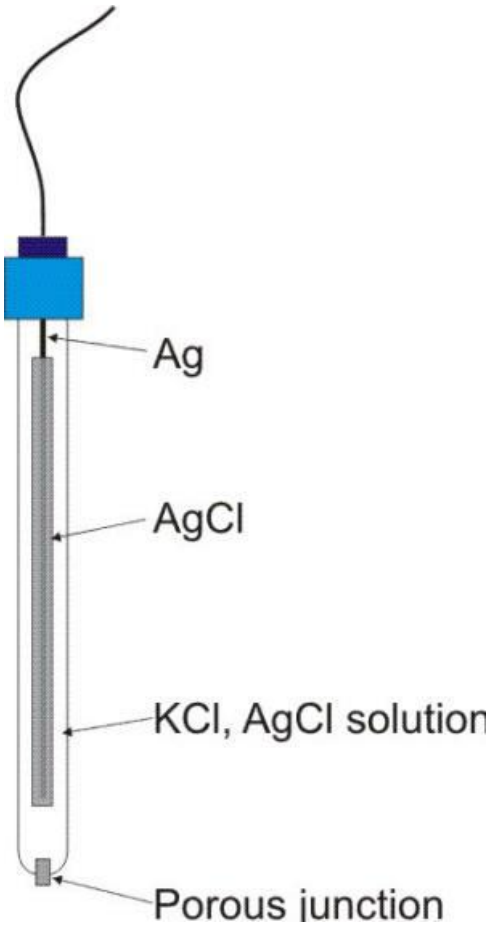

Figure 2.11 - Ag|AgCl|KCl reference electrode.

Working Electrode (WE).

Since it is the electrode on which the electrochemical reaction of interest occurs, its properties are crucial. Its material, composition, geometry and superficial area deeply influence the voltammetric analysis. A good WE should have a high signal-to-noise ratio, well-characterised geometry, low cost, should give reproducible results and should cover a wide range of potential values.

The choice of the WE is mainly made depending on the redox behaviour of the analyte and the background current in the potential range required for the analysis.

The most widely used materials are mercury, carbon or noble metals as platinum and gold.

References

[1] J. Wang, Analytical Electrochemistry, Third Edition. Wiley, 2006

[2] J. R. Maloy, "Factors affecting the shape of current-potential curves." *J. Chem. Educ.* 60, 285. 1983

[3] PSTrace manual (2019). PalmSens BV

[4] N. Elgrishi,K. J. Rountre, B.d. McCarthy, E. S. Rountree, T. T. Eisenhart, J. L. Dempsey, "A Practical Beginner's Guide to Cyclic Voltammetry" *J. Chem. Educ.* 95, 197−206, 2018, https://doi.org/10.1021/acs.jchemed.7b00361

[5] K. Brainina,E. Neyman, Electroanalytical Stripping Methods. John Wiley & Sons. 1983

[6] T. R. Copeland, R. K. Skogerboe, "Anodic stripping voltammetry." *Anal. Chem.* 46, 1257A–1268A, 1974, https://doi.org/10.1021/ac60350a021

[7] W. D. Ellis, "Anodic stripping voltammetry." *J. Chem. Educ.* 50, A131, 1973, https://doi.org/10.1021/ed050pA131

[8] C. D. Harris, Quantitative Chemical Analysis. IX. W.H. Freeman & Co. 2015

EXPERIMENTAL SECTION

3. MERCURY – METHYLMERCURY IN FISH SAMPLES

3.1 General introduction

All the work conducted during the doctoral research regarding the speciation of mercury in fish products has been published in two significant scientific papers, which will be reported below.

The first article reports the procedure for on-site determination of total mercury and inorganic mercury in fish samples. The second paper deals with the next stage of the work in which the procedure was improved to allow the direct methylmercury determination.

3.2 Published research papers

3.2.1 Development of an easy portable procedure for on-site determination of mercury and methylmercury

Agnese Giacomino [a] *, Andrea Ruo Redda [a], Rocco Caligiuri [b], Paolo Inaudi [a], Stefania Squadrone [c], Maria Cesarina Abete [c], Ornella Abollino [a], Sara Morandi [b], Eleonora Conca [b], Mery Malandrino [b]

[a] Department of Drug Science and Technology, University of Torino, Via Pietro Giuria 9, 10125 Turin, Italy

[b] Department of Chemistry, University of Torino, Via Pietro Giuria 5, 10125 Torino, Italy

[c] Istituto Zooprofilattico Sperimentale del Piemonte, Liguria e Valle d'Aosta (IZSPLV), 10100 Torino, Italy

* Corresponding author

Received: 15 July 2020

Revised: 2 October 2020

Accepted: 7 October 2020

Published: 12 October 2020

https://doi.org/10.1016/j.foodchem.2020.128347

FOOD CHEMISTRY – 2021, 342, 128347

3.2.2 Abstract

A portable measurement and speciation procedure for inorganic mercury (Hg_{IN}) and methylmercury (CH_3Hg) was developed. A portable sample pretreatment was optimized to determine total mercury content. A new homemade sorbent (CYXAD, CHYPOS 101 modified Amberlite XAD), was prepared to separate Hg_{IN} and CH_3Hg. Mercury species were determined using square wave anodic stripping voltammetry (SW-ASV) with a solid gold electrode (SGE) and using a portable potentiostat. A certified reference material, five freeze-dried samples and three fresh samples were analysed with conventional voltammetric analyzer, after dissolution of the samples in microwave oven, and with a portable potentiostat after the mild eating procedure. The results obtained by SWASV were compared with those obtained using Direct Mercury Analyser (DMA). The quantification with the portable method is comparable to that obtained with the DMA. Retention tests showed the selectivity of CYXAD for Hg_{IN}, its stability and the possibility to re-use the same aliquot of resin.

3.2.3 Introduction

Mercury is one of the most toxic heavy metals present in nature. It is released into the environment from natural sources and human activities, such as gold mining and burning of fossil fuels (Horowitz et al., 2014); thereafter, it reaches human beings mainly through ingestion of food (Ariya et al., 2015; Voegborlo & Adimado, 2010). In particular, elemental mercury in aquatic ecosystems is firstly oxidized in the inorganic form (Hg_{IN}), then sulphate and iron reducing bacteria (SRB and IRB) transform it into its methylated forms (Cossa et al., 2009) and, finally, it accumulates in fish as methylmercury (CH_3Hg).

Fish is considered one of the best sources of important substances for the human diet, providing, for instance, omega 6, useful against hypertension, coronary heart diseases and cancer, as well as high quality proteins and nutrients, such as selenium and antioxidants (Costa et al., 2015; Galimberti et al., 2016). However, the accumulation of CH_3Hg in fish tissues results in the incorporation of mercury into the food chain (de Paiva et al., 2017; Savery et al., 2013).

Several studies have been carried out on the damage to human health caused by mercury. A multi-year (2004–2011) work by the European Food Safety Authority (EFSA) («EFSA, 2004-2011», s.d.) showed that the presence of Hg and, in particular of CH_3Hg, causes neurodevelopmental, neurological and locomotion deficits, cardiovascular diseases and carcinogenicity.

Moreover, CH_3Hg can also compromise brain development in fetuses, since it is able to cross the placental barrier causing damages in the development phase of the fetus. CH_3Hg has a high affinity for sulphide groups of proteins and enzymes, therefore it is effectively absorbed in the gastrointestinal tract and easily passes both the ematoencephalic barrier and the placenta (Baer et al., 2011). Over the years, the Food Drug Administration (FDA) has issued a warning for pregnant and breastfeeding women to reduce their consumption of fish such as swordfish, needlefish, dogfish and tuna, which, due to their high mercury content, could compromise the development of normal cognition in fetuses and children.

In the European Legislation, a maximum limit of CH_3Hg in food has not been established yet. Provisional Tolerable Weekly Intake (PTWI) of 1.3 mg kg^{-1} CH_3Hg and 4 mg kg^{-1} Hg body weight were set (EFSA, 2012), while the maximum levels of total mercury (Hg_{TOT}) were 0.5 mg kg^{-1} for small

and medium fishes, mussels and most of seafood and 1 mg kg^{-1} for predatory fish respectively (2006/1881/EC, s.d.).

For all these reasons it is very important to be able to discriminate between the inorganic and organic forms of mercury in food. Several techniques have been used for Hg determination: classical methods include cold vapor atomic fluorescence spectrometry (CV-AFS) (Zhang et al., 2016), cold vapor capacitively coupled plasma microtorch optical emission spectrometry (CV-μCCP-OES) (Frentiu et al., 2015), gas chromatography (GC) (Renedo et al., 2017) and high-performance liquid chromatography (HPLC) (Wang et al., 2010) combined with a variety of detection techniques such as atomic absorption spectroscopy (AAS) (Lemos et al., 2013), inductively coupled plasma mass spectrometry (ICP-MS) (Renedo et al., 2017) or optical emission spectroscopy (OES) (Fernández et al., 2015), and capillary electrophoresis (CE) (Kubáň et al., 2007). Alternative methods include Direct Mercury Analyzer (DMA) (Squadrone et al., 2015) or electrochemical techniques, such as anodic stripping voltammetry (ASV) (Chaiyo et al., 2014; Giacomino et al., 2017; Laffont et al., 2015; Somerset et al., 2010), potentiometric stripping analysis (PSA) and current stripping chronopotentiometry (CSP).

All these techniques for monitoring mercury concentration in food (fish, in particular) present some drawbacks: some methods require very expensive instruments and/or highly specialized personnel and they either do not allow to perform on-site real time measurements or they not allow speciation studies.

The scientific literature continues to focus the attention on the improvement of the sensitivity of the electrochemical methods. For this purpose, many interesting chemical modifications have been proposed for different pollutants (Kokab et al., 2020; Ottakam Thotiyl et al., 2012; Shang et al., 2020; Shang, Xu, Jin, et al., 2019; Shang, Xu, Liu, et al., 2019), and, in particular, for Hg determination (Giacomino et al., 2017; Ruo Redda et al., 2019). In fish very low limits of detection (LODs) have been obtained, for example, using a gold nanoparticle modified glassy carbon electrode (Giacomino et al., 2017) or multiwalled carbon nanotubes gold nanoparticles (Bagheri et al., 2013; Ramezani et al., 2015) with value of 0.001 μg L^{-1}, 0.0003 μg L^{-1} and 0.19 μg L^{-1}, respectively.

The main drawback of modified electrodes is that they are often not applicable for routine analysis.

The aim of this paper is to report the development and validation of a simple analytical method (patent pending) that allows to overcome the problems previously exposed. For this reason, a commercial solid gold electrode (SGE) is applicable for quality control purposes, since the maximum admissible level of mercury in fish is higher than the limit of quantification obtained by voltammetry with this electrode (Giacomino et al., 2017).

The method is coupled to a kit for on-site analysis, e.g. on boats or in ports, in order to have a quick quantification of both Hg_{IN} and CH_3Hg content in freshly fished fish.

A certified reference material (Tuna Fish ERM-CE 464), five freeze-dried fishes and three fresh fishes were analysed. The results were compared with those obtained using Direct Mercury Analyser (DMA), considered as a reference method for Hg and CH_3Hg determination, to evaluate the real applicability, advantages and disadvantages of the proposed technique.

3.2.4 Material and methods

3.2.4.1 Instruments and reagents

Sample dissolutions were performed in polytetrafluoroethylene (PTFE) vessels, using Milestone MLS-1200 Mega (Milestone, Sorisole, Italy), a microwave laboratory unit.

The portable sample pretreatment was performed using a commercial food warmer, which can be used in the field combined with a portable battery. The samples, contained in 50 mL Falcon tubes, were heated in "bain-marie".

The electrochemical analyses carried out in laboratory (hereinafter referred to as laboratory procedure or ASV_{lab}), were performed with a PGSTAT 10 potentiostat (Eco Chemie, Utrecht, Netherlands) coupled to a 663 VA Metrohm (Herisau, Switzerland) stand. The analyser was interfaced with a personal computer; the operational conditions were selected and voltammograms were recorded and processed through the IME 663 interface and the GPES software (General Purpose Electrochemical System).

The electrochemical on-site analyses (hereinafter referred to as portable procedure or ASV_{port}) were performed using a PalmSens^3 portable potentiostat (PalmSens, Houten, Netherlands). It was interfaced with a tablet or laptop computer and the software PSTrace 4.6 was used to set the process parameters. The potentiostat was connected to a KIA-Topolino magnetic stirred and fed with a portable battery.

The voltammetric cell, equipped with a commercial Metrohm solid gold electrode (SGE), a glassy carbon counter electrode and an Ag/ AgCl/KCl (3 M) reference electrode, was the same for the two instruments.

All the reagents were of analytical grade. Standard solutions of Hg were prepared from 1000 g· L^{-1} Sigma-Aldrich solutions. CH_3Hg standard solutions were prepared in 0.01 M nitric acid, using the necessary safety devices, from methylmercury chloride powder (Pestanal, analytical standard, Sigma Aldrich) stored away from light to prevent decomposition.

Nitric acid (65%, Sigma Aldrich), hydrogen peroxide (Sigma Aldrich) and hydrochloric acid (ACS Reagent, 37%, Honeywell Fluka) were also used.

The atomic absorption spectrometry analyses were made using a DMA-80 Direct Analyser (FKV SrL, Torre Boldone, BG, Italy) in Istituto Zooprofilattico Sperimentale del Piemonte, Liguria e Valle d'Aosta (IZSPLV) laboratory in Torino. Analytical grade reagents were used.

A 1000 mg L^{-1} standard solution of mercury was prepared from $HgCl_2$ in 0.012 M HCl. More diluted Hg standard solutions were prepared from the concentrated standard. Calibration standards for DME-80 were prepared using a NIST traceable stock solution of 1000 mg L^{-1} Hg preserved in 5% HNO_3. Working standards of 0.1 and 1 mg L^{-1} were prepared, preserved in 3.7% HCl and stored in amber glass vials. All solutions were prepared in ultrapure water (Milli-Q, Milli-pore, 18.2MΩ cm).

A commercial polymeric sorbent, i.e. Amberlite XAD-1180 (Sigma Aldrich), was used after modification with a commercial ionic liquid (IL), namely trihexyl(tetradecyl)phosphonium chloride (CYPHOS 101 solution, Sigma Aldrich) to separate inorganic and organic Hg species. The modified polymeric sorbent is named CYXAD (CYPHOS-modified XAD) in the following.

Absorption/transmission infrared (IR) spectra were run on a Perkin- Elmer FT-IR 2000 spectrophotometer equipped with a Hg-Cd-Te cryodetector, working in the range of wavenumbers 7200–1000 cm^{-1} at a resolution of 2 cm^{-1} (number of scans, ~60). For IR analysis, XAD-1180 and

CYXAD were diluted in KBr and then were pelletized in selfsupporting disks. IR spectra were collected in air at room temperature.

3.2.4.2 Samples

The reference material, namely Tuna Fish ERM-CE 464 ([Hg_{TOT}] = 5.24 ± 0.10 mg kg^{-1}; [CH_3Hg] = 5.50 ± 0.10 mg kg^{-1}), was analysed to evaluate efficiency and accuracy of each adopted technique. Five samples, namely fillet of dogfish (S1), slice of tuna fish (S2), cat food (S3), canned tuna (S4) and cormorant's liver (S5) were firstly lyophilized and subsequently analyzed; other three samples, namely slice of swordfish (S6), Marlin Blue (S7) and slice of emery fish (S8), were analyzed fresh, as received, in order to demonstrate the applicability of the proposed technique for on-site analysis. The whole list of samples is reported in Table 1. All the samples were provided by the IZSPLV laboratory and they were samples in the northwestern Italy. Fish and pet food samples

Table 1 List of samples with correspondent code and sample pretreatment.

Code	Sample	Sample form
RM	Tuna Fish ERM-CE 464	Freeze-dried
S1	Fillet of dogfish	Freeze-dried
S2	Slice of tuna fish	Freeze-dried
S3	Food for cat	Freeze-dried
S4	Canned tuna	Freeze-dried
S5	Cormorant's liver	Freeze-dried
S6	Slice of swordfish	Fresh
S7	Marlin Blue	Fresh
S8	Slice of emery fish	Fresh

were received at the IZSPLV laboratory as part of official controls. The cormorant liver was a sample inherent in the wild species monitoring plan in which IZSPLV laboratory is involved.

3.2.4.3 Procedures

3.2.4.3.1 ASV analysis

3.2.4.3.1.1 *Extraction of Hg_{TOT}*. Two aliquots of each sample were simultaneously subjected to two different pretreatment procedures for the determination of the total content of mercury.

Conventional procedure. 0.5 g of lyophilized sample or 1 g of fresh fish were placed in contact with 3 mL of HNO_3 and 3 mL of H_2O_2 in the vessels of the microwave oven. The following heating program of the microwave unit was adopted: 250 W for 1 min; 0 W for 1 min; 250 W for 5 min; 400 W for 5 min; 650 W for 5 min; ventilation for 25 min. The vessels were then left to cool at room temperature. The solutions were filtered through Whatman Grade 5 cellulose filters, then diluted to 15 mL with HPW. Afterwards, the solutions were analysed using ASV_{lab}.

Portable procedure. 0,5 g of reference material were placed in contact with different extractant solutions, namely mixture 1: HNO_3/H_2O_2 = 1:1 (the same adopted for microwave digestion); mixture 2: H_2SO_4 / HNO_3 / $HClO_4$ = 5: 1: 1 ratio (Ruo Redda et al., 2019) and mixture 3: $HNO_3/HCl/H_2O_2$ = 5: 1:1 (suggested by the producer of the microwave oven).

The sample and the digestion mixtures were put into 50 mL Falcon test tubes and heated for 20 min at 60–70 °C by immersion in a "bainmarie" in a portable food warmer. Then, the suspension

was filtered through 0,45 μm PTFE syringe filters and the filtrate was diluted to 15 mL with HPW. Afterwards, the solutions ($SolHg_{TOT}$) were analysed with ASV_{port}.

0.5 g of samples S1-S5 or 1 g of samples S6-S8 were treated with the same procedure using mixture 1 (see Paragraph 3.1).

3.2.4.3.1.2. *Speciation scheme with ASV*. Two aliquots of each sample were simultaneously subjected to the two different pretreatment procedures. One aliquot was digested as described in 3.2.4.3.1.1 using the portable procedure for the determination of Hg_{TOT} ($SolHg_{TOT}$), while the other aliquot was treated for the determination of inorganic mercury, Hg_{IN} as follows. 0.5 g of lyophilized sample or 1 g of fresh sample were placed in contact with 8 mL of 12 M HCl in a test tube and heated for 20 min at 60–70 °C as described in Paragraph 3.2.4.3.1.1. The solution was then diluted 1: 3 with HPW to obtain a concentration of chloride ions of about 4 M, at which the maximum resin efficiency is achieved. The solution was driven through a column holder containing the cartridge packed with the CYXAD solid phase (described in Paragraph 3.2.4.3.1.4): the latter retained Hg_{IN} quantitatively, while CH_3Hg was eluted. The eluate containing CH_3Hg was discarded because it had a too high Cl- content that would damage the surface of the SGE.

The recovery of Hg_{IN} immobilized on the CYXAD took place by elution with 5 mL of 6 M HNO_3 ($SolHg_{IN}$).

3.2.4.3.1.3. *ASV measurement*. The SGE was polished and activated following the procedure reported in our previous paper (Ruo Redda et al., 2019). During all the analyses, there was no need to renew electrode surface with alumina powder.

Aliquots of 2 mL of solutions for the determination of Hg_{TOT} and Hg_{IN} were transferred into the voltammetric cell and diluted to 20 mL with 60 mM HCl. After 120 s of deposition at 0 V, a voltammetric scan was performed, adopting the parameters, previously optimised in our laboratory (Abollino et al., 2008).

After each determination the electrode was maintained in a mixture of 0.2 M $HClO_4$/3 mM NaCl/1 mM NaEDTA for 30 s at 0.80 V, to remove residues of mercury from its surface.

Each sample was analysed in duplicate. The quantification of mercury concentrations in the solutions was carried out using the standard additions method. After recording the voltammogram of the sample solutions, aliquots of Hg at known concentration were added and the corresponding signals were recorded. The contents of Hg_{TOT} (for both ASV_{lab} and ASV_{port}) and Hg_{IN} (ASV_{port}) were thus determined. In the case of the portable procedure, the concentration of CH_3Hg was obtained by difference from these two values ($[CH_3Hg] = [Hg]_{SolHgTOT} - [Hg]_{SolHgIN}$).

3.2.4.3.1.4. *The new sorbent material "CYXAD". Preparation of CYXAD-sorbent*. An aliquot of a commercial resin Amberlite XAD-1180 was washed with HPW, 1 M hydrochloric acid and ethanol, consecutively. After that, the resin was dried at room temperature. Then, it was functionalized with a commercial ionic liquid (IL), namely trihexyl (tetradecyl)phosphonium chloride (CYPHOS 101), with a ratio resin:IL = 2:1 in 5 mL of ethanol for 6 h. The suspension was filtered through a polytetrafluoroethylene (PFTE) filter (diameter = 0.45 μm) and the solid phase obtained (CYPHOS-modified XAD, called CYXAD) was dried for 1 h in an oven at 60 °C, then stored at room temperature. An aliquot of CYXAD was inserted in a polyethylene tube (diameter = 4,5 mm). The CYXAD sorbent is stable and can be stored for long periods, making it possible to prepare batches of packaged cartridge ready for use.

The cartridge was inserted into the central part of a column support having a suitable housing, fitted with an inlet and an outlet tube at the ends to allow for the passage of the sample solution (Fig. 1, Fig. S1).

Retention/recovery test. The performance of the CYXAD-sorbent was tested by passing 10 mL aliquots of a 40.0 μg L^{-1} solution of CH_3Hg or Hg_{IN} in 4 M HCl and washing each time the resin with 5 mL of 6 M HNO_3 to elute retained Hg_{IN}. The three aliquots were collected after flowing through the column, diluted (1:10) and analysed by ASV. CH_3Hg or Hg_{IN} concentrations were determined and compared to the initial concentration of the solution in order to obtain the recovery percentage. The quantification of each analyte concentration was carried out using the standard addition method, by adding aliquots of CH_3Hg or Hg_{IN} at known concentration into the voltammetric cell.

Subsequently, the efficiency of the resin was evaluated by driving 20 mL aliquots of synthetic solutions containing both CH_3Hg and Hg_{IN}, at a concentration of 20 μg L^{-1} through the column, then the resin was washed with 5 mL of 6 M HNO_3 to elute Hg_{IN}. The synthetic solutions after flowing through the column and the acid eluate were analyzed by ASV to assess mercury retention and recovery.

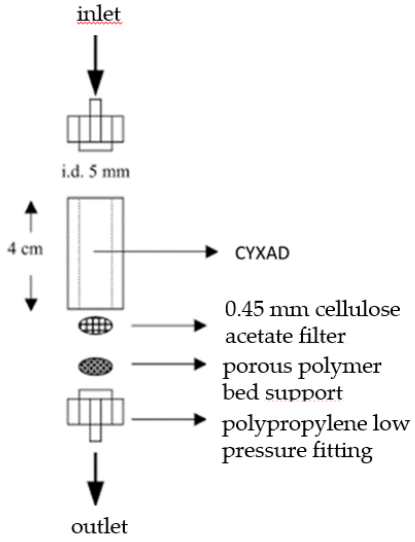

Fig. 1. The support column contained the cartridge filled with CYXAD.

3.2.4.3.2 DMA analysis

3.2.4.3.2.1. *Determination of Hg_{TOT}*. For the determination of Hg_{TOT} with DMA, as reported in the U.S. EPA Method 7473 (EPA, Method 7473, 2007), the analysis was performed directly on three aliquots (0.2–0.5 g) of each sample, since no other pretreatment was required.

3.2.4.3.2.2. *Speciation scheme with DMA.* The method for the determination of CH_3Hg with DMA is based on a double liquid–liquid extraction, first with an organic solvent and subsequently with L-cysteine, according to the protocol proposed by Cordeiro et al (Cordeiro et al., 2013). The obtained solution was then introduced into the DMA and analyzed.
Specifically, the sample preparation procedure involved several steps:

1. All the glasswares used for this procedure were left immersed in 10% (V/V) HNO_3 for 24 h;

2. 0.7–0.8 g of fresh fish sample or 0.2 g of lyophilized sample and 0.5 mL of ultrapure water were inserted into a 50 mL Falcon tube; 10 mL of hydrobromic acid were added and manually stirred;

3. 20 mL of toluene were added and the solution was vigorously shaken with vortex for at least 2 min and then centrifuged for 10 min at 3000 rpm;

4. If, after centrifugation, an emulsion phase between the two phases was present, it was broken down by slightly tapping the test tube against the laboratory bench, and centrifugation was repeated;

5. About 15 mL from the overlying organic phase were withdrawn and transferred into a 50 mL Falcon tube containing 6.0 mL of 1% L-cysteine solution;

6. About 15 mL of toluene were added into the initial centrifuge tube a second extraction with the organic phase was repeated; after centrifugation, the remaining upper organic phase was withdrawn and inserted into the previous 50 mL tube with the L-cysteine solution;

7. The solution was vigorously shaken with vortex for at least 2 min and centrifuged for 10 min at 3000 rpm; an aliquot of 2–3 mL from the lower phase was then withdrawn with a Pasteur pipette, taking care not to drag toluene, transferred into a glass vial and stoppered (Squadrone et al., 2015).

3.2.5 Results

3.2.5.1 Determination of total Hg concentration

The recovery (%) obtained for RM with the portable extraction using the three mixtures were 95%, 90% and 70% for mixture 1, 2 and 3 respectively. The best results were obtained using the HNO_3/H_2O_2 extractant solution, probably because it is very effective for the degradation of organic matter even using a mild heating. The dissolution reaction proved to be slightly exothermic and the final solution was easily filterable even with a paper filter.

When mixture 2 was used, the dissolution reaction was strongly exothermic, and the consistency of the final solution was very viscous, causing many problems during the filtration phase. The digestion with mixture 3 generated a lot of foam during the filtration step.

Therefore, all the samples were digested with HNO_3: H_2O_2 1: 1, because this mixture proved to be the most effective and the easiest to use for in-field analysis.

The performances of SGE for the determination of Hg_{IN} in aqueous solutions were shown in our previous work (Abollino et al., 2008), which reports the repeatability, linearity, accuracy and detection limit of the procedure. Briefly, the height of the Hg peak increased with increasing deposition time; a value of 120 s was found to be suitable for concentrations excess of 50 $\mu g\ L^{-1}$. In synthetic solution, the limit of detection (estimated as LOD = $3\sigma B$/slope) was 0.40 $\mu g\ L^{-1}$ and the sensitivity was 1.71 $\mu A/\mu g\ L^{-1}$; 1 $\mu g\ L^{-1}$ of Hg was quantified as $1.00 \pm 0.01\ \mu g\ L^{-1}$.

Working in fish-matrices, the peak shape remained almost unchanged when the scan parameters were varied. The repeatability was evaluated with 10 replicates on 10 different cells containing the same sample. The relative standard deviation was 3.70%. This value can be considered satisfactory, taking into account the relatively low concentration level and the matrix involved. Moreover, the interference of several ions (As(V), Bi(III), Cd(II), Co(II), Cr(III), Cu(II), Fe(II), Mn(II), Ni(II), Pb(II), and Se(IV)) on the Hg signal was investigated.

The voltammogram of a standard solution with 3 μg L^{-1} of Hg was recorded in the presence of each element (added in 1:100 and 1:1000 concentration ratios with respect to the analyte). As our previous study and other researchers found, no interference was observed and the linearity of the calibration curve of mercury was maintained also in the presence of 3 mg L^{-1} of the other ions in the electrochemical cell.

Table 2 reports the main parameters of the proposed method compared with those of the DMA referred to the determination of Hg_{IN}. DMA has a greater sensitivity than the proposed method, but LOQ (in fish matrix) ASV_{port} is lower than the legislative limit for Hg in fish, so it is broadly sufficient to assess the healthiness of a fish product.

Table 3 shows the results for $[Hg]_{TOT}$ determined with laboratory (digestion and ASV_{lab}) and portable procedure (portable extraction and ASV_{port}), compared with the results obtained using the DMA used as "reference concentrations". Fig. S2 shows an example of voltammogram obtained for samples.

The recovery obtained for RM, 96.0% and 93.3% for $[Hg]_{ASV\ port}$ and $[Hg]_{ASV\ port}$, respectively, showed a very good accuracy of the results for both the procedures.

By analyzing the recovery percentages, calculated with respect to the DMA value, it was possible to see that for $[Hg]_{ASV\ lab}$ the %rec/ $[Hg]_{DMA}$ were in the range 81.5 – 110.3%, while for $[Hg]_{ASV\ port}$ the % rec/$[Hg]_{DMA}$ were in the range 81.5 – 113 %.

Table 2. Analytical parameters of ASV_{port} and DMA (LOD = Limit of Detection; LOQ = Limit of Quantification)

Parameters	**Matrix**	**$[Hg_{TOT}]_{DMA}$**	**$[Hg_{iTOT}]_{ASVport}$**
Linear range	*Blank*	*0.010-1.5 mg*	*0.2-100 mg L^{-1}*
R^2	*Blank*	*0.9996*	*0.9991*
Sensitivity	*Blank*	*3.2 Abs/mg[a]*	*1.71 μA/μg L^{-1}*
LOD	*Blank*	*0.001 μg*	*0.02 μg L^{-1}*
LOQ_{cell}	*Blank*	*0.010 mg*	*0.2 μg L^{-1}*
LOQ_{cell}[b]	*Fish*	*0.037 mg*	*0.5 μg L^{-1}*
LOQ_{FS}[c]		*0.037 mg kg^{-1}*	*0.3 mg kg^{-1}*

[a]Absorbance units [b] Measured concentration in cell [c] Corresponding concentration in the fresh sample

Table 3. $[Hg]_{TOT}$ (mg kg^{-1}) and % of recovery determined by ASV with respect to $[Hg]_{TOT}$ found with DMA (**$[Hg]_{DMA}$**). For RM the recovery with respect to the certified value is also reported (**$[Hg]_{c.v.}$**).

Sample	$[Hg]_{ASV\ lab}$	$\%rec/[Hg]_{DMA}$	$[Hg]_{ASV\ port}$	$\%rec/[Hg]_{DMA}$	$[Hg]_{DMA}$
RM	5.03 ± 0.04 (95.9)*	100.6	4.89 ± 0.56 (93.3)*	97.8	5.00 ± 0.01 (95.4)*
S1	5.64 ± 0.42	104.4	5.16 ± 0.01	95.6	5.40 ± 0.01
S2	2.08 ± 0.38	98.6	2.40 ± 0.08	113.7	2.11 ± 0.04
S3	0.22 ± 0.01	81.5	0.22 ± 0.01	81.5	0.27 ± 0.01
S4	1.21 ± 0.08	88.3	1.21 ± 0.08	88.3	1.37 ± 0.04
S5	4.22 ± 0.11	101.4	4.39 ± 0.14	105.5	4.16 ± 0.03
S6	2.67 ± 0.34	110.3	2.56 ± 0.29	105.8	2.42 ± 0.04
S7	2.02 ± 0.13	98.1	2.07 ± 0.12	100.5	2.06 ± 0.03
S8	2.61 ± 0.51	90.0	2.98 ± 0.21	102.8	2.90 ± 0.05

* $\%rec/[Hg]_{c.v}$

For S1, S2, S5, S6, S7 and S8 recoveries higher than 95.5% were obtained. For S3 and S4 the $\%rec/[Hg]_{DMA}$ was lower, due to the low analyte content in these samples.

For all the samples, a good correlation (Fig. S3) was observed between $[Hg]_{ASV\ lab}$ and $[Hg]_{ASV\ port}$.

The results obtained for $[Hg]_{TOT}$ with the proposed method (ASV_{lab}), proved to be not significantly different from those obtained with the official method. R2 values equal to 0.9948 and 0.9925 were obtained for ASV_{port} and ASV_{lab}, respectively.

The t-test was applied and the results were not significantly different at a level of confidence of 95% ($p < 0.05$) for all the considered samples.

The good recoveries obtained with fresh fish (S6, S7 and S8) can be explained considering the effect of the water present in the sample, which improves the efficiency of the extraction ("wetting techniques" are sometimes adopted for microwave oven digestions). In particular, the recoveries obtained using the portable procedure with respect to the concentrations found with DMA, were better than those obtained with the conventional procedure. The compliance observed between

$[Hg]_{ASV}$ port and $[Hg]_{DMA}$ for fresh samples was a very important result, considering the final application of the proposed method.

3.2.5.2 Speciation

The method is based on ASV coupled to separation of Hg_{IN} and CH_3Hg by solid phase extraction and was applied to the analysis of fresh and freeze-dried fish.

The first step of the developed portable procedure consists of a very simple sample pretreatment, i.e. a small commercial food warmer was used for performing the extracting step, instead of the commonly adopted microwave oven. The efficiency of the portable pretreatment was compared with that obtained using a microwave laboratory unit. Then, home-made cartridges were packed with an Ionic Liquid (IL) modified resin (Escudero et al., 2013). Recently, considerable interest has been manifested in the use of ILs as an alternative to regular solvents. Ionic liquids display unique physicochemical properties, including air and moisture stability, good thermal stability even at high temperatures, very low volatility, relatively favorable viscosity and miscibility with water and organic solvents, as well as good extractability for several ions (Guibal et al., 2008).

CYPHOS, a class of phosphonium derivatives, is one of the most widely used ILs and can be used for extraction of ionic species, but has been developed mainly for the purpose of immobilizing metals (Marták & Schlosser, 2006). ILs can be immobilized on a solid matrix so that it can perform its action and trap ions when put in contact with a sample solution. The solid support is then treated with an extractant solution, in order to recover the ions and, then, it is washed and can be reused. In this work, a commercial polymeric sorbent, Amberlite XAD-1180 (Arias et al., 2011) was modified with CYPHOS 101 obtaining a modified adsorbent material, called CYXAD. This new material permitted to separate inorganic and organic Hg species.

In order to differentiate between Hg_{IN} and CH_3Hg, the two species were separated by solid phase extraction. Extraction with 4 M HCl gives rise to two different species in solution: $Hg_{in}Cl_4^{2-}$ anion and a CH_3HgCl neutral complex. According to Escudero et al. (Escudero et al., 2013), $Hg_{in}Cl_4^{2-}$ would probably interact with tetradecyl(trihexyl)phosphonium cation bound to CYXAD, exhibiting an anion exchange mechanism with Cl^- counterions. This would also explain the inability of CH_3HgCl to be retained by the resin. Other authors suggested that anion-pairing mechanisms could be involved in the retention of $Hg_{in}Cl_4^{2-}$ on CYXAD (Vincent et al., 2008).

3.2.5.1 Retention test

The three aliquots of 10 mL of CH_3Hg standard solution were analysed with ASV after their elution through the column. The recovery expected in this case was about 100%, since no retention should occur for the organic form. The results confirmed this hypothesis, since the recoveries were all above 95%: 98.0% (39.2 μg L^{-1}), 95.3% (38.1 μg L^{-1}) and 97% (38.8 μg L^{-1}) for the three aliquots respectively.

In the case of the three aliquots of Hg_{IN} standard solutions, the concentrations measured after the elution through the column were below the LOQ (< 0.1 μg L^{-1}), demonstrating the quantitative adsorption of Hg_{IN} on the sorbent. HNO_3 was eluted through the column and the solution was then analysed: the use of HNO_3 caused the release of Hg with a recovery of 103.3% (62.1 μg L^{-1} compared to an expected concentration of 60 μg L^{-1}).

Regarding the experiments with mixtures of both analytes, the results were very satisfactory, since the recovery percentage of CH_3Hg was 99.7% (79.7 μg L^{-1} compared to an expected concentration of 80 μg L^{-1}) demonstrating the very good selectivity of the retention on CYXAD.

3.2.5.2 IR analysis of CYXAD

Infrared spectroscopy was used to gain insight into the interaction between XAD-1180 and CYPHOS IL 101. In Fig. S4 the spectrum of XAD-1180 (black line) is compared with that of CYXAD (light grey line) in the region characteristic of C-H and aromatic C-C stretching modes. In particular, the bands related to $\nu(C^{sp2}\text{-}H)$ and ν(C-C) modes of the aromatic rings and to $\nu(C^{sp3}\text{-}H)$ modes of the alkyl chains are detected in the ranges 3120–3000, 1650–1570 and 3000–2800 cm^{-1}, respectively. For defining the modifications induced by the impregnation with CYPHOS IL 101, the spectra were normalized with respect to the intensity of the absorption related to the ν(C-C) mode of the aromatic rings in the 1650–1570 cm^{-1} region. In this way the comparison is made for the same amount of aromatic rings.

After normalization, CYXAD shows a drastic decrease in intensity of the bands related to the stretching modes of aromatic C-H. Moreover, the introduction of IL, causes the intensity decrease of the bands related to the $\nu(C^{sp3}\text{-}H)$ modes, in contrast with the addition of the CYPHOS alkyl chains. XAD-1180 is a porous resin with an average pore diameter of 140 Å (Escudero et al., 2013). It is possible to assume that the IL enters inside the pores and interacts with exposed C-H groups of the resin through its alkyl chains. This interaction can significantly red-shift the vibration frequency of both aromatic and aliphatic C-H. Therefore, only the fraction of not interacting C-H groups continues to show absorptions in the 3120–2800 cm^{-1} range. The interaction between the chains of sorbent and IL would be broken by ethanol, while this does not happen when an aqueous solution is eluted: the water is polar and this ensures the proper functioning of the CYXAD to separate the species of interest.

3.2.5.3 Determination of CH_3Hg and Hg_{IN}

Regarding the determination of CH_3Hg, the performances of SGE in aqueous solutions showed sensitivity and detection limits comparable to Hg_{IN}. By analyzing synthetic solutions containing only CH_3Hg, the limit of detection (estimated as LOD = 3σB/slope) was 0.45 μg L^{-1} and the sensitivity was 1.67 μA/μg L^{-1}; the relative error for the determination of 1 μg L^{-1} of Hg was −1%.

Table 4 shows the results for CH_3Hg determination with portable procedures, $[CH_3Hg]_{ASV\ port}$, and the recovery percentages with respect to $[CH_3Hg]_{DMA}$.

The correlation between $[CH_3Hg]_{ASV}$ port and $[CH_3Hg]_{DMA}$, was very good (R^2 = 0.996) with the exception of S5 and S7. It is well known that the percentage of CH_3Hg is generally in the range 70–85 % of $[Hg]_{TOT}$. (Lescord et al., 2018). The percentages obtained for these samples were lower than 40% in the case of DMA, and greater than 80% with the proposed method: these samples showed very high percentages of fats, which may have caused the extraction with the organic solvent to be inefficient.

Table 4. [CH_3Hg] (mg kg^{-1}) and % of recovery with respect to $[CH_3Hg]_{DMA}$.

Sample	$[CH_3Hg]_{ASV\ port}$	$\%rec/[Hg]_{DMA}$	$[CH_3Hg]_{DMA}$
RM	4.65 ± 0.02 (95.1)*	116.0	4.01 ± 0.04 (80.0)*
S1	4.00 ± 0.05 (77.5)	85.1	4.70 ± 0.04 (87.1)
S2	2.04 ± 0.01 (85.0)	112.1	1.82 ± 0.05 (86.7)
S3	0.17 ± 0.01 (77.3)	68.0	0.25 ± 0.01 (94.4)
S4	1.12 ± 0.02 (92.6)	98.2	1.14 ± 0.01 (83.3)
S5	3.57 ± 0.03 (81.3)	215.1	1.66 ± 0.02 (39.9)
S6	2.52 ± 0.01 (98.4)	106.3	2.37 ± 0.03 (98.7)
S7	1.95 ± 0.01 (94.2)	672.4	0.29 ± 0.01 (14.3)
S8	2.35 ± 0.01 (78.9)	85.5	2.75 ± 0.04 (95.0)

*Percentage recovery in comparison with the certified value ($[Hg]_{c.v.}$).

3.2.5.4 Proposed "portable kit for Hg/CH_3Hg speciation studies" (patent pending)

The kit for the on-site analysis of Hg_{IN} and CH_3Hg consists of:

- Test tubes previously filled with HNO_3/H_2O_2 mixture for the determination of Hg_{TOT};
- Test tubes previously filled with HCl for the determination of Hg_{IN};
- A squeeze bottle containing the washing solution (0.1 M $HClO_4$, 1.5 mM NaCl and 0.5 mM EDTA-Na_2) ready to use;
- A squeeze bottle containing HPW;
- A squeeze bottle containing Hg standard solution;
- A squeeze bottle containing the supporting electrolyte (60 mM NaCl);
- A small balance to weigh aliquots of fish to be inserted into each tube;
- A food warmer;
- A portable battery;
- Some syringes to withdraw the sample solution at the end of the extraction to transfer an aliquot into the measuring cell;
- Some syringe filters to filter the aliquot of sample solution to be transferred into the measuring cell;
- Some cartridges containing the CYXAD phase ready to be insert in the column equipped with a disposable inlet filter;
- Micropipettes and tips for transferring the sample solution and adding known concentrations of mercury for calibration by standard additions;
- A portable cell with perforated cap for housing the electrodes;
- Electrodes (WE: SGE; RE: Ag/AgCl/KCl; AE: Pt);
- Portable potentiostat;
- Laptop computer;
- Container for the collection of wastes, consisting of sample solutions after analysis. The wastes can be transported to a laboratory to be properly disposed or delivered to specialized companies for disposal.

Based on our experience (Abollino et al., 2019), a travel bag (like a trolley) is useful to transport the whole kit.

3.2.6. Conclusion

In view of the more restrictive law requiring the determination of both Hg_{IN} and CH_3Hg form of mercury in food and environmental samples, it is very important that an easy procedure for the quantification of the two forms becomes available. The proposed method is based on a portable pretreatment procedure, consisting of the treatment of the sample with two different extractants: HNO_3/H_2O_2 to extract the total mercury, and HCl to obtain different chemical species in solution. The analyses were performed by ASV using a commercial SGE without modification. The solution containing the total amount of Hg is analysed after dilution with the supporting electrolyte in the voltammetric cell, while the second one requires a treatment to obtain the separation of the two Hg forms. For this step, a new modified resin was optimized, namely CYXAD. A column holder was also developed. CYXAD held Hg_{IN} quantitatively, while CH_3Hg was washed off. Then, Hg_{IN} was eluted with nitric acid and the resulting solution was analysed.

A certified material, some freeze-dried and some fresh samples were analysed and the results compared with those obtained with a reference technique, i.e. DMA analysis. The results obtained by ASV showed a very good compliance with those obtained using DMA.

The proposed procedure is simple, easy to carry out and quick to implement. It does not involve the use of gases or organic solvents having a high environmental impact (which are used, instead, in the consolidated techniques for the determination of CH_3Hg). The official method for mercury and methylmercury quantification, based on DMA measurement, presented higher sensitivity: However, the LOQs for the proposed method resulted lower than the legislative limit, therefore broadly sufficient to assess the compliance and healthiness of a food product. Moreover, the proposed procedure demonstrates good accuracy both for Hg_{IN} and CH_3Hg even in presence of a high fat content, it is faster than the DMA in speciation studies, it does not require the use of organic solvent, it allows accurate and precise measurements to be made without the use of expensive and large instruments, making it possible to analyze the samples directly on the fishing site or in the port.

The proposed procedures can be applied for fast screening tests, allowing for the increase of controls on different matrices. In fact, it can have many applications, such as monitoring of fish products for the protection of consumer health, on site screening analysis and environmental monitoring (i.e. bioaccumulation of mercury in fish and seabirds as pollution indicator).

Supplementary Material

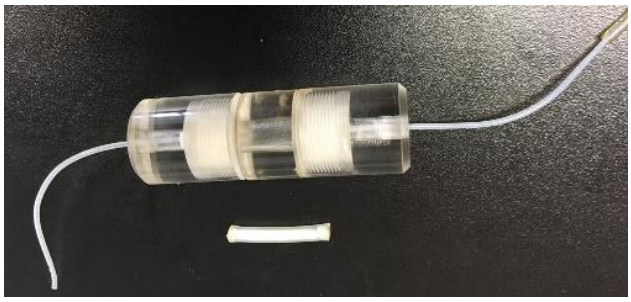

Figure S1. Column holder and the cartridge containing CYXAD

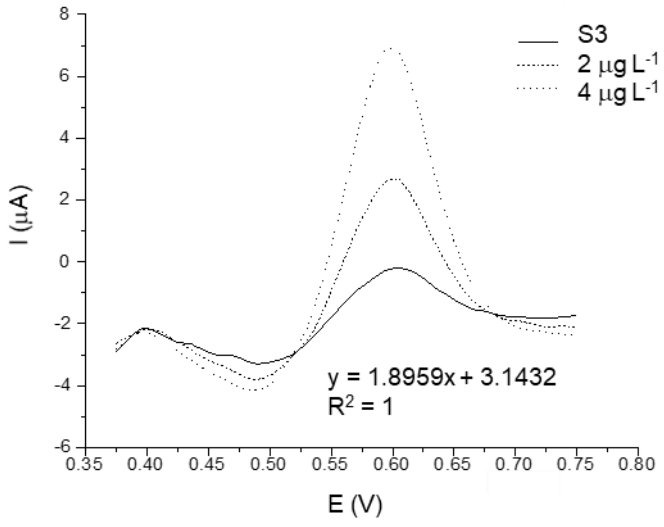

Figure S2 Voltammograms obtained for Hg quantification in sample S3 using ASVport

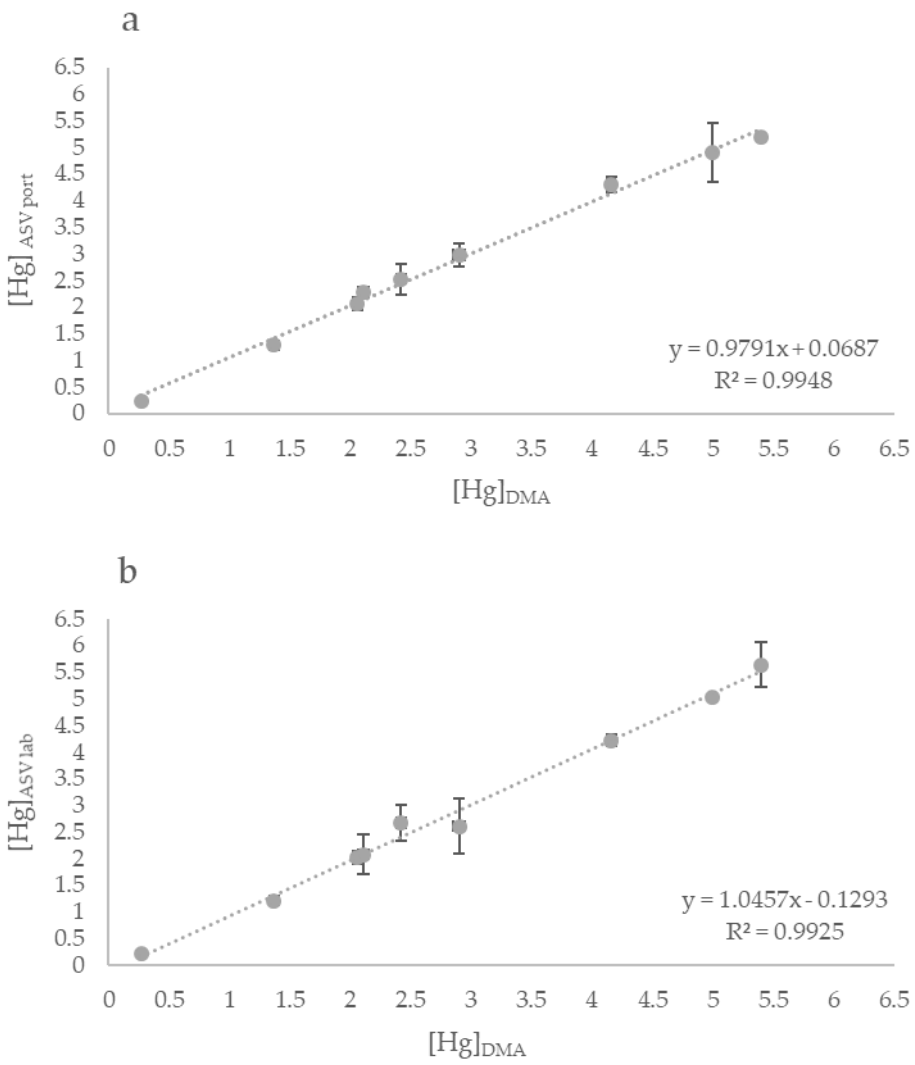

Figure S3 – Scatter plots of mercury concentration (mg kg-1) determined in sample by DMA versus a) ASVport and b) ASVlab

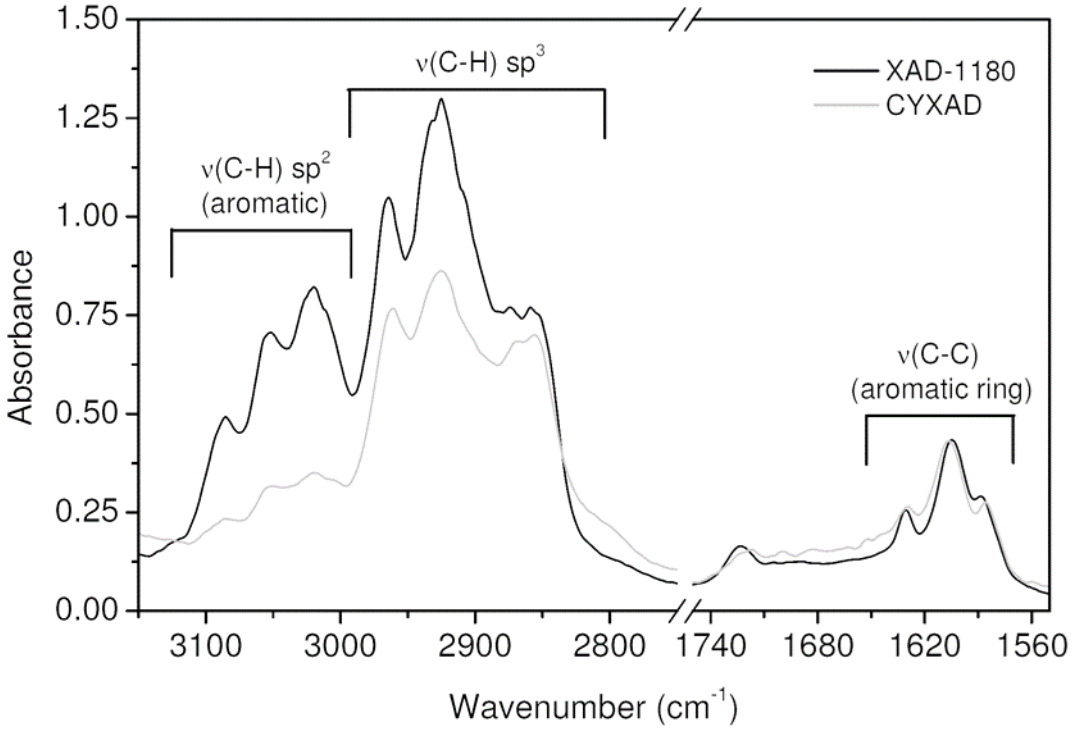

Figure S4 - IR spectra of XAD-1180 (black line) and CYXAD diluted in KBr (light gray line).

References

Abollino, O., Giacomino, A., Malandrino, M., Piscionieri, G., & Mentasti, E. (2008). Determination of mercury by anodic stripping voltammetry with a gold nanoparticle modified glassy carbon electrode. Electroanalysis, 20(1), 75–83. https://doi.org/10.1002/elan.200704044.

Abollino, O., Malandrino, M., Berto, S., La Gioia C., Maruccia, V., et al. (2019). Stripping voltammetry for field determination of traces of copper in soil extracts and natural waters. Microchemical Journal 149, 104015 doi: 10.1016/j.microc.2019.104015.

Arias, A., Saucedo, I., Navarro, R., Gallardo, V., Martinez, M., & Guibal, E. (2011). Cadmium(II) recovery from hydrochloric acid solutions using Amberlite XAD-7 impregnated with a tetraalkyl phosphonium ionic liquid. Reactive and Functional Polymers, 71(11), 1059–1070. https://doi.org/10.1016/j.reactfunctpolym.2011.07.008.

Ariya, P. A., Amyot, M., Dastoor, A., Deeds, D., Feinberg, A., Kos, G., et al. (2015). Mercury physicochemical and biogeochemical transformation in the atmosphere and at atmospheric interfaces: A review and future directions. Chemical Reviews, 115(10), 3760–3802. https://doi.org/10.1021/cr500667e.

Baer, I., Baxter, M., Devesa, V., Vélez, D., Raber, G., Rubio, R., et al. (2011). Performance of laboratories in speciation analysis in seafood – Case of methylmercury and inorganic arsenic. Food Control, 22(12), 1928–1934. https://doi.org/10.1016/j.foodcont.2011.05.005.

Bagheri, H., Afkhami, A., Khoshsafar, H., Rezaei, M., & Shirzadmehr, A. (2013). Simultaneous electrochemical determination of heavy metals using a triphenylphosphine/MWCNTs

composite carbon ionic liquid electrode. Sensors and Actuators B:Chemical, 186, 451–460. https://doi.org/10.1016/j.snb.2013.06.051.

Chaiyo, S., Chailapakul, O., & Siangproh, W. (2014). Highly sensitive determination of mercury using copper enhancer by diamond electrode coupled with sequential injection anodic stripping voltammetry. Analytica Chimica Acta, 852, 55–62. https://doi.org/10.1016/j.aca.2014.09.011.

Cordeiro, F., Gonçalves, S., Emteborg, H., Conneely, P., Calderón, J., Robouch, P., Tumba-Tshilumba, M.-F., Kortsen, B., Calle, B. de la, & Institute for Reference Materials and Measurements. (2013). IMEP-115: Determination of methylmercury in seafood: collaborative trial report. Publications Office. http://dx.publications.europa.eu/10.2787/76278.

Cossa, D., Averty, B., & Pirrone, N. (2009). The origin of methylmercury in open Mediterranean waters. Limnology and Oceanography, 54(3), 837–844. https://doi.org/10.4319/lo.2009.54.3.0837.

Costa, S., Afonso, C., Cardoso, C., Batista, I., Chaveiro, N., Nunes, M. L., & Bandarra, N. M. (2015). Fatty acids, mercury, and methylmercury bioaccessibility in salmon (Salmo salar) using an in vitro model: Effect of culinary treatment. Food Chemistry, 185, 268–276. https://doi.org/10.1016/j.foodchem.2015.03.141.

de Paiva, E. L., Milani, R. F., Boer, B. S., Quintaes, K. D., & Morgano, M. A. (2017). Methylmercury in fish species used in preparing sashimi: A case study in Brazil. Food Control, 80, 104–112. https://doi.org/10.1016/j.foodcont.2017.04.027.

EFSA, 2004-2011. (s.d.). EFSA Journal, 241.

Escudero, L. B., Olsina, R. A., & Wuilloud, R. G. (2013). Polymer-supported ionic liquid solid phase extraction for trace inorganic and organic mercury determination in water samples by flow injection-cold vapor atomic absorption spectrometry. Talanta, 116, 133–140. https://doi.org/10.1016/j.talanta.2013.05.001.

Fernández, Z. H., Valcárcel Rojas, L. A., Álvarez, A. M., Estevez Álvarez, J. R., Araújo dos Santos, J., González, I. P., et al. (2015). Application of Cold Vapor-Atomic Absorption (CVAAS) Spectrophotometry and Inductively Coupled Plasma-Atomic Emission Spectrometry methods for cadmium, mercury and lead analyses of fish samples. Validation of the method of CVAAS. Food Control, 48, 37–42. https://doi.org/10.1016/j.foodcont.2014.05.056.

Frentiu, T., Butaciu, S., Darvasi, E., Ponta, M., Senila, M., Petreus, D., & Frentiu, M. (2015). Analytical characterization of a method for mercury determination in food using cold vapour capacitively coupled plasma microtorch optical emission spectrometry – Compliance with European legislation requirements. Analytical Methods, 7(2), 747–752. https://doi.org/10.1039/C4AY02161D.

Galimberti, C., Corti, I., Cressoni, M., Moretti, V. M., Menotta, S., Galli, U., & Cambiaghi, D. (2016). Evaluation of mercury, cadmium and lead levels in fish and fishery products imported by air in North Italy from extra-European Union Countries. Food Control, 60, 329–337. https://doi.org/10.1016/j.foodcont.2015.08.009.

Giacomino, A., Ruo Redda, A., Squadrone, S., Rizzi, M., Abete, M. C., La Gioia, C., et al. (2017). Anodic stripping voltammetry with gold electrodes as an alternative method for the routine determination of mercury in fish. Comparison with spectroscopic approaches. Food Chemistry, 221, 737–745. https://doi.org/10.1016/j.foodchem.2016.11.111.

Guibal, E., Gavilan, K. C., Bunio, P., Vincent, T., & Trochimczuk, A. (2008). CYPHOS IL 101 (tetradecyl(trihexyl)phosphonium chloride) immobilized in biopolymer capsules for Hg(II) recovery from HCl solutions. Separation Science and Technology, 43(9–10),2406–2433. https://doi.org/10.1080/01496390802118970.

Horowitz, H. M., Jacob, D. J., Amos, H. M., Streets, D. G., & Sunderland, E. M. (2014). Historical mercury releases from commercial products: Global environmental implications. Environmental Science & Technology, 48(17), 10242–10250. https://doi.org/10.1021/es501337j.

Kokab, T., Manzoor, A., Shah, A., Siddiqi, H. M., Nisar, J., Ashiq, M. N., & Shah, A. H. (2020). Development of tribenzamide functionalized electrochemical sensor for femtomolar level sensing of multiple inorganic water pollutants. Electrochimica Acta, 353, Article 136569. https://doi.org/10.1016/j.electacta.2020.136569.

Kubáň, P., Houserová, P., Kubáň, P., Hauser, P. C., & Kubáň, V. (2007). Mercury speciation by CE: A review. Electrophoresis, 28(1–2), 58–68. https://doi.org/10.1002/elps.200600457.

Laffont, L., Hezard, T., Gros, P., Heimbürger, L.-E., Sonke, J. E., Behra, P., & Evrard, D. (2015). Mercury(II) trace detection by a gold nanoparticle-modified glassy carbon electrode using square-wave anodic stripping voltammetry including a chloride desorption step. Talanta, 141, 26–32. https://doi.org/10.1016/j.talanta.2015.03.036.

Lemos, L. S., de Moura, J. F., Hauser-Davis, R. A., de Campos, R. C., & Siciliano, S. (2013). Small cetaceans found stranded or accidentally captured in southeastern Brazil: Bioindicators of essential and non-essential trace elements in the environment. Ecotoxicology and Environmental Safety, 97, 166–175. https://doi.org/10.1016/j.ecoenv.2013.07.025.

Lescord, G. L., Johnston, T. A., Branfireun, B. A., & Gunn, J. M. (2018). Percentage of methylmercury in the muscle tissue of freshwater fish varies with body size and age and among species: Percentage of MeHg in fish. Environmental Toxicology and Chemistry, 37(10), 2682–2691. https://doi.org/10.1002/etc.4233.

Marták, J., & Schlosser, Š. (2006). Phosphonium ionic liquids as new, reactive extractants of lactic acid. Chemical Papers, 60(5), https://doi.org/10.2478/s11696-006-0072-2.

Ottakam Thotiyl, M. M., Basit, H., Sánchez, J. A., Goyer, C., Coche-Guerente, L., Dumy, P., et al. (2012). Multilayer assemblies of polyelectrolyte–gold nanoparticles for the electrocatalytic oxidation and detection of arsenic(III). Journal of Colloid and Interface Science, 383(1), 130–139. https://doi.org/10.1016/j.jcis.2012.06.033.

Ramezani, S., Mashhadizadeh, M. H., Jalilian, S., & Aghili, M. (2015). Structure-switching of an organothiol neutral carrier by gold nanoparticles decorated on SH-MWCNTs for ultra-trace voltammetric assay of Hg(II) using a carbon paste electrode. Analytical Methods, 7(18), 7765–7775. https://doi.org/10.1039/C5AY01660F.

Regulation (EU) No 420/2011 of the European Parliament and of the Council of April 29th 2011. European: Amending Regulation (EC) No 1881/2006 of the European Parliament., n. 2006/1881/EC. Recuperato 6 maggio 2020, da https://eur-lex.europa.eu/LexUriServ/LexUriServ.do?uri=CONSLEG:2006R1881:20120901:EN:PDF.

Renedo, M., Bustamante, P., Tessier, E., Pedrero, Z., Cherel, Y., & Amouroux, D. (2017). Assessment of mercury speciation in feathers using species-specific isotope dilution analysis. Talanta, 174, 100–110. https://doi.org/10.1016/j.talanta.2017.05.081.

Ruo Redda, A., Abollino, O., Malandrino, M., Squadrone, S., Abete, M. C., Berto, S., et al. (2019). A portable setup for the voltammetric determination of total mercury in fish with solid and

nanostructured gold electrodes. Molecules, 24(10), 1910. https://doi.org/10.3390/molecules24101910.

Savery, L. C., Evers, D. C., Wise, S. S., Falank, C., Wise, J., Gianios, C., et al. (2013). Global mercury and selenium concentrations in skin from free-ranging sperm whales (Physeter macrocephalus). Science of The Total Environment, 450–451, 59–71. https://doi.org/10.1016/j.scitotenv.2013.01.070.

Somerset, V., Leaner, J., Mason, R., Iwuoha, E., & Morrin, A. (2010). Development and application of a poly(2,2′-dithiodianiline) (PDTDA)-coated screen-printed carbon electrode in inorganic mercury determination. Electrochimica Acta, 55(14), 4240–4246. https://doi.org/10.1016/j.electacta.2009.01.029.

Shang, H., Xu, H., Jin, L., Chen, C., Song, T., Wang, C., & Du, Y. (2019). Electrochemicalphotoelectrochemical dual-mode sensing platform based on advanced Cu9S8/polypyrrole/ ZIF-67 heterojunction nanohybrid for the robust and selective detection of hydrogen sulfide. Sensors and Actuators B: Chemical, 301, Article 127060. https://doi.org/10.1016/j.snb.2019.127060.

Shang, H., Xu, H., Jin, L., Wang, C., Chen, C., Song, T., & Du, Y. (2020). 3D ZnIn2S4 nanosheets decorated ZnCdS dodecahedral cages as multifunctional signal amplification matrix combined with electroactive/photoactive materials for dual mode electrochemical – photoelectrochemical detection of bovine hemoglobin. Biosensors and Bioelectronics, 159, Article 112202. https://doi.org/10.1016/j.bios.2020.112202.

Shang, H., Xu, H., Liu, Q., & Du, Y. (2019). PdCu alloy nanosheets-constructed 3D flowers: New highly sensitive materials for H2S detection. Sensors and Actuators B: Chemical, 289, 260–268. https://doi.org/10.1016/j.snb.2019.03.101.

Squadrone, S., Chiaravalle, E., Gavinelli, S., Monaco, G., Rizzi, M., & Abete, M. C. (2015). Analysis of mercury and methylmercury concentrations, and selenium: Mercury molar ratios for a toxicological assessment of sperm whales (Physeter macrocephalus) in the most recent stranding event along the Adriatic coast (Southern Italy, Mediterranean Sea). Chemosphere, 138, 633–641. https://doi.org/10.1016/j.chemosphere.2015.07.047.

Vincent, T., Parodi, A., & Guibal, E. (2008). Pt recovery using Cyphos IL-101 immobilized in biopolymer capsules. Separation and Purification Technology, 62(2), 470–479. https://doi.org/10.1016/j.seppur.2008.02.025.

Voegborlo, R. B., & Adimado, A. A. (2010). A simple classical wet digestion technique for the determination of total mercury in fish tissue by cold-vapour atomic absorption spectrometry in a low technology environment. Food Chemistry, 123(3), 936–940. https://doi.org/10.1016/j.foodchem.2010.04.059.

Wang, Z., Yin, Y., He, B., Shi, J., Liu, J., & Jiang, G. (2010). L-cysteine-induced degradation of organic mercury as a novel interface in the HPLC-CV-AFS hyphenated system for speciation of mercury. Journal of Analytical Atomic Spectrometry, 25(6), 810. https://doi.org/10.1039/b924291k.

Zhang, R., Peng, M., Zheng, C., Xu, K., & Hou, X. (2016). Application of flow injection–green chemical vapor generation–atomic fluorescence spectrometry to ultrasensitive mercury speciation analysis of water and biological samples. Microchemical Journal, 127, 62–67. https://doi.org/10.1016/j.microc.2016.02.006.

3.2.2 On-Site Determination of Methylmercury by Coupling Solid-Phase Extraction and Voltammetry

Paolo Inaudi [1*], Elio Mondino [2], Ornella Abollino [1], Mery Malandrino [2], Monica Argenziano [1], Laura Favilli [1], Roberto Boschini [3] and Agnese Giacomino [1,*]

[1] Department of Drug Science and Technology, University of Torino, Via Pietro Giuria 9, 10125 Turin, Italy

[2] Department of Chemistry, University of Torino, Via Pietro Giuria 5, 10125 Torino, Italy

[3] FKV SrL, Largo delle Industrie, 10, 24020 Torre Boldone, Italy;

* Corresponding authors

Received: 6 April 2022

Accepted: 14 May 2022

Published: 16 May 2022

https://doi.org/10.3390/molecules27103178

MOLECULES - 2022, 27, 3178

3.2.2.1 Abstract

A measurement and speciation procedure for the determination of total mercury (Hg_{TOT}), inorganic mercury (Hg_{IN}), and methylmercury (CH_3Hg) was developed and the applicability for on-site determination was demonstrated. A simple, portable sample pretreatment procedure was optimized to extract the analytes. Home-made columns, packed with a new sorbent material called CYXAD (CYPHOS 101 modified Amberlite XAD), were used to separate the two forms of the analyte. Hg_{TOT} and CH_3Hg were determined by anodic stripping voltammetry (ASV), using a solid gold electrode (SGE). Two certified reference materials (BCR-463 Tuna Fish and Tuna Fish ERM-CE 464) and eight fresh fishes were analyzed. Then, the results that were obtained following the optimized portable procedure were compared with the concentrations obtained, using a direct mercury analyzer (DMA). This quantification, using the two techniques, demonstrated the good performance of the proposed method.

3.2.2.2 Introduction

In aquatic systems, bacteria transform inorganic mercury, Hg_{IN}, into methylmercury, CH_3Hg [1]. CH_3Hg is considered the most toxic form of Hg and is very harmful due to its ability to bioaccumulate. As a result of its biomagnification capacity, organisms at the top of a food chain are especially exposed [2], but CH_3Hg is present in varying amounts in all seafood. In fact, for humans, fish is the main source of mercury and methylmercury in the diet. CH_3Hg binds to the sulfhydryl groups of amino acids and is absorbed from the gastrointestinal tract. Furthermore, it is able to cross the blood-brain barrier [3]. For this reason, due to their developing brain, infants and children are considered the most at risk of CH_3Hg toxicity. Health problems such as numbness around the mouth or limbs, difficulty thinking clearly, hair loss, stomach pain and fatigue have been reported in cases involving the consumption of fish with high mercury content. People who frequently eat fish, as well as fauna that feed mainly on fish, are highly exposed to the risks associated with the bioaccumulation of CH_3Hg. For many populations, fish make a vital contribution to the diet in terms of survival and health, particularly in many developing countries. For some populations, for example, in Asia, it is estimated that 75% of the daily proteins ingested as part of the diet are derived from the consumption of fish [4]. They provide essential nourishment, especially quality proteins and fats, vitamins and minerals. Furthermore, fish is a source of income from the fish trade, which can, consequently, enable the purchase of other food products [5,6]. In European Union legislation, the maximum levels of total mercury (Hg_{TOT}) are 0.5 mg kg^{-1} for small and medium fishes, mussels and most forms of seafood, and 1 mg kg^{-1} for predatory fish (e.g., tuna and swordfish) [7], while a maximum limit of CH_3Hg in food has not as yet been established. A provisional tolerable weekly intake (PTWI) of 1.3 μg kg^{-1} CH_3Hg and 4 μg kg^{-1} Hg body weight has been set [8]. For all these reasons, it is essential to monitor the concentration of Hg and its distribution, in its inorganic and organic forms, in fish products [9]. Hg_{TOT} can be quantified by cold-vapor atomic fluorescence spectrometry (CV AFS) [10], cold-vapor capacitively coupled plasma micro-torch optical emission spectrometry (CV-μCCP-OES) [11], cold-vapor atomic absorption, or high-resolution inductively coupled plasma mass spectrometry [12] and capillary electrophoresis (CE) [13]. All these techniques involve long sample pretreatment methods, high management costs and specialized personnel. Gas chromatography (GC) with various detectors, relying on mass spectroscopy (MS) [14], electron capture detection [15], atomic fluorescence spectrometry [16] and high-performance liquid

chromatography (HPLC), coupled with atomic emission detection [17] or coupled with high-performance liquid chromatography [18], have been used to determine CH_3Hg. For example, isotope dilution-GC/ICP-MS [19] and purge-and-trap GC-MS [20] have also been reported as analytical tools. In the literature, some papers also report the application of electrochemical techniques for the determination of CH_3Hg [21,22], such as potentiometric stripping analysis (PSA), current stripping chronopotentiometry (CSP) [23] and, in particular, voltammetry [24]. Anodic stripping voltammetry (ASV) was used for the determination of CH_3Hg at concentrations starting from 2×10^{-8} mol L^{-1} [25]. To our knowledge, the first example of the application of ASV to the determination of CH_3Hg was based on a linear calibration diagram obtained using a mercury drop electrode, which allowed the researchers to obtain a linear response in a concentration range from 10^{-4} to 10^{-7} mol L^{-1} [26]. The method of double standard additions was used for the quantification of CH_3Hg. Agraz et al. reported the use of a particular modified carbon paste electrode for the determination of Hg^{2+} and CH_3Hg after a pre-concentration period, with a detection limit (DL) of 1×10^{-8} mol L^{-1} [27]. Differential pulse voltammetry (DPV), coupled with a glassy carbon electrode modified with Nafion, was tested for CH_3Hg analysis, with a DL equal to 4.5×10^{-8} mol L^{-1} [28]. The DL dropped to 4.5×10^{-11} mol L^{-1} using a multiple square-wave voltammetric technique; the lowest determined concentration of CH_3Hg in this study was 4×10^{-8} mol L^{-1}. The reduction of CH_3Hg and its subsequent re-oxidation is the most exploited voltammetric technique for the quantification of this analyte. Most notably, a detection limit of 5.6×10^{-7} mol L^{-1} was described using conditions optimized for the determination of CH_3Hg in dogfish muscle samples [29]. In another study [22], carbon microelectrodes were used for the analysis of CH_3Hg in chloride media. A positive response to the technique was also demonstrated at nanomolar concentrations for CH_3Hg, but the linearity of the method was not optimal [30]. Several studies using mercury [29] or gold [31] film electrodes were carried out. The use of polymer-coated carbon electrodes [28] or gold nanoparticle-modified electrodes [32] allowed researchers to lower the DL to the nanomolar concentration range. Korolczuk and Rutyna proposed a method for analyzing the organic forms of mercury by eliminating the interference of inorganic forms, complexing Hg^{2+} ions with diethylenetriaminepentaacetic acid (DTPA): in this way, a selective preconcentration on the electrode is obtained by applying a reduction potential to the metallic state to more negative values than the potential of the CH_3Hg^+ reduction to elemental mercury [31].

The purpose of this paper is to highlight the applicability of a patented procedure with freshly caught fish for the determination of Hg_{TOT}, Hg_{IN} and CH_3Hg content via ASV outside laboratories. The work was mainly focused on facilitating the portability and ease of execution of the different steps involved in the treatment of the solid samples, along with the voltammetric determination of the analytes in the obtained sample solution, using a simple solid gold electrode. Two certified reference materials (BCR-463 Tuna Fish and Tuna Fish ERM-CE 464) and eight fresh fish samples were tested. A sample analysis was also conducted using a direct mercury analyzer (DMA), considered a reference method for Hg_{TOT} and CH_3Hg determination [33], in order to compare the results of the two methods.

3.2.2.3 Results

In our previous work, we optimized an easy procedure for mercury speciation in the laboratory. In the present study, the procedure was further improved and its applicability for outside analysis was assessed.

The procedure, once further improved and applied on-site, permitted us to obtain performance data in terms of repeatability, linearity, accuracy and detection limits comparable to those previously obtained in the laboratory. A deposition time of 120 s was found to be the best option for analyte concentrations of up to 50 μg L^{-1}. In a blank matrix, the LOD of Hg_{IN} and CH_3Hg was expected to show a 3σB/slope; it was 0.40 μg L^{-1} for Hg_{IN} and 0.50 μg L^{-1} for CH_3Hg, while sensitivity was 1.71 μA/μgL^{-1} and 1.68 μA/μgL^{-1} for Hg_{IN} CH_3Hg, respectively. The relative error for the quantification of 1 μg L^{-1} of the analytes was −1% and +1% for Hg_{IN} and CH_3Hg, respectively.

All the samples were analyzed outdoors, following the entire portable procedure (extraction of the analytes and voltammetric determination) and adopting the proposed kit.

Figure 1a,b shows the voltammograms obtained during the analysis of ERM-CE 464 for the quantification of Hg and CH_3Hg, respectively.

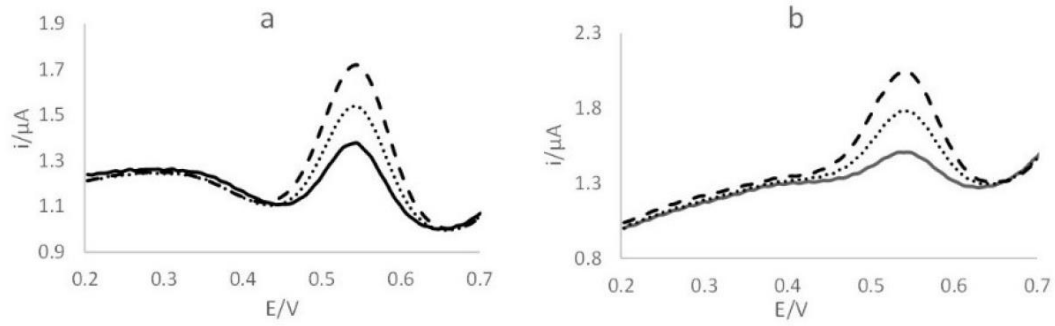

Figure 1. Voltammograms obtained using the portable kit for (a) Hg and (b) CH_3Hg quantification: —, ERM-CE 464; ···· , first addition (5 μg L^{-1}); ----, second addition (10 μg L^{-1}).

For Hg determination, the linear regression equation obtained from the standard additions was y = 0.0756x + 0.0018 (R^2 = 0.9948), while for CH_3Hg, the equation was y = 0.0651x + 0.019 (R^2 = 0.9958). The method shows the good linearity of the technique for both considered analytes. The concentrations of Hg_{TOT} and CH_3Hg found in the reference materials and in the examined fishes are described in Table 1, which shows the results obtained by the portable voltammetric kit and by using DMA.

Table 1. Concentrations ($mg \cdot kg^{-1}$) and recoveries (%) obtained for Hg_{TOT} and CH_3Hg for the analysis of certified materials Tuna fish

Hg_{TOT}					
Sample	$[Hg]_{TOT\ certified}$	ASV	Recovery	DMA	Recovery
ERM-CE 464	5.24±0.10	5.03±0.04	96	5.04±0.01	96
BCR 463	2.85±0.16	2.65±0.44	93	2.06±0.03	72
CH_3Hg					
Sample	$[CH_3Hg]_{certified}$	ASV	Recovery	DMA	Recovery
ECM-CE 464	4.89±0.16	4.65±0.04	95	4.01±0.04	82
BCR 463	3.04±0.16	2.08±0.37	68	2.34±0.01	77

In the case of Hg_{TOT}, recoveries of 96% and 93% were obtained for ERM-CE464 and BCR 463, respectively, in the case of ASV measurement and 96% and 72%, respectively, using DMA. For CH_3Hg, recoveries of 95% and of 68% were obtained for ERM-CE464 and BCR 463, respectively, in the case of ASV measurement, and 82% and 77%, respectively, using DMA. Then, the portable procedure was applied to the fish samples. As an example, Figure 2a,b shows the voltammograms obtained when analyzing commercial fresh tuna fish for Hg and CH_3Hg determination, respectively. For all the samples, R^2 values higher than 0.99 were obtained.

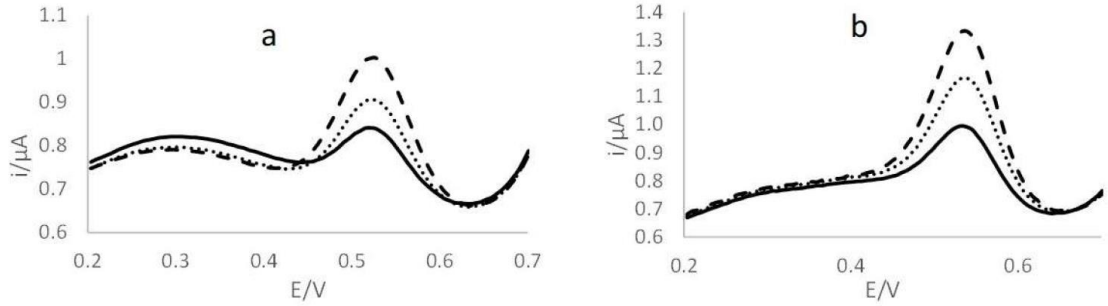

Figure 2. Voltammograms obtained using the portable kit for (a) Hg_{IN} and (b) CH_3Hg quantification: — tuna fish; ···· first addition (5 μg L^{-1}); ---- second addition (10 μg L^{-1}).

The concentrations of Hg_{TOT} and CH_3Hg achieved using the proposed portable procedure and DMA are compared in Table 2.

Table 2. Concentrations (mg·kg^{-1}) obtained for Hg_{TOT} and CH_3Hg in fish-samples analysed by voltammetry and by DMA.

Sample	Hg_{TOT}		CH_3Hg	
	Portable procedure	DMA	Portable procedure	DMA
Swordfish 1	2.67±0.34	2.60±0.03	4.55±0.04	4.11±0.04
Swordfish 2	3.53±1.52	3.40±0.01	1.91±0.14	2.06±0.01
Tuna fish 1	1.78±0.41	1.76±0.02	1.29±0.23	1.36±0.02
Tuna fish 2	1.04±0.30	1.02±0.02	0.84±0.20	0.82±0.01
Marlin Blue	2.02±0.13	2.09±0.05	0.23±0.01	0.29±0.01
Cod fish	<0.20	0.08± 0.01	<0.20	0.07±0.01
Rainbow trout	<0.20	0.04±0.01	<0.20	0.02±0.01
Salmon trout	<0.20	0.2±0.01	<0.20	0.08±0.01

No measurable Hg peaks were detected in the trout samples or in the codfish, while in all the other samples, the concentrations for fresh fish exceeded the legal limits for the predator fish. In fact, all the concentrations were higher than 1 mg kg^{-1}, the limit for the predator fish; in particular, both the slices of swordfish that were tested showed an Hg content two to three times higher than the maximum permitted value. These results were confirmed by the results obtained using DMA. The LOQ in the fish matrix, calculated as the minimum quantity determined with good accuracy, was 0.2 mg kg^{-1} with the solid gold electrode (SGE). Our new method can be considered appropriate for testing the mercury content in this matrix since the highest permissible concentration in tuna fish is set to 0.5 mg kg^{-1} wet fish by the European Commission [7]. For the sake of completeness, it should be said that the Hg_{IN} retained in the column was recovered with 5 mL of HNO_3, and then diluted and analyzed. The recovery was quantitative (comparing the obtained concentrations with those of Hg_{TOT} and CH_3Hg found in each sample). The results were always compared with the DMA. The data are not reported here since the aim of this work was to optimize the procedure in order to make possible the direct quantification of CH_3Hg. To better compare the results, Figure 3a,b shows the correlation between the concentrations obtained (analyzing swordfish, tuna fish and blue marlin samples) using the two techniques for Hg and CH_3Hg, respectively.

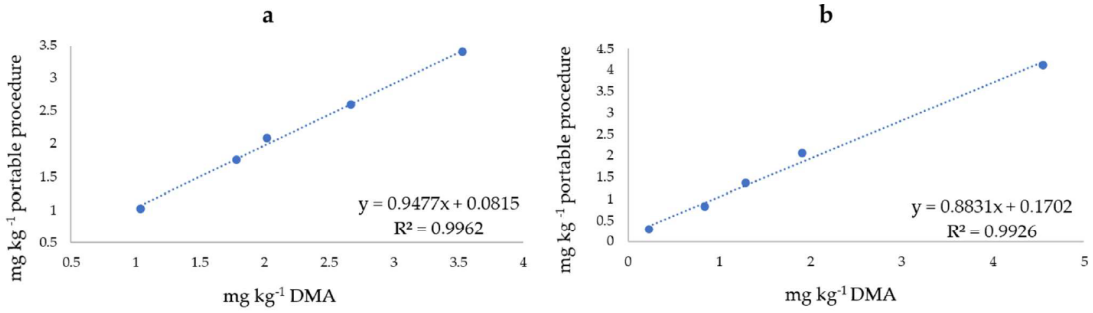

Figure 3. Correlation between the concentrations (mg kg^{-1}) of (a) Hg_{TOT} and (b) CH_3Hg obtained using the portable procedure and DMA. ● = samples (tuna fish 2, tuna fish 1, blue marlin, swordfish 1 and swordfish 2, reported in ascending order of concentration).

A value of $R^2 > 0.99$ was obtained for both the analytes, demonstrating the good applicability of the proposed portable procedure for mercury speciation studies.

Novelty of the Study and Concerns about the Portable Kit

The novelty of this study is the further optimization of the procedure and its on-site application for mercury speciation in fish samples. To our knowledge, this is the first method that permits the treatment of solid samples for the extraction of Hg and CH_3Hg, separating them before analysis and the determination of their concentration, directly in the field.

The most significant improvements have been: (i) the use of piston syringes, which permits carrying out the procedure manually, without the aid of supports or pumps. Moreover, this type of syringe can be packed with CYXAD and then stored at room temperature for up six months. (ii) The possibility of determining CH_3Hg in the sample solutions after elution. In this way, the elution of Hg_{IN} that was retained in the CYXAD cartridge was not required, reducing the number of solutions that need to be carried in the field and speeding up the procedure.

The modifications simplified the applicability of the procedure for on-site analysis while maintaining the same performance, in terms of accuracy and precision, as that obtained in the laboratory.

The transportable battery assures 15 h of autonomy, with the battery recharging overnight. Consequently, the possibility of performing analyses on subsequent days is secured.

The use of a mini dry bath to warm the samples during the extraction step permits more uniform heating; the dissolution of the sample appears more homogeneous, consequently facilitating the filtration step; furthermore, the heating takes place in dry conditions, reducing the volume of high-purity water (HPW) needing to be brought into the field. In order to reduce waste, it is important to use small volumes of the reagents for both the analysis and pre-treatment of the sample. In particular, additions of mercury standards should be made in small volumes to the voltammetric cell, in order to reduce the volumes of solutions containing mercury; for this reason, it is essential that they are collected and transported to the laboratory for proper disposal. In our previous study, the direct determination of CH_3Hg did not seem possible since the concentration of chlorides and residues of organic matter in the solution eluted by the CYXAD were too high: chlorides could cause damage to the gold surface of the electrode, while organic matter created problems during the phase of the deposition of the analyte onto the electrode. Therefore, CH_3Hg concentration was determined by the difference between Hg_{TOT} and Hg_{IN}. Since Hg_{IN} was previously retained by the column and had to be eluted with concentrated HNO_3, there was higher variability in the recovery of the analyte and in its quantification. In this work, after elution, the solution was treated with H_2O_2 to oxidize most of the organic matter. Moreover, the analysis was performed using the "medium exchange" technique. These procedures reduce the passivation phenomena on the electrode's active surface due to the deposition of other substances on the WE surface and increase the sensitivity of the method.

3.2.2.4 Materials and Method

3.2.2.4.1 Instruments and Reagents

A mini dry bath, coupled with a metal block for 2 × 50 mL tubes, was used in the pre-treatment of the samples (Starlab S.r.l, Milano, Italy). A PalmSens^4 portable potentiostat (PalmSens, Houten, the Netherlands) was adopted for the electrochemical analyses. It was then connected to a portable computer; the different parameters for the analysis were set using the PSTrace 5.8 software. A magnetic stirrer (IKA-Topolino, Staufen, Germany) was connected to the PalmSens^4 and was

powered by a portable battery. An electrochemical cell with 15 mL minimum usable volume (Kit BASI, West Lafayette, IN, USA), equipped with an SGE (peek OD: 6 mm, ID: 1.6 mm, glass-bodied; Ionode, Tennyson, Australia) as a working electrode, a Pt auxiliary electrode with 6 mm × 6 mm foil (Ionode, Tennyson, Australia) and a glass-bodied refillable reference electrode, single-junction, with Ag/AgCl (Ionode, Tennyson, Australia) was used. A DMA-80 Direct Analyzer (FKV SrL, Torre Boldone, Italy) in the FKV laboratory in Torre Boldone (BG, Italy) was used for the atomic absorption spectrometry analyses. Analytical grade reagents were used. Nitric acid (HNO_3, 65%, Sigma-Aldrich Merck, Darmstadt, Germany), hydrogen peroxide (H_2O_2, 30%, Sigma-Aldrich Merck, Darmstadt, Germany) and hydrochloric acid (HCl, ACS Reagent, 37%, Fisher Scientific Italy, Rodano (MI), Italy) were also used. Briefly, 1000 mg L^{-1} of Sigma-Aldrich Hg solution was used to prepare working standard solutions of 1 mg L^{-1}. CH_3Hg standard solutions were prepared in high-purity water (HPW-Milli-Q, Millipore, 18.2 MΩ cm), using due precautions, from CH_3HgCl crystals (Pestanal, analytical standard, Sigma-Aldrich Merck, Darmstadt, Germany), then stored in a cool, dry place away from oxidizers. Calibration standards for DMA-80 were prepared using a NIST traceable stock solution of 1000 mg L^{-1} Hg, preserved in 5% HNO_3. All the working standards were freshly prepared weekly. An ionic liquid, namely, trihexyl(tetradecyl)phosphonium chloride (CYPHOS 101 solution, Sigma-Aldrich) was used to modify a polymeric sorbent, i.e., Amberlite XAD-1180 (Sigma-Aldrich). This new sorbent material (CYXAD: CYPHOS-modified XAD) was used to separate the Hg_{IN} and CH_3Hg after extraction with HCl.

The patented equipment for the outdoor analysis adopted in this work can be easily transported in a backpack and consists of: (i) test tubes filled with H_2O_2 at 30%, HNO_3 at 65%, or HCl at 37%; (ii) a bottle containing the solution for the electrochemical cleaning (0.1 mol L^{-1} $HClO_4$, 1.5 mmol L^{-1} NaCl and 0.5 mmol L^{-1} -Na_2-EDTA); (iii) two bottles containing HPW; (iv) test tube with 1 mg L^{-1} Hg standard solution; (v) a bottle containing 60 mmol L^{-1} HCl as the supporting electrolyte; (vi) a small balance to weigh aliquots of the sample; (vii) a mini dry bath for sample pretreatment; (viii) a portable battery; (ix) syringes to transfer the aliquot of a solution and filters to filter the aliquot of the sample solutions; (x) cartridges containing the CYXAD phase, equipped with a disposable inlet filter; (xi) micropipettes and tips for transferring the sample solution and adding known concentrations of analytes for calibration by standard additions; (xii) a cell, its perforated cap and the three electrodes (SGE; Ag/AgCl/KCl; Pt); (xiii) a Palmsens[4] portable potentiostat; (xiv) a portable computer; (xv) a tank for the wastewater.

3.2.2.4.2 Samples

The reference materials (RMs), namely, BCR-463 Tuna Fish ([Hg_{TOT}] = 2.85 ± 0.16 mg kg^{-1}; [CH_3Hg] = 3.04 ± 0.16 mg kg^{-1}) and ERM-CE464 Tuna Fish ([Hg_{TOT}] = 5.24 ± 0.10 mg kg^{-1}; [CH_3Hg] = 5.50 ± 0.17 mg kg^{-1}) were analyzed to assess the quality and accuracy of the analytical technique in question. Eight samples, specifically, two slices of tuna fish and one slice each of swordfish, blue marlin, codfish, rainbow trout and salmon trout were analyzed with the aim of testing the applicability of the technique for in situ analysis. The analyses were carried out near the experimental breeding tanks of the Department of Agricultural, Forest and Food Sciences, located in Carmagnola (Turin, Italy), where the rainbow trout was also caught from a tank. The other samples were purchased in local supermarkets or fish-markets located in the province of Turin (Italy). In all cases, the samples were analyzed outdoors to test the applicability of the whole procedure in the field.

3.2.2.4.3 Procedures

3.2.2.4.3.1 Extraction of Hg_{TOT}

Aliquots of 0.5 g of RM or the sample were added with a 1:1 mixture of HNO_3/H_2O_2 into 50 mL test tubes and warmed for 20 min at 70 ± 5 °C with the mini dry bath. Afterward, the solution was filtered through 0.45 μm polytetrafluoroethylene (PTFE) syringe filters and diluted to 15 mL with HPW. Subsequently, all the solutions were analyzed. All the analyses were performed in duplicate.

3.2.2.4.3.2 Preparation of the Modified New Sorbent—CYXAD

HPW, HCl (10% v/v) and ethanol were used in order to wash the Amberlite XAD-1180 resin to remove inorganic contaminants and residues; afterward, it was left to dry at room temperature. Lastly, it was functionalized using CYPHOS 101 with a resin:IL = 2:1 ratio in 5 mL of ethanol for 6 h. The suspension was then filtered through a PTFE filter and the new sorbent material that was obtained (CYXAD) was dried in an oven (1 h—60 °C), then collected in a vessel.

At this point, 40 mg of CYXAD was inserted into a Combitips 500 μL advanced Eppendorf syringe, as shown in Figure 4 (diameter = 4.5 mm).

Figure 4. Eppendorf syringe packed with CYPHOS

Previously, a Teflon filter was inserted into the syringe to maintain the resin inside the tube. The CYXAD material is durable and can be stored for up to six months; this way, it is possible to prepare packed cartridges that are ready for use.

3.2.2.4.3.3 Speciation System with Voltammetry

Each sample was subjected to two different types of pretreatment. The first aliquot was treated as explained earlier for the quantification of Hg_{TOT}, while the second aliquot was treated for the speciation study, as follows: 1 g of sample was placed into a 50 mL test tube, in contact with 6 mL of 8 mol L^{-1} HCl, and heated in the mini dry bath (20 min—70 °C). The high concentration of Cl^- in the solution permits the formation of a negative complex with Hg^{2+} (tetrachloromercurate (II), $[HgCl_4]^{2-}$) and a neutral complex with CH_3Hg (methylmercury chloride, CH_3HgCl) [34]. Later, to lower the concentration of chloride ions (4 mol L^{-1}), the solution was diluted to 1:2 with HPW, at

which ratio the highest resin efficiency is realized. The solution was forced through the CYXAD cartridge that retained Hg_{IN} quantitatively, while the CH_3Hg was eluted. In this step, the CYXAD retains the anionic species of Hg, while the neutral species is eluted. In our former work [24], the eluate containing CH_3Hg was useless because it had too high a level of Cl^-, which would damage the SGE. The Hg_{IN} immobilized on the CYXAD was recovered with 5 mL of 6 mol L^{-1} HNO_3 and the voltammetric analysis was performed. The content of CH_3Hg was determined by difference ($[CH_3Hg] = [Hg]_{TOT} - [Hg]_{IN}$). After the elution in this scenario, the solution was added with concentrated H_2O_2 (1:1 ratio); then, 0.5 mL was added to 9.5 mL of 60 mmol L^{-1} HCl and analyzed. To reduce the matrix effect, the analysis was made utilizing the "medium exchange" procedure: the deposition step at 0 V was achieved by placing the electrode into the sample solution, then, with the aid of the "hold" function, the potential was kept constant and the cell was changed for a new one containing 20 mL of supporting electrolyte; then, the stripping step was begun.

3.2.2.4.3.4 ASV Measurement

Every day, the SGE was polished with alumina powder and activated by utilizing a potential of +0.6 V for 30 s in 60 mmol L^{-1} HCl [35]. There was no need to repeat these procedures during the analysis. Many researchers use CV treatment as an activation step for solid electrodes, for example, in the case of SGE, using H_2SO_4 as the supporting electrolyte; however, in our experience, an activation step of applying a potential of 0.60 V for 60 s in 60 mmol L^{-1} HCl before mercury determination is sufficient to keep the electrode surface active to enhance the quality and reproducibility of the mercury signal. The CV voltammogram, recorded in H_2SO_4, presents the characteristic anodic and cathodic peaks at +1.25 V and at +0.90 V, respectively [36]. Cyclic voltammetry is commonly used to check the quality and the area of the electrode surface [37].

After each quantification, the SGE was stored in a solution of 0.2 mol L^{-1} $HClO_4$/3 mmol L^{-1} NaCl/1 mmol L^{-1} NaEDTA (0.8 V—30 s), to eliminate the residues of Hg from its surface. For the development of the procedure, Hg standard solutions were used. Firstly, 10 mL of the aliquot test solution of 60 mmol L^{-1} HCl was transferred into the voltammetric cell to register the blank signal. The values of the voltammetric parameters were: frequency 15 Hz, step potential 0.006 V, and amplitude 0.03 V. The standard additions method was used for the determination of Hg content in the samples. After recording the voltammogram of the sample solution when spiked with a known concentration of analyte, the aliquots of Hg at a known concentration were added and the corresponding signals were recorded.

Aliquots of 0.5–1 mL of sample solutions were placed into the cell for the determination of analytes and diluted to 10 mL with the supporting electrolyte. The concentrations of Hg_{TOT} and CH_3Hg were determined in the sample extract. The content of CH_3Hg was determined directly in the extractant solution after the addition of H_2O_2.

3.2.2.4.3.5 DMA Analysis

All the data acquired using the proposed procedure were evaluated by comparing them with those obtained using DMA [33], the official method for the determination of Hg_{TOT}, according to the protocol proposed by J. Calderón [38] for the speciation study. For the quantification of Hg_{TOT}, aliquots of each sample were directly analyzed. For the determination of CH_3Hg, a double liquid-liquid extraction, initially with an organic solvent and then with L-cysteine, was required.

3.2.2.5 Conclusions

In this work, the suitability of a patented portable kit for on-site Hg_{TOT} and CH_3Hg determination in fish samples was demonstrated. SGE is the best option for in situ studies because it does not require surface modification. Since the LOQ (0.2 mg kg^{-1}) of the technique is less than the maximum allowable concentration in fish products (0.5 mg kg^{-1}), it is possible to use SGE to monitor the concentration of mercury in these matrices. ASV with SGE has proved to be an interesting technique, also in terms of on-site usage, particularly because of its ease of use, portability and sensitivity. The modern portable potentiostat permits on-site analysis. For the determination of Hg_{TOT}, an easy treatment with 1:1 HNO_3:H_2O_2 solution using a dry mini-bath allows the user to quantitatively extract mercury from the sample in the field. The major criticality was linked to the speciation step, particularly the need to create a simple, portable and fast technique for the determination of methylmercury. The development of the patented, homemade new resins, CYXAD, permitted us to separate the different forms of mercury: after the extraction of the two forms with HCl, the sample solution was eluted through a cartridge packed with CYXAD. The CH_3Hg was eluted, while the Hg_{IN} was retained in the cartridge. The direct determination of CH_3Hg was made possible by using two expedients that facilitate the determination of content during one step of the voltammetric analysis: the addition of H_2O_2 to degrade the organic matrix and the use of the medium exchange technique to avoid the electrode passivation effect due to the elevated concentration of chlorides in the eluent solution. With this method, the certified samples were first analyzed with the aim of assessing the accuracy of the technique; subsequently, the applicability of the portable procedure was evaluated by analyzing genuine samples such as fresh tuna steaks, swordfish and trout. The portable procedure has shown excellent applicability for the on-site determination of Hg_{TOT}, CH_3Hg and/or Hg_{IN} since the results obtained with it are consistent with those obtained with DMA.

The new CYXAD cartridges permit the simplification of the application of the procedure out of doors. This cartridge could also be used in the laboratory for the separation of mercury and methylmercury before analysis. For example, the researcher could substitute the long procedure for methylmercury extraction, avoiding the use of organic solvent, e.g., before DMA analysis, making the separation procedures both more eco-friendly and faster.

With regard to the mercury content found in the considered samples, the situation appears worrying, in particular with regard to the sea fish, which showed concentrations above the legal limit for predatory fish. This underlines the importance of having a fast and simple technique that allows researchers to increase the number of controls on these matrices. The proposed procedure meets these needs precisely: it proved to be suitable for rapid screening analyses, permitting an increase in the monitoring of Hg_{TOT} and CH_3Hg in fish products to protect the health of consumers.

3.2.2.6 Patents

The "Portable kit for mercury speciation analysis" obtained an Italian patent license (priority n° 102019000005904).

References

1. Morel, F.M.M.; Kraepiel, A.M.L.; Amyot, M. The Chemical Cycle and Bioaccumulation of Mercury. Annu. Rev. Ecol. Syst. 1998, 29, 543–566.

2. Lehnherr, I. Methylmercury Biogeochemistry: A Review with Special Reference to Arctic Aquatic Ecosystems. Environ. Rev. 2014, 22, 229–243.
3. Wolfe, M.F.; Schwarzbach, S.; Sulaiman, R.A. Effects of Mercury onWildlife: A Comprehensive Review. Environ. Toxicol. Chem. 1998, 17, 146–160.
4. Udaya Kumar, Y.D.; Christopher, V.; Sobha Rani, D.; Nagendra Sastri, Y. A study on distribution of protein, lipids and carbohydrates in muscle and liver of marine associated upeneus vittatus. Int. J. Pharm. Sci. Res. 2015, 6, 1294–1301.
5. Liu, Y.; Buchanan, S.; Anderson, H.A.; Xiao, Z.; Persky, V.; Turyk, M.E. Association of Methylmercury Intake from Seafood Consumption and Blood Mercury Level among the Asian and Non-Asian Populations in the United States. Environ. Res. 2018, 160, 212–222.
6. Zheng, N.; Wang, S.; Dong, W.; Hua, X.; Li, Y.; Song, X.; Chu, Q.; Hou, S.; Li, Y. The Toxicological Effects of Mercury Exposure in Marine Fish. Bull. Environ. Contam. Toxicol. 2019, 102, 714–720.
7. Regulation (EU) No 420/2011 of the European Parliament and of the Council of April 29th 2011. European: Amending Regulation (EC) No 1881/2006 of the European Parliament. Available online: https://eur-lex.europa.eu/legal-content/EN/ALL/?uri= celex%3A32011R0420 (accessed on 12 May 2022).
8. EFSA Panel on Contaminants in the Food Chain (CONTAM). Scientific Opinion on the Risk for Public Health Related to the Presence of Mercury and Methylmercury in Food. EFS2 2012, 10, 2985.
9. Madenjian, C.P.; Chipps, S.R.; Blanchfield, P.J. Time to Refine Mercury Mass Balance Models for Fish. Facets 2021, 6, 272–286.
10. Method 1630: Methyl Mercury inWater by Distillation, Aqueous Ethylation, Purge and Trap, and Cold Vapor Atomic Fluorescence Spectrometry. 1998; Volume 55. Available online: https://www.epa.gov/sites/default/files/2015-08/documents/method_1630_1998.pdf (accessed on 12 May 2022).
11. Frentiu, T.; Butaciu, S.; Darvasi, E.; Ponta, M.; Senila, M.; Levei, E.; Frentiu, M. Sono-Induced Cold Vapour Generation Interfaced with Capacitively Coupled Plasma Microtorch Optical Emission Spectrometry: Analytical Characterization and Comparison with Atomic Fluorescence Spectrometry. J. Anal. At. Spectrom. 2015, 30, 1161–1168.
12. Sørmo, E.G.; Ciesielski, T.M.; Øverjordet, I.B.; Lierhagen, S.; Eggen, G.S.; Berg, T.; Jenssen, B.M. Selenium Moderates Mercury Toxicity in Free-Ranging Freshwater Fish. Environ. Sci. Technol. 2011, 45, 6561–6566.
13. Kubá ˇ n, P.; Houserová, P.; Kubá ˇ n, P.; Hauser, P.C.; Kubá ˇ n, V. Mercury Speciation by CE: A Review. Electrophoresis 2007, 28, 58–68.
14. Chen, S.-S.; Chou, S.-S.; Hwang, D.-F. Determination of Methylmercury in Fish Using Focused Microwave Digestion Following by Cu2+ Addition, Sodium Tetrapropylborate Derivatization, n-Heptane Extraction, and Gas Chromatography–Mass Spectrometry. J. Chromatogr. A 2004, 1024, 209–215.
15. Lee, D.; Lee, K.-G. Mercury and Methylmercury in Korean Herbal Medicines and Functional Health Foods. Food Addit. Contam. Part B 2013, 6, 279–284.
16. Kongchum, M.; Devai, I.; DeLaune, R.D.; Jugsujinda, A. Total Mercury and Methylmercury in Freshwater and Salt Marsh Soils of the Mississippi River Deltaic Plain. Chemosphere 2006, 63, 1300–1303.

17. Kuballa, T.; Leonhardt, E.; Schoeberl, K.; Lachenmeier, D.W. Determination of Methylmercury in Fish and Seafood Using Optimized Digestion and Derivatization Followed by Gas Chromatography with Atomic Emission Detection. Eur. Food Res. Technol. 2009, 228, 425–431.
18. Narukawa, T.; Iwai, T.; Chiba, K.; Feldmann, J. A Method for Methylmercury and Inorganic Mercury in Biological Samples Using High Performance Liquid Chromatography–Inductively Coupled Plasma Mass Spectrometry. Anal. Sci. 2018, 34, 1329–1334.
19. Inagaki, K.; Kuroiwa, T.; Narukawa, T.; Yarita, T.; Takatsu, A.; Okamoto, K.; Chiba, K. Certification of Methylmercury in Cod Fish Tissue Certified Reference Material by Species-Specific Isotope Dilution Mass Spectrometric Analysis. Anal. Bioanal. Chem. 2008, 391, 2047–2054.
20. Park, J.-S.; Lee, J.-S.; Kim, G.-B.; Cha, J.-S.; Shin, S.K.; Kang, H.-G.; Hong, E.-J.; Chung, G.-T.; Kim, Y.-H. Mercury and Methylmercury in Freshwater Fish and Sediments in South Korea Using Newly Adopted Purge and Trap GC-MS Detection Method. Water Air Soil Pollut. 2010, 207, 391–401.
21. Afonso, F.; Ribeiro, F.; Proença, L.; Lopes, M.I.S.; Rocha, M.M.; Neto, M.M.M.; Fonseca, I.T.E. Voltammetric Studies on the Electrochemical Reduction of Methylmercury in HCl Aqueous Medium at a Carbon Microelectrode. Electroanalysis 2005, 17, 127–133.
22. Ribeiro, F.; Neto, M.M.M.; Rocha, M.M.; Fonseca, I.T.E. Voltammetric Studies on the Electrochemical Determination of Methylmercury in Chloride Medium at Carbon Microelectrodes. Anal. Chim. Acta 2006, 579, 227–234.
23. Augelli, M.; Abarza Munoz, R.; Richter, E.; Gouveia Junior, A.; Angnes, L. Chronopotentiometric Stripping Analysis Using Gold Electrodes, an Efficient Technique for Mercury Quantification in Natural Waters. Electroanalysis 2005, 17, 755–761.
24. Giacomino, A.; Ruo Redda, A.; Caligiuri, R.; Inaudi, P.; Squadrone, S.; Abete, M.C.; Abollino, O.; Morandi, S.; Conca, E.; Malandrino, M. Development of an Easy Portable Procedure for On-Site Determination of Mercury and Methylmercury. Food Chem. 2021, 342, 128347.
25. Ireland-Ripert, J.; Bermond, A.; Ducauze, C. Determination of methylmercury in the pressure of inorganic mercury by anodic stripping voltammetry. Anal. Chim. Acta 1982, 143, 249–254.
26. Heaton, R.C.; Laitinen, H.A. Electroanalytical Studies of Methylmercury in Aqueous Solution. Anal. Chem. 1974, 46, 547–553.
27. Agraz, R.; Sevilla, M.T.; Hernandez, L. Voltammetric Quantification and Speciation of Mercury Compounds. J. Electroanal. Chem. 1995, 390, 47–57.
28. Moretto, L.M.; Ugo, P.; Lacasse, R.; Champagne, G.Y.; Chevalet, J. Determination of Methylmercury at Nafion® Coated Electrodes by Single and Multiple Pulse Voltammetric Techniques. J. Electroanal. Chem. 1999, 467, 193–202.
29. Lai, R.; Huang, E.L.; Zhou, F.;Wipf, D.O. Selective Determination of Methylmercury by Flow-Injection Fast-Scan Voltammetry. Electroanal. Int. J. Devoted Fundam. Pract. Asp. Electroanal. 1998, 10, 926–930.
30. Jaworski, A.; Stojek, Z.; Osteryoung, J.G. Oxidation of Mercury Microelectrodes in Complexing Media in the Presence and Absence of Supporting Electrolyte. J. Electroanal. Chem. 2003, 558, 141–153.
31. Korolczuk, M.; Rutyna, I. New Methodology for Anodic Stripping Voltammetric Determination of Methylmercury. Electrochem. Commun. 2008, 10, 1024–1026.

32. Abollino, O.; Giacomino, A.; Malandrino, M.; Piscionieri, G.; Mentasti, E. Determination of Mercury by Anodic Stripping Voltammetry with a Gold Nanoparticle-Modified Glassy Carbon Electrode. Electroanalysis 2008, 20, 75–83.
33. United States Environmental Protection Agency (EPA). Mercury in Solids and Solutions by Thermal Ecomposition, Amalgamation, and Atomic Absorption Spectrophotometry; EPA: Washington, DC, USA, 2007. Available online: https://www.epa.gov/esam/epamethod-7473-sw-846-mercury-solids-and-solutions-thermal-decomposition-amalgamation-and (accessed on 12 May 2022).
34. Escudero, L.B.; Olsina, R.A.; Wuilloud, R.G. Polymer-Supported Ionic Liquid Solid Phase Extraction for Trace Inorganic and Organic Mercury Determination in Water Samples by Flow Injection-Cold Vapor Atomic Absorption Spectrometry. Talanta 2013, 116, 133–140.
35. Ruo Redda, A.; Abollino, O.; Malandrino, M.; Squadrone, S.; Abete, M.C.; Berto, S.; Toniolo, R.; Durbiano, F.; Giacomino, A. A Portable Setup for the Voltammetric Determination of Total Mercury in Fish with Solid and Nanostructured Gold Electrodes. Molecules 2019, 24, 1910.
36. Giacomino, A.; Ruo Redda, A.; Squadrone, S.; Rizzi, M.; Abete, M.C.; La Gioia, C.; Toniolo, R.; Abollino, O.; Malandrino, M. Anodic stripping voltammetry with gold electrodes as an alternative method for the routine determination of mercury in fish. Comparison with spectroscopic approaches. Food Chem. 2017, 221, 737–745.
37. Su, C.; Li, Z.; Zhang, D.; Wang, Z.; Zhou, X.; Liao, L.; Xiao, X. A highly sensitive sensor based on a computer-designed magnetic molecularly imprinted membrane for the determination of acetaminophen. Biosens. Bioelectron. 2020, 148, 111819.
38. Calderón, J.; Gonçalves, S.; Cordeiro, F. Determination of Methylmercury in Seafood by Direct Mercury Analysis: Standard Operating Procedure; European Commission Joint Research Center: Ispra, Italy, 2013; Available online: https://www.africanfoodsafetynetwork.org/wp-content/uploads/2020/08/SOP-for-Analysis-of-Methyl-Mercury.pdf (accessed on 12 May 2022).

4. IRON SPECIATION FOR THE EARLY DIAGNOSIS OF NEURODEGENERATIVE DISEASES

4.1 General introduction

During the conducted doctoral research, various methods were tested for iron speciation in view of its use as a potential marker in neurodegenerative diseases.

In particular, modifications of different voltametric parameters were tested, in order to enhance iron accumulation on the working electrode, including the modification of the active surface of WE (a glassy carbon electrode, GCE) with mercury film, nafion film, cysteine and gold nanoparticles. Several ligands were tested, such as 2,2'-bipyridine (BP), 2,3-dihydroxynaphthalene (DHN), sodium pyrophosphate ($Na_4O_7P_2$), deferoxamine ($C_{25}H_{48}N_6O_8$), ferrozine ($C_{20}H_{12}N_4Na_2O_6S_2 \cdot H_2O$), along with various supporting electrolytes like Britton Robinson buffer, hydrochloric acid, potassium chloride, lithium chloride, tetra-n-butylammonium hexafluorophosphate (NBu_4PF_6), acetate buffer, HEPES (4-(2-hydroxyethyl)-1-piperazineethanesulfonic acid), perchloric acid and sulfuric acid.

During these tests, several challenges were encountered, including stability issues of the applied modification, selectivity of the chosen ligand, difficulty in maintaining iron in the predetermined form, and choice of suitable voltammetric parameters. The most effective approach, both as a modification to the working electrode (WE) and in terms of applicability, is detailed in the following paper, where it was possible to determine iron (III) in lake waters. The next step in the coming years will involve testing the method on samples of biological fluids.

4.2 Published research paper

4.2.1 Advancements in Portable Voltammetry: A Promising Approach for Iron Speciation Analysis

Paolo Inaudi[1,*], Ornella Abollino[1], Monica Argenziano[1], Mery Malandrino[2], Caterina Guiot[3], Stefano Bertinetti[2], Laura Favilli[1] and Agnese Giacomino [1]

[1] Department of Drug Science and Technology, University of Torino, Via Pietro Giuria 9, 10125 Turin, Italy

[2] Department of Chemistry, University of Torino, Via Pietro Giuria 5, 10125 Torino, Italy

[3] Department of Neurosciences “Rita Levi Montalcini”, University of Torino, 10125 Torino, Italy;

∗ Corresponding authors

Received: 3 October 2023

Revised: 23 October 2023

Accepted: 1 November 2023

Published: 3 November 2023

https://doi.org/10.3390/molecules28217404

MOLECULES – 2023, 28, 21**4.2.1.1 Abstract**

Iron, a crucial element in our environment, plays a vital role in numerous natural processes. Understanding the presence and concentration of iron in the environment is very important as it impacts various aspects of our planet's health. The on-site detection and speciation of iron are significant for several reasons. In this context, the present work aims to evaluate the applicability of voltammetry for the on-site determination of iron and its possible speciation using a portable voltammetric analyzer. Voltammetry offers the advantage of convenience and cost-effectiveness. For iron (III) determination, the modification of a glassy carbon electrode (GCE) with an antimony bismuth film (SbBiFE) using the acetate buffer (pH = 4) as a supporting electrolyte was used. The technique adopted was Square Wave Adsoptive Cathodic Stripping Voltammetry (SW-AdCSV), and we used 1-(2-piridylazo)-2-naphthol (PAN) as the iron (III) ligand. Linearity, repeatability, detection limit, and accuracy were determined using synthetic solutions; then, a Standard Reference Material (SRM) of 1643f Trace Elements in Water (iron content: 93.44 ± 0.78 μg L^{-1}) was used for validation measurements in the real matrix. the accuracy of this technique was found to be excellent since we obtained a recovery of 103.16%. The procedure was finally applied to real samples (tap, lake, and seawater), and the results obtained were compared via Inductively Coupled Plasma-Optical Emission Spectroscopy (ICP-OES). The amount of iron found was 207.8 ± 6.6 μg L^{-1} for tap water using voltammetry and 200.9 ± 1.5 μg L^{-1} with ICP-OES. For lake water, 171.7 ± 3.8 μg L^{-1}, 169.8 ± 4.1 μg L^{-1}, and 187.5 ± 5.7 μg L^{-1} were found using voltammetry in the lab both on-site and using ICP-OES, respectively. The results obtained demonstrate the excellent applicability of the proposed on-site voltammetric procedure for the determination of iron and its speciation in water.

4.2.1.2 Introduction

Iron has both positive and negative impacts on the environment, depending on its form, concentration, and distribution [1,2]. Iron is an essential micronutrient for living organisms, including humans, plants, and animals. As for humans, it plays a crucial role in various biological processes, such as oxygen transport, energy production, and enzyme function. Furthermore, it is a component of soil minerals and plays a vital role in maintaining soil fertility [3,4]. It affects soil structure, pH balance, and nutrient availability [1]. Adequate iron levels promote healthy plant growth and development. On the other hand, high concentrations of iron in water can lead to contamination. Iron-rich groundwater or surface water can lead to discoloration, presenting a reddish or brownish tint. This iron-contaminated water may be unsuitable for certain uses, such as drinking, irrigation, or industrial processes.

Iron is present in waters at concentrations that vary greatly among sea, lake, or drinking water. Soluble iron is found in seawater in very low concentrations (nanomolar or picomolar) due to some phenomena, such as particle scavenging, low solubility, and the effective removal caused by biological absorption. These processes are less present in other waters, such as lake water or drinking water, in which iron concentrations are higher [5,6,7,8].

Iron also has a relevant influence on human health: whereas it is an essential nutrient required for various physiological processes, its dysregulation can contribute to the pathogenesis of neurodegenerative disorders such as Alzheimer's disease, Parkinson's disease, and Huntington's disease [9,10,11,12,13]. In a recent paper, Baringer et al. [14] emphasized the fundamental role that

iron plays in human neurological health and, in this way, many studies have been carried out in order to understand its role and facilitate its determination as a marker of such diseases [10,15].

Electrochemical methods are widely used for iron determination and speciation due to their sensitivity, selectivity, and ability to provide real-time measurements [4,16]. Over the years, different voltammetric techniques and iron complexants that are able to enhance the selectivity and sensitivity of responses, have been tested. Differential pulse voltammetry (DPV), Cyclic Voltammetry (CV) and Square Wave Voltammetry (SWV) are the most commonly used techniques [17,18,19,20,21]. A wide range of complexing agents have been used, such as 1-nitroso-2-naphthol (NN) [22], 4,4'-[3-(2-pyridyl)1,2,4-triazine-5,6-diyl]bis(benzene sulfonic acid) disodium salt hydrate (ferrozine, FZ) [23], dihydroxynaphthalene (DHN) [24,25], 2-(5-bromo-2-pyridylazo)-5-diethylaminophenol (5-Br-PADAP) [26] and 2-(2-thiazolylazo)-p-cresol (TAC) [27]. Another fundamental aspect is the use of suitably modified working electrodes (WE); in the literature, there are some important examples, such as chemically modified carbon-paste electrodes (CMCPEs) [28,29], nafion-coated electrodes (NCE) [30], thick-film graphite containing electrode modified with calomel (TFGME) [31], boron-doped diamond (BDD) electrodes [32], bismuth-coated glassy carbon electrodes (BiFE) [33,34], gold and bismuth bimetallic nanoparticles decorated with l-cysteine-functionalized graphene oxide nanocomposites (Au-BiNPs/SH-GO) [35] and gold 2-mercaptosuccinic acid self-assembled monolayers (AuMSA SAM) [36]. In recent years, even more complex electrode modifications have been tested for simultaneous iron (II) and iron (III) detection using, e.g., nitrogen-doped carbon quantum dot silver nanoparticle β-cyclodextrin nanomaterials (N-CQDs/AgNPs/β-CD) [37]. The use of electrode-specific modifiers and complexants greatly helps increase the selectivity and sensitivity of these voltammetric methods.

An advantage of voltammetry is the availability of portable instruments that enable on-site measurements and are useful in various fields, such as clinical practice, quality control, and environmental monitoring.

The aim of this study was to develop a new portable voltammetric method for the on-site determination of iron (III) in different types of water. This work is focused on the use of a new antimony-bismuth film-modified glassy carbon electrode (SbBiFE-GCE) coupled with 1-(2-piridylazo)-2-naphthol (PAN) as a ligand for iron (III). All the analyses were carried out in triplicate with the use of a portable potentiostat and tested outside laboratories.

4.2.1.3 Results and Discussion

The aim of this paper was to develop a method that allowed iron (III) to be selectively analyzed when present in different matrices directly in the field.

The decision to modify the electrode with a film of Sb-Bi was made starting from the study of Segura et al. [33], where only Bi was used, integrating with other recent studies using Sb for the modification of WE.

The optimization of conditions for film formation was carried out by testing different concentrations of Bi and Sb and different deposition times. As for the potential of deposition and the supporting electrolyte, it was decided to use those reported in some papers regarding only the bismuth film [33,34]. The tests were carried out by evaluating the accuracy of determining a concentration of 5 μg L^{-1} of iron (III) in a synthetic solution (10 mL of 0.1 mol L^{-1} acetate buffer (pH 4) and 5 μmol L^{-1} PAN).

In particular, the conditions reported in Table 1 were tested.

Table 1 - Tests for best SbBiFE performance.

Test	Bi concentration (mg L^{-1})	Sb concentration (mg L^{-1})	Deposition time (s)	Accuracy (% of recovery)
1	300	200	300	76.7
2	300	200	120	n.d.
3	300	200	30	n.d.
4	**100**	**50**	**300**	**95.3**
5	100	50	120	89.8
6	100	50	30	88.7
7	20	10	300	80.5
8	20	10	120	n.d.
9	20	10	30	n.d.

In tests 2–3, using 300 and 200 mg L^{-1} of Bi and Sb, respectively, with a deposition time of 120 and 30 s, the film did not stick to the WE surface, and iron was not determined (n.d. in Table 1); after 300 s (test 1), the results were better, but the film was thicker, and the sensitivity (data not showed) was worse than the analog with lower concentrations of Bi and Sb (test 4) as well as the obtained recovery.

Tests 7–9 experienced similar problems as follows: with short deposition times, iron was not determinable. The best results were obtained with test number 4, with a percentage recovery of 95.3%.

All the preliminary tests were made first on synthetic solutions (Table 1) and then on a SRM 1643f using the SWAdSW parameters reported.

To obtain good results in terms of sensitivity, different concentrations of PAN were tested, namely 1, 5, and 10 μmol L^{-1}. The concentration that permitted the best response was 5 μmol L^{-1} in the cell, confirming the findings by Segura et al. [33]; tests made at higher and lower concentrations (10 μmol L^{-1} and 1 μmol L^{-1}) gave rise to a worsening performance for this method. In particular, with a higher concentration, we lost sensitivity (87.5% recovery), and with a lower concentration, iron was not displayed.

Tests were also made using a standard of iron (II), showing an absence in the signal and consequently certifying the selectivity of the method and of the complexant used for iron (III) in the experimental conditions adopted.

In the second step of this work, samples were analyzed for the total iron, as described in Section 2.2 and Section 2.3, after the addition of nitric acid in order to oxidize any iron (II) present.

The results obtained for total iron were also confirmed by another analytical technique, namely ICP-OES.

4.2.1.3.1. Synthetic Solutions

The first tests were carried out on synthetic solutions. The electrochemical cell was composed of 10 mL of a 0.1 mol L^{-1} acetate buffer (pH 4) and 5 μmol L^{-1} of PAN, to which subsequent aliquots of iron (III) were added.

Figure 1 reports voltammograms for the blank and four successive additions of iron (III). The analytical signal was the current intensity registered for the potential of −0.475 V.

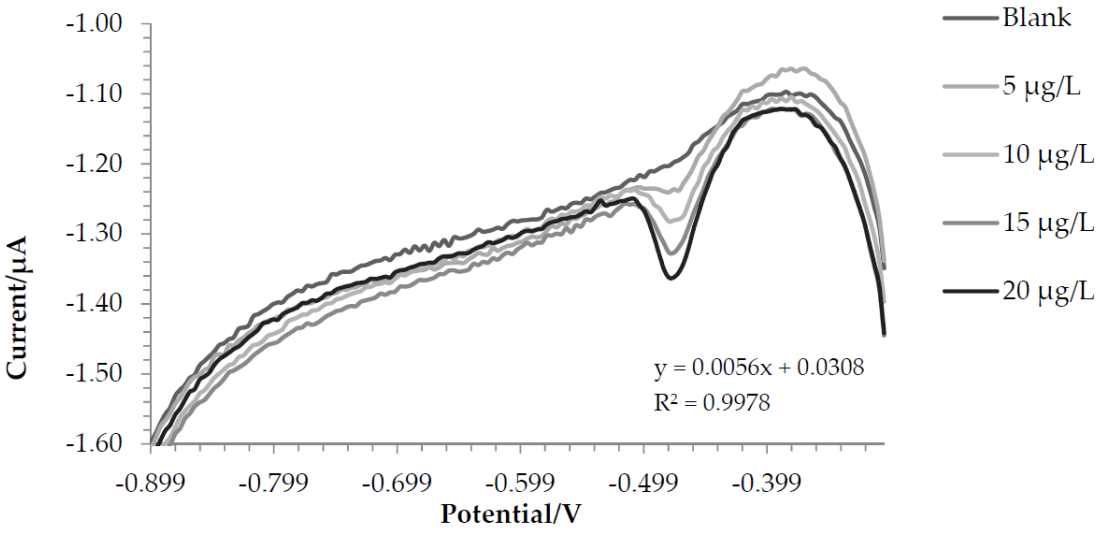

Figure 1. Voltammograms of the blank solution and successive additions of iron (III).

The results obtained are shown in Table 2.

Table 2 – Figures of merit of the developed method.

WE	Analyte	Repeatability (RSD %, n=3)	Linearity	LOD* (µg L^{-1})	LOQ * (µg L^{-1})	Accuracy (% recovery)
SbBiFE	Iron (III)	3.05	y = 0.056x + 0.0308 R^2 = 0.9978	0.54	1.78	95.4

* Limit of Detection (LOD) and Limit of Quantification (LOQ) were estimated as 3 and 10 times the standard deviation of the blank (n=3), respectively.

Reproducibility studies were performed intracell, intercell, in the laboratory and in the field with a relative % RSD of 2.8%, 3.0%, 4.1%, and 3.9%. In Figure 2, the voltammogram of three standard additions of iron (II) and a subsequent one of iron (III) demonstrates the selectivity of this method for iron (III).

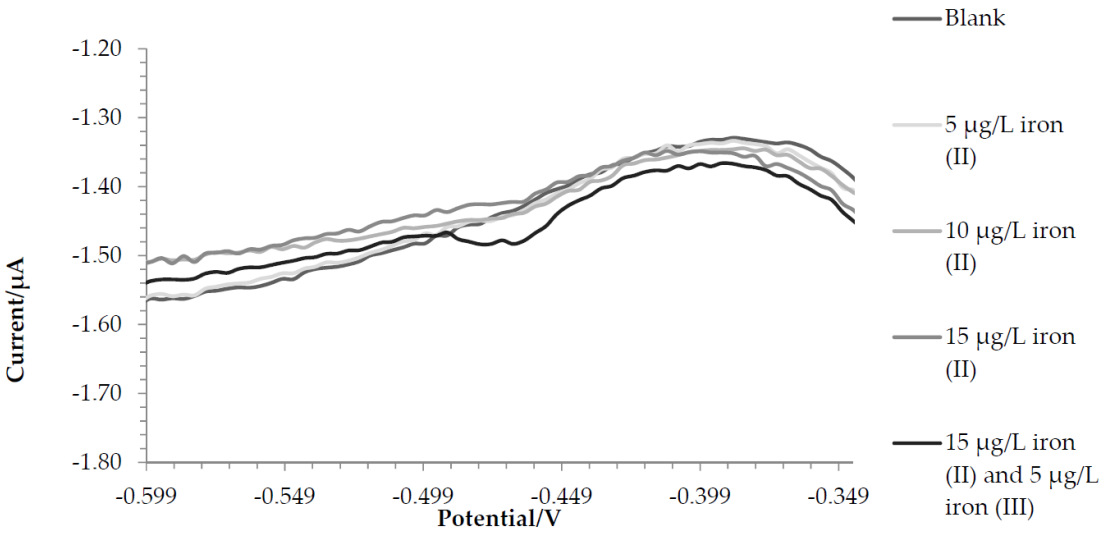

Figure 2. Voltammograms of the blank solution, successive additions of iron (II) and an addition of iron (III).

The true iron concentration of the home-made standards used for the preparation of synthetic solutions was checked using ICP-OES for the analysis of the total iron present in the solution. The concentrations were computed by means of an external calibration obtained via dilution from a concentrated (1000 mg L^{-1}) Sigma-Aldrich standard solution. The results obtained, as shown in Table 3, confirm the reliability of the iron (III) and iron (II) standards.

Table 3 – Analysis of prepared iron standards vs ICP-OES.

Analyte	Theoretical concentration prepared (µg L^{-1})	Results with ICP-OES (µg L^{-1})	Recovery (%)
Iron (II)	1000	1058	105.8
Iron (III)	1000	1034	103.4

4.2.1.3.2 Certified Reference Material

After that, the accuracy of the method was tested on a Standard Reference Material (SRM) 1643f—Trace Elements in Water—with a total iron-certified concentration of 93.44 ± 0.78 µg L^{-1}.

The iron (III) concentration in SRM was estimated using the standard addiction method, as reported before. The accuracy of this technique was found to be excellent since we found 96.40 ± 2.45 µg L^{-1} of iron with a recovery of 103.16%. The SRM 1643f contained HNO_3 as a stabilizer; therefore, it was not surprising to find all the iron as iron (III).

Figure 3 shows the voltammogram for this test.

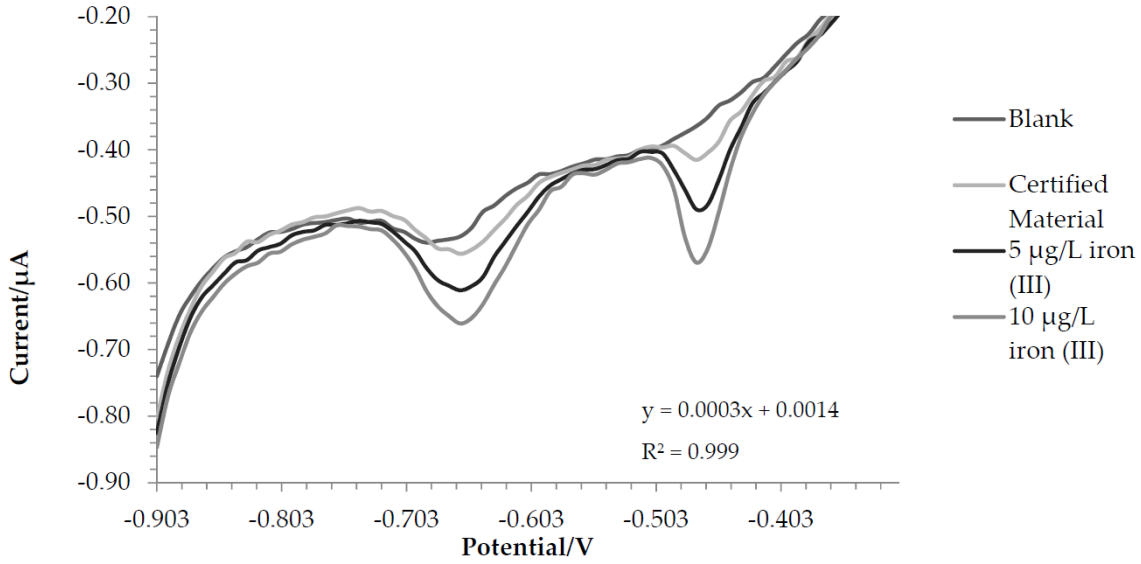

Figure 3. Voltammograms of SRM and two standard additions of Fe(III).

4.2.1.3.3 Water Samples

After optimizing and verifying the effectiveness of this method, it was tested on real samples of water (tap water, sea water, and lake water).

For lake water, the same sample was analyzed both in the laboratory and in the field to demonstrate the applicability of this method outside the laboratory.

Figure 4 and Figure 5 show the voltammograms of lake water and tap water, respectively.

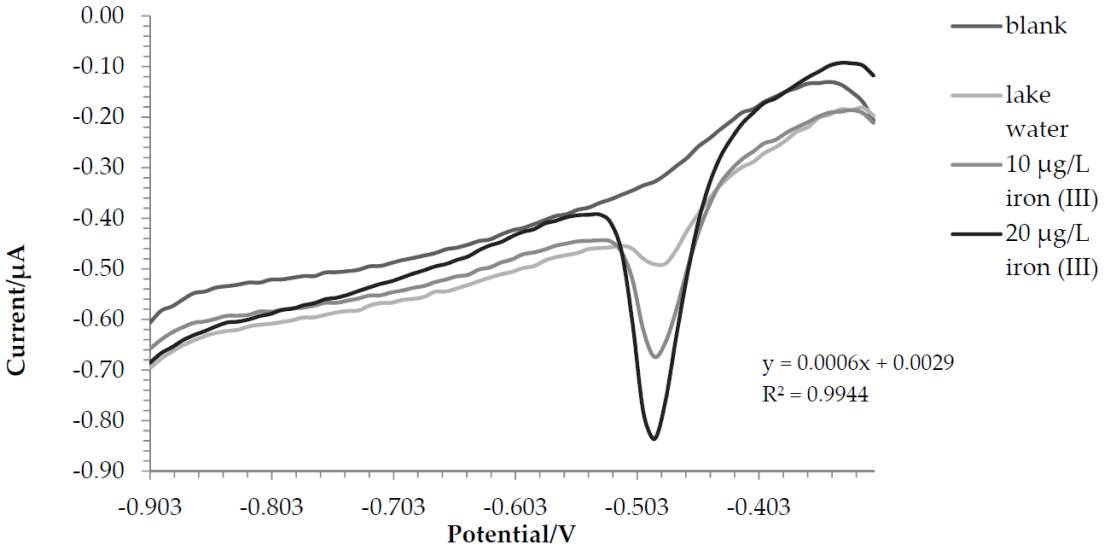

Figure 4. Voltammograms recorded for lake water analysis.

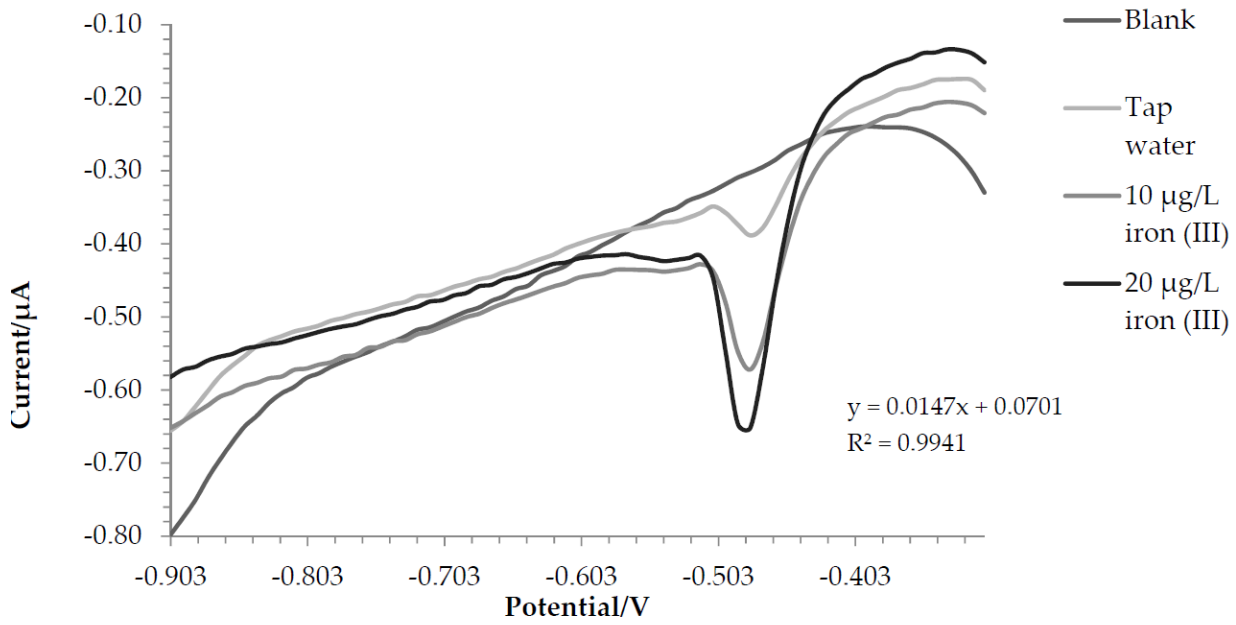

Figure 5. Voltammograms recorded for tap water analysis.

For lake and tap water, the method responded excellently; in detail, the tests were carried out in triplicate, and a comparison with ICP-OES was also made. Before the analysis, nitric acid (final concentration 0.01 mol L^{-1}) was added to the water samples. In this way, all the iron in the solution was present as iron (III), and a direct comparison was performed between voltametric and ICP-OES analysis.

The amount of iron found was 171.7 ± 3.8 µg L^{-1} using voltammetry in the first test and 187.5 ± 5.7 µg L^{-1} with ICP-OES. For tap water, 207.8 ± 6.6 µg L^{-1} and 200.9 ± 1.5 µg L^{-1} were found via voltammetry and ICP-OES, respectively. A T-test was conducted to assess whether the results obtained with the two techniques were significantly different. For tap water, there were no significant differences between the two data (p-value = 0.14). In the case of lake water, the values were statistically different (p-value = 0.03); this was probably due to the fact that being a more complex matrix, not all iron (II) was oxidized to iron (III). In fact, the value at the ICP-OES, which evaluates the total iron, turned out to be higher.

However, it was not possible to determine the concentration of iron in seawater, probably due to the fact that the concentration of iron is presumably lower than the LOQ of the proposed technique. As an example, seawater from the eastern Mediterranean Sea contains around 83 ng L^{-1} of iron [38]. In any case, standard additions are displayed, and the instrumental LOQ was 2.07 µg L^{-1}.

This technique was found to be very accurate for water analysis even in the field; the lake water was also analyzed directly on-field, and the result was 169.8 ± 4.1 µg L^{-1} compared to the 171.7 ± 3.8 µg L^{-1} of the laboratory. Figure 6 shows a voltammogram of an on-site analysis of lake water. However, the greatest limitation of this procedure was the limited duration of the antimony and bismuth film. In fact, it was necessary to regenerate it every three samples in order not to lose sensitivity. The primary objective was to identify optimal conditions that could enhance the film's longevity. Subsequently, it is anticipated that future investigations could encompass additional surface modifications of the glassy carbon electrode (GCE) to explore further enhancements.

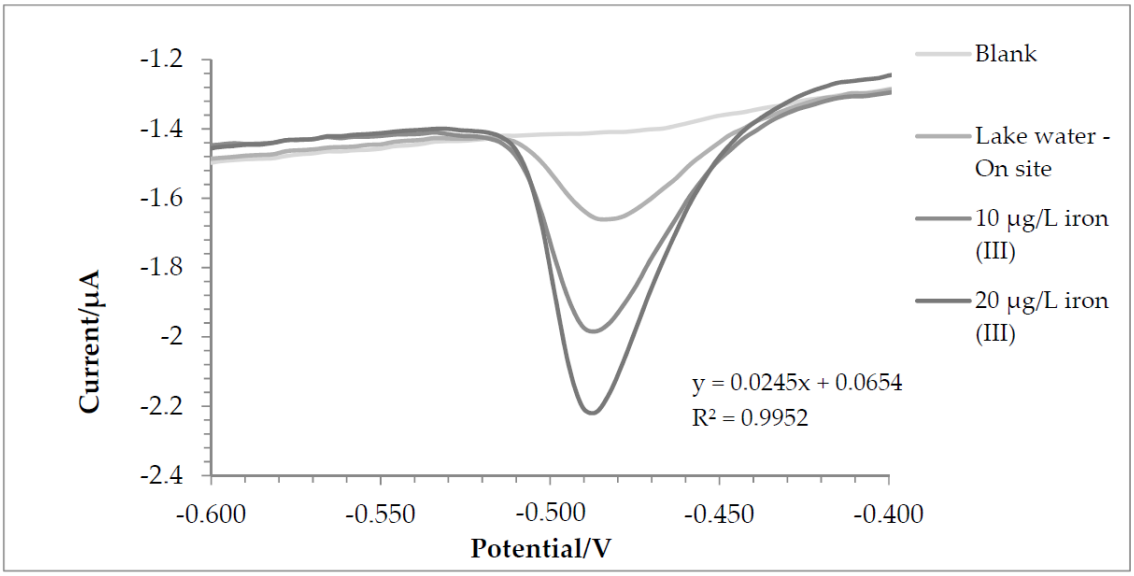

Figure 6. Voltammograms recorded for lake water for on-site analysis.

The innovative nature of this technique concerns its capacity to facilitate direct analytical assessments in remote geographic areas, enabling the real-time monitoring of iron concentrations while avoiding the logistical complexities associated with sample collection and transportation, particularly in challenging environmental contexts.

The future development of this study will be testing the applicability of the procedure to the analysis of biological samples (such as plasma or serum). Even more challenging is the detection of iron in Cerebrospinal Fluid (CSF), ranging from about 30 in controls to 70 µg L^{-1} in AD patients [39]. The determination of iron in CSF samples is carried out by means of a Graphite Furnace Atomic Absorption Spectrometer (GF-AAS), which is a very precise but time-requiring method. For the voltammetric analysis of CSF, matrix effects have to be removed. The following approaches may be used: centrifuge the sample to separate solid particles or precipitates from the liquid phase, adjust the pH of the sample, and dilute the samples with the supporting electrolyte at least 1:10.

4.2.1.4 Material and Method

4.2.1.4.1 Instruments

Square Wave Adsorptive Cathodic Stripping Voltammetry (SW-AdCSV) was carried out with a Palmsens[4] portable potentiostat (PalmSens, Houten, The Netherlands). The height of the peaks was always taken in "automatic mode" by the software (PS trace 5.9). A classic electrochemical cell was equipped with a glassy carbon WE (GCE, 2 mm diameter, Metrohm, Herisau, Switzerland), a Ag/AgCl/KCl 3 mol L^{-1} reference electrode (RE), and an auxiliary platinum electrode. A mechanical stirrer (IKA-Topolino, Staufen, Germany) was connected to the PalmSens[4] and powered by a portable battery for on-site analysis. A Cyberscan 2100 pH meter (Eutech Instruments srl, Thermo Fisher Scientific, Waltham, MA, USA) was used to adjust the solution's pH, and the pH meter was calibrated daily with pH 4 and pH 7 buffers. An Inductively Coupled Plasma-Optical Emission Spectrometer (ICP-OES), in particular Perkin Elmer Optima 7000 (Perkin Elmer, Norwalk, CT, USA), was used for the measurement of total iron in the test analysis.

4.2.1.4.2 Reagents

All solutions were prepared with high-purity water (HPW-Milli-Q, Millipore, 18.2 MΩ cm, Milford, MA, USA). Antimony and bismuth standard solutions were obtained via dilution from concentrated (1000 mg L^{-1}) Merck TraceCERT stock solutions (Merck, Darmstadt, Germany). Ammonium iron (II) sulfate hexahydrate and iron (III) nitrate nonahydrate (Sigma Aldrich-Merck, Darmstadt, Germany) were used for the preparation of iron (II) and iron (III) standards, respectively. Standard solutions were prepared for both analytes at a 1000 mg L^{-1} concentration and subsequently diluted to 1 mg L^{-1}. Acetate buffers (0.1 mol L^{-1}, pH 3.0–6.0) were prepared using potassium acetate and acetic acid (Sigma Aldrich-Merck, Darmstadt, Germany). A 0.001 mol L^{-1} solution of PAN (Sigma Aldrich-Merck, Darmstadt, Germany) was prepared in ethanol. Standard Reference Material (SRM) 1643f Trace Elements in Water (NIST, National Institute of Standards and Technology, Gaithersburg, MD, USA) with a total iron-certified concentration of 93.44 ± 0.78 μg L^{-1} were used for validation measurements.

4.2.1.4.3 Preparation of –SbBiFE-GCE

Before using the GCE was sequentially polished with three different alumina powders of different granulometry, namely 0.05, 0.3, and 1 μm (CH Instruments, Austin, TX, USA) on a microcloth pad (BASi, West Lafayette, IN, USA) and then rinsed with HPW and ethanol. This mechanical cleaning of the GCE was carried out daily.

After that, GCE was modified by the formation of a double film of bismuth and antimony in two successive steps. All parameters for film deposition and the amount of bismuth and antimony were optimized and are reported below.

The first step was the deposition of the antimony film; in particular, a cell containing 0.1 mol L^{-1} of the acetate buffer at pH 4.5 and 10 mL of the solution with an antimony concentration of 50 mg L^{-1} was prepared. A −1.0 V deposition potential was applied for 300 s.

The second step, analogously to the first one, allowed the subsequent deposition of bismuth onto the WE surface in the same supporting electrolyte but with a bismuth concentration equal to 100 mg L^{-1} in the 10 mL cell. The parameters for deposition were the same as those adopted for antimony.

4.2.1.4.4 Parameters for Iron Determination

For iron determination in a synthetic solution, a cell containing 10 mL of a 0.1 mol L^{-1} acetate buffer (pH 4) with an optimized and known concentration of PAN (5 μmol L^{-1}) was used.

For the analysis of the certified sample, the cell consisted of 0.5 mL of the sample, 9.5 mL of the acetate buffer 0.1 mol L^{-1} (pH 4), and an amount of 50 μL of PAN (final concentration 5 μmol L^{-1} in the cell). The concentration was quantified with the standard addition method by adding two successive aliquots of 5 μg L^{-1} of iron (III). The test was carried out in triplicate.

Lake water was collected from Avigliana Lake (Avigliana, TO, Italy), while the sea water was sampled in Savona (Italy). The water samples were sampled using 1 L plastic bottles, stored in the fridge, and the analysis of the sample was carried out within 24 h of collection.

For these samples, analyses were carried out using a voltammetric cell containing 0.25 mL of the sample, 9.75 mL of the 0.1 mol L^{-1} acetate buffer (pH 4), and 5 μmol L^{-1} of PAN. Then, two

standard additions of iron (III) (10 μg L^{-1} each) were made, and only two standard additions were performed on the samples due to the limited durability of the film.

The parameters optimized for iron (III) determination included deposition at −0.4 V for 180 s and a subsequent scan from −0.3 V to −0.9 with a frequency of 10 Hz and an amplitude of 0.025 V.

4.2.1.5 Conclusions

The proposed method has been shown to be excellent for the determination of iron (III) in water, using a method that is also applicable in the field.

The results obtained and the precision and accuracy of the optimized procedure make it possible to hypothesize its application in different areas. A future development of this method could be to increase the stability of Bi/Sb, thus reducing the frequency of its regeneration.

Overall, the time required for a complete voltammetric analysis, including film deposition, is 30 min; this value is acceptable, and a throughput of 25 samples for 8 h of operation is expected. This method is also suitable for speciation studies when considering that iron (II) is not detected using the proposed experimental conditions. This can allow for a potential increase in water analyses in cases of iron contamination or to investigate the role of this metal in biogeochemical cycles, even directly on site. This possibility could enable researchers to perform the rapid and immediate monitoring of iron concentrations, testing its suitability as a possible marker for the early detection of neurodegenerative diseases.

References

1. Nagajyoti, P.C.; Lee, K.D.; Sreekanth, T.V.M. Heavy metals, occurrence and toxicity for plants: A review. Environ. Chem. Lett. 2010, 8, 199–216.
2. Statham, P.J.; Jacobson, Y.; Van Den Berg, C.M.G. The measurement of organically complexed FeII in natural waters using competitive ligand reverse titration. Anal. Chim. Acta 2012, 743, 111–116.
3. Hopwood, M.J.; Birchill, A.J.; Gledhill, M.; Achterberg, E.P.; Klar, J.K.; Milne, A. A Comparison between Four Analytical Methods for the Measurement of Fe(II) at Nanomolar Concentrations in Coastal Seawater. Front. Mar. Sci. 2017, 4, 192.
4. Lu, M.; Rees, N.V.; Kabakaev, A.S.; Compton, R.G. Determination of Iron: Electrochemical Methods. Electroanalysis 2012, 24,1693–1702.
5. Liu, X.; Millero, F.J. The solubility of iron in seawater. Mar. Chem. 2002, 77, 43–54.
6. Bowie, A.R.; Maldonado, M.T.; Frew, R.D.; Croot, P.L.; Achterberg, E.P.; Mantoura, R.C.; Worsfold, P.J.; Law, C.S.; Boyd, P.W. The fate of added iron during a mesoscale fertilisation experiment in the Southern Ocean. Deep Sea Res. Part II Top. Stud. Oceanogr. 2001, 48, 2703–2743.
7. Wells, M.L. The level of iron enrichment required to initiate diatom blooms in HNLC waters. Mar. Chem. 2003, 82, 101–114.
8. Boyd, P.W.; Ellwood, M.J. The biogeochemical cycle of iron in the ocean. Nat. Geosci. 2010, 3, 675–682.
9. Zecca, L.; Youdim, M.B.H.; Riederer, P.; Connor, J.R.; Crichton, R.R. Iron, brain ageing and neurodegenerative disorders. Nat. Rev. Neurosci. 2004, 5, 863–873.
10. Ward, R.J.; Zucca, F.A.; Duyn, J.H.; Crichton, R.R.; Zecca, L. The role of iron in brain ageing and neurodegenerative disorders. Lancet Neurol. 2014, 13, 1045–1060.

11. Liu, J.-L.; Fan, Y.-G.; Yang, Z.-S.; Wang, Z.-Y.; Guo, C. Iron and Alzheimer's Disease: From Pathogenesis to Therapeutic Implications. Front. Neurosci. 2018, 12, 632.
12. Jasiecki, J.; Targon´ ska, M.;Wasa˛g, B. The Role of Butyrylcholinesterase and Iron in the Regulation of Cholinergic Network and Cognitive Dysfunction in Alzheimer's Disease Pathogenesis. Int. J. Mol. Sci. 2021, 22, 2033.
13. Kim, N.; Lee, H.J. Redox-Active Metal Ions and Amyloid-Degrading Enzymes in Alzheimer's Disease. Int. J. Mol. Sci. 2021, 22, 7697.
14. Baringer, S.L.; Simpson, I.A.; Connor, J.R. Brain iron acquisition: An overview of homeostatic regulation and disease dysregulation. J. Neurochem. 2023, 165, 625–642.
15. Xu, Y.; Huang, X.; Geng, X.; Wang, F. Meta-analysis of iron metabolism markers levels of Parkinson's disease patients determined by fluid and MRI measurements. J. Trace Elem. Med. Biol. 2023, 78, 127190.
16. Laglera, L.M.; Monticelli, D. Iron detection and speciation in natural waters by electrochemical techniques: A critical review. Curr. Opin. Electrochem. 2017, 3, 123–129.
17. Cuculi´c, V.; Pižeta, I.; Branica, M. Voltammetry of Dissolved Iron(III)-Nitrilotriacetate-Hydroxide System in Water Solution. Electroanalysis 2005, 17, 2129–2136.
18. Abualhaija, M.M.; Van Den Berg, C.M.G. Chemical speciation of iron in seawater using catalytic cathodic stripping voltammetry with ligand competition against salicylaldoxime. Mar. Chem. 2014, 164, 60–74.
19. Demir, E.; Göktug, Ö.; ˙Inam, R.; Doyduk, D. Development and characterization of iron (III) phthalocyanine modified carbon nanotube paste electrodes and application for determination of fluometuron herbicide as an electrochemical sensor. J. Electroanal. Chem. 2021, 895, 115389.
20. Vukosav, P.; Mlakar, M. Speciation of biochemically important iron complexes with amino acids: L-aspartic acid and L-aspartic acid—Glycine mixture. Electrochim. Acta 2014, 139, 29–35.
21. Van Huis, A. Edible Insects: Future Prospects for Food and Feed Security. In FAO Forestry Paper, No. 171; Food and Agriculture Organization of the United Nations: Rome, Italy, 2013.
22. Gledhill, M.; Van Den Berg, C.M.G. Measurement of the redox speciation of iron in seawater by catalytic cathodic stripping voltammetry. Mar. Chem. 2013, 50, 51–61.
23. Iwai, H.; Fukushima, M.; Yamamoto, M. Determination of Labile Fe(II) Species Complexed with Seawater Extractable Organic Matter Under Seawater Conditions Based on the Kinetics of Ligand-exchange Reactions with Ferrozine. Anal. Sci. 2013, 29, 723–728.
24. Laglera, L.M.; Caprara, S.; Monticelli, D. Towards a zero-blank, preconcentration-free voltammetric method for iron analysis at picomolar concentrations in unbuffered seawater. Talanta 2016, 150, 449–454.
25. Sanvito, F.; Pacileo, L.; Monticelli, D. Fostering and Understanding Iron Detection at the Ultratrace Level by Adsorptive Stripping Voltammetry with Catalytic Enhancement. Electroanalysis 2019, 31, 212–216.
26. Ghoneim, M.M.; Hassanein, A.M.; Hammam, E.; Beltagi, A.M. Simultaneous determination of Cd, Pb, Cu, Sb, Bi, Se, Zn, Mn, Ni, Co and Fe in water samples by differential pulse stripping voltammetry at a hanging mercury drop electrode. Fresenius J. Anal. Chem. 2000, 367, 378–383.
27. Croot, P.L.; Johansson, M. Determination of Iron Speciation by Cathodic Stripping Voltammetry in Seawater Using the Competing Ligand 2-(2-Thiazolylazo)-p-cresol (TAC). Electroanalysis 2000, 12, 565–576.

28. Gao, Z. Determination of iron with chemically-modified carbon-paste electrodes. Talanta 1991, 38, 1177–1184.
29. Gholivand, M.B.; Geravandi, B.; Parvin, M.H. Anodic Stripping Voltammetric Determination of Iron(II) at a Carbon Paste Electrode Modified with Dithiodianiline (DTDA) and Gold Nanoparticles (GNP). Electroanalysis 2011, 23, 1345–1351.
30. Ugo, P.; Moretto, L.M.; De Boni, A.; Scopece, P.; Mazzocchin, G.A. Iron(II) and iron(III) determination by potentiometry and ion-exchange voltammetry at ionomer-coated electrodes. Anal. Chim. Acta 2002, 474, 147–160.
31. Stozhko, N.Y.; Inzhevatova, O.V.; Kolyadina, L.I. Determination of Iron in Natural and DrinkingWaters by Stripping Voltammetry. J. Anal. Chem. 2005, 60, 668–672.
32. Ferreira, R.; Chaar, J.; Baldan, M.; Braga, N. Simultaneous voltammetric detection of Fe3+, Cu2+, Zn2+, Pb2+ e Cd2+ in fuel ethanol using anodic stripping voltammetry and boron-doped diamond electrodes. Fuel 2021, 291, 120104.
33. Segura, R.; Toral, M.I.; Arancibia, V. Determination of iron in water samples by adsorptive stripping voltammetry with a bismuth film electrode in the presence of 1-(2-piridylazo)-2-naphthol. Talanta 2008, 75, 973–977.
34. Bobrowski, A.; Nowak, K.; Zar˛ebski, J. Application of a bismuth film electrode to the voltammetric determination of trace iron using a Fe(III)–TEA–BrO3⊙ catalytic system. Anal. Bioanal. Chem. 2005, 382, 1691–1697.
35. Zhou, N.; Li, J.; Wang, S.; Zhuang, X.; Ni, S.; Luan, F.; Wu, X.; Yu, S. An Electrochemical Sensor Based on Gold and Bismuth Bimetallic Nanoparticles Decorated L-Cysteine Functionalized Graphene Oxide Nanocomposites for Sensitive Detection of Iron Ions in Water Samples. Nanomaterials 2021, 11, 2386.
36. Shervedani, R.K.; Hatefi-Mehrjardi, A.; Asadi-Farsani, A. Sensitive determination of iron(III) by gold electrode modified with 2-mercaptosuccinic acid self-assembled monolayer. Anal. Chim. Acta 2007, 601, 164–171.
37. Ma, X.; Yu, J.; Wei, L.; Zhao, Q.; Ren, L.; Hu, Z. Electrochemical sensor based on N-CQDs/AgNPs/-CD nanomaterials: Application to simultaneous selective determination of Fe(II) and Fe(III) irons released from iron supplement in simulated gastric fluid. Talanta 2023, 253, 123959.
38. Statham, P.J.; Hart, V. Dissolved iron in the Cretan Sea (eastern Mediterranean). Limnol. Oceanogr. 2005, 50, 1142–1148.
39. Ficiarà, E.; Boschi, S.; Ansari, S.; D'Agata, F.; Abollino, O.; Caroppo, P.; Di Fede, G.; Indaco, A.; Rainero, I.; Guiot, C. Machine Learning Profiling of Alzheimer's Disease Patients Based on Current Cerebrospinal Fluid Markers and Iron Content in Biofluids. Front. Aging Neurosci. 2021, 13, 607858.

5. MONITORING ENVIRONMENTAL POLLUTANTS (UV FILTERS)

5.1 General introduction

The work produced in this topic will be summarized in the following paragraphs, culminating in the submission of a patent application titled: "Portable Procedure for the Determination of Residues of Organic Solar Filters". Inventors: Agnese Giacomino, Paolo Inaudi, Debora Fabbri, Stefano Bertinetti, Silvia Berto.

5.2 Octocrylene - OC

Octocrylene (OC, 2-Ethylhexyl 2-cyano-3,3-diphenylprop-2-enoate) is an organic compound (Figure 5.1) used as a component in sunscreens and cosmetics. It is an ester formed through the condensation of 2-ethylhexyl cyanoacetate with benzophenone.

It is an organic UV filter primarily absorbing UV-B and short-wavelength UV-A radiations. Due to its UV radiation absorption properties, it is employed in sunscreens to protect the skin from the harmful effects of solar radiation. Additionally, OC is used in sunscreens to stabilize other UV filters, such as avobenzone, an effective UV-A filter, providing optimal UV protection through this combination.

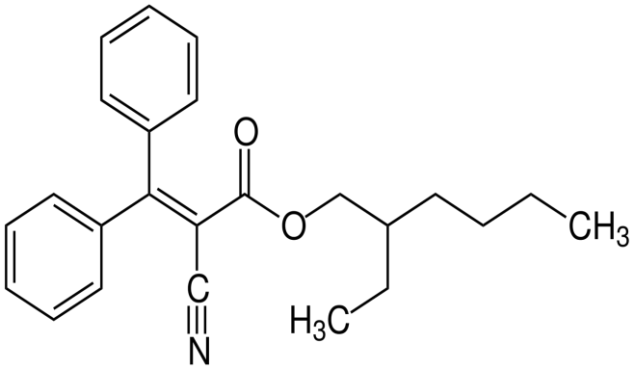

Figure 5.1 – Octocrylene

Despite its widespread use in sun care products, in recent years, the scientific community has raised concerns about its the potential adverse effects. Specifically, OC can cause contact allergy (a relatively rare effect), photoallergy (photoallergic dermatitis has been observed in 4 % of adult patients undergoing patch tests), and is suspected to be an endocrine disruptor [1]. OC has a logP>6 (partition coefficient representing the ratio of concentrations of a compound in two immiscible liquids, namely octanol and water) and, being a lipophilic compound, may give rise to bioaccumulation and biomagnification, potentially appearing throughout the food chain.

Furthermore, octocrylene undergoes a slow retro-aldol condensation reaction that results in benzophenone, a molecule classified by the IARC as a possible human carcinogen (Group 2B). According to a 2021 study by Downs et al., the retro-aldol condensation reaction occurred in all tested commercial sunscreens containing octocrylene, and the concentration of benzophenone increased with product aging [2].

In addition to potential effects on humans, octocrylene can cause significant harm to the aquatic ecosystem. In study by He et al. (2019), it was demonstrated that octocrylene can lead to

visual bleaching and death of coral reefs [3]. For this reason, starting from January 1, 2021, through the Hawaii Reef Safe Sunscreen Act, Hawaii has prohibited the sale and use of sunscreens containing octocrylene to protect their coral reefs.

5.3 Oxybenzone – BP3

Oxybenzone or benzophenone-3 (BP3, 2-hydroxy-4-methoxybenzophenone) is an organic compound (Figure 5.2) belonging to the aromatic ketones family, known as benzophenones. It is a widely used molecule in sunscreens and cosmetic products, but it is also utilized in plastics and toys to limit their degradation from UV radiation. BP3 is produced through the Friedel-Crafts reaction of benzoyl chloride with 3-methoxyphenol.

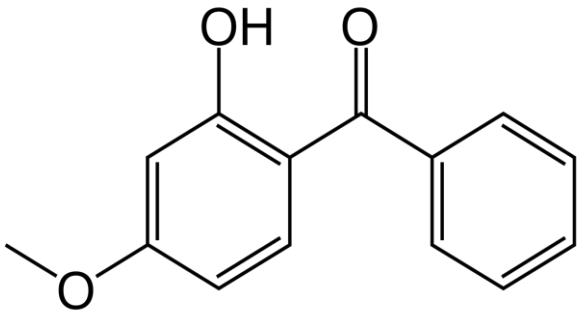

Figure 5.2 - Oxybenzone

The BP3 molecule was approved by the Food and Drug Administration (FDA) in the early 1980s and has become one of the most used organic UV-A filters in sunscreens. BP3 has an absorption profile ranging from 270 to 350 nm, covering UV-B and part of UV-A radiations[4].

Despite its significant photoprotective effects, BP3 can induce toxic pathological damage. Oxybenzone, like other benzophenones, is considered a mutagenic agent that causes an increased rate of DNA damage, especially when exposed to sunlight. Additionally, BP3 is genotoxic or can become so after activation by cytochrome P450 enzymes.

Genetic damage caused by benzophenones and, in particular, by BP3 can include: i) oxidative damage to DNA, ii) formation of pyrimidine dimers, iii) single-strand DNA breaks, iv) DNA cross-linking to proteins v) increased formation of abasic DNA sites (i.e. sites that have neither a purine nor a pyrimidine base).

Furthermore, BP3 exhibits pro-carcinogenic activity and can generate reactive oxygen species that are potential mutagens [5].

In addition to humans, BP3 can cause significant harm to fish and invertebrates. In fish, BP3 can cause endocrine disruption by modulating oestrogen receptor signalling pathways, inducing reproductive pathologies, and reducing reproductive fitness [5]. A study by Coronado et al. (2008) demonstrated that chronic exposure of fish to BP3 resulted in reduced egg production, induction of vitellogenin protein in males, and a significant reduction in egg hatching [6].

Gao et al. (2013) studied the possible effects of oxybenzone on the ciliate protozoan *Tetrahymena thermophila*. Exposure to BP3 caused oxidative damage, reduced glutathione, and negatively influenced the vitality of the protozoan [7].

5.4 – Octinoxate - EHMC

Octinoxate (EHMC, octyl methoxycinnamate) is an organic molecule (Figure 5.3) used in sunscreens to protect the skin from UV radiation and is one of the most widely used UV-B absorbers. It is an ester formed by methoxy cinnamic acid and ethyl hexanol. EHMC is unstable, and when exposed to sunlight, it undergoes isomerization, transforming from trans-EHMC to cis-EHMC. A study by Sharma et al. (2017) evaluated the potential toxic effects of the cis isomer, revealing that the cis isomer has a significant genotoxic effect under laboratory conditions. This implies that EHMC can damage human DNA and induce genome mutations that pose serious risks to human health [8].

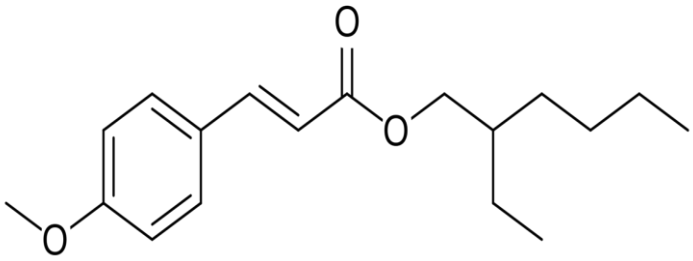

Figure 5.3 - Octinoxate

Moreover, EHMC can react with hypochlorite, a compound used in swimming pools to disinfect water, leading to the formation of chlorinated intermediates. Nakajima et al. (2009) highlighted that chlorinated intermediates have mutagenic effects on *Salmonella typhimurium* TA 100 bacteria [9].

EHMC also has adverse effects on coral reefs; in conjunction with other UV filters, it contributes to coral bleaching and mortality. For this reason, both Hawaii and the government of Palau (a republic located in western Pacific Ocean) have banned the sale and use of sunscreens containing certain UV filters, including EHMC.

5.5 Avobenzone - AVO

Avobenzone (AVO, Butyl Methoxydibenzoylmethane) is a compound used in sunscreens to protect the skin from UVA rays. AVO is an organic molecule (see Figure 5.4) formed through Claisen condensation between the methyl ester of 4-tert-butylbenzoic acid and 4-methoxyacetophenone in toluene in the presence of $NaNH_2$.

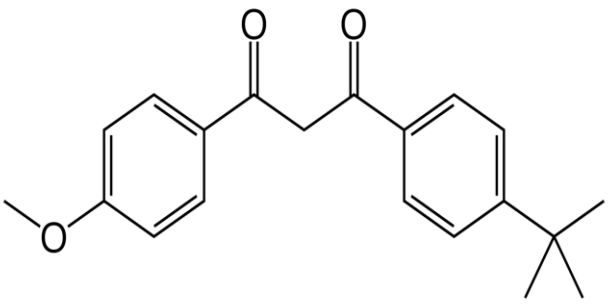

Figure 5.4 - Avobenzone

AVO can exist in solution in various tautomeric forms, and in its ground state, it exhibits a keto-enolic equilibrium favouring the enolic form. When it absorbs UV radiation, AVO generates a triplet state in which the ketonic form prevails, potentially causing the degradation of the filter or transferring energy to biological targets, leading to deleterious effects. Additionally, AVO is sensitive to solvent properties, being stable in polar protic solvents and unstable and photolabile in nonpolar solvents [10].

AVO degrades significantly when exposed to UV radiation. A study conducted by Tarras-Wahlberg et al. (1999) demonstrated that after UV irradiation, avobenzone degrades, and the photoproduct exhibits strong absorption in the UV-B region [11]. This results in AVO no longer absorbing UV-A rays, which are the primary culprits of skin cancers. To prevent this, stabilizers such as OC, benzoates, or camphor derivatives are added to cosmetic products containing AVO.

Although AVO is still the only UVA filter (3 % concentration) and approved by FDA and by the EU (5 % concentration), some countries, such as Hawaii, Mexico, and Bonaire, have banned it due to its potential negative impacts on the aquatic ecosystem. The effects of AVO on the aquatic ecosystem were evaluated by Clergeaud et al., (2023). Exposure of the coral *P. damicornis* to AVO induced metabolic alterations due to the accumulation of AVO derivatives originating from in vivo reduction followed by esterification. The derivatives were present in the coral in higher quantities than AVO and exhibited greater toxicity. Furthermore, this study also demonstrated that AVO, at a concentration of 300 $\mu g\ L^{-1}$, alters the photosynthetic capacity of the *Symbiodiniaceae* coral [12].

5.6 Optimization of the voltammetric method

The objective of this work is to determine the presence of UV filters in both water and sunscreens by voltammetry. However, before analyzing water samples, it is necessary to assess the instrumental response of UV filters using certified standards at known concentrations. In particular, octocrylene (OC), oxybenzone (BP3), and octinoxate (EHMC) have been studied.

Initially, the three UV filters were considered individually, and after optimizing the operational parameters, the application of the technique for the simultaneous determination of the analytes was evaluated. Voltammograms were recorded using a square wave potential scan in the cathodic direction, capturing the signal corresponding to their reduction at the electrode.

For the preparation of the OC standard, 1 g of certified standard (Sigma Aldrich) was dissolved in 30 mL of ethanol, resulting in a stock solution at 0.09 M (33333 $mg\ L^{-1}$). Subsequently, intermediate standard solutions were prepared from the stock solution to carry out standard additions. The intermediate standards had concentrations of 1.84 mM (666.66 $mg\ L^{-1}$) and 138 μM (50 $mg\ L^{-1}$).

The BP3 standard was prepared by dissolving 1 g of certified standard (Sigma Aldrich) in 30 mL of ethanol, obtaining a stock solution at 0.146 M (333333 $mg\ L^{-1}$). Intermediate standards were then prepared with concentrations of 2.92 mM (666.66 $mg\ L^{-1}$) and 219 μM (50 $mg\ L^{-1}$).

The EHMC standard was prepared by dissolving 1 g of certified standard (Parsol MCX) in 30 mL of ethanol, resulting in a stock solution at 0.115 M (33333 $mg\ L^{-1}$). Intermediate standards were prepared by diluting the stock solution, resulting in standards at 2.296 mM (666.66 $mg\ L^{-1}$) and 172 μM (50 $mg\ L^{-1}$).

For the determination of OC, BP3 and EHMC the parameters given in Table 5.1 were initially used.

Table 5.1 – Parameters initially adopted for the voltammetric determination of UV filters (E_{dep}= deposition potential, t_{dep}= deposition time, t_{eq}= equilibrium time, E_{start}= initiation potential, E_{end} = end potential, E_{step}= potential step, A= amplitude, F= frequency)

Parameter	Value
E_{dep}	-0.4 V
t_{dep}	120s
t_{eq}	10 s
E_{start}	-0.4 V
E_{end}	-1.8 V
E_{step}	0.006 V
A	0.018 V
F	10 Hz

Determination of Octocrylene.

The first UV filter considered was OC. To perform the initial analysis, a supporting electrolyte solution was used, consisting of 8 mL of 0.1 M NaCl, 2 mL of ethanol, and 0.30 mM CTAB (cetyltrimethylammonium bromide). This solution is referred to as the blank and the corresponding voltammogram represents the background signal.

Initially, a series of scans of this solution were conducted, and after confirming the stability of the background, known concentrations of OC were added. Specifically, five subsequent additions were made, each at a concentration of 2.766 μM (1 mg L^{-1}).

Following the additions of OC, an increase in peak intensity was observed at the potential of -0.95 V.

Quantification of a known concentration of OC was achieved at 2.77 μM using the standard addition method. The obtained result was not optimal, yielding a recovery of 69.7 %. The non-quantitative recovery is attributed to OC's low solubility in water (0.00157 mg mL^{-1}), and the inability of ethanol to fully solubilize it. For this reason, the composition of the supporting electrolyte was modified.

A solution composed of 8 mL of 0.1 M NaCl, 2 mL of methanol, and 0.30 mM CTAB was used, and known concentrations of OC were added to this solution. The additions allowed the construction of a calibration curve (y=13.664x+0.0154) with an R^2 of 0.9836. Quantification of the added OC at 2.77 μM resulted in a recovery of 90.08 %.

Given the improved recovery using methanol instead of ethanol, accuracy at lower OC concentrations was assessed. Despite the positive results obtained, since the goal is to develop a method for determining multiple UV filters simultaneously, further variations to the supporting electrolyte were considered using a mixture of organic solvents. The solution comprised 8 mL of 0.1 M NaCl, 1 mL of ethanol, 1 mL of methanol, and 0.30 mM CTAB. Known quantities of OC were added to this solution, and quantification of the OC addition at 2.77 μM resulted in a recovery of 98.24 %.

Comparing the analyses conducted using different synthetic solutions, it was decided to use the mixture consisting of 8 mL of 0.1 M NaCl, 1 mL of ethanol, 1 mL of methanol, and 0.30 mM CTAB. This solution provides good linearity and a high percentage recovery for OC additions. Additionally, this solution has a linear background signal with low currents (-1.0 μA), allowing for increased sensitivity.

After optimizing the supporting electrolyte composition, operational parameters were varied to enhance instrumental sensitivity. To the solution composed of 8 mL of 0.1 M NaCl, 1 mL of ethanol, 1 mL of methanol, and 0.30 mM CTAB, OC at 0.553 μM (0.2 mg L^{-1}) was added, and various parameters of square wave voltammetry (SWV) were adjusted. As expected, the frequency parameter significantly influences sensitivity. Increasing the frequency enhances the signal intensity corresponding to OC, owing to the increase in scan rate.

Reducing the deposition time and increasing the equilibration time ensured better background stability. Values for potential step and amplitude were selected to achieve an improved redox profile without current spikes.

The optimized parameters used in SWV are reported in Table 5.2.

Table 5.2 – Optimized parameters for OC determination by SWV

Parameter	Value
E_{dep}	-0.4 V
t_{dep}	60s
t_{eq}	20 s
E_{start}	-0.8 V
E_{end}	-1.7 V
E_{step}	0.009 V
A	0.021 V
F	50 Hz

Utilizing the same supporting electrolyte and the optimized parameters, instrumental sensitivity was increased. The voltammogram and calibration curve obtained by performing five subsequent additions of OC, each at 0.276 μM, to the solution are presented below (Figure 5.5). Using this set of parameters, excellent results in terms of linearity, accuracy, repeatability, and sensitivity were achieved. Table 5.3 shows the performance of the method for the determination of the OC present in the solution.

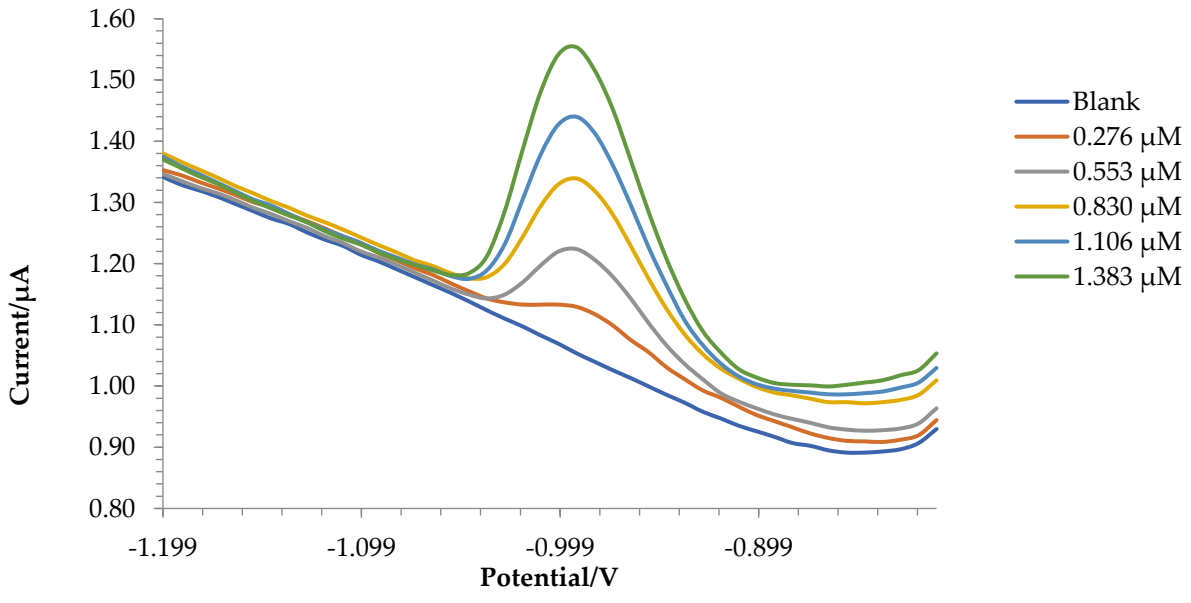

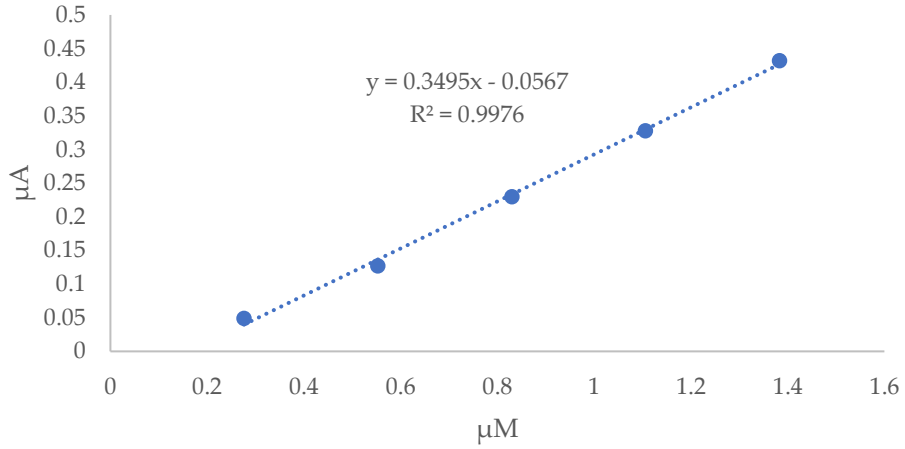

Figure 5.5 - Voltammograms and calibration line obtained after five additions of OC (0.27 µM) in a solution of 0.1 M NaCl, EtOH, MeOH, and 0.30 mM CTAB.

Table 5.3 - Performance obtained by the method following five additions of OC (0,276 µM) in a solution consisting of NaCl 0,1M, MeOH, EtOH and CTAB 0,30mM

Parameters	Values
Concentration range (µM)	0.276-1.38
Correlation coefficient R^2	0.9977
Sensitivity (µA/µM)	0.35
Recovery %	93.17
RSD %	3.62
LOD (µM)	0.07
LOQ (µM)	0.25

Determination of Oxybenzone.

The second UV filter considered was BP3. For the initial analysis, the parameters listed in Table 5.1 were employed, and a supporting electrolyte solution of 8 mL 0.1 M NaCl, 2 mL ethanol, and CTAB was used. Five subsequent additions of BP3, each at a concentration of 4.38 µM, were made to this solution. Following the BP3 additions, a calibration curve with the equation y=9.6548x-0.0063 and an R^2 of 0.991 was obtained.

Using the standard addition method, a known concentration of BP3 at 4.38 µM was quantified, yielding a percentage recovery of 85.1%. Subsequently, similar to the approach with OC, the composition of the supporting electrolyte was modified, and a mixture of 8 mL 0.1 M NaCl, 2 mL methanol, and 0.30 mM CTAB was used. Five additions of BP3 were made to this solution.

The resulting calibration curve y=10.591x + 0.0764, with an R^2 of 0.9901, showed a quantitative recovery of 101.6% for the addition of 4.38 µM BP3. Once again, methanol proved to be more effective in solubilizing UV filters. When using the NaCl-methanol solution as the supporting electrolyte, a higher percentage recovery was achieved compared to using the NaCl-ethanol solution.

Given the positive results, the linearity and accuracy at lower concentrations of BP3 were evaluated. Tests were conducted at concentrations of BP3 equal to 2.19, 1.0, and 0.43 µM.

Subsequently, similar to the OC analysis, the composition of the supporting electrolyte was altered. A mixture of 8 mL 0.1 M NaCl, 1 mL ethanol, 1 mL methanol, and 0.30 mM CTAB was used. Subsequent additions were made to this solution, and the quantification of the 4.38 µM BP3 addition resulted in a recovery of 98.08%.

A subsequent test was conducted using the support electrolyte solution consisting of 8 mL 0.1 M NaCl, 1 mL methanol, 1 mL ethanol, and 0.30 mM CTAB, along with the optimized parameters listed in Table 5.3. Five additions of BP3, each at 0.43 µM, were made to this solution (Figure 5.6).

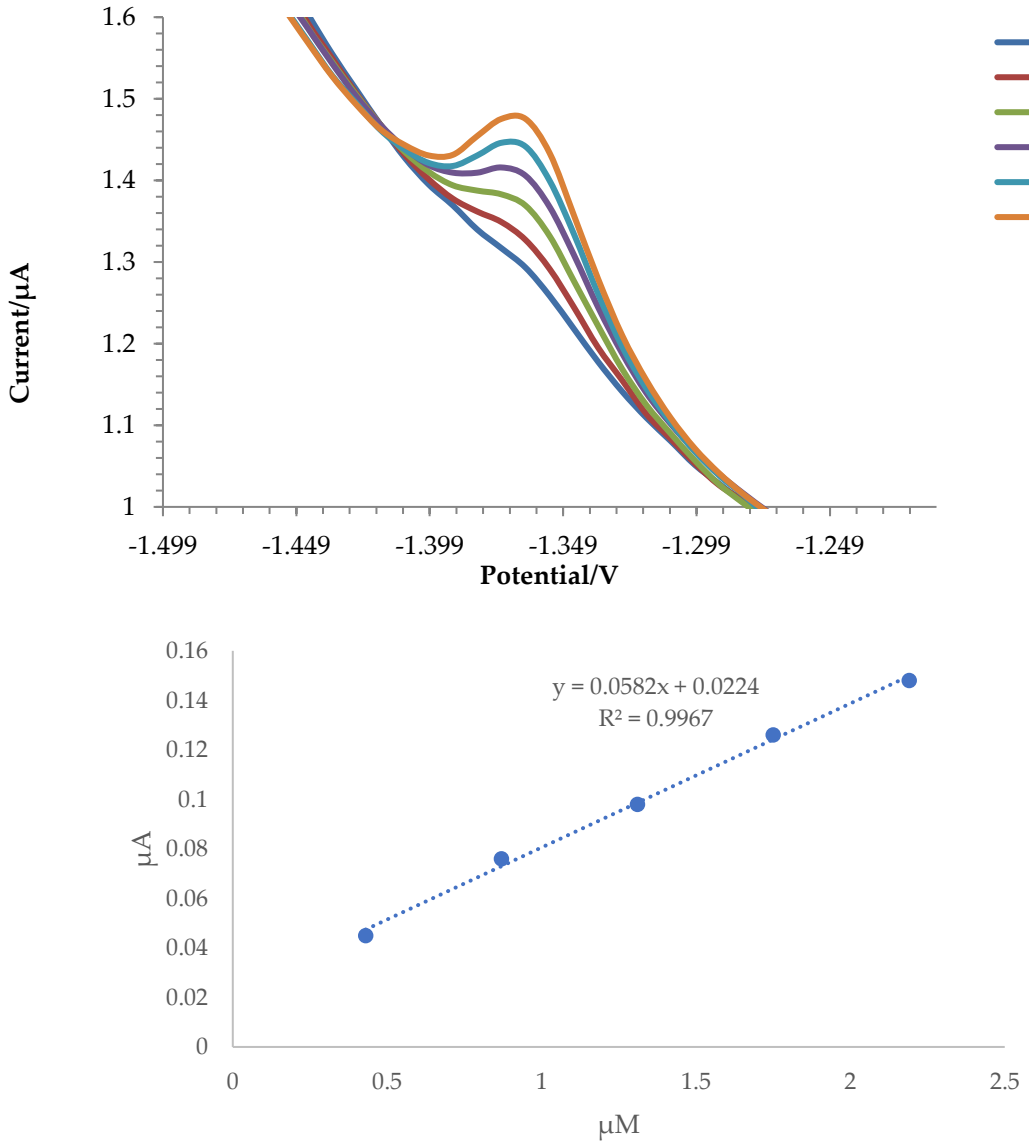

Figure 5.6 -Voltammograms and calibration line obtained after five additions of BP3 (0.43 µM) in a solution of 0.1 M NaCl, EtOH, MeOH, and 0.30 mM CTAB.

Similar to OC, this parameter set yielded very good results in terms of linearity, repeatability, and accuracy. Table 5.4 reports the performance obtained by the methodology in determining BP3 in the solution.

Table 5.4 - Performance obtained by the method following five additions of BP3 (0,483 μM) in a solution consisting of 0,1M NaCl, MeOH, EtOH and 0,30 mM CTAB

Parameters	Values
Concentration range (μM)	0.483-2.19
Correlation coefficient R^2	0.9967
Sensitivity (μA/μM)	0.058
Recovery %	96.72
RSD %	3.22
LOD (μM)	0.11
LOQ (μM)	0.39

Determination of Octinoxate.

The third UV filter considered was EHMC. The initial test was conducted using the parameters listed in Table 5.1 and a supporting electrolyte solution consisting of 8 mL 0.1 M NaCl, 2 mL methanol, and 0.30 mM CTAB. Five subsequent additions of EHMC, each at a concentration of 1.72 μM, were made to this solution.

Using the standard addition method, a known concentration of EHMC at 1.72 μM was quantified, resulting in a recovery of 108.5%.

Subsequently, the linearity and accuracy at lower concentrations of EHMC were evaluated. Additions of 0.86 μM and 0.34 μM were made to the solution composed of 0.1 M NaCl, methanol, and 0.30 mM CTAB.

Following the same approach adopted for OC and BP3, the composition of the supporting electrolyte was modified. A solution consisting of 8 mL 0.1 M NaCl, 1 mL methanol, 1 mL ethanol, and 0.30 mM CTAB was used, and subsequent additions of EHMC at known concentrations were made to this solution.

The resulting calibration curve $y=40.076x+0.0087$ with an R^2 of 0.9916 was obtained, and the quantification of the 1.72 μM EHMC addition led to a recovery of 93.69%.

Finally, a test was conducted using the optimized parameters (Table 5.2) and a supporting electrolyte solution of 0.1 M NaCl, methanol, ethanol, and 0.30 mM CTAB. Five additions of EHMC, each at 0.34 μM, were made to this solution.

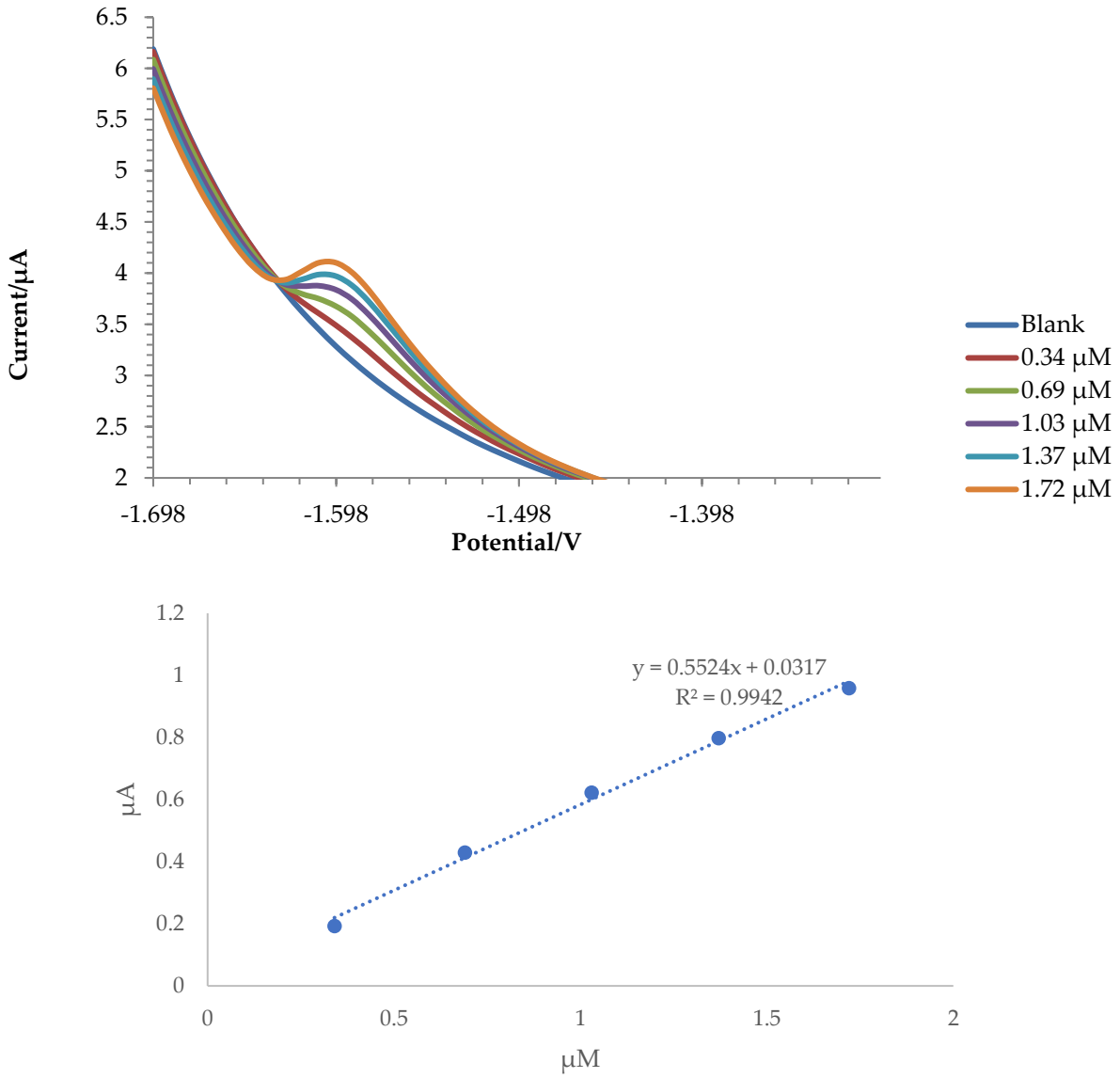

Figure 5.7 - Voltammograms and calibration line obtained after five additions of EHMC (0.34 µM) in a solution of 0.1 M NaCl, MeOH, EtOH, and 0.30 mM CTAB.

Similar to OC and BP3, this parameter set yielded very good results in terms of linearity, repeatability, and accuracy. Table 5.5 reports the performance obtained by the methodology in determining EHMC in the solution.

Table 5.5 - Performance obtained by the method following five additions of EHMC (0,34 μM) in a solution consisting of NaCl 0,1M, MeOH, EtOH and CTAB 0,30mM

Parameter	Value
Concentration range (μM)	0.34-1.72
Correlation coefficient R^2	0.994
Sensitivity (μA/μM)	0.5518
Recovery %	93.17
RSD %	0.67
LOD (μM)	0.065
LOQ (μM)	0.223

Determination of Octocrylene, Oxybenzone, and Octinoxate Simultaneously Present in Solution

Given the satisfactory results obtained for individual analytes using the supporting electrolyte consisting of 8 mL 0.1 M NaCl, 2 mL methanol, and 0.30 mM CTAB, it was decided to use the same solution and simultaneously add the three analytes. Three additions were made for OC, each at 0.69 μM, three additions for BP3, each at 1.09 μM, and three additions for EHMC, each at 0.86 μM.

The optimized parameters shown in Table 5.2 were adopted for the voltammetric measurement. The corresponding voltammograms are displayed in Figure 5.8.

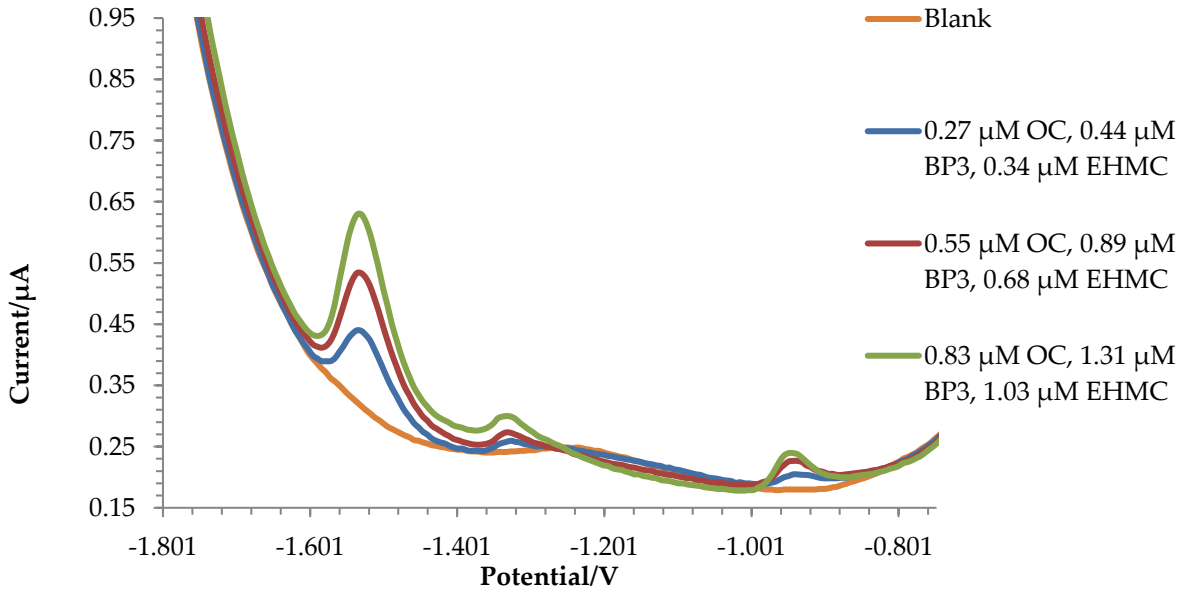

Figure 5.8 - Voltammograms obtained following three additions of OC (0.27 μM), BP3 (0.44 μM), and EHMC (0.34 μM) in a solution of 0.1 M NaCl, EtOH, MeOH, and 0.30 mM CTAB.

Using all the previously optimized conditions, good results were obtained in terms of linearity, repeatability and accuracy for all analytes simultaneously present in the solution. The performance obtained for the simultaneous determination of OC, BP3, and EHMC is reported below.

Table 5.6 - Performance obtained by the method following three additions of OC (0.27μM), BP3 (0.44μM) and EHMC (0,34 μM) in a solution consisting of 0,1M NaCl, MeOH, EtOH and 0,30 mM CTAB

Parameters	OC	BP3	EHMC
Concentration range (μM)	0.27-0.83	0.44-1.31	0.34-1.03
Correlation coefficient R^2	0.995	0.994	0.995
Sensitivity (μA/μM)	0.161	0.084	0.425
Recovery %	91.66	96.72	100
RSD %	1.96	0.93	3.48
LOD (μM)	0.06	0.087	0.079
LOQ (μM)	0.21	0.29	0.26

It can be observed that the simultaneous presence of the three analytes does not seem to affect quantification, as the results obtained exhibit high accuracy and precision.

When compared with the method developed by Sunyer et al. (2019) [13], the proposed methodology appears to be more sensitive and has lower LOD and LOQ values.

Compared to the method developed by Ferreira et al. (2013) [14], the proposed methodology has higher LOD and LOQ values for OC. However, in addition to allowing simultaneous determination of three UV filters, it is more environmentally friendly, as Ferreira et al. use a hanging mercury drop electrode.

The proposed method has lower LOD and LOQ values for EHMC compared to the method proposed by Cardoso et al. (2008) [15]. Additionally, the developed method is more environmentally friendly as it uses a GCE, while Cardoso et al. use a hanging mercury drop electrode.

5.7 Tests on synthetic samples

After optimizing the voltammetric technique for the simultaneous determination of OC, BP3, and EHMC, tests were conducted on synthetic solutions containing a known quantity of these three UV filters. Since the final objective of our research study is to monitor the content of UV filters in lake waters, which typically have concentrations in the order of units to tens of ng L^{-1}, it was decided to include a preconcentration step using solid-phase extraction (SPE).

The considered analytes are low-polarity substances; therefore, it was decided to work in reverse phase. Three different types of cartridges were used, and their specifications are listed in Table 5.7, whereas the structures of their active groups are displayed in Figure 5.9.

- Oasis HLB

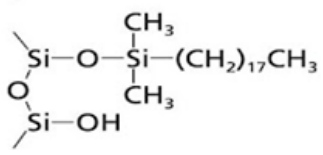

;

- Discovery DSC-Ph

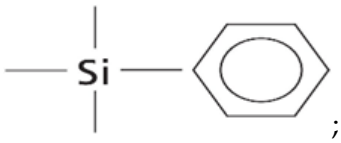

;

- Discovery DSC-18Lt

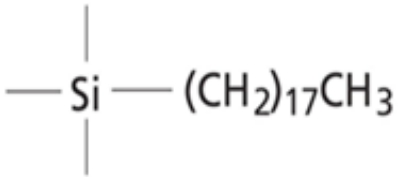

;

Figure 5.9. Structure of the active groups of Oasis HLB, Discovery DSC-Ph and- Discovery DSC-18Lt cartridges

Table 5.7 - Specifications of the three cartridges used for SPE

Cartridge	Volume (cc)	Quantity of stationary phase (mg)	Specific surface area (m^2/g)	Total pore volume (cm^3/g)
Oasis HLB	3	60	781	1.27
Discovery DSC-Ph	6	500	513	0.88
Discovery DSC-18Lt	6	500	485	0.89

Oasis HLB cartridge

The first cartridge used was the Oasis HLB cartridge (3 cc, 60 mg). The synthetic sample was prepared using 100 mL of tap water to which known quantities of UV filters were added. In particular, 100 μg L^{-1} of each analyte was added, corresponding to 0.276 μM of OC, 0.438 μM of BP3, and 0.344 μM of EHMC. After preparing the sample, the SPE cartridge was conditioned using 3 mL of methanol to activate the resin's active sites and 3 mL of ultrapure water to remove any potential interferents present on the resin. Once the stationary phase was conditioned, the sample was driven through with a constant flow of 5 mL min^{-1}. This flow rate was chosen as a good compromise between fast flows, which could result in low retention of analytes on the resin, and slow flows, which would make the method unsuitable for routine analysis. After this step, the analytes retained on the resin were recovered using a solution consisting of 1 mL of methanol and 1 mL of ethanol. The eluate was then placed inside the electrochemical cell along with 8 mL of 0.1 M NaCl and 0.30 mM CTAB, and a voltammetric measurement was carried out. To this solution, two additions of OC (2.76 μM), BP3 (4.38 μM), and EHMC (3.44 μM) were subsequently made to determine the amount of recovered analytes. Figure 5.10 shows the corresponding voltammograms and Table 5.8 reports the results obtained.

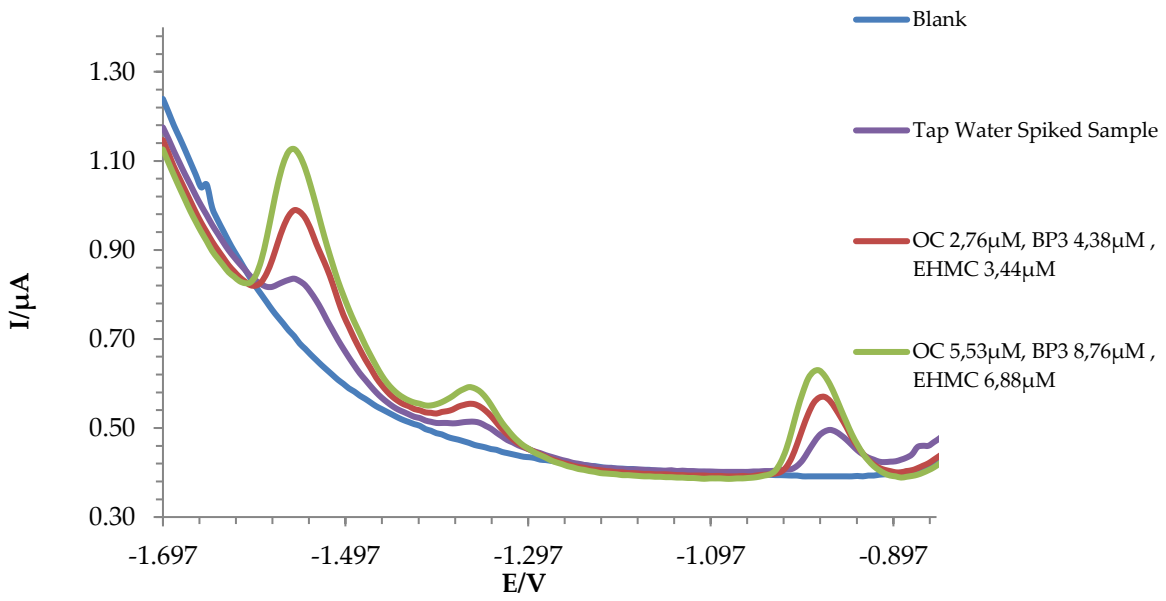

Figure 5.9 - Voltammograms obtained following the potential scan and two additions of 2.76 µM OC, 4.38 µM BP3, and 3.44 µM EHMC.

Table 5.8 - Percentage recoveries and concentrations of UV filters obtained after SPE treatment with Oasis cartridge (3cc, 60mg; ; 50 mL of starting solution containing 100 µg L^{-1} analytes)

Analyte	Added UV Filter Concentration (µM)	Recovered UV Filter Concentration (µM)	Recovery (%)
OC	0.276	0.258	93.41
BP3	0.438	0.421	96.13
EHMC	0.344	0.342	99.52

The results obtained with this cartridge were very good, as a recovery exceeding 90% was achieved for all analytes. For this reason, further tests were carried out by decreasing the concentration of UV filters and increasing the volume of synthetic solution.

For the second test, a synthetic solution was prepared from 200 mL of tap water to which 0.138 µM of OC, 0.219 µM of BP3, and 0.172 µM of EHMC were added, corresponding to 50 µg L^{-1}.

After conditioning the cartridge and loading the sample onto the SPE cartridge, the analytes adsorbed on the stationary phase were recovered with a solution consisting of 1 mL of methanol and 1 mL of ethanol. This solution was added to the electrochemical cell with 8 mL of 0.1 M NaCl and 0.30 mM CTAB: the concentrations expected in the cell are the same as those present in the previous experiement. Subsequently, to determine the amount of recovered UV filters, two additions of OC (2.76 µM), BP3 (4.38 µM), and EHMC (3.44 µM) were made to the solution.

Table 5.9 shows the concentrations of the recovered analytes and the percentage recoveries.

Table 5.9 - Percentage recoveries and concentrations of UV filters obtained after SPE treatment with Oasis cartridge (3cc, 60mg; 100 mL of starting solution containing 50 μg L^{-1} analytes)

Analyte	Added UV Filter Concentration (μM)	Recovered UV Filter Concentration (μM)	Recovery (%)
OC	0.138	0.112	81.31
BP3	0.219	0.21	96.07
EHMC	0.172	0.09	52.26

Unfortunately, the increase in the volume of the sample solution passed through the column led to a decrease in the recovery of analytes. This could be caused by the fact that, following the passage of a high volume of solution, "cracks" may be created in the packing that no longer allow the retention of analytes. Preferential channels may be formed in which the retention sites are saturated while others are less available: consequently, the contact between analytes and sorbent is not complete.

Finally, using the same type of cartridge, a synthetic sample of 200 mL of tap water with 0.069 μM of OC, 0.109 μM of BP3, and 0.086 μM of EHMC, corresponding to 25 μg L^{-1}, was also analyzed.

In this case as well, after conditioning the SPE cartridge and loading the sample, the analytes retained by the resin were recovered using 1 mL of methanol and 1 mL of ethanol. To this solution, 8 mL of 0.1 M NaCl and 0.30 mM CTAB were added. After recording the voltammogram of the sample, two additions of OC (1.38 μM), two additions of BP3 (2.19 μM), and two additions of EHMC (1.72 μM) were made. Table 5.10 shows the concentrations of the recovered analytes and the percentage recoveries.

Table 5.10 - Percentage recovery and concentration of UV filters recovered after SPE treatment with Oasis cartridge (3cc, 60mg; 200 mL of starting solution containing 50 μg L^{-1} analytes)

Analyte	Added UV Filter Concentration (μM)	Recovered UV Filter Concentration (μM)	Recovery (%)
OC	0.069	0.045	65.33
BP3	0.109	0.106	97.16
EHMC	0.086	0.049	57.97

From the results obtained, it was observed that for OC and EHMC, the recovery decreased with increasing sample volume and decreasing analyte concentration within the solution, while for BP3, the recovery was always quantitative. This may be due to the fact that the analytes (OC and EHMC) are not quantitatively retained by the resin (due to the formation of preferential channels within the packing) or that the analytes are not released from the resin because a too low eluent volume or an insufficiently strong extracting solution is being used, preventing quantitative recovery.

Discovery DSC-Ph and Discovery DSC-18Lt cartridge

The second SPE cartridge used was the Discovery DSC-Ph (6cc, 500mg). Initially, a preliminary test was performed to assess the treatment efficiency by comparing the results obtained through voltammetry with those obtained using HPLC-PDA (High-Performance Liquid Chromatography-Photodiode Array). In particular, a C8 Synergi 4 μm reverse phase stainless steel

chromatographic column was used at a temperature of 40 ºC and a mobile phase: 50% ultra pure water acidified with acetic acid 0.05% v/v, 50% acetonitrile. The synthetic sample was prepared using 100 mL of tap water to which 2.76 µM of OC, 4.38 µM of BP3, and 3.44 µM of EHMC were added. The cartridge was conditioned using 6 mL of methanol and 6 mL of ultrapure water, and after this step, the sample was loaded using a constant flow of 5 mL min^{-1}.

After completing the sample loading phase, the cartridge was eluted using a solution consisting of 2.5 mL of methanol and 2.5 mL of ethanol. A portion of this solution (0.5 mL) was introduced into the electrochemical cell with 8 mL of 0.1 M NaCl and 0.30 mM CTAB, and a potential scan was performed.

Two additions of OC (2.76 µM), BP3 (4.38 µM), and EHMC (3.44 µM) were made to this solution to determine the concentrations of analytes.

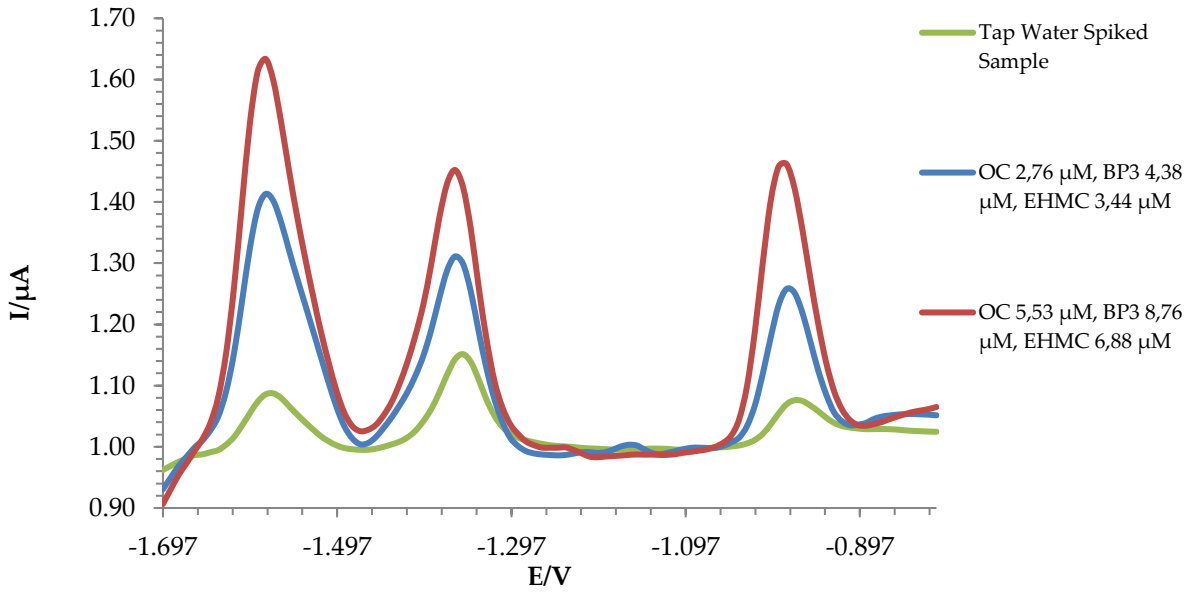

Figure 5.10 - Voltammograms obtained following the sample scan and two additions of 2.76 µM OC, 4.38 µM BP3, and 3.44 µM EHMC.

The same eluate was then analyzed using HPLC-PDA. For the analysis, an aliquot of the eluate (0.05 mL) was transferred into an HPLC vial with 0.475 mL of acetonitrile and 0.475 mL of HPW acidified with 0.05% v/v acetic acid.

Additionally, two other vials were prepared, one containing 0.05 mL of eluate, 0.465 mL of acetonitrile, 0.465 mL of HPW acidified with 0.05% v/v acetic acid, and 0.02 mL of UV filter standards (0.138 mM OC, 0.219 mM BP3, 0.172 mM EHMC), and the other containing 0.05 mL of eluate, 0.455 mL of acetonitrile, 0.455 mL of HPW acidified with 0.05% v/v acetic acid, and 0.04 mL of UV filter standards (0.138 mM OC, 0.219 mM BP3, 0.172 mM EHMC).

Table 5.11 shows the comparison between the results obtained by voltammetric analysis and chromatographic analysis.

Table 5.11 - Comparison of Voltammetry recoveries and HPLC recoveries after SPE treatment with Discovery DSC-Ph cartridge

Analyte	Voltammetry		HPLC-PDA	
	Recovered UV filter concentration (μM)	Recovery (%)	Recovered UV filter concentration (μM)	Recovery (%)
OC	0.99	36.07	1.22	44.15
BP3	3.72	84.94	3.30	75.50
EHMC	1.28	37.29	1.45	42.19

It can be observed that the results obtained by voltammetry are consistent with the values obtained by HPLC. However, the percentage recoveries are unsatisfactory, as the recoveries for OC and EHMC are less than 50%. For this reason, it was considered to change the extracting phase and use a less polar solvent, such as dichloromethane (CH_2Cl_2). A solution was prepared with 100 mL of tap water to which 1.38 μM of OC, 2.19 μM of BP3, and 1.72 μM of EHMC were added.

After conditioning the cartridge with 6 mL of methanol and 6 mL of ethanol and loading the sample with a constant flow of 5 mL min^{-1}, the cartridge was eluted using 2 mL of CH_2Cl_2. The eluate was evaporated to dryness, both to recover the eluate with a smaller solvent volume and because dichloromethane could pose issues during analysis. The analytes were subsequently dissolved into 0.2 mL of methanol, and the solution was added to a cell with 8 mL of 0.1 M NaCl, 1 mL of methanol, 1 mL of ethanol, and 0.30 mM CTAB. Two additions of OC (5.53 μM), BP3 (8.76 μM), and EHMC (6.88 μM) were made to the solution to determine the concentrations of analytes. Table 5.11 shows the results obtained.

Table 5.12 - Percentage recoveries and concentrations of UV filters recovered after SPE treatment with DSC-Ph cartridge (6cc, 500mg)

Analyte	Added UV Filter Concentration (μM)	Recovered UV Filter Concentration (μM)	Recovery (%)
OC	1.38	0.97	70.49
BP3	2.19	1.86	84.92
EHMC	1.72	1.48	85.58

A recovery greater than 70% was observed for all considered analytes. Given the better results obtained using dichloromethane as an extracting solvent, it was decided to decrease the concentration of UV filters in the synthetic sample.

A solution of 100 mL of tap water with 0.138 μM OC, 0.219 μM BP3, and 0.172 μM EHMC was prepared. After conditioning the column and loading the sample, the analytes were eluted from the cartridge using 2 mL of CH_2Cl_2. Once dried, the analytes were dissolved into 0.2 mL of methanol. This solution was added to 8 mL of 0.1 M NaCl, 1 mL of methanol, 1 mL of ethanol, and 0.30 mM CTAB, and a voltammetric measurement was carried out. Two additions of OC (1.38 μM), BP3 (2.19 μM), and EHMC (1.72 μM) were subsequently made to the solution.

Table 5.13 reports the concentrations of UV filters recovered following SPE and the percentage recoveries.

Table 5.13 - Percentage recoveries and concentrations of UV filters recovered after SPE treatment with DSC-Ph cartridge (6cc, 500mg)

Analyte	Added UV Filter Concentration (μM)	Recovered UV Filter Concentration (μM)	Recovery (%)
OC	0.138	0.101	73.57
BP3	0.219	0.201	92.14
EHMC	0.172	0.141	82.12

In this case, recoveries greater than 70% were obtained for all analytes, which were deemed acceptable, so the concentrations in the starting synthetic sample were further decreased. In this case, the chosen concentrations were in the nM range, so it was decided to increase the volume of the sample solution.

A synthetic sample of 500 mL of tap water containing 0.014 μM OC, 0.021 μM BP3, and 0.017 μM EHMC was then processed with the DSC-Ph cartridge. After conditioning the column, loading the sample, and eluting the analytes with CH_2Cl_2, the eluate was evaporated to dryness, and it was subsequently recovered with 0.2 mL of methanol. The solution containing the analytes was added to a cell with 8 mL of 0.1 M NaCl, 1 mL of methanol, 1 mL of ethanol, and 0.30 mM CTAB, and the sample was scanned. Two subsequent additions of OC (0.69 μM), BP3 (1.09 μM), and EHMC (0.86 μM) were made to the solution.

Table 5.14 reports the concentrations of UV filters recovered following SPE and the percentage recoveries.

Table 5.14 - Percentage recoveries and concentrations of UV filters recovered after SPE treatment with DSC-Ph cartridge (6cc, 500mg)

Analyte	Added UV Filter Concentration (μM)	Recovered UV Filter Concentration (μM)	Recovery (%)
OC	0.014	0.008	62.96
BP3	0.022	0.015	70.38
EHMC	0.017	0.017	99.71

Following the flow of a larger volume (500 mL), the recoveries were acceptable for OC and BP3, exceeding 60%, and excellent for EHMC. With the Discovery DSC-Ph cartridge, there is no observed decrease in percentage recovery as the analyte concentration in the sample decreases and the sample volume increases, as seen with the Oasis HLB cartridge. Therefore, it is possible to process high sample volumes with this cartridge.

The third cartridge used for preconcentrating the synthetic sample through SPE was the Discovery DSC-18Lt. Similar to the DSC-Ph cartridge, a preliminary test was conducted for the DSC-18Lt cartridge to assess the efficiency of the SPE treatment by comparing the results obtained in voltammetry with those obtained through HPLC-PDA.

The synthetic sample was prepared using 100 mL of tap water to which 2.76 µM OC, 4.38 µM BP3, and 3.44 µM EHMC were added. The cartridge was conditioned using 6 mL of methanol and 6 mL of ultra-pure water. After this step, the sample was loaded using a constant flow of 5 mL/min.

Once the sample loading phase was completed, the cartridge was eluted using a solution consisting of 2.5 mL of methanol and 2.5 mL of ethanol. A portion of this solution (0.5 mL) was introduced into the electrochemical cell with 8 mL of 0.1 M NaCl and 0.30 mM CTAB, and a voltammetric measurement was carried out. Two additions of OC (2.76 µM), BP3 (4.38 µM), and EHMC (3.44 µM) were made to this solution to determine the quantity of recovered analytes.

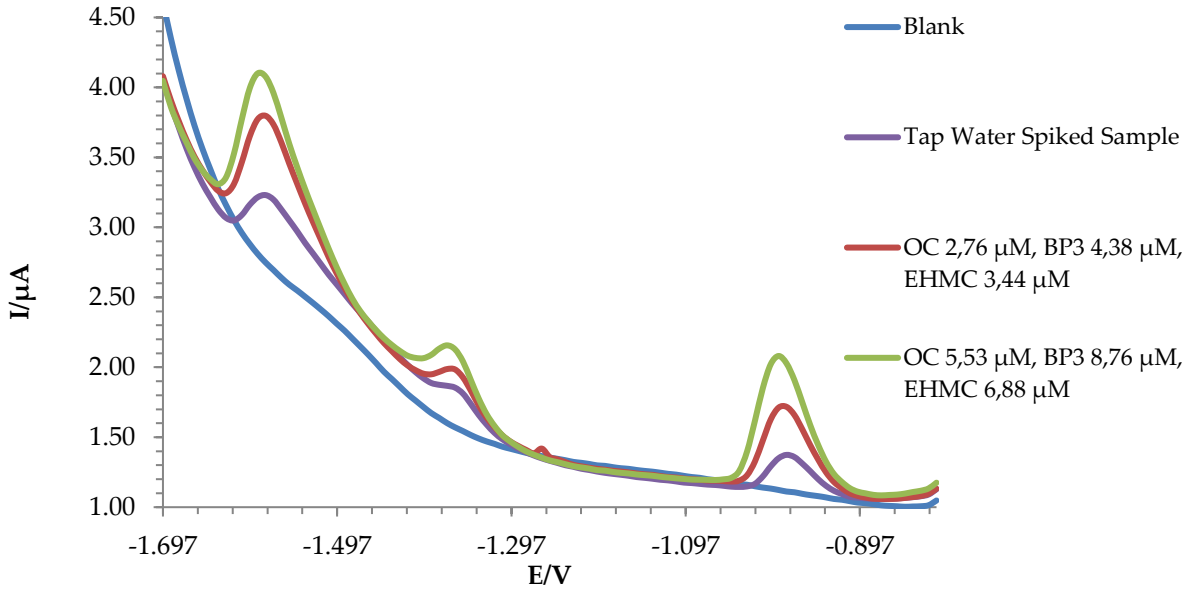

Figure 5.11 - Voltammograms obtained following the sample scan and two additions of 2.76 µM OC, 4.38 µM BP3, and 3.44 µM EHMC.

The same eluate was analyzed using HPLC-PDA. For the analysis, a sample aliquot (0.05 mL) was withdrawn and placed into an HPLC vial containing 0.475 mL of acetonitrile and 0.475 mL of high-purity water (HPW) acidified with 0.05% v/v acetic acid.

Additionally, two other vials were prepared. One contained 0.05 mL of eluate, 0.465 mL of acetonitrile, 0.465 mL of HPW acidified with 0.05% v/v acetic acid, and 0.02 mL of UV filter standards (0.138 mM OC, 0.219 mM BP3, 0.172 mM EHMC). The second vial contained 0.05 mL of eluate, 0.455 mL of acetonitrile, 0.455 mL of HPW acidified with 0.05% v/v acetic acid, and 0.04 mL of UV filter standards (0.138 mM OC, 0.219 mM BP3, 0.172 mM EHMC).

Table 5.15 presents a comparison between the results obtained through voltammetric analysis and chromatographic analysis.

Table 5.15 - Comparison of Voltammetry recoveries and HPLC recoveries with Discovery DSC-18Lt cartridge

Analyte	Voltammetry		HPLC-PDA	
	Recovered UV filter concentration (μM)	Recovery (%)	Recovered UV filter concentration (μM)	Recovery (%)
OC	2.10	76.15	1.89	68.33
BP3	3.45	78.81	3.60	82.39
EHMC	2.69	78.09	2.44	70.88

With the DSC-Lt18 cartridge, overall better results were achieved compared to those obtained with the DSC-Ph cartridge. In this case as well, tests were conducted using dichloromethane as the eluent phase to enhance release and preconcentration.

A synthetic tap water sample was prepared, to which 1.38 μM of OC, 2.19 μM of BP3, and 1.72 μM of EHMC were added. After conditioning the cartridge with 6 mL of methanol and 6 mL of HPW, the sample was loaded using a constant flow of 5 mL/min. After completing this phase, the analytes were eluted using 2 mL of CH_2Cl_2, and the eluate was evaporated to dryness. The analytes were redissolved using 0.2 mL of methanol, and this solution was added to 8 mL of 0.1 M NaCl, 1 mL of methanol, 1 mL of ethanol, and 0.30 mM CTAB. After scanning the sample, two subsequent additions were made: OC (5.53 μM), BP3 (8.76 μM), and EHMC (6.88 μM).

Table 5.16 reports the concentrations of UV filters recovered following SPE and the percentage recoveries.

Table 5.16 - Percentage recovery and concentration of UV filters recovered after SPE treatment with DSC-Lt18 cartridge (6cc, 500mg)

Analyte	Added UV Filter Concentration (μM)	Recovered UV Filter Concentration (μM)	Recovery (%)
OC	1.38	1.31	94.79
BP3	2.19	1.99	91.16
EHMC	1.72	1.57	91.24

As seen in Table 5.16, recoveries exceeding 90% were obtained for all considered analytes. The test was then conducted with lower concentrations: it was decided to decrease the concentration of UV filters in the synthetic sample. A synthetic solution was prepared consisting of 100 mL of tap water, 0.138 μM of OC, 0.219 μM of BP3, and 0.172 μM of EHMC.

After conditioning the column, loading the sample, eluting the analytes, and evaporating the eluate to dryness, the analytes were solubilized in 0.2 mL of methanol. This solution was added to 8 mL of 0.1 M NaCl, 1 mL of methanol, 1 mL of ethanol, and 0.30 mM CTAB, and a voltammetric measurement was carried out. Subsequently, two additions were made to the solution: OC (1.38 μM), BP3 (2.19 μM), and EHMC (1.72 μM).

Table 5.17 reports the concentrations of UV filters recovered following SPE and the percentage recoveries.

Table 5.17 - Percentage recovery and concentration of UV filters recovered after SPE treatment with DSC-Lt18 cartridge (6cc, 500mg)

Analyte	Added UV Filter Concentration (μM)	Recovered UV Filter Concentration (μM)	Recovery (%)
OC	0.138	0.074	53.91
BP3	0.219	0.187	85.37
EHMC	0.172	0.104	60.87

Subsequently, a synthetic sample consisting of 500 mL of tap water to which 0.014 μM of OC, 0.021 μM of BP3, and 0.017 μM of EHMC were added was treated using DSC-Lt18. After performing the various steps of SPE, and after solubilizing the analytes in 0.2 mL of methanol. This solution was added to 8 mL of 0.1 M NaCl, 1 mL of methanol, 1 mL of ethanol, and 0.30 mM CTAB, and a voltammetric measurement was carried out. Two subsequent additions of OC (0.69 μM), BP3 (1.09 μM), and EHMC (0.86 μM) were made to the solution composed of 0.2 mL of the sample, 8 mL of 0.1 M NaCl, 1 mL of methanol, 1 mL of ethanol, and 0.30 mM CTAB.

Table 5.18 reports the concentrations of UV filters recovered following SPE and the percentage recoveries.

Table 5.18 - Percentage recovery and concentration of UV filters recovered after SPE treatment with DSC-Lt18 cartridge (6cc, 500mg)

Analyte	Added UV Filter Concentration (μM)	Recovered UV Filter Concentration (μM)	Recovery (%)
OC	0.0.14	0.0074	53.38
BP3	0.022	0.0074	34.11
EHMC	0.017	0.011	65.10

It has been observed that with the DSC-Lt18 cartridge, the percentage recovery decreases as the sample volume to be processed increases and the concentration of UV filters in the solution decreases. The same trend had been found with the Oasis cartridge.

Mix cartridges

Given the results obtained using the DSC-Ph and DSC-Lt18 cartridges, it was decided to mix the two resins. After removing the resins from the cartridges, they were blended in a 1:1 ratio, with 250 mg of DSC-Ph and 250 mg of DSC-Lt18, and placed inside an SPE cartridge, which was then packed. The "MIX" cartridge was initially used to preconcentrate synthetic samples containing individual analytes and subsequently to preconcentrate synthetic solutions containing all three UV filters simultaneously.

The first analyte treated with the "MIX" cartridge was OC. A synthetic solution was prepared with 50 mL of tap water to which 0.55 μM OC was added. After preparing the sample, the cartridge was conditioned with 6 mL of methanol and 6 mL of HPW. Once this step was completed, the sample was loaded, and subsequently, the analyte was eluted using a mixture composed of 1 mL of methanol and 1 mL of ethanol. Finally, an aliquot of the eluate (1 mL) was added to 8 mL of 0.1 M NaCl, 0.5 mL of methanol, 0.5 mL of ethanol, and 0.30 mM CTAB.

Using the standard addition method, it was possible to quantify the recovery obtained through SPE treatment (Table 5.19).

Table 5.19 - Percentage recovery and recovered concentration of OC following SPE treatment with the "MIX" cartridge (6cc, 250mg DSC-Ph, 250mg DSC-Lt18).

Octocrylene			
Added concentration of UV filters (μM)	Recovered concentration of UV filters (μM)	Recovery (%)	RSD (%)
0.55	0.48 ± 0.087	87.81 ± 6.32	7.19

By employing the "MIX" cartridge, consisting of 250 mg of DSC-Ph and 250 mg of DSC-Lt18, and using a extracting phase composed of 1 mL of methanol and 1 mL of ethanol, a high percentage recovery of OC and good repeatability were achieved.

After evaluating the percentage recovery of OC, the same treatment was carried out for BP3. A synthetic sample was prepared with 50 mL of tap water to which BP3 at 0.87 μM was added. After conditioning the cartridge and loading the sample, BP3 was eluted using a solution composed of 1 mL of methanol and 1 mL of ethanol. An aliquot of the solution (1 mL) was added to a cell with 8 mL of 0.1 M NaCl, 0.5 mL of methanol, 0.5 mL of ethanol, and 0.30 mM CTAB, and the sample was scanned. Finally, two subsequent additions of BP3 at 2.19 μM were made to the solution.

Through the standard addition method, it was possible to quantify the recovery obtained through SPE treatment (Table 5.20).

Table 5.20 - Percentage recovery and recovered concentration of BP3 following SPE treatment with the "MIX" cartridge (6cc, 250mg DSC-Ph, 250mg DSC-Lt18).

Oxybenzone			
Added concentration of UV filters (μM)	Recovered concentration of UV filters (μM)	Recovery (%)	RSD (%)
0.87	0.77 ± 0.089	93.67 ± 4.08	4.36

The use of the "MIX" cartridge allowed for a very high percentage recovery of BP3, and the treatment proved to be repeatable, with a percentage RSD below 10%.

The last analyte treated using the "MIX" cartridge was EHMC. A sample of 50 mL tap water with an addition of 0.69 μM EHMC was prepared. After completing all SPE steps, such as conditioning, sample loading, and elution, an aliquot (1 mL) of the eluate was added to a cell with 8 mL of 0.1 M NaCl, 0.5 mL of methanol, 0.5 mL of ethanol, and 0.30 mM CTAB.

Using the standard addition method, it was possible to quantify the recovery obtained through SPE treatment (Table 5.21).

Table 5.21 - Percentage recovery and recovered concentration of EHMC following SPE treatment with the "MIX" cartridge (6cc, 250mg DSC-Ph, 250mg DSC-Lt18).

Octinoxate			
Added concentration of UV filters (μM)	Recovered concentration of UV filters (μM)	Recovery (%)	RSD (%)
0.68	0.60 ± 0.002	92.41 ± 0.16	0.17

As seen for BP3 and OC, also for EHMC, the use of the "MIX" cartridge and the extracting solution consisting of 1 mL of methanol and 1 mL of ethanol allowed for a high percentage recovery and good repeatability.

Given the satisfactory results, a synthetic solution containing all three analytes (OC, BP3, EHMC) was treated using SPE. The sample was prepared using 50 mL of tap water with additions of 0.55 μM OC, 0.87 μM BP3, and 0.69 μM EHMC. After conditioning the cartridge with 6 mL of methanol and 6 mL of HPW, and loading the sample, the analytes were eluted using a mixture of 1 mL of ethanol and 1 mL of methanol. An aliquot of the eluate (0.5 mL) was placed into a cell with 4 mL of 0.1 M NaCl, 0.25 mL of methanol, 0.25 mL of ethanol, and 0.30 mM CTAB, and the sample was scanned. Two additions of 1.38 μM OC, 2.19 μM BP3, and 1.72 μM EHMC were made to the solution, resulting in the voltammograms in Figure 5.12. The results obtained are reported in Table 5.22.

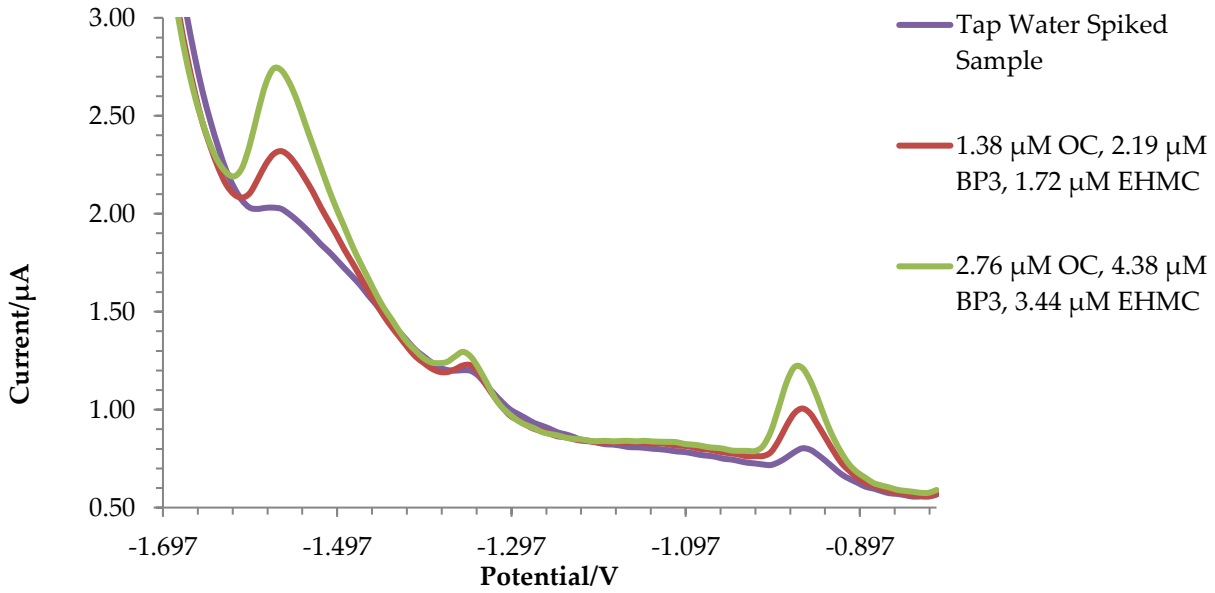

Figure 5.12 - Voltammogram obtained following the sample scan and two additions of 1.38 μM OC, 2.19 BP3 μM, and 1.72 μM EHMC.

Table 5.22 - Percentage recovery and recovered concentration of UV filters following SPE treatment with the "MIX" cartridge (6cc, 250mg DSC-Ph, 250mg DSC-Lt18).

Analyte	Added concentration of UV filters (μM)	Recovered concentration of UV filters (μM)	Recovery (%)	RSD (%)
OC	0.55	0.44 ± 0.041	79.34 ± 2.97	3.74
BP3	0.87	0.73 ± 0.05	83.75 ± 2.38	2.84
EHMC	0.68	0.50 ± 0.07	72.6 ± 4.09	5.64

Considering the satisfactory results obtained in terms of percentage recovery and repeatability, it was decided to further decrease the concentration of UV filters in the sample and increase the volume of the solution to be treated by SPE.

Using the "MIX" cartridge, a synthetic sample consisting of 100 mL of tap water with additions of 0.27 μM OC, 0.43 μM BP3, and 0.34 μM EHMC was treated through SPE. After conditioning the cartridge and loading the sample, the analytes were eluted using 1 mL of methanol and 1 mL of ethanol. This solution was then dried, and the analytes were solubilized using 0.25 mL of methanol and 0.25 mL of ethanol. An aliquot of the eluate (0.25 mL) was added to a cell with 4 mL of 0.1 M NaCl, 0.5 mL of methanol, 0.5 mL of ethanol, and 0.30 mM CTAB, and the sample was scanned. Finally, two subsequent additions of 1.38 μM OC, 2.19 μM BP3, and 1.72 μM EHMC were made to the solution. Table 5.23 reports the concentrations of UV filters recovered following SPE and the percentage recoveries.

Table 5.23 - Percentage recovery and recovered concentration of UV filters following SPE treatment with the "MIX" cartridge (6cc, 250mg DSC-Ph, 250mg DSC-Lt18).

Analyte	Added concentration of UV filters (μM)	Recovered concentration of UV filters (μM)	Recovery (%)	RSD (%)
OC	1.38	1.16 ± 0.055	84.30 ± 3.97	4.71
BP3	2.19	2.11 ± 0.033	96.61 ± 1.5	1.55
EHMC	1.72	1.35 ± 0.08	78.39 ± 4.6	5.85

Considering the very good results, it was decided to further decrease the concentration of UV filters in the sample.

Three different samples were analyzed:

- Sample A: 500 mL of tap water with 0.055 μM OC, 0.087 μM BP3, 0.068 μM EHMC

- Sample B: 500 mL of tap water with 0.014 μM OC, 0.022 μM BP3, 0.017 μM EHMC

- Sample C: 1 L of tap water with 2.76 nM OC, 4.38 nM BP3, 3.44 nM EHMC

The samples were treated with the same procedure. After conditioning the cartridge and loading the sample, the analytes were eluted using a mixture of 1 mL of ethanol and 1 mL of methanol. Subsequently, the eluate was dried, and the analytes were solubilized into 0.2 mL of methanol. This solution was then added to 4 mL of 0.1 M NaCl, 0.5 mL of methanol, 0.5 mL of ethanol, and 0.30 mM CTAB.

For all samples (A, B, C), accurate quantification was not possible since the resulting concentrations were close to the LOQ. However, a qualitative analysis was conducted, demonstrating that the "MIX" cartridge allows for the detection of UV filters in samples containing a low concentrations of these analytes and can also handle large sample volumes. This is considered a good result since the concentrations considered in these last tests were similar to those typically found in natural waters: the preconcentration and analysis procedure demonstrated the ability to identify the presence of these substances even at trace levels.

5.8 Voltammetric Analysis of Lake Water Samples

The analyzed waters are from lakes located in Piedmont. In particular, waters from four lakes were sampled:

- **Afframont Lake**: a small alpine lake located in Val d'Ala, in the municipality of Balme, at an elevation of 1986 m above sea level (a.s.l.). 45°17'29.49" N; 7°14'13.15" E.

- **Ceresole Reale Lake**: an artificial lake situated in the Orco Valley, in the municipality of Ceresole Reale, at an elevation of 1582 m a.s.l. 45°25'46.95" N; 7°13'48.66" E.

- **Small Avigliana Lake**: a moraine-origin lake located in the municipality of Avigliana at an elevation of 356 m a.s.l. 45°03'57.09" N; 7°23'13.73" E.

- **Large Avigliana Lake**: a moraine-origin lake located in the municipality of Avigliana at an elevation of 352 m a.s.l. 45°03'57.09" N; 7°23'13.73" E.

Lake waters are generally rich in organic matter and suspended solids. For this reason, after sampling, they were filtered using glass fiber filters. Subsequently, the waters were stored in amber glass containers and placed in a refrigerator at a temperature of 4 °C to prevent the degradation of the analytes.

The sampled waters were analyzed using voltammetry with optimized parameters. After conditioning the SPE cartridge with 6 mL of methanol and 6 mL of HPW, 100 mL of the sample were passed through the cartridge. Subsequently, the retained analytes were eluted using a solution composed of 1 mL of methanol and 1 mL of ethanol. The eluate was dried, and the analytes were solubilized in 0.2 mL of methanol. This solution was placed inside the electrochemical cell with 4 mL of 0.1 M NaCl, 0.5 mL of ethanol, 0.5 mL of methanol, and 0.30 mM CTAB. After scanning the sample, two additions of 1.38 μM OC, 2.19 μM BP3, and 1.72 μM EHMC were made to the solution.

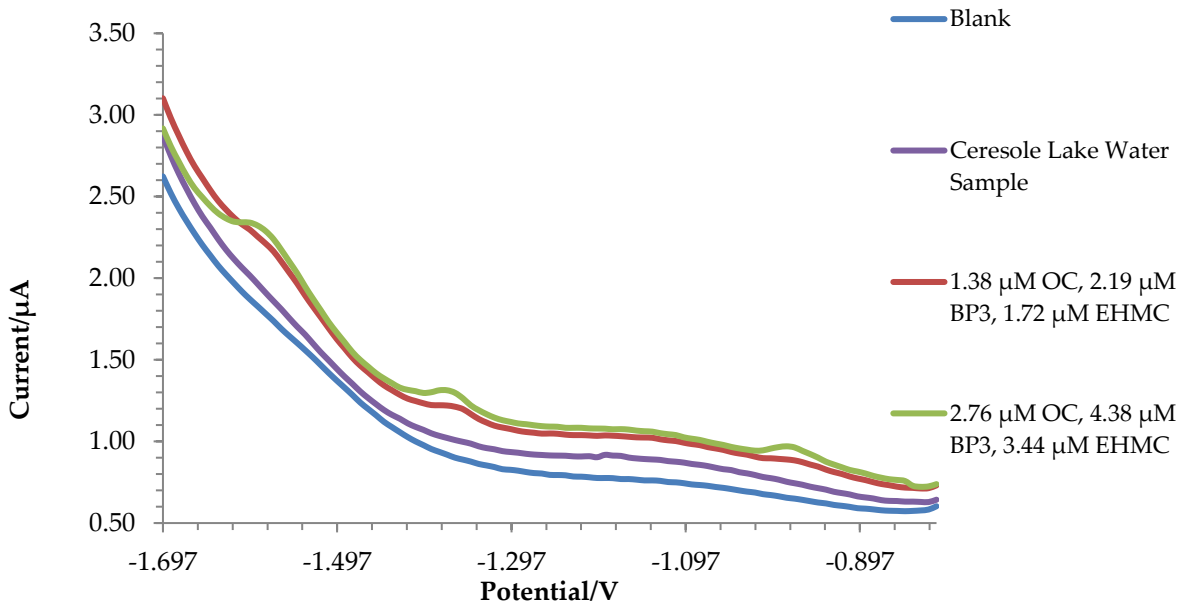

Figure 5.13 -Voltammogram obtained following the scan of the sample from Lake Ceresole Reale and two additions of 1.38 µM OC, 2.19 µM BP3, and 1.72 µM EHMC.

Figure 5.13 shows, by way of example, the voltammograms obtained for the sample from Lake Ceresole Reale. Indeed, the concentrations of analytes in all water samples collected were found to be below the method's limit of quantification (LOQ). In addition to laboratory analyses, field analysis was conducted for the Avigliana lakes (Figure 5.14).

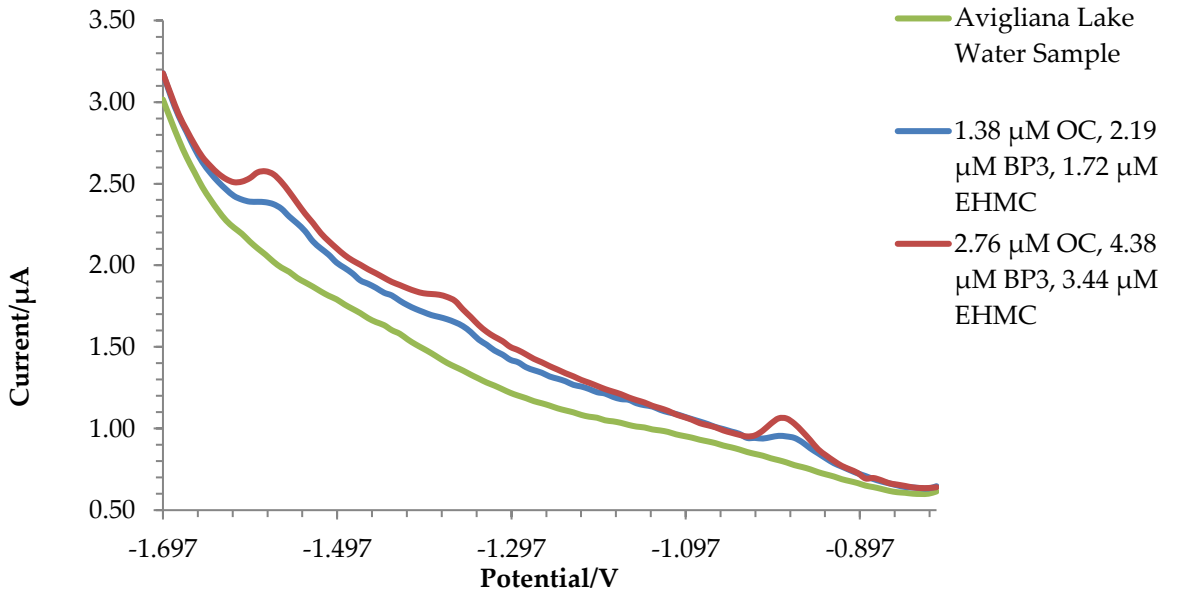

Figure 5.14 - Voltammogram obtained following the field scan of the Avigliana lake sample and two additions of 1.38 µM OC, 2.19 µM BP3, and 1.72 µM EHMC.

In this case, 100 mL of the sample was treated using SPE, and subsequently, the cartridge was eluted using a solution composed of 1 mL of methanol and 1 mL of ethanol. It was not feasible to dry the eluate in the field since this process requires too much time. Therefore, 0.5 mL of the eluate was placed into the cell with 4 mL of 0.1 M NaCl, 0.25 mL of methanol, 0.25 mL of ethanol, and 0.30

mM CTAB. After, two subsequent additions of 1.38 μM OC, 2.19 μM BP3, and 1.72 μM EHMC were made. This field analysis was conducted to assess the applicability and potential challenges of the on-site analysis procedure. Clearly, in this case as well, the analyte content was confirmed to be below the instrumental LOQ.

After analyzing lake waters and observing that the concentration of UV filters in the samples was below the LOQ, lake waters spiked with a known concentration of each analyte were analyzed. To perform the spike, 69.16 nM OC (25 μg L^{-1}), 109.53 nM BP3 (25 μg L^{-1}), and 86.08 nM EHMC (25 μg L^{-1}) were added to 100 mL of the sample.

All samples were treated with the same procedure. After spiking 100 mL of lake water with 69.16 nM OC, 109.53 nM BP3, and 86.08 nM EHMC, the sample was treated with an SPE cartridge at a constant flow rate of 5 mL min^{-1}. After this step, a methanol : ethanol = 1 : 1 mixture was eluted through the cartridge, and the eluate was dried. Subsequently, the analytes were recovered using 0.2 mL of methanol, which were then added to a cell containing 4 mL of 0.1 M NaCl, 0.5 mL of methanol, 0.5 mL of ethanol, and 0.30 mM CTAB. Two additions of 1.38 μM OC, 2.19 μM BP3, and 1.72 μM EHMC were made to this solution.

As an example, the voltammograms for two lake samples are shown in Figures 5.15 and 5.16. Table 5.24 presents the % recoveries and concentrations of UV filters recovered following the SPE treatment for all investigated lakes.

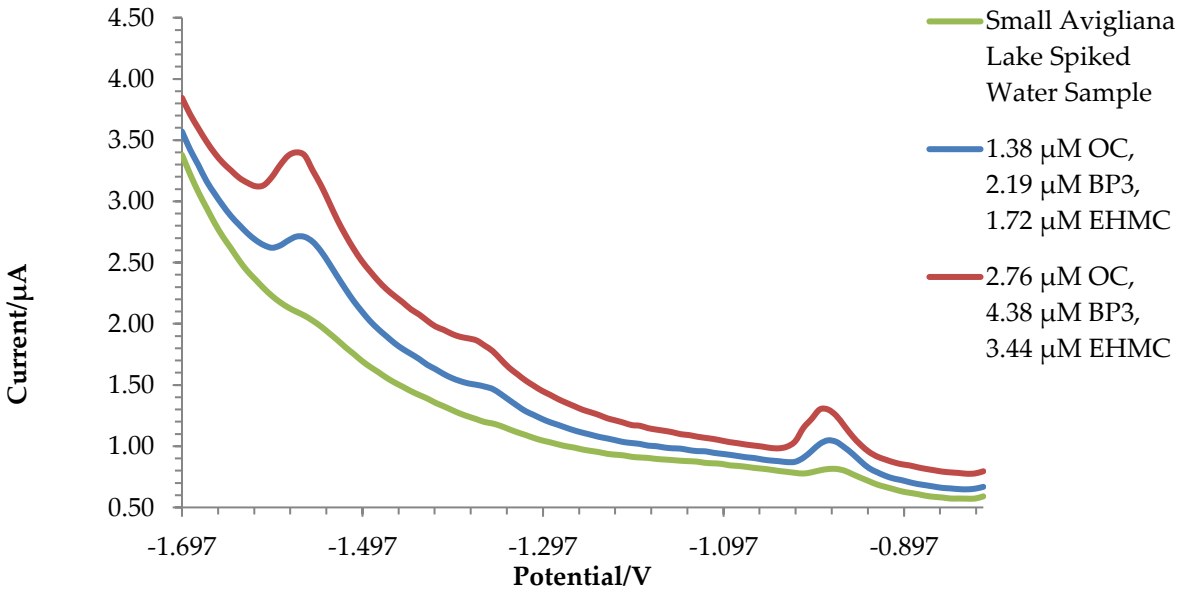

Figure 5.15 - The voltammogram obtained following the scanning of the sample from the small lake of Avigliana and two additions of 1.38 μM OC, 2.19 μM BP3, and 1.72 μM EHMC.

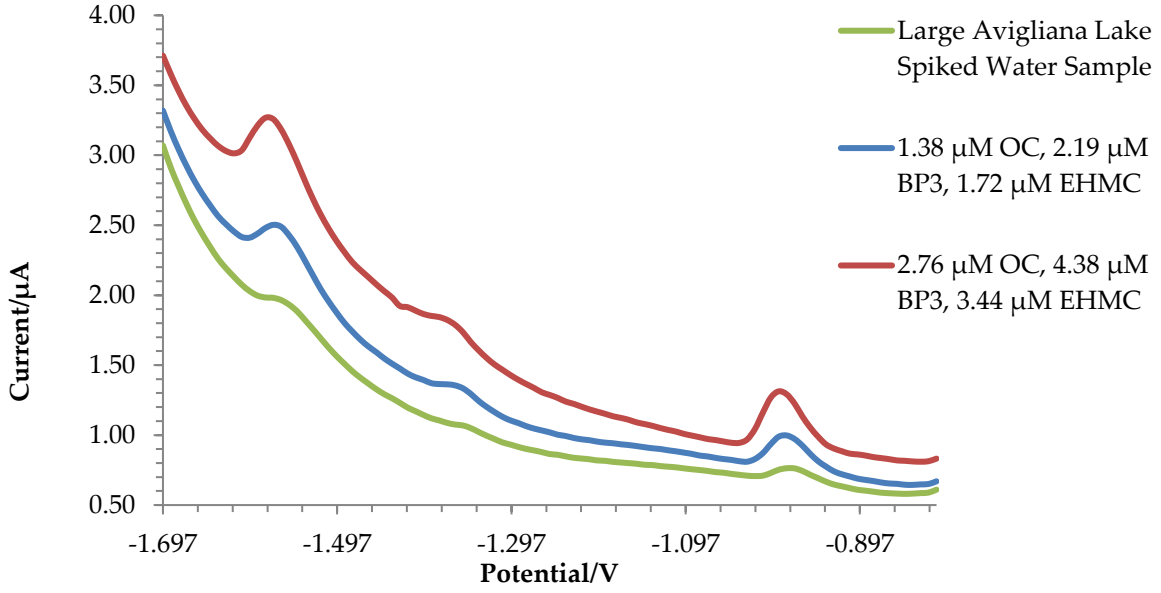

Figure 5.16 - The voltammogram obtained following the scanning of the sample from the large lake of Avigliana and two additions of 1.38 µM OC, 2.19 µM BP3, and 1.72 µM EHMC.

Table 5.24 - Percentage recoveries and concentrations of recovered UV filters following the Solid Phase Extraction (SPE) treatment of the four analyzed lakes.

	Analyte	Expected concentration of UV filters (nM)	Recovered concentration of UV filters (nM)	Recovery (%)
Afframont lake	OC	69.16	66.08	95.55
	BP3	109.53	46.00	42.00
	EHMC	86.08	84.52	98.18
Ceresole Reale Lake	OC	69.16	46.92	67.85
	BP3	109.53	103.07	94.11
	EHMC	86.08	87.51	101.65
Small Avigliana Lake	OC	69.16	65.14	94.20
	BP3	109.53	50.26	45.89
	EHMC	86.08	18.99	222.07
Large Avigliana Lake	OC	69.16	41.83	60.49
	BP3	109.53	83.52	76.25
	EHMC	86.08	59.73	69.38

From Table 5.24, it can be noted that for some lakes and analytes, recoveries are greater than 90%, while for others, they are relatively low. This issue could be attributed to the presence of other organic substances, of natural of anthropic origin, which might interact with the analytes, or might compete with them for the sorbent in the cartridge. This problem could be addressed by increasing instrumental sensitivity or using SPE cartridges that allow a higher sample volume to pass through, thereby increasing preconcentration ratio.

Regarding the analysis of "unspiked" lake samples, passive "disk" samplers containing adsorbent resins could be considered to detect the presence of UV filters. These disks could be left in the lake for a longer period (e.g. days) to accumulate a higher amount of UV filters, facilitating the determination of these substances. This approach would provide a monitoring technique to verify the presence of these contaminants in natural waters. If positive, i.e. if UV filters are detected, the samples could then be taken to the laboratory for quantification.

5.9 Analysis on Sunscreen Samples

The optimized analytical technique was employed to analyze samples of sunscreens to determine the quantity of UV filters present. Initially, two sunscreen samples (Sample 1 and Sample 2) were analyzed to optimize sample pretreatment. Subsequently, the remaining sample aliquots were analyzed to characterize the UV filters present within them. Furthermore, the results obtained through voltammetry were compared with the concentrations found using HPLC-DAD as the analytical technique.

To optimize the sample pretreatment, particularly the extraction procedure, two sunscreen samples were initially analyzed: Sample 1, containing OC according to the label, and Sample 2, whose label indicated the presence of EHMC.

Three different extraction procedures were tested:

- Extraction Procedure A: 0.1 g of sunscreen was added to 50 mL of 0.1 M NaCl, and the solution was stirred for 30 minutes.

- Extraction Procedure B: 0.1 g of sunscreen was added to 50 mL of 0.1 M NaCl, and the solution was stirred for 24 hours.

- Extraction Procedure C: 0.1 g of sunscreen was added to 30 mL of methanol, and the solution was sonicated for 10 minutes.

Upon completion of the extraction procedure, 0.1 mL of the solution was placed in an electrochemical cell with 8 mL of 0.1 M NaCl, 1 mL of methanol, 1 mL of ethanol, and 0.30 mM CTAB. After the voltammetric measurement, standard additions were performed. Finally, the percentage (% w/w) of UV filter present in each sunscreen sample was calculated.

The results obtained by voltammetry were compared with those obtained through HPLC-DAD analysis, assuming that the latter provides accurate results. In particular, Hypersil GOLD PFP (5×2.1 mm, 1.9 μm particle size) was used at a temperature of 30 ºC and a mobile phase: 52% ultra pure water acidified with formic acid 0.1% v/v, 48% acetonitrile acidified with formic acid 0.1% v/v. For the HPLC-DAD analysis, 0.1 g of sunscreen were added to 4 mL of methanol, and the solution was sonicated for 15 minutes. To the sample, 6 mL of the mobile phase, composed of HPW and acetonitrile acidified with 0.1% formic acid, were added, and the mixture was centrifuged for 10 minutes. Subsequently, the sample was diluted 1:200 with the mobile phase, and after filtration, 5 μL of the solution were injected into the chromatograph.

It was observed that the extraction procedure yielding the best results in terms of % w/w is extraction procedure A. This procedure, for both Sample 1 and Sample 2, provides percentages that

closely approximate those obtained with HPLC-DAD. Below, in Figure 5.17, the voltammograms of Sample 2 are presented.

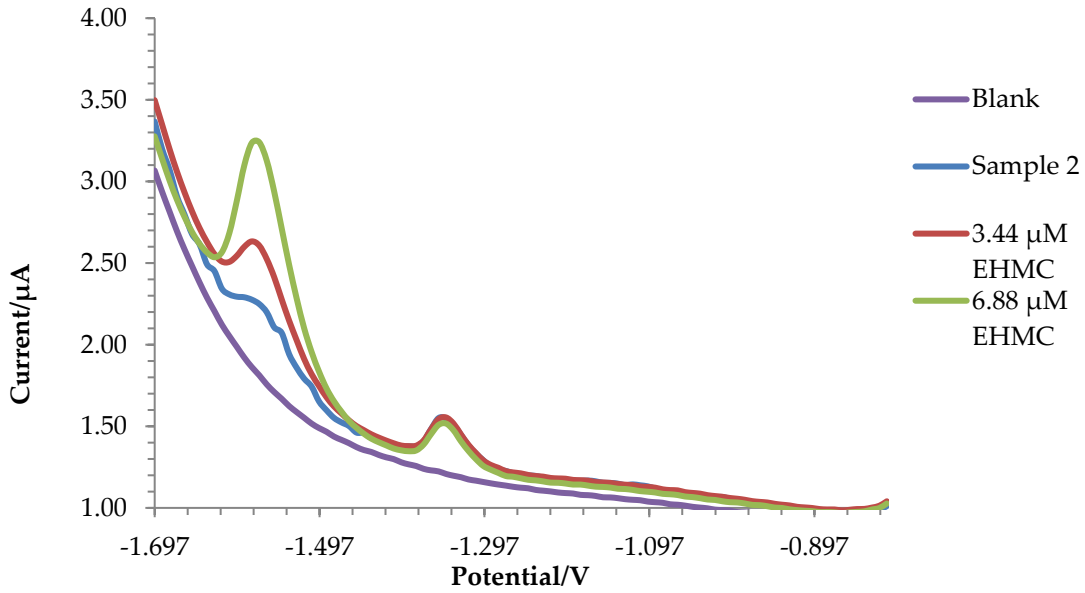

Figure 5.17 - The voltammogram of sample 2 obtained following the scan of the sample and two additions of 3.44 µM EHMC.

After optimizing the sample pretreatment, various sunscreens were analysed. The results are reported in table 5.25 compared with those obtained with HPLC-DAD.

Table 5.25 - Quantification of UV filters in sunscreens – results reported as % (w/w) of UV filters, voltammetry vs HPLC-DAD

	Voltammetry			HPLC-DAD		
Sunscreen	EHMC	OC	AVO	EHMC	OC	AVO
1	3,54±0,4			3.49		
2	2,47±0,24	2,31±0,08		2.48	2.30	0.14
3						
4		3,44±0,21	1,51±0,11		3.64	1.51
5					2.80	1.85
6			3,88±0,14	2.46		3.66
7	1,88±0,03			1.88		
8			3,81±0,07			3.81
9			2,04±0,03			2.19
10			1,53±0,04			1.26
11	1,25±0,08	2,42±0,21	1,75±0,1	1.38	2.46	1.73
12	<LOQ			0.37		
13			<LOQ			0.17
14	2,09±0,12			2.32		
15			4,42±0,23	0.03		4.28
16	1,3±0,2	<LOQ	<LOQ	1.13	0.26	1.03
17	<LOQ		<LOQ	0.07		0.04
18	4,22±0,54		<LOQ	4.14		0.74
19		1,3±0,35	1,32±0,05		1.17	1.30
20			<LOQ			0.26
21		4,11±0,02			5.37	
22	2,68±0,33			3.70		
23		8,38±0,67	3,6±0,48		8.85	4.61
24	2,1±0,19		1,17±0,28	1.84		1.29
25		<LOQ	<LOQ		0.26	0.57

Each sample was treated using extraction procedure A, i.e. 0.1 g of cream were added to 50 mL of 0.1 M NaCl, and the solution was stirred for 30 minutes. Afterwards, a voltammetric measurement was carried out, then two subsequent additions of EHMC 3.44 μM were made to the solution containing the sample, 8 mL of 0.1 M NaCl, 1 mL of methanol, 1 mL of ethanol, and 0.30 mM CTAB.

For all the analyzed sunscreen samples, the results obtained with the voltammetric technique were in agreement with those obtained using a conventional method, such as HPLC-DAD. Therefore, the analytical procedure optimized proved suitable not only for detecting the presence of UV filters in aqueous matrices but also for determining UV filters in complex matrices such as sunscreens.

In terms of the percentage of filters found in the products, all results comply with both the limits set by European Chemicals Agency (ECHA) (OC < 10%, EHMC < 10%) and the limits set by the FDA (OC < 10%, EHMC < 7.5%). In fact, all analyzed sunscreen samples exhibit UV filter percentages much lower than the legal limits. Therefore, these sunscreens are considered "safe" from an environmental standpoint, although continued use could potentially have various impacts on the aquatic ecosystem.

References

[1] E. Berardesca, T. Zuberbier, M. Sanchez Viera, and M. Marinovich, "Review of the safety of octocrylene used as an ultraviolet filter in cosmetics," J. Eur. Acad. Dermatol. Venereol., vol. 33, no. S7, pp. 25–33, Nov. 2019, doi: 10.1111/jdv.15945.

[2] C. A. Downs, J. C. DiNardo, D. Stien, A. M. S. Rodrigues, and P. Lebaron, "Benzophenone Accumulates over Time from the Degradation of Octocrylene in Commercial Sunscreen Products," Chem. Res. Toxicol., vol. 34, no. 4, pp. 1046–1054, Apr. 2021, doi: 10.1021/acs.chemrestox.0c00461.

[3] T. He, M. M. Tsui, C. J. Tan, C. Y. Ma, S. K. F. You, L- H. Wang, T. H. Chen, T. Y. Fan, P. K. Lam, M. Murphy, "Toxicological effects of two organic ultraviolet filters and a related commercial sunscreen product in adult corals," Environ. Pollut., vol. 245, pp. 462–471, Feb. 2019, doi: 10.1016/j.envpol.2018.11.029.

[4] M. E. Burnett and S. Q. Wang, "Current sunscreen controversies: a critical review," Photodermatol. Photoimmunol. Photomed., vol. 27, no. 2, pp. 58–67, Apr. 2011, doi: 10.1111/j.1600-0781.2011.00557.x.

[5] C. A. Downs, E. Kramarsky-Winter, R. Segal, J. Fauth, S. Knutson, O. Bronstein, F. R. Ciner, R. Jeger, Y. Lichtenfeld, C. M. Woodley, P. Pennington, K. Cadenas, A. Kushmaro, Y. Loya, "Toxicopathological Effects of the Sunscreen UV Filter, Oxybenzone (Benzophenone-3), on Coral Planulae and Cultured Primary Cells and Its Environmental Contamination in Hawaii and the U.S. Virgin Islands," Arch. Environ. Contam. Toxicol., vol. 70, no. 2, pp. 265–288, Feb. 2016, doi: 10.1007/s00244-015-0227-7.

[6] M. Coronado, H. De Haro, X. Deng, M. A. Rempel, R. Lavado, and D. Schlenk, "Estrogenic activity and reproductive effects of the UV-filter oxybenzone (2-hydroxy-4-methoxyphenyl-methanone) in fish," Aquat. Toxicol., vol. 90, no. 3, pp. 182–187, Nov. 2008, doi: 10.1016/j.aquatox.2008.08.018.

[7] L. Gao, T. Yuan, C. Zhou, P. Cheng, Q. Bai, J. Ao, W. Wang, H. Zhang, "Effects of four commonly used UV filters on the growth, cell viability and oxidative stress responses of the Tetrahymena thermophila," Chemosphere, vol. 93, no. 10, pp. 2507–2513, Nov. 2013, doi: 10.1016/j.chemosphere.2013.09.041.

[8] A. Sharma, K. Bányiová, P. Babica, N. El Yamani, A. R. Collins, and P. Čupr, "Different DNA damage response of cis and trans isomers of commonly used UV filter after the exposure on adult human liver stem cells and human lymphoblastoid cells," Sci. Total Environ., vol. 593–594, pp. 18–26, Sep. 2017, doi: 10.1016/j.scitotenv.2017.03.043.

[9] M. Nakajima, T. Kawakami, T. Niino, Y. Takahashi, and S. Onodera, "Aquatic Fate of Sunscreen Agents Octyl-4-methoxycinnamate and Octyl-4-dimethylaminobenzoate in Model Swimming Pools and the Mutagenic Assays of Their Chlorination Byproducts," J. Health Sci., vol. 55, no. 3, pp. 363–372, 2009, doi: 10.1248/jhs.55.363.

[10] C. Paris, V. Lhiaubet-Vallet, O. Jiménez, C. Trullas, and M. Á. Miranda, "A Blocked Diketo Form of Avobenzone: Photostability, Photosensitizing Properties and Triplet Quenching by a

Triazine-derived UVB-filter," Photochem. Photobiol., vol. 85, no. 1, pp. 178–184, Jan. 2009, doi: 10.1111/j.1751-1097.2008.00414.x.

[11] N. Tarras-Wahlberg, A. Rosén, G. Stenhagen, O. Larkö, A.-M. Wennberg, and O. Wennerström, "Changes in Ultraviolet Absorption of Sunscreens After Ultraviolet Irradiation," J. Invest. Dermatol., vol. 113, no. 4, pp. 547–553, Oct. 1999, doi: 10.1046/j.1523-1747.1999.00721.x.

[12] F. Clergeaud, M. Giraudo, A. M. S. Rodrigues, E. Thorel, P. Lebaron, and D. Stien, "On the Fate of Butyl Methoxydibenzoylmethane (Avobenzone) in Coral Tissue and Its Effect on Coral Metabolome," Metabolites, vol. 13, no. 4, p. 533, Apr. 2023, doi: 10.3390/metabo13040533.

[13] A. Sunyer, A. González-Navarro, M. P. Serra-Roig, N. Serrano, M. S. Díaz-Cruz, and J. M. Díaz-Cruz, "First application of carbon-based screen-printed electrodes for the voltammetric determination of the organic UV filters oxybenzone and octocrylene," Talanta, vol. 196, pp. 381–388, May 2019, doi: 10.1016/j.talanta.2018.12.092.

[14] V. S. Ferreira, J. B. G. Júnior, C. M. S. C. Oliveira, R. M. Takeuchi, A. L. Santos, and M. A. G. Trindade, "Voltammetric analysis of sun-block preparations containing octocrylene and its association with 2-Hydroxy-4-methoxybenzophenone and octyl methoxycinnamate," Microchem. J., vol. 106, pp. 378–383, Jan. 2013, doi: 10.1016/j.microc.2012.10.002.

[15] J. C. Cardoso, B. M. L. Armondes, and J. B. G. J. E. V. Ferreira, "Simultaneous electrochemical determination of three sunscreens using cetyltrimethylammonium bromide," Colloids Surf. B Biointerfaces, vol. 63, no. 1, pp. 34–40, May 2008, doi: 10.1016/j.colsurfb.2007.11.001.

6. CONCLUSIONS

The aims of the PhD project focused on the development of sensors for the rapid determination of contaminants in different matrices, using a low-cost and easy-to-use voltammetric technique that allows analysis directly in the field, with a focus on topics related to food, environment, and human health.

In conclusion, this work represents a significant contribution to the advancement of sensor technology in the fields of food and environmental monitoring. The successful development of a innovative kit for on-site speciation of mercury and methylmercury stands out as a remarkable achievement. This innovation not only enhances the accuracy and efficiency of mercury determination but also offers a practical solution for field applications, particularly in areas where real-time monitoring is critical.

Furthermore, the devised method for the determination of Fe(III) in lake waters showcases the PhD's commitment to addressing environmental concerns. The demonstrated efficacy of this method underscores its potential as a valuable tool for monitoring iron levels in aquatic ecosystems, contributing to the broader understanding of water quality and ecological health. A further development of the method will be to test its applicability to the analysis of biological samples, taking into account its potential role as a biomarker of Alzheimer’s disease.

A noteworthy aspect of this thesis is the introduction of an innovative method, protected by a patent, for the determination of chemical UV filters in water and creams. This novel approach not only meets the growing demand for accurate and precise analysis of personal care products but also highlights the researcher's creativity in developing proprietary methods with potential applications in various industries.

The overall success of these developments underscores the thesis's impact on both scientific knowledge and practical applications. As the global community fights with increasingly complex challenges related to environmental pollution and food safety, the advancements presented in this work offer tangible solutions and avenues for further research. The patented method for chemical UV filter determination, in particular, holds promise for commercial applications, exemplifying the potential for academic research to drive technological innovation and address pressing societal needs.

In summary, the outcomes of this thesis not only contribute significantly to the academic advancement of sensor technology but also provide practical tools that can be instrumental in safeguarding the environment and ensuring the safety of food products. The combination of scientific rigor, innovation, and real-world applicability positions this research as a noteworthy milestone in the field of sensors for food and environmental analysis.

7 SCIENTIFIC PUBLICATIONS

P. Inaudi*, O. Abollino, M. Argenziano, M. Malandrino, C. Guiot, S. Bertinetti, L. Favilli, A. Giacomino, "Advancements in Portable Voltammetry: A Promising Approach for Iron Speciation Analysis", Molecules 2023, 28, 7404, https://doi.org/10.3390/molecules28217404

A. Diana, S. Bertinetti, O. Abollino, A. Giacomino, S. Buoso, L. Favilli, **P. Inaudi**, M. Malandrino, "PM10 element distribution and environmental-sanitary risk analysis in two Italian industrial cities", Atmosphere 2023, 14, 48. https://doi.org/10.3390/atmos14010048

A. Giacomino, **P. Inaudi*,** G. Silletta, A. Diana, S. Bertinetti, E. Gaggero, M. Malandrino, F. Stilo, O. Abollino, "Analytical methods for the characterization of vegetable oils", Molecules 2023, 28, 153. https://doi.org/10.3390/molecules28010153

L. Favilli, A. Giacomino, M. Malandrino, **P. Inaudi**, A. Diana, O. Abollino, "Strategies for mercury speciation with single and multi-element approaches by HPLC-ICP-MS", Frontiers in Chemistry 2022, 10:1082956 doi: 10.3389/fchem.2022.1082956

S. Berto, E. Cagno, E. Prenesti, G. Aragona, S. Bertinetti, A. Giacomino, **P. Inaudi,** M. Malandrino, E. Terranova, O. Abollino, "Voltammetric study for the determination of diclofenac in aqueous solutions using electro-activated carbon electrodes", Applied Science 2022, 12, 7983. https://doi.org/10.3390/app12167983

F. Solano, **P. Inaudi***, O. Abollino, A. Giacomino, M. Chiesa, E. Salvadori, G. Kociok-Kohn, E. da Como, T. Salzillo, C. Fontanesi, "Charge transfer modulation in Charge Transfer co-crystal driven by crystal structure morphology", Physical Chemistry Chemical Physics 2022, DOI https://doi.org/10.1039/D2CP01408D

P. Inaudi*, E. Mondino, O. Abollino, M. Malandrino, M. Argenziano, R. Boschini, A. Giacomino "On-site determination of methylmercury by coupling solid phase extraction and voltammetry", Molecules 2022, 27, 3178. https://doi.org/10.3390/molecules27103178

E. Conca, M. Malandrino, A. Giacomino, **P. Inaudi,** A. Giordano, F. Ardini, R. Traversi, O. Abollino "Chemical fractionation of trace elements in Arctic PM10 samples", Atmosphere 2021, 12(9), 1152 https://doi.org/10.3390/atmos12091152

F. Solano, **P. Inaudi**, M. Chiesa, G. Kociok-Köhn, E. Salvadori, E. Da Como, D. Vanossi, M. Malandrino, R. Carmieli, A. Giacomino, C. Fontanesi "Spin Multiplicity and Solid-State Electrochemical Behavior in Charge-Transfer Co-crystals of DBTTF/F4TCNQ", The Journal of Physical Chemistry C, 2021: https://doi.org/10.1021/acs.jpcc.1c00020

A. Giacomino, A. Ruo Redda, R. Caligiuri, **P. Inaudi**, S. Squadrone, M. C. Abete, O. Abollino, S. Morandi, E. Conca, M. Malandrino, "Development of an easy portable procedure for on-site determination of mercury and methylmercury", Food Chemistry, 342, 2021, 128347, https://doi.org/10.1016/j.foodchem.2020.128347

E. Conca, M. Malandrino, A. Giacomino, E. Costa, F. Ardini, **P. Inaudi,** O. Abollino, "Optimization of a sequential extraction procedure for trace elements in Arctic PM10", Analytical and Bioanalytical Chemistry, https://doi.org/10.1007/s00216-020-02874-4

E. Gaggero, M. Malandrino, D. Fabbri, G. Bordiglia, A. Fusconi, M. Mucciarelli**, P. Inaudi**, P. Calza, "Uptake of potentially toxic elements by four plant species suitable for phytoremediation of Turin urban soils", Applied Science, 2020, 10, 3948; doi:10.3390/app10113948

E. Conca, M. Malandrino, A. Giacomino, **P. Inaudi**, S. Buoso, S. Bande, M. Sacco, O. Abollino, "Contribution of the Incinerator to the Inorganic Composition of the PM10 Collected in Turin", Atmosphere, 2020, 11, 400, 1-13. doi:10.3390/atmos11040400

P. Inaudi, A. Giacomino, M. Malandrino, C. La Gioia, E. Conca, T. Karak, O. Abollino, "The inorganic component as a possible marker for quality and for authentication of the hazelnut's origin", International Journal of Environmental Research and Public Health, 2020, 17, 447, 1-15. doi:10.3390/ijerph17020447

8 ORAL CONTRIBUTIONS TO CONGRESSES

P. Inaudi, A. Giacomino, O. Abollino, F. Cafaro, E. Fea, S. Squadrone, M. C. Abete, On-site approach for mercury determination and speciation, XVII Italian-Hungarian Symposium on Spectrochemistry, Turin (Italy), 14-18 June 2021

P. Inaudi, O. Abollino, M. Malandrino, F. Stilo, A. Giacomino, Redox Profile as Marker for the Authentication of Vegetable Oil, 72nd Annual Meeting of the International Society of Electrochemistry, Jeju (Korea), 29 August – 3 September 2021

P. Inaudi, F. Solano, M. Chiesa, E. Salvadori, O. Abollino, E. Da Como, M. Malandrino, C. Fontanesi, A. Giacomino, Solid state electrochemical behaviour and spin multiplicity in charge transfer co-crystals of DBTTF:F4TCNQ, SCI2021 XXVII Congresso Nazionale della Società Chimica Italiana, Milan (Italy) 14-23 September 2021

P. Inaudi, L. Favilli, A. Diana, S. Bertinetti, M. Malandrino, O. Abollino, M. Rocci, A. Giacomino, Characterization and monitoring of UV filters in sunscreens by voltammetric methods, XIX Congresso Nazionale della Divisione di Chimica dell'Ambiente e dei Beni Culturali, Turin, 20-23 June 2022

9 POSTER CONTRIBUTIONS TO CONGRESSES

P. Inaudi, C. Mattalia, M. Malandrino, A. Giacomino, O. Abollino, Development of a Voltammetric Screening Method for Pharmaceutical Pollution in Waters, Recent Developments in Pharmaceutical Analysis 2021, Modena (Italy) 6-8 September 2021

P. Inaudi, O. Abollino, M. Malandrino, E. Botticella, A. Giacomino, Monitoring UV filters through the use of voltammetric methods, AISEM 2022 XXI Conferenza Nazionale Sensori e Microsistemi, Rome (Italy), 10/11 February 2022

P. Inaudi, M. Rocci, L. Favilli, A. Diana, S. Bertinetti, M. Malandrino, O. Abollino, A. Giacomino, Voltammetric methods for monitoring UV filters in sunscreens, Giornate dell'Elettrochimica Italiana (GEI) 2022, Orvieto (Italy), 11/15 September 2022

P. Inaudi, L. Favilli, O. Abollino, M. Malandrino, R. Cecire, A. Diana, S. Bertinetti, A. Giacomino, Iron in water: a new procedure for on-site measurement using voltammetric methods, XX Congresso Nazionale della Divisione di Chimica dell'Ambiente e dei Beni Culturali, Ischia (Italy), 28 September 2023 – 1 October 2023

P. Inaudi, L. Favilli, O. Abollino, M. Malandrino, S. Bertinetti, F. Velocci, D. Fabbri, M. Locatelli, A. Giacomino, Analyzing UV Filter Levels in Water and Sunscreens: A Voltammetric Approach, Workshop del Gruppo Interdivisionale "Sensori" della Società Chimica Italiana, Roma (Italy), 13-15 December 2023

10. PARTICIPATION IN RESEARCH PROJECTS

PETKIT - "Valutazione del pet food: impiego di un kit portatile per la determinazione del mercurio "on site" e ricerca di virus emergenti" - Progetto IZPS (Bando Ricerca Corrente 2019 - Ministero della Salute)

MISTICA – "DeterMinazIone e Speciazione del mercurio in un kiT unICo e portAtile" - Progetti di Ricerca di Ateneo PoC Instrument

SVAMITE – "Strategie per la valutazione ed il miglioramento della qualità del te' " - Grant for Internationalization - GFI - Programmazione Triennale 21-23

COALA - "COntaminanti emergenti in laghi prealpini ed ALpine. Monitoraggio del contenuto di residui di prodotti farmaceutici e filtri UV in Acqua e sedimento" - Grant for Internationalization - GFI - Programmazione Triennale 21-23

UPINAN - "Uve PIemontesi e NANotecnologie: tradizione e innovazione per la lotta al tumore al seno (UPINAN)" – Fondazione CRT – Fondi Ordinari 2023

SUSWATER - Sustainable integrated approach to achieve CECs and PTEs removal from contaminated waters. The aquaculture as case study - Marie Skłodowska-Curie Actions (MSCA) – Research and Innovation Staff Exchange - Call: H2020-MSCA-RISE-2020, Project number: 101007578